



CENTRUM FIZYKI TEORETYCZNEJ
POLSKIEJ AKADEMII NAUK

Michele Grasso

**BIGONLIGHT: A NEW PACKAGE FOR
COMPUTING OPTICAL OBSERVABLES IN
NUMERICAL RELATIVITY**

*Thesis submitted in fulfillment of the requirements
for the degree of Doctor of Philosophy in Physics*

Supervisors:

Prof. Mikołaj Korzyński
Dr. Eleonora Villa

WARSAW, NOVEMBER 2021

*“There is a theory which states that if ever anyone discovers exactly what the Universe is for and why it is here, it will instantly disappear and be replaced by something even more bizarre and inexplicable.
There is another theory which states that this has already happened.”*

Douglas Adams

Abstract

With the advent of precision cosmology, our theoretical predictions must aspire to the same level of precision as achieved by experimental probes. In this context, numerical simulations including general relativistic effects represent the state-of-the-art method to describe the formation of structures. However, aside from a detailed description of the dynamics, it is necessary to have an equally accurate explanation of the effects of such structures on light propagation and modelling their impacts on measurable quantities.

The investigation of relativistic effects in the most general way requires a unified treatment of light propagation in cosmology. This goal can be achieved with the new interpretation of the geodesic deviation equation in terms of the bilocal geodesic operators (BGO). The BGO formalism extends the standard formulation, providing a unified framework to describe all possible optical phenomena due to the interaction between light and spacetime curvature.

In my dissertation, I present `BiGONLight`, a `Mathematica` package that applies the BGO formalism to study light propagation in numerical relativity. The package encodes the 3+1 bilocal geodesic operators framework as a collection of `Mathematica` functions. The inputs are the spacetime metric plus the kinematics of the observer and the source in the form of the 3+1 quantities, which may come directly from a numerical simulation or can be provided by the user as analytical components. These data are then used for ray tracing and computing the BGO's in a completely general way, i.e. without relying on symmetries or specific coordinate choices. The primary purpose of the package is the computation of optical observables in arbitrary spacetimes. The uniform theoretical framework of the BGO formalism allows for the extraction of multiple observables within a single computation, while the `Wolfram` language provides a flexible computational framework that makes the package highly adaptable to perform both numerical and analytical studies of light propagation. `BiGONLight` is tested by computing the redshift, angular diameter distance, parallax distance, and redshift drift in well-known cosmological models. We use three different inputs for the metric: two analytical metrics, the homogeneous Λ CDM model and the inhomogeneous Szekeres model, and 3+1 quantities from a simulated dust Universe. The tests show an excellent agreement with known results.

The characteristics of `BiGONLight` make it a suitable tool for studying the impact of inhomogeneities on light propagation. We investigate various sources of nonlinear general relativistic effects on light propagation induced by inhomogeneous cosmic structures. `BiGONLight` is used to calculate observables computed at different approximations in a plane-parallel inhomogeneous spacetime. The nonlinear effects are evaluated as the fractional difference between the observables obtained at the three different approximations: linear perturbation theory, Newtonian, and post-Newtonian approximations. The inhomogeneities are tuned by varying the model's free parameters, and their contributions to the observables are obtained by analysing the variations in the fractional differences. Using this method we estimate the Newtonian and post-Newtonian corrections to the linear observables and analyse how these corrections change as we vary the size and magnitude of the inhomogeneities. We also explain the role of the linear initial seed as the dominant post-Newtonian contribution and show that the remaining post-Newtonian nonlinear corrections are less than 1%, which is consistent with previous results in the literature.

Streszczenie

Polish translation of the abstract

Wraz z początkiem kosmologii precyzyjnej, przewidywania teoretyczne powinny zbliżać się do podobnego poziomu precyzji jak eksperymenty. W tym kontekście symulacje numeryczne uwzględniające poprawki związane z ogólną teorią względności stanowią najlepszą obecnie metodę opisu formowania struktury. Jednakże, oprócz dokładnego opisu dynamiki, niezbędne jest także równie dokładne wyjaśnienie oddziaływania tych struktur na propagację światła i precyzyjne modelowanie ich wpływu na wielkości mierzalne.

Badanie wszystkich relatywistycznych efektów w najbardziej ogólnym sformułowaniu wymaga jednolitego podejścia do problemu propagacji światła w kosmologii. Można to osiągnąć dzięki nowej interpretacji równania dewiacji geodezyjnych w języku bilokalnych operatorów geodezyjnych (bilocal geodesic operators, BGO). Formalizm BGO jest rozszerzeniem standardowego opisu, wprowadzającym jednolity opis różnych zjawisk optycznych związanych z oddziaływaniem krzywizny czasoprzestrzeni na światło.

W tej rozprawie prezentuję **BiGONLight**, pakiet w języku *Mathematica* implementujący formalizm BGO do badania propagacji światła w numerycznej ogólnej teorii względności. Pakiet implementuje formalizm BGO dla danych w rozkładzie 3+1 jako kolekcję funkcji języka *Mathematica*. Dane wejściowe stanowią metryka czasoprzestrzeni oraz kinematyka obserwatora i źródła, oba w rozkładzie 3+1, które mogą pochodzić bezpośrednio z numerycznej symulacji albo zostać dostarczone bezpośrednio przez użytkownika jako funkcje w jawnej postaci. Dane te służą do śledzenia promieni światła (ray-tracing) i obliczenia bilokalnych operatorów geodezyjnych w najogólniejszy możliwy sposób, bez korzystania z symetrii czasoprzestrzeni lub własności układu współrzędnych. Głównym zadaniem pakietu jest obliczanie obserwablów optycznych w dowolnej czasoprzestrzeni. Formalizm BGO pozwala na wyznaczenie wszystkich obserwablów podczas jednego obliczenia, a język *Wolfram* dostarcza narzędzi numerycznych, dzięki czemu pakiet łatwo nadaje się do zarówno numerycznych, jak i analitycznych badań nad propagacją światła. Pakiet **BiGONLight** został przetestowany przez obliczenie przesunięcia ku czerwieni, odległości kątowej, odległości paralaktycznej i dryfu przesunięcia ku czerwieni w prostych modelach kosmologicznych. Badania przeprowadzamy dla trzech przykładów: dwóch metryk podanych analitycznie, tzn. modelu jednorodnego Λ CDM bez perturbacji i niejednorodnego modelu z klasy Szekeresa, oraz dla symulowanego wszechświata z pyłem w rozkładzie 3+1. Testy pokazały bardzo dobrą zgodność z analitycznymi wzorami.

Dzięki wyżej wymienionym cechom pakiet **BiGONLight** jest dobrym narzędziem do badania wpływu niejednorodności na propagację światła. Zbadaliśmy źródła efektów relatywistycznych w propagacji światła spowodowane przez niejednorodne struktury. Pakiet **BiGONLight** został użyty do obliczenia obserwablów obliczonych w różnych przybliżeniach w niejednorodnym modelu typu plane-parallel. Efekty nieliniowe obliczone zostały jako względne różnice między trzema przybliżeniami: liniowy rachunek perturbacyjnym, przybliżeniem newtonowskim oraz post-newtonowskim. Wielkość niejednorodności można regulować zmieniając wolne parametry modelu, a wpływ tych parametrów na obserwable otrzymany został przez analizę zmian względnych różnic. W ten sposób szacujemy wielkość newtonowskich oraz post-newtonowskich poprawek do liniowego rzędu rachunku zaburzeń i badamy jak zmieniają się one przy zmianie rozmiaru i amplitudy niejednorodności. Wyjaśniamy także rolę początkowej perturbacji metryki przez potencjał skalarny i pokazujemy, że nieliniowe poprawki są mniejsze niż 1%. Wyniki te są zgodne z wcześniejszymi badaniami na ten temat.

Declaration

The work described in this thesis was undertaken between October 2017 and November 2021 while the author was a research student at the Center for Theoretical Physics, Polish Academy of Sciences. The work was done under the scientific supervision of Prof. Mikołaj Korzyński and co-supervised by Dr. Eleonora Villa at Center for Theoretical Physics, Polish Academy of Sciences. Under the same period, the author completed his coursework at the Institute of Physics, Polish Academy of Sciences. No part of this thesis has been submitted for any other degree at the Center for Theoretical Physics, Polish Academy of Sciences or any other university. The abstract is translated into Polish by Prof. Mikołaj Korzyński.

This thesis is based on the original results published in the following articles:

- *Chapter 4: “BiGONLight: light propagation with bilocal operators in Numerical Relativity.”* Authors: Michele Grasso and Eleonora Villa, published in Classical and Quantum Gravity (Class. Quant. Grav.) ([89]).
- *Chapter 5: “Isolating nonlinearities of light propagation in inhomogeneous cosmologies.”* Authors: Michele Grasso, Eleonora Villa, Mikołaj Korzyński, and Sabino Matarrese, published in Physical Review D (Phys. Rev. D) ([90]).

Author’s contributions

The work described in Chapters 4-5 was performed in collaboration with the other co-authors (listed above). The author’s main results are summarised in Sec. 1.1, while a detailed description of the author’s contribution is provided in the introductions of Chapters 4-5.

Other works

Apart from the two original works mentioned above, the author has contributed to the article [88]

- **“Geometric optics in general relativity using bilocal operators.”** Authors: Michele Grasso, Mikołaj Korzyński, and Julius Serbenta, published in Physical Review D (Phys. Rev. D) ([88]).

In the former work, a new formulation for light propagation in geometric optics by means of the bilocal geodesic operators is presented. This novel formulation offers a consistent approach to optical phenomena in curved spacetimes, and it may be used to compute observables like angular diameter distance, luminosity distance, magnification, as well as new real-time observables like parallax and redshift drift, all within the same framework. Although the results in [88] are not included as original work of this thesis, the mathematical machinery of the BGO is presented in Chapter 3 as it provides the theoretical framework on which the results in [89, 90] are based.

Acknowledgements

Searching for the term **P.h.D.**, the Collins dictionary¹ says :

A P.h.D. is a degree awarded to people who have done advanced research into a particular subject. P.h.D. is an abbreviation for “Doctor of Philosophy”.

Similarly, from Oxford dictionary²

P.h.D., noun.

Abbreviation for doctor of philosophy: the highest college or university degree.

These two definitions make it seem like a solo effort, but in reality, I could never have accomplished this journey alone. Therefore, I would like to thank all those who have supported me during these years.

First and foremost, I would like to express my gratitude to my supervisors Prof. Mikołaj Korzyński and Dr. Eleonora Villa, for their helpful advice, unwavering support, and patience throughout my doctoral studies. They introduced me to the broad and complicated world of research with their vast expertise and wealth of experience and inspired me throughout my studies.

I would like to extend my sincere thanks to all other professors of the Center for Theoretical Physics (CFT PAS) for their kind and open-minded attitude and for allowing me to carry out my research in a multidisciplinary and dynamic environment. I would especially like to thank Prof. L. Mankiewicz, Prof. K. Pawłowski, and Prof. M. Bilicki for their help in starting the PhD procedure. I would also like to thank the administrative and secretarial staff of CFT PAS for their unconditional help and endless patience in facilitating the complicated matters of bureaucracy.

At CTP PAS, I also had the opportunity to meet many more friends and colleagues. I am grateful to the other PhD students in room 304A, Julius, Ishika, Grzegorz, and Suhani, for accompanying me during this intense period and rejoicing with me over my achievements. Furthermore, I cannot fail to mention “the boss”, who has been a point of reference for my academic and professional decisions with her sincere and objective advice. *In particular*, thank you for the endless meetings and virtual toasts.

I am immensely grateful to my parents, who have always supported and helped me with every decision I have ever made. Without the support of Orazio and Meletta, as well as Alfredo and Pina, I would never have become who I am today. Thank you for always being there for me. I would also like to thank those who have become a second family to me: without the delightful distractions from my studies provided by my briscola-enthusiasts friends Mario, Lucia, Silvia, Stefano, Valeria, Fabrizio, Paola and Ruggero, I would not have been able to finish this dissertation.

Finally, I would like to express my gratitude to Miriam for her unique understanding (over the past 16 years) and for seeing abilities in me that I did not even know I had. This thesis does not represent the end of an academic path but the beginning of a life together.

¹<https://www.collinsdictionary.com/dictionary/english/phd>

²<https://dictionary.cambridge.org/dictionary/english/phd?q=P.h.D>

CONTENTS

Abstract	i
Streszczenie	ii
Declaration	iii
Acknowledgements	iv
Contents	v
1 Introduction	1
1.1 Main results	2
1.1.1 Structure of the thesis	3
1.2 Conventions and notations	3
2 The standard cosmological model	5
2.1 Cosmological models	6
2.1.1 General relativity	7
2.1.2 The FLRW class of models	8
2.2 The Λ CDM model	11
2.2.1 Early fluctuations and cosmological perturbation theory	13
2.2.2 Analytical approaches to structure formation	15
2.2.3 Inhomogeneous models	17
2.2.4 Numerical simulations	19
2.2.5 Numerical relativity and cosmological observations: the state of the art	22
3 The BGO formalism for light propagation	23
3.1 Light propagation in curved spacetime	23
3.1.1 Geometric description of light beams	27
3.1.2 Properties of the GDE	29
3.2 The bilocal geodesic operators	31
3.2.1 Algebraic properties of the BGO.	35
3.2.2 BGO for light propagation and the quotient space	36
3.2.3 The semi-null frame and the observer's sky	37
3.3 Observables with the BGO: momentary observables and drift effects	41
3.3.1 The redshift	41
3.3.2 The angular diameter distance	42
3.3.3 The luminosity distance	43
3.3.4 The parallax and the parallax distance	43
3.3.5 Position drift	45
3.3.6 The redshift drift formula	47
4 Paper I: “BiGONLight: light propagation with bilocal operators in Numerical Relativity”	51

5	Paper II: “Isolating nonlinearities of light propagation in inhomogeneous cosmologies”	83
6	Summary	107
	List of Figures	111
	Bibliography	113

INTRODUCTION

To answer the most critical questions about the origin, structure, evolution and ultimate destiny of the Universe, cosmologists gather empirical evidence and measurements to create theoretical models that explain real-world observations. The evidence used to formulate the current model of the Universe comes mainly from astronomical observations, namely the observation and analysis of signals emitted from distant sources and propagating at the speed of light. The nature of these light-like signals can vary, and they can reveal a range of information: for example, the electromagnetic signals from a star or galaxy can be analysed to draw conclusions about its physical properties (such as temperature, composition, rotational speed, and relative motion), the distance from us, as well as the characteristics of the space(time) through which the signal has passed. Another notable example is gravitational waves, which are direct evidence of the existence of black holes and provide a new window to peer into regions inaccessible with electromagnetic signals, [1]. Advances in experimental precision or observations of new physical phenomena lead to improvements in the theoretical model that provides a deeper understanding of our Universe.

Today, this constant exchange between theoretical models and observations has led to a scientific revolution, ushering in the era of *precision cosmology*, [99, 103]. The term “precision” refers to the targeted accuracy of 1%, which is aimed at both experimental observations and theoretical predictions: the next generation of galaxy surveys¹ will scan almost the whole extragalactic sky to unprecedented depth and resolution, producing the most detailed map of the Universe ever made. Moreover, this remarkable precision of the experimental data opens up the possibility of measuring small temporal variations in cosmological observables known as *optical drift effects*, [148]. These “real-time” effects have the potential to provide new and crucial insights into the structure and evolution of the Universe, [150, 65, 147, 152, 30]. In terms of theoretical predictions, numerical simulations have made great strides in describing the formation of cosmic structures, ranging from large to small scales and accounting for relativistic effects, [82, 32, 5, 122, 123, 21]. In addition, cosmological simulations are used to study nonlinear relativistic effects in lensing observations, [83, 39, 114], and distance measurements, [7, 3, 121].

In this view, the fundamental problem is to describe how an observer perceives signals emitted by a distant object in any spacetime. The difficulty of such an analysis is that the observed quantities depend on the curvature of spacetime and the motion of the emitter and the observer [152, 110]. This problem is easily overcome in the new formulation of light propagation in geometric optics that we presented in [88]. All possible effects on light distortions caused by the curvature between the observer and the source are encoded in the bilocal geodesic operators, which are the fundamental quantities of our formalism. In

¹See e.g. <https://www.skatelescope.org>, <https://www.euclid-ec.org>, <https://www.lsst.org>, <http://litebird.jp/eng/>, <https://www.jpl.nasa.gov/missions/spherex>.

this way, the effects on the light due to curvature and those caused by the kinematics of the observer and the source can be clearly distinguished, [88]. Once the bilocal geodesic operators are computed, they can be combined with the source and observer motion to obtain all possible optical observables such as magnification, shear, angular distance, and the real-time observables (i.e., parallax, redshift drift and position drift). In this sense, the bilocal geodesic operators formalism provides a unified framework for studying light propagation and the calculation of optical observables, [88, 89].

1.1 Main results

This thesis is devoted to the presentation of **BiGONLight**, Bilocal Geodesic Operators framework for Numerical Light propagation, the **Wolfram** package² I have developed for the study of light propagation in numerical simulations. The original results of this thesis were published in the two peer-reviewed articles [89, 90], and are summarised as follows:

The 3 + 1 bilocal geodesic operators framework: numerically generated spacetimes are evolved in full general-relativistic simulations using the ADM formalism, based on the 3 + 1 splitting of the Einstein equations. To make **BiGONLight** compatible with such computer-generated spacetimes, I have obtained the expressions of the parallel transport equations, the optical tidal matrix, and the geodesic deviation equations for the bilocal operators in 3+1 form. Once the geodesic connecting observer and emitter is found (as shown in [182]), the above equations can be used to perform the parallel transport of a reference frame and obtain the bilocal geodesic operators along that geodesic. The computation is simplified by using the general matrix form of the optical tidal matrix and the bilocal operators projected into the semi-null frame, which I have obtained.

BiGONLight: the 3+1 bilocal geodesic operators framework is encoded in the package as a collection of **Mathematica** functions. These functions take as input the ADM quantities directly from a numerical simulation or provided by the user in analytical components to find the bilocal geodesic operators. The bilocal operators are the starting point to obtain all possible optical observables by combining them with the observer and emitter four-velocities and four-accelerations. The package leaves complete control to the user, who can choose the position of the source and the observer anywhere along the null geodesic with any four-velocities and four-accelerations.

From forward to backwards-integrated bilocal operators: I have used the properties of the geodesic deviation equation to obtain the transformation between forward-integrated and backwards-integrated bilocal geodesic operators. Forward-integrated bilocal geodesics operators can be helpful in cosmological simulations to study the properties of light propagation on-the-fly with the simulation of spacetime. However, observables are obtained using backwards-integrated bilocal geodesic operators since they express observations performed by the observer receiving the light emitted by a source in the past. The explicit transformations between these two methods enlarge the range of applicability of the package.

Tests using three cosmological models: the accuracy of the package is tested by computing redshift, angular diameter distance, parallax distance, and redshift drift in

² <https://github.com/MicGrasso/bigonlight.git>.

well-known cosmological models. Three different kinds of inputs are provided: analytical metric components of a homogeneous Λ CDM model, analytical metric components of the inhomogeneous Szekeres model (as presented in [130, 131]), numerical data of a uniform dust Universe (EdS) evolved with the `Einstein Toolkit` and `FLRWSolver`, [117, 122].

Isolating nonlinear effects of light propagation: we present a detailed analysis of the different ways in which inhomogeneities contribute to nonlinearities in cosmological observables. In this study, I have applied `BiGONLight` to compute observables calculated at different approximations in a plane-parallel inhomogeneous spacetime. The nonlinear effects are evaluated as the fractional difference between observables obtained at the three different approximations linear perturbation theory, Newtonian, and post-Newtonian approximations. The inhomogeneities are tuned by varying the model’s free parameters, and their contributions to the observables are obtained by analysing the variations in the fractional differences.

1.1.1 Structure of the thesis

The outline of the thesis is the following: the basis of modern cosmology and the description of light propagation with the bilocal geodesic operators are described in Chapters 2 and 3, respectively. A detailed presentation of `BiGONLight` and its code tests is given in Chapter 4. Chapter 5 presents the application of the package to study the nonlinear contributions to light propagation in the inhomogeneous plane-symmetric Universe. Finally, the conclusions and a detailed summary of the results of my research are addressed in Chapter 6.

1.2 Conventions and notations

This dissertation is a collection of articles, and every effort has been made to make the notation as consistent and clear as possible. Throughout the text, we assume that the spacetime metric $g_{\mu\nu}$ has signature $(-, +, +, +)$. We also assume the Einstein summation notation $\sum_{\mu} a_{\mu} b^{\mu} \equiv a_{\mu} b^{\mu}$, with the range of the sum depending on the nature of the index μ . Greek indices (α, β, \dots) run from 0 to 3, while Latin indices (i, j, \dots) run from 1 to 3 and refer to spatial coordinates only. Latin indices (A, B, \dots) run from 1 to 2. Tensors and bitensors expressed in a semi-null frame are denoted using boldface indices: Greek boldface indices $(\boldsymbol{\alpha}, \boldsymbol{\beta}, \dots)$ run from 0 to 3, Latin boldface indices $(\mathbf{a}, \mathbf{b}, \dots)$ run from 1 to 3 and capital Latin boldface indices $(\mathbf{A}, \mathbf{B}, \dots)$ run from 1 to 2. Boldface letters $(\mathbf{X}, \mathbf{Y}, \dots)$ are also used for vectors in quotient space \mathcal{P}_p , while objects in \mathcal{Q}_p are denoted using square brackets $([X], [Y], \dots)$. Objects defined in tangent spaces $T_p\mathcal{M}$ are denoted by standard letters. Overdotted quantities denote a derivative with respect to conformal time, i.e. $\dot{A} = \frac{dA}{d\eta}$. Quantities with a subscript 0 are meant to be evaluated at present, whereas the subscript “in” indicates the initial time. Quantities with a subscript \mathcal{S} (or \mathcal{O}) are meant to be evaluated at the source (observer) position. A description on how to set physical units in `BiGONLight` is presented in Chapter 4 (appendix A in [89]).

List of Acronyms		
Acronym	Signification	page
ADM	Arnowitt-Deser-Misner formalism	19
BGO	bilocal geodesic operators	33
CMB	cosmic microwave background	5
EdS	Einstein-de Sitter	11
EOS	equation of state	9
FLA	flat lightcone approximation	31
FLRW	Friedmann-Lemaître-Robertson-Walker	9
GDE	geodesic deviation equation	29
GR	general relativity	7
h.o.t.	higher-order term	25
Λ CDM	Λ -cold dark matter	11
Lin	first-order in perturbation theory	13
LSS	large-scale structure	5
LTB	Lemaître-Tolman-Bondi	17
ODE	ordinary differential equations	33
PN	post-Newtonian approximation	15
PT	cosmological perturbation theory	13
SNF	semi-null frame	37
SnIa	type Ia supernovæcandels	5

THE STANDARD COSMOLOGICAL MODEL

The increasing amount of data collected by experimental probes like SDSS, Planck, LSST, SKA and others¹ have produced a generally coherent picture of our Universe. The general purpose of these experiments is to investigate the three main pieces of evidence in cosmology:

- the *cosmic microwave background* (CMB): the CMB is the electromagnetic radiation that pervades the Universe as homogeneous and isotropic background noise. It was discovered by A. Penzias and R. Wilson in 1965 [138], when they observed a thermal black body spectrum with a temperature of 3.5 K across the entire sky. Successive measurements [168, 107, 10, 11, 9] have revealed further details in the CMB structure, showing small fluctuations of $\Delta T/T \sim 10^{-5}$ around the average temperature of 2.7 K. Accurate mapping of the small anisotropies in the temperature of the CMB is of fundamental importance to cosmology, as it provides a clue to the structure of the Universe at very early times, see Fig. 2.1a.
- the *large-scale structure* (LSS): observations in different wavelength ranges of electromagnetic radiation have revealed a hierarchical organisation of astrophysical objects: massive objects tend to form gravitationally bound structures such as galaxies and galaxy clusters, which organise themselves on cosmological scales into superclusters, filaments, and voids, forming the so-called *cosmic web* [50]. Increasingly better galaxy surveys, like [188, 61, 127, 184, 29], have measured the distance and shape of cosmological structures with great precision and produced an accurate three-dimensional map of the LSS of the Universe, see Fig. 2.1b. Furthermore, since these cosmological structures observed today are the result of the evolution of the tiny CMB anisotropies under the influence of gravity, we expect to find features of the CMB radiation anisotropy in the observed LSS.
- the *type Ia supernovæ* (SnIa): the distance-redshift relation is one of the landmarks of modern cosmology. It is also known as “Hubble law” and was first derived by G. Lemaître in 1927, [112], as a linear relation between the distance of a galaxy D and its recession velocity v ($v = cz$ for small redshifts $z < 1$), i.e. $z = \frac{H_0}{c}D$. The same relation was measured by E. Hubble in 1929, [100], finding a value of the constant of proportionality $H_0 = 500$ km/s/Mpc. This is considered the first evidence for the expansion of the Universe². An accurate measurement of H_0 requires a precise estimate of the redshift and the distance of the source: the redshift is obtained directly

¹<https://www.sdss.org>, <https://www.cosmos.esa.int/web/planck>, <https://www.lsst.org>,
<http://skatelescope.org/>

²This relationship is universal and does not depend on the location of observation. So if we make the same measurement from another galaxy, we get the same relation with the same constant H_0 . From this, we can conclude that the Universe is expanding isotropically at the expansion rate H_0 .

from spectroscopic analysis, while the distance is derived using indirect methods, such as geometrical relations and/or physical properties of astronomical candles. Precise measurements of the distance-redshift relation in cosmology are performed using SnIa standard candles³, see Fig. 2.1c, which led not only to a better estimate of the present-day expansion rate $H_0 = 73.48 \pm 1.66$ km/s/Mpc [154], but also to the first confirmation of the accelerated expansion of the Universe, [155, 141].

This chapter describes the basics of modern cosmology and how the information obtained from the CMB, LSS, and SnIa observations are merged to produce a theoretical model of the Universe.

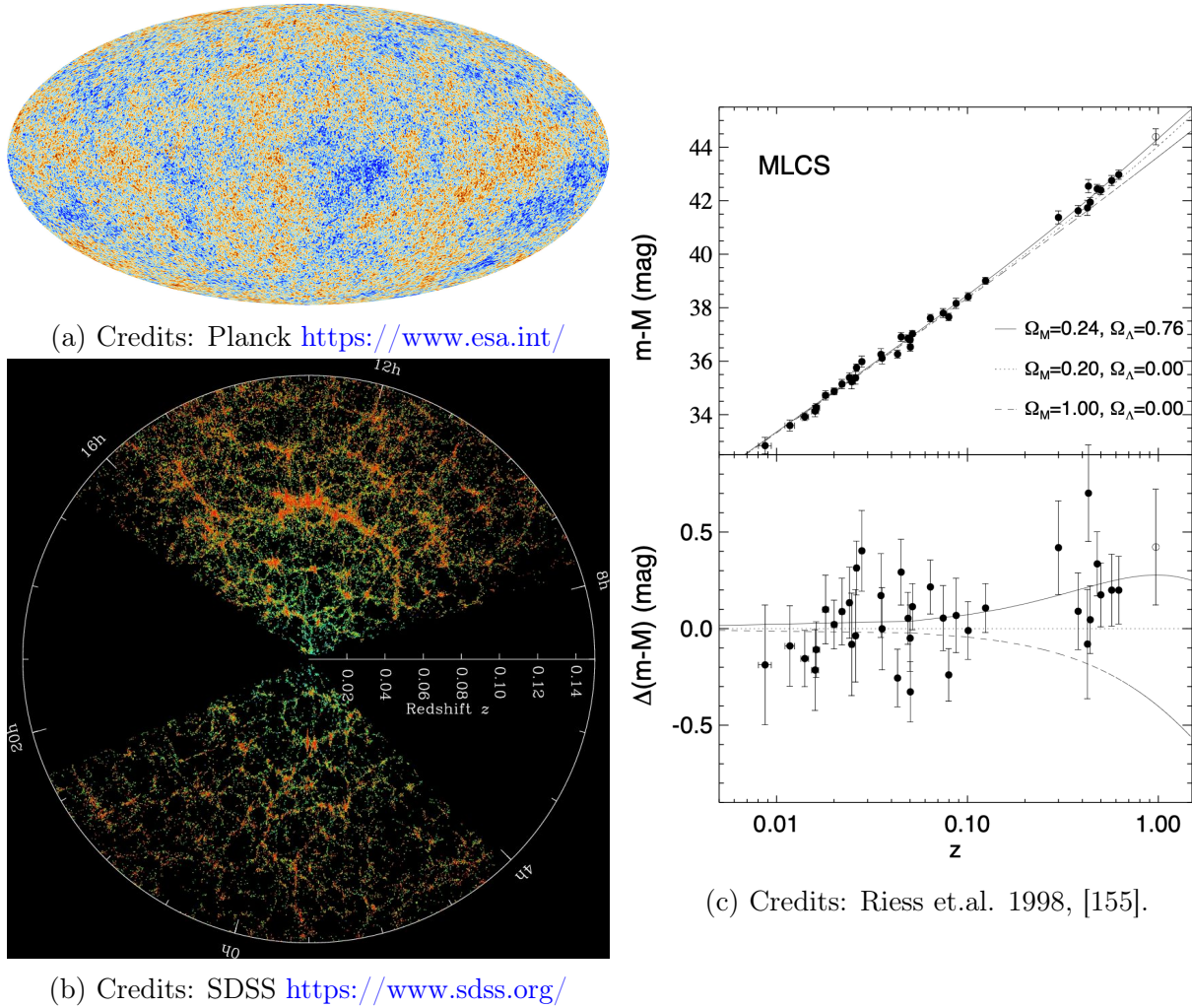


Figure 2.1: Precise measurements of the CMB (Fig. 2.1a), the LSS (Fig. 2.1b), and the SnIa (Fig. 2.1c) have been used to constraint the standard model for cosmology.

2.1 Cosmological models

As noted above, observations on cosmological scales suggest that the gravitational attraction of the primordial anisotropies observed in the CMB shaped the Universe's large-scale

³Standard candles are astronomical objects whose absolute luminosity L is known, so their distance is determined by measuring the luminosity flux at the observer F and using the relation $D = \sqrt{\frac{L}{4\pi F}}$ (see Eq.(3.93)). SnIa are explosions of white dwarf stars characterised by a precise relation between the brightness and the timescale of the explosion.

structure. In general, gravity is the dominant interaction responsible for the formation of structures at all scales (from planets to the LSS), and it represents the fundamental mechanism underlying the formation and evolution of the Universe. Therefore, a model of the Universe must be consistent with the laws of gravity.

2.1.1 General relativity

From a theoretical point of view, the gravitational interaction at the macroscopic level⁴ is described by *general relativity* (GR), which was proposed by A. Einstein in 1915, [72]. The primary distinction between general relativity and Newtonian gravity is Einstein's interpretation of gravity as a geometric property of spacetime. This interpretation was supported by the *equivalence principle*, which states that gravitational acceleration is the same as the acceleration of an inertially moving body and by the fact that there can be no absolute concept of inertia, but only the inertia of masses relative to each other. In this perspective, Einstein assumes that free particles move along geodesics in a four-dimensional Riemannian manifold \mathcal{M} whose points represent physical locations in space and time. Locally, we can specify a reference frame and label the point in \mathcal{M} by a coordinate system $\{x^\mu\}$. However, the coordinate system $\{x^\mu\}$ is not uniquely defined since the laws of physics must be independent with respect to this choice. To manifest this "gauge invariance", general relativity is formulated using the invariant structures of tensors. Indeed, at each point x of the manifold \mathcal{M} , we can introduce a tangent space⁵ $T_x\mathcal{M}$ and the cotangent space $T_x^*\mathcal{M}$, being the dual space to $T_x\mathcal{M}$, and define the type (r, s) tensor \mathbf{T} as the multilinear map

$$\mathbf{T} : \underbrace{T_x^*\mathcal{M} \times \cdots \times T_x^*\mathcal{M}}_r \times \underbrace{T_x\mathcal{M} \times \cdots \times T_x\mathcal{M}}_s \rightarrow \mathbb{R}.$$

Although this invariant coordinate formulation fits well the purposes of general relativity, for practical calculations it is better to express tensors by their components: a type (r, s) tensor may be written as

$$\mathbf{T} = T^{\mu_1 \cdots \mu_r}_{\nu_1 \cdots \nu_s} \frac{\partial}{\partial x^{\mu_1}} \otimes \cdots \otimes \frac{\partial}{\partial x^{\mu_r}} \otimes dx^{\nu_1} \otimes \cdots \otimes dx^{\nu_s} \quad (2.1)$$

where $\frac{\partial}{\partial x^{\mu_i}}$ is a basis for the i -th tangent space, with $i = 1, 2, \dots, r$, and dx^{ν_j} a basis for the j -th cotangent space, with $j = 1, 2, \dots, s$. In other words, the type (r, s) tensor \mathbf{T} associates r vectors $\frac{\partial}{\partial x^{\mu_1}}, \dots, \frac{\partial}{\partial x^{\mu_r}}$ and s covectors $dx^{\nu_1}, \dots, dx^{\nu_s}$ to a scalar $T^{\mu_1 \cdots \mu_r}_{\nu_1 \cdots \nu_s}$. It is indeed evident that the tensor components $T^{\mu_1 \cdots \mu_r}_{\nu_1 \cdots \nu_s}$ depend on the choice of coordinates, although the tensor itself \mathbf{T} is independent. This freedom in the choice of coordinate system can be used to simplify the computation of the tensor components.

The geometry of Riemannian spacetime is encoded in the metric tensor $g_{\mu\nu}$, which is the core object of general relativity. Indeed, the metric is used to define coordinate invariants, such as the squared line element $ds^2 = g_{\mu\nu}dx^\mu dx^\nu$, which expresses the measure of the proper distance between two arbitrarily close events in spacetime x^μ and $x^\mu + dx^\mu$. Moreover, the metric tensor is used to introduce essential structures like the *covariant derivative* (or connection) ∇ , which is the covariant generalization of the partial derivative that allows to

⁴Gravity is the weakest of the four fundamental interactions of nature and has a negligible influence on the behaviour of subatomic particles. However, there are events in the cosmos that involve strong gravitational effects at the quantum scale that can only be described by a theory of quantum gravity.

⁵Defined as the real vector space that intuitively contains all the possible directions in which one can tangentially pass through x .

derive and transport tensors along the manifold. The action of the covariant derivative ∇_σ on a type (r, s) tensor is expressed as

$$\nabla_\sigma T^{\mu_1 \dots \mu_r}_{\nu_1 \dots \nu_s} = \partial_\sigma T^{\mu_1 \dots \mu_r}_{\nu_1 \dots \nu_s} + \sum_i \Gamma_{\sigma\lambda}^{\mu_i} T^{\mu_1 \dots \lambda \dots \mu_r}_{\nu_1 \dots \nu_s} - \sum_j \Gamma_{\sigma\nu_j}^\lambda T^{\mu_1 \dots \mu_r}_{\nu_1 \dots \lambda \dots \nu_s}, \quad (2.2)$$

with $\partial_\mu = \frac{\partial}{\partial x^\mu}$, and Γ being the *Christoffel symbols* expressing the difference between the covariant and the partial derivative⁶ in terms of metric tensor derivatives

$$\Gamma_{\mu\nu}^\rho = \frac{1}{2} g^{\rho\lambda} (\partial_\mu g_{\lambda\nu} + \partial_\nu g_{\mu\lambda} - \partial_\lambda g_{\mu\nu}). \quad (2.3)$$

One application of the covariant derivative is the *directional derivative* $t^\sigma \nabla_\sigma v^\mu$, namely the derivative of a vector field v^μ in the direction of a given vector t^μ . If t^μ is the tangent vector to the curve C in the manifold and $t^\sigma \nabla_\sigma v^\mu = 0$ along all points of the curve, we say that the vector v^μ is *parallel transported along C* . In the special case where the tangent vector t^μ is parallel transported along itself $t^\sigma \nabla_\sigma t^\mu = 0$, we call the curve C a *geodesic*, which in general relativity represents the trajectory of a free particle. In special relativity, the trajectories of free particles are straight lines, but in general relativity, the structure of spacetime is curved by the presence of matter, and this “bends” the particle’s trajectories.

The equations which make it possible to derive the metric tensor associated with a given distribution of matter are the Einstein’s field equations

$$G_{\mu\nu} \equiv R_{\mu\nu} - \frac{1}{2} R g_{\mu\nu} = \frac{8\pi G}{c^4} T_{\mu\nu}, \quad (2.4)$$

where $G_{\mu\nu}$ is the Einstein tensor representing the curvature of the spacetime, $T_{\mu\nu}$ is the stress-energy tensor representing the energy and momentum of matter and radiation, while G and c are the gravitational constant and the speed of light, respectively. The two quantities $R_{\mu\nu} \equiv R^\sigma_{\mu\sigma\nu}$ and $R \equiv g^{\mu\nu} R_{\mu\nu}$ are the Ricci tensor and the Ricci scalar, and they are directly defined from the Riemann tensor

$$R^\rho_{\mu\sigma\nu} = \partial_\sigma \Gamma_{\mu\nu}^\rho - \partial_\nu \Gamma_{\mu\sigma}^\rho + \Gamma_{\lambda\sigma}^\rho \Gamma_{\mu\nu}^\lambda - \Gamma_{\lambda\nu}^\rho \Gamma_{\mu\sigma}^\lambda. \quad (2.5)$$

2.1.2 The FLRW class of models

A valid cosmological model must be based on general relativity, and its spacetime must satisfy the Einstein equations (2.4). Thus, it is a matter of finding the correct stress-energy tensor to describe the correct distribution of energy and momentum in the Universe. According to cosmological observations, the Universe seems to be filled with an isotropic and homogeneous mass distribution on large scales, which can be represented as a perfect fluid characterised by an average energy density $\bar{\rho}$ and isotropic pressure p . The expression for stress-energy tensor of this cosmic fluid is written as

$$T^{\mu\nu} = \left(\bar{\rho} + \frac{p}{c^2} \right) u^\mu u^\nu + p g^{\mu\nu}, \quad (2.6)$$

with $u^\mu = g^{\mu\nu} u_\nu$ the four-velocity vector field of the fluid. In addition, the tensor $T_{\mu\nu}$ satisfies the following conservation rules

$$\nabla_\mu T^{\mu\nu} \equiv \partial_\mu T^{\mu\nu} + \Gamma_{\mu\lambda}^\mu T^{\lambda\nu} + \Gamma_{\mu\lambda}^\nu T^{\mu\lambda} = 0, \quad (2.7)$$

⁶It worth mentioning that Γ are not tensor quantities since they do not transform as tensor. However, the difference $C^\rho_{\mu\nu} = \Gamma_{\mu\nu}^\rho - \Gamma_{\nu\mu}^\rho$ defines a tensor expressing the torsion of the spacetime. In general relativity we assume that the spacetime is torsion-less, implying that $\Gamma_{\mu\nu}^\rho$ are symmetric in the lower indices.

whose components are the continuity equation for the energy density $\bar{\rho}$ and the Euler equation for the fluid.

Under the same assumptions of isotropy and homogeneity, we may derive the following form of the metric⁷

$$ds^2 = -c^2 dt^2 + a(t)^2 \left[\frac{dr^2}{1 - kr^2} + r^2 d\theta^2 + r^2 \sin(\theta)^2 d\phi^2 \right], \quad (2.8)$$

where (t, r, θ, ϕ) are coordinates, $a(t)$ is the scale factor, and k is a constant expressing the spatial curvature: usually the coordinates are rescaled such that k is set to -1 , 1 , or 0 for space of constant negative, positive, or null spatial curvature, respectively. The metric in Eq. (2.8) is the *Friedmann-Lemaître-Robertson-Walker* metric (FLRW) and it represents a class of cosmological models with the dynamics determined by the scale factor $a(t)$. The time coordinate t is known as the *cosmic time*, and it is the proper time measured in a comoving frame with the observer, i.e. the frame in which the observer's position remains unchanged $(r, \theta, \phi) = \text{const.}$ In this frame the four-velocity of a fluid element is simply $u^\mu = (1, 0, 0, 0)$ and the stress-energy conservation, Eq. (2.7), for the FLRW metric simply reduces to

$$\frac{d}{dt}(\bar{\rho}a^3) = -\frac{p}{c^2} \frac{d}{dt}(a^3). \quad (2.9)$$

This formula expresses the mass-energy conservation, relating the change of the energy density in a element volume $\frac{d}{dt}(\bar{\rho}a^3)$ to the pressure acting on that volume $p \frac{d}{dt}(a^3)$. In cosmology Eq. (2.9) is usually written as

$$\frac{d \log(\bar{\rho})}{dt} = -3(1 + w) \frac{d \log(a)}{dt}, \quad (2.10)$$

with $w = p/(c^2\bar{\rho})$. If w is time independent, Eq. (2.10) has solution

$$\bar{\rho} = \bar{\rho}_0 \left(\frac{a_0}{a} \right)^{3(1+w)}, \quad (2.11)$$

with $\bar{\rho}(t_0) = \bar{\rho}_0$ and $a(t_0) = a_0$ the mass-energy density and the scale factor at present time t_0 , respectively. The quantity $w = p/(c^2\bar{\rho})$ gives the *equation of state* (EOS) of the cosmic fluid, where some notable examples are:

- $w = 1/3$ for radiation, which gives $\bar{\rho}_r \propto a^{-4}$;
- $w = 0$ for (pressureless) matter, which gives $\bar{\rho}_m \propto a^{-3}$;
- $w = -1$ for vacuum (dark) energy, which gives $\bar{\rho}_\Lambda = \text{const.}$

From this we can conclude that the mass-energy density is the sum of different species $\bar{\rho}(t) = \sum_x \bar{\rho}_x(t)$ and each species scales as a different power of the scale factor according to its EOS w_x . In cosmology, it is usually assumed that the only species contributing to the mass-energy density are baryonic matter $\bar{\rho}_b$, dark matter $\bar{\rho}_m$, radiation $\bar{\rho}_r$, and dark energy $\bar{\rho}_\Lambda = \frac{\Lambda c^2}{8\pi G}$, i.e. $\bar{\rho} = \bar{\rho}_b + \bar{\rho}_m + \bar{\rho}_r + \bar{\rho}_\Lambda$. Similarly, the species contributing to the cosmic pressure are the radiation pressure p_r and the dark energy pressure $p_\Lambda = -\frac{\Lambda c^4}{8\pi G}$, since the (baryonic and dark) matter have vanishing⁸ pressure $w = 0$. More often we refer

⁷It is customary to express the metric components by specifying the line element.

⁸The baryonic and dark particles are non-relativistic and therefore their energy density is much larger than their pressure.

to “dust”, or simply matter, to indicate both baryonic and dark matter components as the part of the perfect fluid that has positive mass density and vanishing pressure. By defining the *Hubble parameter* (also known as expansion rate) $H = \frac{1}{a} \frac{da}{dt}$ and the *critical density* as $\rho_c(t) = \frac{3H(t)^2}{8\pi G}$, we express the mass-energy density by the dimensionless *density parameter* $\Omega(t) = \frac{\bar{\rho}(t)}{\rho_c(t)}$. This is particularly convenient in cosmology, since using Eq. (2.11) one can write the density parameter of each species $\Omega_x(t)$ in terms of its value at the present time, $\Omega_x(t_0) = \Omega_{x_0}$, i.e.

$$\Omega_x = \frac{8\pi G}{3H_0^2} \bar{\rho}_x = \Omega_{x_0} \left(\frac{a_0}{a} \right)^{3(1+w_x)}, \quad (2.12)$$

and thus clearly separate the contributions of the different species at present time in the density parameter $\Omega(t)$ as

$$\Omega(t) = (\Omega_{b_0} + \Omega_{m_0}) \left(\frac{a_0}{a(t)} \right)^3 + \Omega_{r_0} \left(\frac{a_0}{a(t)} \right)^4 + \Omega_{\Lambda_0}. \quad (2.13)$$

The Einstein field equations in Eq. (2.4) for the FLRW metric give the *Friedmann equations*

$$\frac{1}{a^2} \left(\frac{da}{dt} \right)^2 = \frac{8\pi G}{3} \bar{\rho} - \frac{kc^2}{a^2} \quad (2.14)$$

$$\frac{1}{a} \frac{d^2a}{dt^2} = -\frac{4\pi G}{3} \left(\bar{\rho} + \frac{3p}{c^2} \right). \quad (2.15)$$

The first Friedmann equation, Eq. (2.14), expressed in terms of the density parameter Eq. (2.13) reads

$$H(t)^2 = H_0^2 \left[\Omega_{r_0} \left(\frac{a_0}{a(t)} \right)^4 + (\Omega_{b_0} + \Omega_{m_0}) \left(\frac{a_0}{a(t)} \right)^3 + \Omega_{k_0} \left(\frac{a_0}{a(t)} \right)^2 + \Omega_{\Lambda_0} \right], \quad (2.16)$$

with $\Omega_{k_0} = -\frac{kc^2}{H_0^2 a_0^2}$. Similarly, the second Friedmann equation, Eq. (2.15), in terms of density parameters reads

$$q \equiv -\frac{\frac{dH}{dt} + H^2}{H^2} = \frac{1}{2} \sum_x (1 + 3w_x) \Omega_x, \quad (2.17)$$

where q is the *deceleration parameter*, and we remind that $\Omega_x(t) = \frac{8\pi G}{3H(t)^2} \bar{\rho}_x(t)$ and w_x are the density parameter and the EOS parameter for the x^{th} specie at time t , respectively.

The peculiarity of the FLRW models is that they predict the beginning of the Universe from a singularity point at $t = 0$, i.e. $a(0) = 0$: this is known as *Big Bang* and corresponds to the origin of the Universe (13.8 billion years, according to the standard cosmological model, [74, 10]) from extreme conditions of density, pressure, and temperature. From this extreme initial state, the Universe began its adiabatic expansion, becoming less dense and colder, allowing the formation of all elementary particles and gradually, electrons, photons, and baryons. One of the strongest evidence in favour of the Big Bang theory is the CMB, corresponding to the radiation relict formed 379000 years after the Big Bang in the *recombination epoch*, [74]. Before that time, the Universe was indeed a plasma of electrons, protons, and nuclei, in which the photons were constantly scattered. Due to cosmic expansion, conditions

in the era of recombination became favourable for the formation of atoms (mainly hydrogen and helium) until the photons decoupled from matter and began to move freely through the expanding Universe: this is observed today as the CMB thermal radiation. Thus, on the one hand, the CMB is an excellent source of information, as it provides a “snapshot” of the Universe as it was 379000 years after the Big Bang, but on the other hand, it also constitutes a limit to cosmological observations with electromagnetic radiation.

Some notable examples from the class of FLRW models are the *de Sitter* and *Einstein-de Sitter* (EdS) models, each representing a (spatially flat) Universe containing only dark energy and only dark matter, respectively. The de Sitter model represents an empty Universe (without matter) containing only dark energy, which determines the expansion rate $H \propto \sqrt{\Lambda}$. It is characterised by an exponentially growing scale factor $a(t) = e^{Ht}$, which causes an accelerated expansion of the de Sitter Universe. Since no other mechanism opposes the accelerated expansion, at a certain point, any observer in a de Sitter Universe will start experiencing event horizons, beyond which it is impossible to see or perceive anything. In contrast, the Einstein-de Sitter model represents a Universe containing only dust (pressureless matter) with a density of $\bar{\rho}_m \propto H^2$. In this model, the distance between two comoving observers increases with $t^{2/3}$, but this expansion is balanced by gravitational attraction so that it tends asymptotically to zero as time approaches infinity. Although these models do not explain current observations, they can be considered reasonable approximations for past epochs of the Universe, [74]. Using Friedmann equation Eq. (2.16), we can distinguish the following epochs: at very early times, i.e. $a(t)$ small, the Universe was dominated by radiation, since $H^2 \sim H_0^2 \Omega_{r_0} a^{-4}$. After that, followed a matter-dominated era (for a spatially flat Universe), with $H^2 \sim H_0^2 \Omega_{m_0} a^{-3}$, which lasted until dark energy took over, leading to an accelerated expansion of the Universe, $q = \Omega_{m_0}/2 - \Omega_{\Lambda_0} < 0$.

2.2 The Λ CDM model

The Friedmann equations Eqs. (2.16)-(2.17), together with the EOS and Eq. (2.10), completely define the dynamics and composition of the cosmological model. Therefore, to build a complete picture of the cosmological model that best fits our Universe, one must measure the values of the cosmological parameters H_0 , Ω_{r_0} , Ω_{b_0} , Ω_{m_0} , Ω_{k_0} , and Ω_{Λ_0} from the observations, and determine the dynamics by solving the Friedmann equations. The first important constraint on the total energy-density of the Universe is provided by the Friedmann equation Eq. (2.16) evaluated at present time, i.e.

$$\Omega_{r_0} + \Omega_{b_0} + \Omega_{m_0} + \Omega_{k_0} + \Omega_{\Lambda_0} = 1. \quad (2.18)$$

Several cosmological parameters can be measured within the same observation, and the specific observation can constrain each parameter differently: their values are obtained by best-fitting the different measurements of the cosmological parameters by the CMB, SnIa, and LSS. The latest results, published in 2018 by the Planck Collaboration [10], depict a cosmological model consistent with a spatially flat Universe $\Omega_{k_0} = 0.001 \pm 0.002$, and dominated by the dark sector, i.e. dark matter $\Omega_{m_0} = 0.315 \pm 0.007$ and dark energy $\Omega_{\Lambda} = 0.685 \pm 0.0073$. The baryonic matter represents only few percent of all the energy content of the Universe, i.e. $\Omega_{b_0} = 0.022 \pm 0.0001$, while the radiation component (intended as photons and massless neutrinos) have a negligible effect at present time $\Omega_{r_0} \sim 10^{-5}$. The value of the Hubble constant⁹ is $H_0 = 67.4 \pm 0.5$ km/s/Mpc. This parametrization defines the standard cosmological model, also dubbed as the Λ CDM model.

⁹This value of H_0 is in 3.7σ tension with the local measurement of H_0 from SnIa, $H_0 = 73.48 \pm 1.66$ km/s/Mpc [154].

The dynamics of the Λ CDM model is prescribed by the Friedmann equations Eqs. (2.16)-(2.17), with $\Omega_{\text{m}_0} + \Omega_{\Lambda} = 1$ (here Ω_{m_0} considers both baryonic and dark matter), and completely encoded in the scale factor. Before proceeding to find the expression for the scale factor, let us make some considerations about the coordinates. The FLRW line element, Eq. (2.8), for the Λ CDM model simplifies to

$$ds^2 = -c^2 dt^2 + a(t)^2 \delta_{ij} dq^i dq^j, \quad (2.19)$$

where q^i are the spatial coordinates in flat space. As for time, we prefer to use the *conformal time* η coordinate, which is related to the cosmic time t as $dt = a(\eta)d\eta$. The advantage is that in conformal time the metric further reduces to

$$ds^2 = a(\eta)^2 (-c^2 d\eta^2 + \delta_{ij} dq^i dq^j), \quad (2.20)$$

simplifying also the calculations. Moreover, the conformal time has the clear physical meaning of particle horizon $c\eta$, i.e. the maximum distance ideally travelled by a photon since the beginning of the Universe, [68, 74]. In conformal time $dt = a(\eta)d\eta$, the Hubble parameter transforms as

$$H(t) = \frac{\mathcal{H}(\eta)}{a(\eta)}, \quad (2.21)$$

where we have defined the conformal Hubble parameter $\mathcal{H}(\eta) = \frac{1}{a(\eta)} \frac{da(\eta)}{d\eta}$. The Friedmann equations (2.16)-(2.17) for Λ CDM in conformal time reads

$$\mathcal{H}^2 = \mathcal{H}_0^2 \left[\frac{\Omega_{\text{m}_0}}{a} + \Omega_{\Lambda_0} a^2 \right] \quad (2.22)$$

$$\dot{\mathcal{H}} = \mathcal{H}^2 - \frac{3}{2} \frac{\mathcal{H}_0^2 \Omega_{\text{m}_0}}{a}, \quad (2.23)$$

where dotted quantities indicates derivative with respect to conformal time, i.e. $\dot{\mathcal{H}} = \frac{d\mathcal{H}}{d\eta}$, and we have used the standard convention of setting the scale factor today to unit $a_0 = 1$. The expression for the density parameters in conformal time [181] is

$$\Omega_{\text{m}} = \frac{8\pi G a^2}{3\mathcal{H}^2} \bar{\rho}_{\text{m}} = \frac{\mathcal{H}_0^2 \Omega_{\text{m}_0}}{a\mathcal{H}^2} \quad (2.24)$$

$$\Omega_{\Lambda} = \frac{a^2 c^2 \Lambda}{3\mathcal{H}^2} = \frac{a^2 \mathcal{H}_0^2 \Omega_{\Lambda_0}}{\mathcal{H}^2}. \quad (2.25)$$

The scale factor for the Λ CDM model can be explicitly found (using the results in [87]) by solving Eq. (2.22)

$$a(\eta) = \frac{\sqrt[3]{\frac{\Omega_{\text{m}_0}}{\Omega_{\Lambda}}}}{(\sqrt{3}-1) + (\sqrt{3}+1)\text{cn}(y|r)}, \quad (2.26)$$

where $\text{cn}(y|r)$ is the Jacobi elliptic cosine function, with $y = (\sqrt[4]{3}\sqrt[6]{\Omega_{\Lambda}}\sqrt[3]{\Omega_{\text{m}_0}}) \mathcal{H}_0 \eta$, and $r = \sqrt{\frac{\sqrt{3}+2}{4}}$.

The Λ CDM model presented so far is based on the fundamental assumptions of homogeneity and isotropy of the Universe. However, as has been noted several times, these properties are only satisfied on average and on very large scales, with the transition from clustered structures to a homogeneous distribution beginning on scales¹⁰ of ~ 100 Mpc, [187, 162, 55]. So, while the Λ CDM model describes the overall dynamics of the Universe, we still need to account for the evolution of structures such as galaxies and galaxy clusters that are visible on smaller scales.

¹⁰This scale is also known as *End of Greatness*.

2.2.1 Early fluctuations and cosmological perturbation theory

The features of the CMB map have been thoroughly examined, revealing that in the first moments after the Big Bang, small temperature variations were generated by quantum fluctuations on microscopic scales generating the seeds for galaxies and clusters, [168, 107, 9]. Thanks to the inflationary paradigm¹¹, [177], the early evolution of perturbations is well described on cosmological scales by relativistic *perturbation theory* (PT), [106]. Indeed, the small primordial fluctuations can be conceived as tiny perturbations $\delta\rho$ over a homogeneous and isotropic density distribution $\bar{\rho}$, so that the real mass-energy density is expanded as $\rho = \bar{\rho} + \delta\rho$ up to linear order. Similarly, the real spacetime is modelled by a perturbed metric $g_{\mu\nu} = \bar{g}_{\mu\nu} + \delta g_{\mu\nu}$, where $\bar{g}_{\mu\nu}$ is the background metric and $\delta g_{\mu\nu}$ is the small linear perturbation. It is important to note that $\delta g_{\mu\nu}$ is not uniquely defined due to coordinate gauge freedom: the same physical perturbation can be described by a different tensor perturbation

$$\widetilde{\delta g_{\mu\nu}} = \delta g_{\mu\nu} + \mathcal{L}_\xi \bar{g}_{\mu\nu}, \quad (2.27)$$

see e.g. [185]. The term $\mathcal{L}_\xi \bar{g}_{\mu\nu} \equiv \xi^\sigma \partial_\sigma \bar{g}_{\mu\nu} + \bar{g}_{\mu\nu} \partial_\mu \xi^\sigma + \bar{g}_{\mu\nu} \partial_\nu \xi^\sigma$ is the Lie derivative and it represents the action on $\bar{g}_{\mu\nu}$ of an ‘‘infinitesimal diffeomorphism’’ generated by the vector field ξ^μ (see e.g. App. C in [185]). In other words, the form of the perturbed metric $g_{\mu\nu}$ depends¹² on the specific choice of the gauge, and the first-order transformation between two different gauge choices is given by Eq. (2.27) (see [181] for gauge transformations of 3 different gauges up to second-order PT).

Considering linear perturbations (Lin) over the flat FLRW background Eq. (2.20), the most general form of the spacetime metric is [181]

$$\begin{aligned} g_{00} &= -a^2(1 + 2\Psi) \\ g_{0i} &= a^2(\partial_i B + \omega_i) \\ g_{ij} &= a^2\{(1 - 2\Phi)\delta_{ij} + 2D_{ij}E + \partial_{(i}F_{j)} + \chi_{ij}\}, \end{aligned} \quad (2.28)$$

where Ψ , Φ , B , E are the scalar modes, ω_i , F_i are the transverse vector modes ($\partial^i \omega_i = \partial^i F_i = 0$), and χ_{ij} is the transverse and tracefree tensor mode ($\partial^i \chi_{ij} = \chi^i_i = 0$). The operator $D_{ij} = \partial_i \partial_j - 1/3 \delta_{ij} \nabla^2$ is the traceless symmetric double gradient operator, see e.g. [38]. The expressions in Eq. (2.28) define the *scalar-vector-tensor decomposition* of the metric tensor [106, 19]. Usually, in the study of structure formation, the linear vector and tensor modes can be neglected, i.e. $\omega_i \sim F_i \sim \chi_{ij} \sim 0$ [125, 24], simplifying the expression of Einstein equations. The reason is that linear vector modes are decaying in time and linear tensor modes, i.e. primordial gravitational waves, are decoupled from the other perturbation modes. Each gauge corresponds to a specific choice of Ψ , Φ , B , E :

- the *Lagrangian frame* (or *synchronous-comoving gauge*) is defined by choosing $B = \Psi = 0$ and corresponds, in analogy with fluid dynamics, to the reference frame associated with the coordinates comoving with the cosmic flow. In this reference frame, the positions of the fluid particles do not evolve in time, see Fig. 2.2.
- *Eulerian gauges* are all gauges identified by the (spatial) choice $E = 0$. They correspond to a frame associated with the observer measuring the matter stream, i.e. not comoving with the cosmic flow. The expression of B fully specifies the gauge. For example, a common choice in PT is the *Poisson gauge* identified by $B = 0$, [38]. With

¹¹*Inflation* is an epoch of accelerated expansion in the early Universe, and it was introduced to explain the coherence of CMB anisotropies on angular scales larger than the apparent cosmological horizon at recombination.

¹²For a different approach see [19, 106].

this coordinate choice, the positions of the particle of the fluid evolve from their initial positions, see again Fig. 2.2.

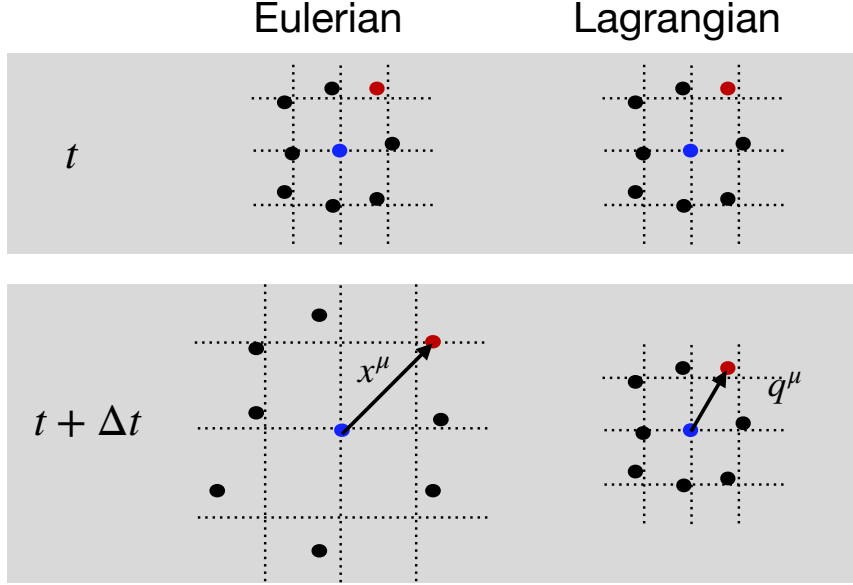


Figure 2.2: Illustration of the evolution of a group of particles in an expanding Universe in the Eulerian (left) and Lagrangian (right) frames. At the initial time t , the particles have a certain position with respect to the uniform grid. Due to the expansion and the gravitational interaction, at a later time $t + \Delta t$ the particles are in a different position with respect to the grid in the Eulerian frame (left), with the new position being marked by the vector x^μ . In the Lagrangian frame (right), on the other hand, the positions of the particles q^μ do not change with time.

The form of the first-order line element in the Poisson gauge considering scalar perturbations only is [181]

$$ds^2 = a(\eta)^2 \left[- \left(1 + 2 \frac{\Psi(\eta, q^i)}{c^2} \right) c^2 d\eta^2 + \left(1 - 2 \frac{\Phi(\eta, q^i)}{c^2} \right) \delta_{ij} dq^i dq^j \right], \quad (2.29)$$

where the perturbations $\Psi(\eta, q^i)$ and $\Phi(\eta, q^i)$ are obtained by solving¹³ the Einstein equations, Eq. (2.4), expanded up to linear order, see [38]. Let us start by noting that $\Psi = \Phi = \phi$, as it follows from the trace-free part of the (i, j) components. At first order, the $(0, 0)$ component returns the Poisson equation

$$\nabla^2 \phi(\eta, q^i) - \frac{3}{2} \frac{\mathcal{H}_0^2 \Omega_{m0}}{a} \delta_{\text{Lin}}(\eta, q^i) = 0, \quad (2.30)$$

with $\delta_{\text{Lin}}(\eta, q^i)$ the *linear Newtonian density contrast* defined as $\delta_{\text{Lin}} = \frac{\delta\rho}{\bar{\rho}} + \mathcal{O}(\delta\rho^2)$, and $\nabla^2 = \partial^i \partial_i$. From the other components of Einstein equations, we obtain that the scalar perturbation decomposes¹⁴ into the *present time gravitational potential* $\phi_0(q^i)$ and a time-dependent part containing the *growth factor* $\mathcal{D}(\eta)$

$$\phi(\eta, q^i) = \frac{\mathcal{D}(\eta)}{a(\eta)} \phi_0(q^i). \quad (2.31)$$

¹³The equations are solved order by order, with the zeroth-order resembling the Friedmann equations Eqs. (2.22)-(2.23).

¹⁴Actually, the scalar perturbation is composed by growing and decaying modes like $\phi(\eta, q^i) = g_+(\eta)\phi_+(q^i) + g_-(\eta)\phi_-(q^i)$. However the decaying modes are quickly suppressed leaving only with growing modes.

The growth factor $\mathcal{D}(\eta)$ is the growing mode solution for the linear density contrast, i.e. $\delta_{\text{Lin}}(\eta, q^i) = \mathcal{D}(\eta)\delta_{\text{Lin}}(\eta_0, q^i)$, and it is found by solving the evolution equation for the first-order density contrast [137]

$$\ddot{\delta}_{\text{Lin}} + \mathcal{H}\dot{\delta}_{\text{Lin}} - \frac{3}{2}\mathcal{H}_0^2\Omega_{m0}\frac{\delta_{\text{Lin}}}{a} = 0. \quad (2.32)$$

The analytical solution for \mathcal{D} is given in [181],

$$\mathcal{D}(\eta) = \frac{a}{\frac{5}{2}\Omega_{m0}} \sqrt{1 + \frac{\Omega_{\Lambda}}{\Omega_{m0}}a^3} {}_2F_1\left(\frac{3}{2}, \frac{5}{6}, \frac{11}{6}, -\frac{\Omega_{\Lambda 0}}{\Omega_{m0}}a^3\right), \quad (2.33)$$

with ${}_2F_1(a, b, c, y)$ being the Gaussian (or ordinary) hypergeometric function. In conclusion at early times the small inhomogeneities are described by the density contrast

$$\delta_{\text{Lin}} = \frac{2}{3\mathcal{H}_0^2\Omega_{m0}} \left(\mathcal{D}\nabla^2\phi_0 - 3\mathcal{H}\dot{\mathcal{D}}\phi_0 \right). \quad (2.34)$$

The evolution of inhomogeneities can be modelled by linear PT only if $\delta \ll 1$. Initially, this is the case, but at later times the density fluctuations become larger under the influence of gravity, reaching values of $\delta \sim 10^2$ for filaments and $\delta \sim 10^6$ for galaxies. The evolution of the gravitational instability that led from the early linear perturbations to the present-day inhomogeneities is the primary goal of the study of *structure formation*.

2.2.2 Analytical approaches to structure formation

The equations of GR control gravitational instability, but some applications are well described by the *Newtonian approximation*, namely by a weak-field and slow-motion limit of GR. These requirements are indeed satisfied on small scales, where the dimensionless peculiar gravitational potential ϕ_g/c^2 remains small ($\phi_g/c^2 \sim 10^{-5}$), and the peculiar velocity is never relativistic. In particular, for a fluctuation of proper scale L , the dimensionless peculiar gravitational potential is

$$\frac{\phi_g}{c^2} \sim \delta \left(\frac{L}{r_H} \right)^2 \quad (2.35)$$

with $r_H = cH^{-1}$ the Hubble radius, implying that ϕ_g/c^2 remains small even if $\delta \gg 1$. Usually, this legitimises the use of cosmological simulations based on Newtonian dynamics to describe the nonlinear structure growth on small scales. Formally, the Newtonian approach is obtained by perturbing only the time-time component of the FLRW metric Eq. (2.20) by $2\phi_g/c^2$

$$ds^2 = a^2 \left[- \left(1 + 2\frac{\phi_g}{c^2} \right) c^2 d\eta^2 + \delta_{ij} dx^i dx^j \right]. \quad (2.36)$$

The Einstein equations give the Poisson equation Eq. (2.30) again, while the dynamics is described by the stress-energy conservation Eq. (2.7) with continuity and Euler equations. Recently, cosmologists have begun to investigate cosmic dynamics beyond the Newtonian approximation and to search for measurable relativistic effects on cosmic scales.

Estimating the importance of relativistic corrections in structure formation is of paramount importance in cosmology (see e.g. [45, 36, 173, 21] and refs. therein), and several approximation techniques have been developed to account for nonlinear GR effects in structure formation: to this list belongs the *post-Newtonian approximation* (PN), which we will encounter in Chapter 5. Formally, it is obtained by expanding the equations of GR in inverse

powers of the speed of light, where the zero-order is the Newtonian limit. For the application of the PN approach to cosmological perturbations, see [176, 165, 49] and [126] for the formulations of PN cosmology in two different gauges. In the following, we give a brief overview of the PN approximation as presented in [126].

The authors use the Lagrangian approach by relating the evolved (Eulerian) position x^μ and the initial (Lagrangian) position q^μ of the fluid particles with the transformation

$$x^\mu(\eta, q^j) = q^\mu + \mathcal{S}^\mu(\eta, q^j). \quad (2.37)$$

The vector $\mathcal{S}^\mu(\eta, q^i)$ is the *displacement vector* and represents the difference in matter flow induced by the inhomogeneities. In a homogeneous Universe, the comoving Eulerian coordinate x^μ matches the Lagrangian coordinate q^μ . The presence of inhomogeneities locally alters the expansion as the perturbations grow with time. This is encoded by the displacement vector $\mathcal{S}^\mu(\eta, q^i)$, which is the fundamental field describing the evolution of the inhomogeneities [52, 51]. Equivalently, the relation in Eq. (2.37) can be expressed by the Jacobian of the transformation [126]

$$\mathcal{J}^\mu{}_\nu = \frac{\partial x^\mu}{\partial q^\nu} = \delta^\mu{}_\nu + \mathcal{S}^\mu{}_\nu, \quad (2.38)$$

where $\mathcal{S}^\mu{}_\nu = \frac{\partial \mathcal{S}^\mu}{\partial q^\nu}$ is the deformation tensor. The expression of $\mathcal{S}^\mu{}_\nu$ is found perturbatively by searching for solutions of the trajectories x^μ : this is the key point of the PN approach presented in [126]. Instead of perturbing over the density fluctuations and the velocity fields, as in the Eulerian approach, the perturbation is performed only in the trajectories.

The post-Newtonian expression of the Jacobian $\mathcal{J}^\mu{}_\nu$ has the form

$$\mathcal{J}^\mu{}_\nu = \begin{pmatrix} 1 + \frac{1}{c} \frac{\partial \mathcal{S}^0}{\partial \eta} & \frac{1}{c} \frac{\partial \mathcal{S}^0}{\partial q^j} \\ v^i & \mathcal{J}^i{}_j \end{pmatrix}, \quad (2.39)$$

with $v^i = \delta^{ij} \frac{\partial \mathcal{S}^0}{\partial q^j}$ the peculiar velocity, and the spatial deformation $\mathcal{J}^i{}_j = \frac{\partial \mathcal{S}^i}{\partial q^j}$ being the Newtonian limit of the Jacobian Eq. (2.39). In synchronous-comoving gauge the post-Newtonian metric assumes the form

$$ds^2 = a^2 \{ -c^2 d\eta^2 + \gamma_{lk} dq^l dq^k \} = a^2 \{ -c^2 d\eta^2 + \left[\left(1 + \frac{\chi}{c^2} \right) \delta_{ij} \mathcal{J}^i{}_l \mathcal{J}^j{}_k + \frac{1}{c^2} \pi_{lk} \right] dq^l dq^k \}. \quad (2.40)$$

The PN scalar and tensor modes χ and π_{ij} are sourced by combinations of the peculiar gravitational field ϕ_g and the peculiar velocity gradient tensor $\theta^i{}_j = 1/2 \gamma^{il} \frac{\partial \gamma_{lj}}{\partial \eta}$. In particular, they are found from

$$\chi = 2\mathcal{H}\mathcal{S}^0 - 2\phi_g - \Upsilon \quad (2.41)$$

$$D^2 \pi_{ij} = D_i D_j \Upsilon + \delta_{ij} D^2 \Upsilon + 2(\theta^k{}_k \theta_{ij} - \theta_{ik} \theta^k{}_j), \quad (2.42)$$

where D_i is the covariant spatial derivative of γ_{ij} in the Newtonian limit, while Υ and \mathcal{S}^0 are the solutions of

$$D^2 \Upsilon = -\frac{1}{2} [(\theta^k{}_k)^2 - \theta^i{}_j \theta^j{}_i] \quad (2.43)$$

$$D^2 \mathcal{S}^0 = \theta^k{}_k. \quad (2.44)$$

Once that γ_{ij} is known, one obtains the density contrast $\delta(\eta, q^i)$ from the exact expression of the continuity equation in Lagrangian frame

$$\delta(\eta, q^i) = (1 + \delta_0(q^i)) \sqrt{\frac{\gamma_0(q^i)}{\gamma(\eta, q^i)}} - 1, \quad (2.45)$$

where $\gamma = \det(\gamma_{ij})$, and $\delta_0(q^i) = \delta(\eta_0, q^i)$ and $\gamma_0(q^i) = \delta(\eta_0, q^i)$ are respectively the density contrast and the determinant of the spatial metric at present time. Note that the expression of the density fluctuations in Lagrangian framework Eq. (2.45) is not expanded in γ . In other words, it is capable of mimicking the nonlinear behaviour of structure formation¹⁵.

The PN approximation is one of the many proposed methods to describe nonlinear GR effects in structure formation. Other perturbative approaches are: the *post-Friedmann approximation* (see [132, 151] for a different approach, which adapts to cosmology the weak-field post-Minkowskian approximation and reproduces linear-order cosmological perturbation theory at their zeroth-order), the *weak-field approximation*¹⁶ (see [91] for the development of the framework and [4] for estimations with the use of N-body simulations for a plane-symmetric Universe), and, more recently, a *two-parameters gauge-invariant approximation* (see [84]).

2.2.3 Inhomogeneous models

Another analytical approach to structure formation is to search for exact (i.e. non-perturbative) inhomogeneous solutions to the Einstein equations. These inhomogeneous solutions are not assumed to have the symmetries of the FLRW models. However, interesting classes of such solutions typically contain the FLRW models as a limit (in [40] this was used to define suitable classes for representing inhomogeneous cosmological models). Two noticeable examples are the *Lemaître-Tolman-Bondi* (LTB) and the *Szekeres* models (see [113, 175, 41] and [172] for the original articles), which have been extensively studied in cosmology. The LTB is a spherically symmetric solution containing only dust that is inhomogeneously distributed along the radial direction, i.e. the matter is condensed into concentric shells (overdensities) separated by underdense regions. In this model, an observer at the centre of a local underdense region measures a local accelerated expansion caused by the large-scale inhomogeneities. This feature of the LTB models has been investigated as an alternative explanation for the SNIa observations without the need for dark energy, [53, 14]. Although the LTB solution has been shown to be a valuable toy model¹⁷ to test possible probes for inhomogeneities and anisotropies at late times, [148], they cannot be considered as a realistic model of the Universe for its intrinsic symmetries.

A further improvement is represented by the Szekeres models, a class of exact solutions of the Einstein equations that includes both LTB and FLRW solutions as limits. In his original paper [172], Szekeres finds all solutions of the form

$$ds_{S_z}^2 = -c^2 dt^2 + e^{2\alpha(t, q_1, q_2, q_3)} dq^1{}^2 + e^{2\beta(t, q_1, q_2, q_3)} (dq^2{}^2 + dq^3{}^2) \quad (2.46)$$

Two distinct classes of spacetime metrics can be distinguished: class I, which are a generalization of the Lemaître-Bondi-Tolman model, and class II, which are a generalization of the Kantowski-Sachs and FLRW models. These original solutions were obtained for a pressureless matter (dust) and later extended by Barrow and Stein-Schabes in [22] to include a

¹⁵However, this perturbation technique is limited by the formation of caustic singularities.

¹⁶The leading order of the last two approximation schemes were shown to be equivalent for a dust Universe in the Poisson gauge in [108], whereas [126, 49] were constructed on purpose to include second-order perturbation theory at their PN order.

¹⁷An interesting review of misleading concepts on LTB models can be found in [111], Sec. 4.

cosmological constant Λ . M. Bruni and N. Meures presented a more recent formulation of the class-II solutions in [130] that will be later used in Chapter 4. This formulation distinguishes the contribution of inhomogeneities from the FLRW background and allows us to express the spacetime metric in a form more convenient for cosmological applications: the expression of the line element Eq. (2.46) for this Szekeres model¹⁸ is rewritten as

$$ds_{\text{Sz}}^2 = a^2 \left[-c^2 d\eta^2 + dq^{12} + dq^{22} + Z^2(\eta, q^1, q^2, q^3) dq^{32} \right]. \quad (2.47)$$

As it is shown in [130], thanks to the symmetry of the problem, the function $Z(\eta, q^1, q^2, q^3)$ is decomposed as

$$Z(\eta, q^1, q^2, q^3) = F(\eta, q^3) + A(q^1, q^2, q^3), \quad (2.48)$$

where the function $F(\eta, q^3)$ satisfies Newton's evolution equation for the first-order density contrast¹⁹, Eq. (2.32). Neglecting the decaying modes, it is therefore possible to factorize $F(\eta, q^3)$ without loss of generality as²⁰

$$F(\eta, q^3) = \mathcal{D}(\eta)\beta_+(q^3), \quad (2.49)$$

where we remind that \mathcal{D} is the growing mode solution for the density contrast, Eq. (2.33). It follows that $F(\eta, q^3)$ coincides with the linear density contrast and more precisely we have $\delta_{\text{Lin}}(\eta, q^3) = -\mathcal{D}(\eta)\beta_+(q^3)$ ²¹.

The purely spatial function $A(q^1, q^2, q^3)$ sets the spatial distribution of the density contrast

$$\delta_{\text{Sz}} = -\frac{F}{F + A}. \quad (2.50)$$

From Einstein equations follows that A is decomposed as, [130]

$$A(q^1, q^2, q^3) = 1 + \beta_+(q^3)B \left\{ [q^1 + \omega(q^3)]^2 + [q^2 + \gamma(q^3)]^2 \right\}. \quad (2.51)$$

with ω and γ being two real functions which reduces to $\omega = \gamma = 0$ for the special case of axial symmetry around q^3 . The term B in Eq. (2.51) is a constant and is given by (see App. C in [90])

$$B = \frac{5}{4} \mathcal{H}_0^2 \Omega_{\text{m}0} \frac{\mathcal{D}_{\text{in}}}{a_{\text{in}}}, \quad (2.52)$$

where $\mathcal{D}_{\text{in}} = a_{\text{in}}$ for initial conditions set deeply in the matter-dominated era. As noted before, the function β_+ is the part of A which specifies the spatial distribution of the first-order density contrast, and it can be related to the peculiar gravitational potential ϕ_0 via the cosmological Poisson equation Eq. (2.30).

Other examples of exact inhomogeneous cosmological models are *black-hole lattices* (see [115, 59, 60, 33] and [34, 35] for numerical investigations), *plane symmetric models* or *wall Universe* (see [64, 7, 180] for an exact, numerical, and PN analysis of the wall Universe), and *Swiss Cheese* models ([73]).

¹⁸We choose here to use our notation instead that of [130]. The line element (2.47) is different from the one presented in [130] because we use conformal time. Of course, this does not affect the results, since it can be easily shown that the two metrics are equivalent under a coordinate transformation.

¹⁹This was implicitly shown in Sec. 5 of the Szekeres' original paper [172] and later by many other authors such as those of [42]. However, it was Goode and Wainwright who explicitly recognized that the relativistic equations for the density fluctuations in Szekeres model are the same as in Newtonian gravity, [85]. They also provide a new formulation of Szekeres solutions which is much more useful in cosmology and in which the relation to the FLRW solution is clarified.

²⁰The time-dependent-only growing mode is denoted by f_+ in [130] and is given in Eq. (11b) in a dimensionless time variable τ . To reconcile \mathcal{D} in (2.33) and f_+ , one must: first transform $f_+(\tau)$ into a conformal time $f_+(\eta)$ and then normalise so that $f_+(\eta_0) = 1$. The final result is $F(\eta, q^3)$ as in (2.49).

²¹The minus sign between F and δ follows from the fact that in eq. (A8) of [130] the authors set, in full generality, $\delta_{\text{in}} = -\frac{F_{\text{in}}}{F_{\text{in}} + A}$.

2.2.4 Numerical simulations

Together with the latter two approaches, numerical simulations in cosmology have become a valuable tool for modelling nonlinear regimes in structure formation. The first generation of numerical codes in cosmology used the Newtonian approximation of GR to simulate systems of N self-gravitating identical objects. A pioneering application of these *N-body simulations* was proposed by J. Peebles in 1970, [136], to model the formation of the Coma cluster. The steep growth in computational power led to the development of more detailed N-body codes capable of simulating up to 10^{12} particles and producing a realistic structure of the cosmic web, [134, 135]. A number of attempts have been made to incorporate relativistic corrections into N-body simulations using some of the perturbation methods listed above, see e.g. [43, 92, 37], as well as N-body simulations have been used as an input for approximated GR equations, as in [46, 8, 79].

Another approach to cosmological simulations is represented by *full-GR numerical codes*, which use numerical methods to directly solve Einstein’s equations (see [117, 31, 129, 6, 122, 70, 62, 20] for the codes used in cosmology, and [2] for the comparison between them). Numerical solutions of the Einstein equations were used early on to study the dynamics of strong-field gravitational systems, such as the study of the two-body problem for the two ends of a wormhole (Hahn and Lindquist in 1964, [94]) and the generation of pure gravitational waves (Eppley in 1977, [75]), where the highly nonlinear relativistic phenomena dominate. Since these early applications, continuous improvements in numerical techniques have shaped *numerical relativity* and enabled many successes in the description of compact astrophysical objects [145, 17, 48, 47, 97, 16, 54] and in cosmological dynamics, [82, 32, 5, 122, 123, 21].

To simulate full-GR dynamics in numerical relativity, the Einstein equations Eq. (2.4) must be reformulated as an initial value problem, clearly separating the temporal and spatial dependence in the equations. This procedure is known as the $3 + 1$ *splitting of spacetime* (or *ADM formalism*) [15, 167], and forms the common theoretical framework for most of the numerical codes mentioned so far. In what follows, we will discuss some of the key concepts of the $3 + 1$ approach to GR that we will encounter later in this thesis. For comprehensive references on the $3+1$ formalism, see [12, 26, 86].

Let us start by considering a manifold $(\mathcal{M}, g_{\mu\nu})$ which is globally foliated by a family of three-dimensional space-like hypersurfaces Σ_t . We also assume that the foliation is labelled by a monotonic function t such that $t = \text{const}$ on each slice, see Fig. 2.3. In other words, each slice Σ_t is identified as the level (hyper)surface of $t = \text{const}$ and is characterised by the timelike vector $\nabla^\mu t = g^{\mu\nu}\nabla_\nu t$ orthogonal to the hypersurface and such that $(\nabla^\mu t)(\nabla_\mu t) = -\alpha^{-2}$. In this view, the function t can be interpreted²² as a “global time” (synchronising all points on Σ_t), whose flow is represented by $\nabla^\mu t$. The unit *normal vector* to Σ_t n^μ is given as $n^\mu = -\alpha\nabla^\mu t$ and represents the normalised time-like vector colinear to the time flow $\nabla^\mu t$. The *lapse function* α gives the flow rate of the proper time τ of an “Eulerian observer”, i.e. an observer moving along the normal vector $n^\mu = \frac{dx^\mu}{d\tau}$, with respect to the global time t [12]

$$d\tau = \alpha dt. \quad (2.53)$$

This can be shown by computing the variation of the global time flow $\nabla^\mu t$ along n^μ

$$n^\mu\nabla_\mu t = (-\alpha\nabla^\mu t)\nabla_\mu t = \frac{1}{\alpha}. \quad (2.54)$$

The adjective “Eulerian” refers to the fact that it is the observer who measures how the points on the foliation evolve in time. In general, any other observer is called a “coordinate”

²²Note that t will not necessary coincide with the proper time of any particular observer.

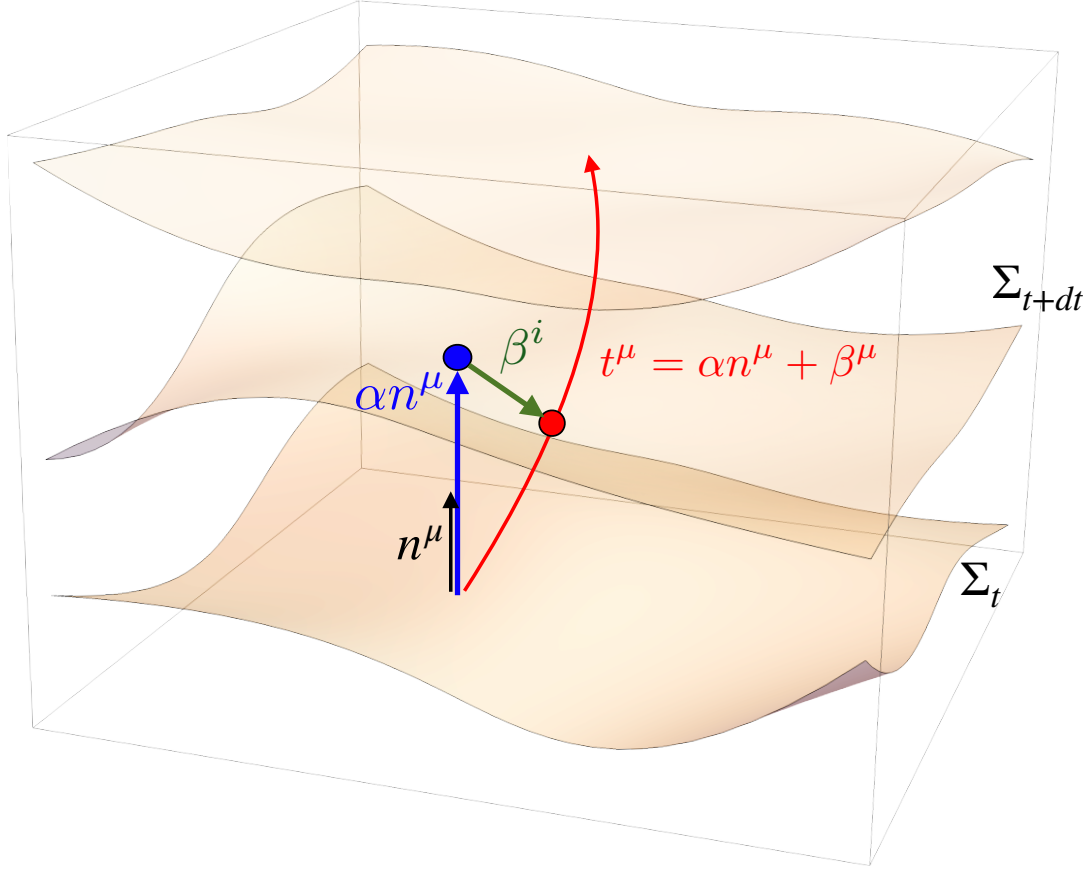


Figure 2.3: The constant-time hypersurfaces Σ_t foliating the four-dimensional spacetime $\mathcal{M}, g_{\mu\nu}$, introduce a unit normal vector n^μ orthogonal to Σ_t . The coordinate flow, i.e. the lines of constant spatial coordinates, is given in terms of the lapse α and the shift β^i gauge functions.

observer and identified by the timelike vector field

$$t^\mu = \alpha n^\mu + \beta^\mu, \quad (2.55)$$

where β^μ is the *shift vector* quantifying the displacement on Σ_t of the coordinate observer t^μ with respect to the position of the Eulerian observer. The choice of $\alpha = 1$ and $\beta^i = 0$ for t^μ is equivalent to choosing a Lagrangian observer. The unit normal vector n^μ , together with the spacetime metric $g_{\mu\nu}$ define the induced *spatial metric* on each slice [86]

$$\gamma^\mu{}_\nu = g^\mu{}_\nu + n^\mu n_\nu, \quad (2.56)$$

which is linked to the orthogonal projector tensor on Σ_t as $\gamma^\mu{}_\nu = g^{\mu\rho} \gamma_{\rho\nu}$. In the adapted coordinate system t^μ , the components of the normal vector and the metric $g_{\mu\nu}$ are written in terms of $(\alpha, \beta^i, \gamma_{i,j})$ as

$$n^\mu = \left(\frac{1}{\alpha}, -\frac{\beta^i}{\alpha} \right), \quad n_\mu = (-\alpha, 0) \quad (2.57)$$

and

$$g_{\mu\nu} = \begin{pmatrix} \beta_i \beta^i - \alpha^2 & \beta_i \\ \beta_j & \gamma_{ij} \end{pmatrix}, \quad g^{\mu\nu} = \begin{pmatrix} -\alpha^{-2} & \alpha^{-2} \beta^i \\ \alpha^{-2} \beta^j & \gamma^{ij} - \alpha^{-2} \beta^i \beta^j \end{pmatrix}, \quad (2.58)$$

where the Latin indices runs from 1 to 3, and $\beta_i = \gamma_{ij} \beta^j$, [12].

The projection of a generic (r, s) tensor ${}^{(4)}T^{\mu_1 \dots \mu_r}_{\nu_1 \dots \nu_s}$ on the slice is obtained by using the projector γ^μ_ν

$${}^{(3)}T^{\mu_1 \dots \mu_r}_{\nu_1 \dots \nu_s} = {}^{(4)}T^{\rho_1 \dots \rho_r}_{\sigma_1 \dots \sigma_s} \gamma^{\mu_1}_{\rho_1} \dots \gamma^{\mu_r}_{\rho_r} \gamma^{\sigma_1}_{\nu_1} \dots \gamma^{\sigma_s}_{\nu_s}, \quad (2.59)$$

where we have denoted as ${}^{(3)}T^{\mu_1 \dots \mu_r}_{\nu_1 \dots \nu_s}$ the projected tensor, [86]. The very same projector is also used to define the operation of *covariant derivative on the slice* $D_\mu = \gamma^\sigma_\mu \nabla_\sigma$: for the (r, s) tensor ${}^{(4)}T^{\mu_1 \dots \mu_r}_{\nu_1 \dots \nu_s}$ (see e.g. [86])

$$D_\lambda T^{\mu_1 \dots \mu_r}_{\nu_1 \dots \nu_s} = \gamma^{\mu_1}_{\rho_1} \dots \gamma^{\mu_r}_{\rho_r} \gamma^{\sigma_1}_{\nu_1} \dots \gamma^{\sigma_s}_{\nu_s} \gamma^\epsilon_\lambda \nabla_\epsilon T^{\rho_1 \dots \rho_r}_{\sigma_1 \dots \sigma_s}, \quad (2.60)$$

which is written in terms of the 3D Christoffel symbol ${}^{(3)}\Gamma^k_{ij} = \frac{1}{2} \gamma^{kl} \left(\frac{\partial \gamma_{lj}}{\partial x^i} + \frac{\partial \gamma_{li}}{\partial x^j} - \frac{\partial \gamma_{ij}}{\partial x^l} \right)$.

With the introduction of the spacetime foliation, one must distinguish between the *intrinsic curvature* of the hypersurface and an *extrinsic curvature* in order to fully characterise the curvature of spacetime. The intrinsic curvature is the curvature of the hypersurface and is defined by the three-dimensional Riemann tensor, i.e. the Riemann tensor with respect to the spatial metric γ_{ij}

$${}^{(3)}R^k_{isj} = \partial_s {}^{(3)}\Gamma^k_{ij} - \partial_j {}^{(3)}\Gamma^k_{is} + {}^{(3)}\Gamma^k_{ls} {}^{(3)}\Gamma^l_{ij} - {}^{(3)}\Gamma^k_{lj} {}^{(3)}\Gamma^l_{is}. \quad (2.61)$$

On the other hand, the *extrinsic curvature* $K_{\mu\nu}$ represents the curvature of the hypersurfaces with respect to the embedding higher-dimensional spacetime \mathcal{M} . It can be determined as the covariant variation of the normal vector $\nabla_\mu n_\nu$ along the slice Σ_t , namely

$$K_{\mu\nu} = -\gamma^\sigma_\mu \gamma^\rho_\nu \nabla_\sigma n_\rho. \quad (2.62)$$

In conclusion, after the introduction of the foliation, the geometry of spacetime $(\mathcal{M}, g_{\mu\nu})$ is completely defined by the four quantities $(\alpha, \beta_i, \gamma_{ij}, K_{ij})$.

The projection of the Einstein equations Eq. (2.4) decomposes the system into 3 relations [12, 26]:

- the *Hamiltonian constraint*:

$${}^{(3)}R + (K^i_i)^2 - K_{ij} K^{ij} - \frac{16\pi G}{c^2} \rho = 0, \quad (2.63)$$

- the *momentum constraint*:

$$D_j K^j_i - D_i K^j_j - \frac{8\pi G}{c^3} S_i = 0, \quad (2.64)$$

- the *evolution equation*:

$$\left(\frac{\partial}{\partial t} - \mathcal{L}_\beta \right) K_{ij} = \alpha \left[{}^{(3)}R_{ij} - 2K_{il} K^l_j + K_{ij} K^l_l \right] - D_i D_j \alpha \quad (2.65)$$

$$- \frac{8\pi G}{c^4} \alpha \left[S_{ij} - \frac{1}{2} \gamma_{ij} (S^i_i - \rho c^2) \right], \quad (2.66)$$

where we have defined the various components of the stress-energy tensor as $\rho c^2 \equiv T_{\mu\nu} n^\mu n^\nu$, $S_\mu \equiv -\gamma^\sigma_\mu n^\rho T_{\sigma\rho}$, and $S_{\mu\nu} \equiv \gamma^\sigma_\mu \gamma^\rho_\nu T_{\sigma\rho}$. An additional evolution equation

$$\left(\frac{\partial}{\partial t} - \mathcal{L}_\beta \right) \gamma_{ij} = -2\alpha K_{ij}, \quad (2.67)$$

is obtained from Eq. (2.62). The first two are constraints arising from the conservation of energy and momentum, while the last two indicate the evolution of the metric. As mentioned earlier, the covariant formulation of GR leaves us free to choose the gauge in which we perform the computation. The gauge choice in the ADM formalism is represented by a specific choice of the lapse α and the shift β^i . Despite the success of the ADM formalism in transforming the Einstein equations into an initial value problem, the equations obtained are weakly hyperbolic, which prevents the simulations from evolving over a long time and becoming rapidly unstable. This problem is overcome by the *BSSN formalism*, [166, 25], which rewrites the ADM equations into a highly hyperbolic form and allows arbitrarily long and stable evolutions of the Einstein equations.

2.2.5 Numerical relativity and cosmological observations: the state of the art

The methods presented above provide a comprehensive general relativistic description of cosmic dynamics. Although they allow the inclusion of GR effects in the growth of structures, the key aspect is to describe and evaluate the nonlinear GR effects on cosmological observations. This requires an equally accurate description of light propagation, which is necessary for tests and comparisons with real data. These studies are still in the early stages and have been approached in a variety of ways. For example, the distance-redshift relation has been investigated using perturbative methods (see e.g. [66] for calculations up to second order PT, and [160] for PN calculations within a class of cosmological models and the deviation from the homogeneous FLRW), with exact methods (see e.g. [78] for exact calculations in the geodesic light-cone gauge and [53, 14] for calculations in LTB models), and in various cosmological simulations (see e.g. [7, 3, 121]). Another important example is the estimation of the weak gravitational lensing effect, i.e. the phenomenon of light deflection in the presence of massive objects. Weak lensing on cosmic scales can be used to probe the presence of dark matter and gain insight into the constituents of the Universe, [169]. Furthermore, by comparing the statistical features of the distortion map from galaxy surveys with those obtained from theoretical models, weak lensing can be used to distinguish between different models of modified gravity, [118, 161, 157]. Theoretical estimates of weak lensing observables in the post-Friedmann formalism are presented in [174, 93]. Weak lensing map and power spectrum have also been extracted from numerical simulations [83, 114]. According to these initial findings, the codes used to simulate GR dynamics appear to be consistent with Newtonian simulations for predicting weak lensing observables [174, 114], although there is a shift in the luminosity distance statistics [3]. Moreover, the PN approximation leads to results different from Λ CDM for certain cosmological models [160]. However, some efforts still need to be made to adapt the truly GR numerical codes to (observational) cosmology.

The central importance of estimating relativistic effects in cosmological observables requires a theoretical framework that comprehensively describes the propagation of light and all optical effects that result from its interaction with cosmological structures. In the next chapter, we give an overview of the theory of light propagation in geometric optics and introduce the theoretical foundations on which this work is based.

THE BGO FORMALISM FOR LIGHT PROPAGATION

Cosmologists and astronomers use electromagnetic and gravitational radiation as their major tools for studying the structure and development of the Universe. These "light-like" signals contain information about the emitting source as well as of the spacetime geometry, the latter derived from the effects induced by gravity. In the near future, these effects will be measured with unprecedented precision over a wider range of scales and redshift by the next generation of galaxy surveys and CMB experiments¹. This revolution in cosmology marks also the beginning of the *real-time cosmology* era, [148], in which it will be possible to measure small temporal changes in cosmological observables, called *optical drift effects*. These real-time effects can provide important and new information about the structure and evolution of the Universe. From the point of view of the basic theory of light propagation, a new approach was presented in [88]. The key ingredients of this new formulation are the *bilocal geodesic operators* which represent the map from the portion of spacetime occupied by the observer to that occupied by the source and provide the complete description of the distortion of the light rays in between.

This chapter is divided into two parts: in the first part, we review the fundamental equations of light propagation in geometric optics, starting from Maxwell's equations in curved spacetimes. This is standard knowledge, see e.g. [133, 185, 140], and serves here as an introduction to the basic concepts of geometric optics in general relativity. In the second part, we discuss the bilocal geodesic operators formulation of light propagation in geometric optics, based on the results presented in [88]. This part provides the theoretical framework for the original results presented in Chapters 4 and 5.

3.1 Light propagation in curved spacetime

Light signals, intended as radiation travelling at the speed $c = 299792.5$ km/s, are governed by *Maxwell's equations*

$$F_{\mu\nu} = \nabla_\mu A_\nu - \nabla_\nu A_\mu \quad (3.1)$$

$$\nabla_\nu F^{\mu\nu} = 4\pi J^\mu \quad (3.2)$$

$$\nabla_{[\lambda} F_{\mu\nu]} = 0, \quad (3.3)$$

with $J^\mu = (c\rho, J^i)$ the four-current of the charge density ρ and current density J^i . $F^{\mu\nu}$ is the Faraday tensor (also known as field strength or electromagnetic tensor) defined as the

¹<https://www.skatelescope.org>, <https://www.euclid-ec.org>, <https://www.lsst.org>, <http://litebird.jp/eng/>, <https://www.jpl.nasa.gov/missions/spherex>

field strength of the four-vector potential $A^\mu = (\phi/c, A^i)$

$$F_{\mu\nu} = \nabla_\mu A_\nu - \nabla_\nu A_\mu, \quad (3.4)$$

whose components are the electric $F^{0i} = -F^{i0} = E^i$ and magnetic $F^{ij} = \varepsilon^{ijk} B^k$ fields. From the very definition of $F_{\mu\nu}$, Eq. (3.4), we see that the electromagnetic tensor is invariant under the gauge transformation $A_\mu \rightarrow A_\mu + \nabla_\mu \chi$, with χ a scalar function. This constitutes the gauge freedom of electromagnetism. A convenient gauge choice is the Lorentz gauge condition $\nabla_\mu A^\mu = 0$, in which Eq. (3.2) takes the simpler form of a wave equation for the four-vector potential

$$\nabla_\nu \nabla^\nu A^\mu = R^\mu{}_\sigma A^\sigma - 4\pi J^\mu, \quad (3.5)$$

where the Ricci tensor $R^\mu{}_\sigma = R_\sigma{}^\mu = R^\nu{}_{\sigma\nu}{}^\mu$ appear from the commutation of the two covariant derivatives as $\nabla_\nu \nabla^\mu A^\nu = \nabla^\mu \nabla_\nu A^\nu + R^\nu{}_{\sigma\nu}{}^\mu A^\sigma$. The expression in Eq. (3.5) describes the dynamics of electromagnetic potential in a generic spacetime, (see e.g. [133, 185, 140]).

In the absence of sources $J^\mu = 0$ Eq. (3.5) gives the propagation equation for the electromagnetic radiation

$$\nabla_\nu \nabla^\nu A^\mu - R^\mu{}_\sigma A^\sigma = 0, \quad (3.6)$$

which one has to solve to study light propagation in cosmology. However, this equation is too general, and needs to be ‘‘adapted’’ to apply to astronomical observations. As described in [133], one can distinguish three characteristic lengths²:

1. the typical wavelength of the electromagnetic radiation λ ,
2. the typical length over which the amplitude, the polarization and the wavelength vary L ,
3. the typical radius of curvature of the spacetime \mathcal{R} , defined such that $\mathcal{R} = \mathcal{O}(|R^\mu{}_{\rho\sigma\nu}|^{-1/2})$, with $|R^\mu{}_{\rho\sigma\nu}|$ denoting the magnitude of the typical component of the Riemann tensor.

In the range of astrophysical observations, the typical electromagnetic wavelength extends³ from ~ 10 m for radio waves emitted by active radio galaxies to the smaller wavelengths of visible, X-rays, and gamma-rays emissions. On the other hand, the typical curvature’s radius \mathcal{R} of the spacetime where these electromagnetic signals propagate is usually much larger. For instance on cosmological scales we have that⁴ $\mathcal{R} \sim c/H$, with H the Hubble parameter whose value depends on the cosmological era⁵: at present time $H_0 = 67.4 \frac{km}{s Mpc}$, see [10], which gives $\mathcal{R} \sim 4.5$ Gpc. Also on smaller scales the condition $\lambda \ll \mathcal{R}$ remain valid, for instance close to the surface of the Sun, one can calculate that the curvature radius is of the order of 10^8 km. We need to go to very strong gravitational regimes, like close to the event horizon r_s of a black hole where $\mathcal{R} \sim r_s$ to have the condition $\lambda \ll \mathcal{R}$ no longer valid

²These characteristic lengths are evaluated in a local inertial frame, e.g. the one at rest respect a nearby galaxy.

³For gravitational waves the typical wavelength can be larger, as the one of the first gravitational waves detection $\lambda \sim 10^4$ km, [1].

⁴As an estimate of $|R^\mu{}_{\rho\sigma\nu}|$ we use the Ricci scalar that in a flat FLRW metric gives $R = 6 \left(\frac{\dot{a}^2 + a\ddot{a}}{a^2} \right) \sim \left(\frac{\dot{a}}{a} \right)^2 = H^2$. In other cases, like e.g. in a Schwarzschild metric, the Ricci scalar is not a good indicator and we need to use a different estimator for $|R^\mu{}_{\rho\sigma\nu}|$, like the Kretschmann scalar $|R^{\mu\rho\sigma\nu} R_{\mu\rho\sigma\nu}|$.

⁵At the recombination era (around 3.7×10^5 years after the Big Bang, the epoch at which the ionised plasma of electrons and protons first became bound forming neutral hydrogen atoms, which did not scatter the photons but allowed them to travel freely) the Hubble parameter was $H = 1255 \frac{km}{s Mpc}$ corresponding to $\mathcal{R} \sim 0.2$ Mpc.

for part of the electromagnetic spectrum⁶. Except for the last instance, we can treat light propagation within the so called *geometric optics approximation*, which is valid whenever λ is much smaller than each of the other scales involved, i.e.

$$\lambda \ll L \text{ and } \lambda \ll \mathcal{R}. \quad (3.7)$$

Within this approximation one can look for solutions of Eq. (3.6) in the form of a rapidly oscillating wave with a nearly constant amplitude, namely

$$A^\mu = C^\mu e^{i\theta}, \quad (3.8)$$

where the phase $\theta \propto \frac{2\pi}{\lambda}$ is a real function of the spacetime's position, while C^μ is in general a complex four-vector expressing the amplitude and polarization of the electromagnetic wave. Given this ansatz, we note that with λ decreasing to zero, and L and \mathcal{R} fixed, the phase θ will get larger and larger, but C^μ will not vary very much. Therefore, we can express the dependence on λ in Eq. (3.8) by introducing the parameter $\epsilon = \lambda/d$, where $d = \min(L, \mathcal{R})$, and expanding the solution in its powers

$$A^\mu = (a^\mu + \epsilon b^\mu + \epsilon^2 c^\mu + \dots) e^{i\frac{\theta}{\epsilon}}. \quad (3.9)$$

Note that $a^\mu e^{i\frac{\theta}{\epsilon}}$ is the leading order term and it constitutes the geometric optics approximation of our solution. The other higher-order terms (h.o.t.) are all contained in $(\epsilon b^\mu, \epsilon^2 c^\mu, \dots)$, representing the post-geometric optics corrections (see e.g. [101, 102, 95] for approaches beyond geometric optics). Applying the ansatz in Eq. (3.9), the wave equation in geometric approximation gives

$$\ell_\mu a^\mu = 0 \quad (3.10)$$

$$a^\mu \ell_\nu \ell^\nu = 0 \quad (3.11)$$

$$-b^\mu \ell_\nu \ell^\nu + i(a^\mu \nabla_\nu \ell^\nu + 2\ell_\nu \nabla^\nu a^\mu) = 0. \quad (3.12)$$

The first relation, Eq. (3.10) is the orthogonality relation between the vector amplitude a^μ and $\ell^\mu = \nabla^\mu \theta$, the vector normal to the surfaces of constant phase. The relation Eq. (3.11) expresses the fact that in the geometric optics approximation one can consider the electromagnetic signals as travelling along null-like geodesic, whose tangent vector ℓ^μ satisfies the geodesic equation⁷

$$\ell^\nu \nabla_\nu \ell^\mu = 0. \quad (3.13)$$

A generic geodesic can be represented as a parametric curve $\gamma(\lambda)$, where the parameter λ spans the geodesic such that to a small variation of the parameter $d\lambda$ correspond a small displacement along the geodesic itself:

$$dx^\mu = \ell^\mu d\lambda.$$

Therefore, the geodesic equation (3.13) can be expressed as the covariant derivative with respect to λ as

$$\frac{D}{D\lambda} \ell^\mu = \frac{d^2 x^\mu}{d\lambda^2} + \Gamma_{\sigma\rho}^\mu \frac{dx^\sigma}{d\lambda} \frac{dx^\rho}{d\lambda} = 0. \quad (3.14)$$

⁶For instance, for a Sun-like black hole we have that $\mathcal{R} \sim r_s \sim 3$ km which is smaller than the low frequency radio waves, or for a Earth-like black hole $\mathcal{R} \sim 8$ mm which is smaller than micro waves $\lambda \sim 1$ cm.

⁷The geodesic equation (3.13) is related to the condition Eq. (3.11) as $0 = \nabla_\mu(\ell^\nu \ell_\nu) = (\nabla_\mu \ell^\nu) \ell_\nu + \ell^\nu (\nabla_\mu \ell_\nu) = \ell_\nu (\nabla_\mu \nabla^\nu \theta) + \ell^\nu (\nabla_\mu \nabla_\nu \theta) = \ell_\nu (\nabla^\nu \nabla_\mu \theta) + \ell^\nu (\nabla_\nu \nabla_\mu \theta) = \ell_\nu (\nabla^\nu \ell_\mu) + \ell^\nu (\nabla_\nu \ell_\mu) = 2\ell^\nu \nabla_\nu \ell_\mu$, where we have used $\nabla_\mu(\nabla_\nu \theta) = \nabla_\mu(\partial_\nu \theta) = \partial_\mu \partial_\nu \theta - \Gamma_{\mu\nu}^\sigma \partial_\sigma \theta = \partial_\nu \partial_\mu \theta - \Gamma_{\nu\mu}^\sigma \partial_\sigma \theta = \nabla_\nu(\nabla_\mu \theta)$.

It is worth noticing that Eq. (3.14) is satisfied if λ is an affine parameter of the geodesic $\gamma(\lambda)$. However, the parametrisation of the geodesic is not unique, i.e. it is always possible to choose a different parametrisation τ , such that $\gamma(\lambda) \rightarrow \gamma(\tau)$. In general the transformation introduces a new term in Eq. (3.14) proportional to the tangent vector, such that $\frac{D\ell^\mu}{D\tau} \propto \ell^\mu$: in this case τ is said a non-affine parameter. It is easy to show that the transformation

$$\lambda \rightarrow A \cdot \lambda + B, \quad (3.15)$$

with $A, B = \text{const}$, is the only possible transformation that leaves the Eq. (3.14) satisfied, namely it transforms an affine parameter into a new affine parameter (see problem 5 of Sec. 3 in [185]). Moreover, a different parametrisation of the geodesic γ changes the value of the squared norm of the tangent vector. In general for time-like and space-like geodesics we prefer to use an affine parametrisation of the geodesic such that its tangent vector k^μ is normalised as $k^\mu k_\mu = \sigma$, with $\sigma = -1$ for time-like geodesics and $\sigma = 1$ for space-like geodesics. In the particular case of null geodesics we do not have a preferred, normalised parametrisation, since Eq. (3.11) holds, so we may always reparametrise γ by an affine transformation, Eq. (3.15). Then the null tangent vector ℓ^μ transforms according to

$$\ell^\mu \rightarrow \frac{1}{A} \ell^\mu. \quad (3.16)$$

The relation in Eq. (3.12) is the propagation equation for the vector amplitude: it is convenient to express a^μ as $a^\mu = ap^\mu$, where $a = \sqrt{|a^\mu a_\mu|}$ is the scalar amplitude and $p^\mu = a^\mu/a$ is the polarization vector. Thus, Eq. (3.12) becomes

$$p^\mu (a \nabla_\nu \ell^\nu + 2\ell_\nu \nabla^\nu a) + 2a \ell_\nu \nabla^\nu p^\mu = 0. \quad (3.17)$$

The term in parenthesis has an important physical meaning and it represents the flux conservation in geometric optics approximation. This can be easily proved by using the continuity equation $\nabla^\mu T_{\mu\nu} = 0$ for the electromagnetic stress-energy tensor in the geometric optics approximation $T_{\mu\nu} = a^2 e^{2i\theta} \ell_\mu \ell_\nu + h.o.t..$ After some straightforward calculations, one get that at the leading order

$$0 = \nabla^\mu T_{\mu\nu} = 2a \nabla^\mu a \ell_\mu + a^2 \nabla^\mu \ell_\mu = \nabla^\mu (a^2 \ell_\mu). \quad (3.18)$$

The vector $a^2 \ell^\mu$ is the photon flux density and the volume integral $(8\pi\hbar)^{-1} \int a^2 \ell^0 \sqrt{|-g|} d^3x$ gives the number of photons (or geodesics) in the volume of integration on any $x^0 = \text{const}$ hypersurface. Implementing Eq. (3.18) in Eq. (3.17) we obtain the propagation equation for the polarization vector

$$\ell^\nu \nabla_\nu p^\mu = 0, \quad (3.19)$$

or in other words, the polarization vector is parallel transported along the null geodesic.

To conclude, the geometric optics approximation can be summarised as follows:

- when an electromagnetic signal satisfies the conditions $\lambda \ll L$ and $\lambda \ll \mathcal{R}$ we can look for solutions to Eq. (3.6) of the form $A^\mu = ap^\mu e^{i\theta} + h.o.t.$;
- in this approximation we can consider the photons as travelling along light rays (null geodesics), Eq. (3.11), with the tangent vector $\ell_\mu = \nabla_\mu \theta$ being the normal to the surfaces of constant phase θ ;
- the amplitude a is governed by the evolution equation

$$\ell^\mu \nabla_\mu a = -\frac{1}{2} a (\nabla_\mu \ell^\mu),$$

which leads to the conservation of the photon number Eq. (3.18);

- the polarization vector p^μ is perpendicular to the light rays, Eq. (3.10) and it is parallel transported along them Eq. (3.19).

3.1.1 Geometric description of light beams

The geometric optics approximation provides a description of light propagation in terms of rays. In this view, the image of an astronomical object is effectively presented as the cross section of a light beam, namely the bunch of rays emitted by the object and focused at the observer. However, the curved spacetime between the emitting object and the observer can bend the geodesics and hence produce deformations in the cross section of the beam. The result is that the apparent position, size, shape, and luminosity of the emitter will appear modified to the observer. These effects are described using the geodesic deviation equation, which is the equation describing the tendency of nearby geodesics to converge or diverge from each other due to the curvature of the spacetime. In this section we will introduce the geodesic deviation equation from a geometric perspective, without any restriction to its application, and we postpone to the next section, Sec. 3.2, the implementation of the concepts introduced here to describe a typical situation in observational astronomy.

As we just mentioned, the equation of geodesic deviation expresses the changes of the distance between a point $x^\mu(\lambda)$ on one geodesic $\gamma(\lambda)$ to a point $\tilde{x}^\mu(\lambda)$ on a nearby geodesic $\tilde{\gamma}(\lambda)$ at the same value⁸ of λ . The major assumption is that the two geodesics are close enough, so as we can define a deviation vector $\xi^\mu(\lambda) = \tilde{x}^\mu(\lambda) - x^\mu(\lambda)$ expressing the difference between the two points and such that the geodesic deviation equation is derived by expanding the geodesic equation for $\tilde{\gamma}(\lambda)$ up to linear order in ξ^μ . Therefore, the geodesic deviation equation gives only the linear corrections in the deviation vector. Several authors have extended the geodesic deviation equation beyond the linear order, see e.g. [28, 146, 183], but the first-order is enough for the purposes of this work.

This way of deriving the geodesic deviation equation requires the introduction of several details which make the derivation difficult to follow. Instead, we decided to present the geodesic deviation equation as derived in [185]: on the one hand this derivation has the advantage of having a clear physical interpretation, but on the other hand it hides the perturbative nature of the geodesic deviation equation. Here, we will try to solve this question clarifying where the linearisation in the deviation vector takes place. Let us start by representing a light beam as a smooth one-parameter family of geodesics $\{\gamma_\tau(\lambda)\}$, i.e. for each $\tau \in \mathbb{R}$ correspond a null geodesic $\gamma_\tau(\lambda)$ of the beam parametrised by the affine parameter λ , and such that the map $(\lambda, \tau) \rightarrow \{\gamma_\tau(\lambda)\}$ is smooth. For our purposes we have considered light geodesics, but the derivation we will present is completely general and it does not depend on the nature of the geodesics. Defining Σ as the two-dimensional submanifold spanned by the geodesics of the family $\{\gamma_\tau(\lambda)\}$, one can introduce the coordinate base (ℓ^μ, ξ^μ) : the vector $\ell^\mu = \frac{dx^\mu}{d\lambda}$ is tangent to the family of geodesics and it satisfies Eq. (3.13). The vector $\xi^\mu = \frac{dx^\mu}{d\tau}$ is the deviation vector and it represents the infinitesimal displacement between two nearby geodesics, see Fig 3.1. To evaluate the change of the vector field ξ^μ , along the flow defined by the tangent vector to the geodesics ℓ^μ , let us calculate the Lie derivative of ξ^μ with respect to ℓ^μ on Σ

$$\mathcal{L}_\ell \xi^\mu = \ell^\nu \nabla_\nu \xi^\mu - \xi^\nu \nabla_\nu \ell^\mu = \ell^\nu \partial_\nu \xi^\mu - \xi^\nu \partial_\nu \ell^\mu, \quad (3.20)$$

where last equality follows from the symmetry of the Christoffel symbols $\Gamma_{\mu\nu}^\lambda$. Now, since $\ell^\mu = \frac{\partial x^\mu}{\partial \lambda}$ and $\xi^\mu = \frac{\partial x^\mu}{\partial \tau}$, it is easy to see that the Lie derivative vanishes, implying the

⁸Here one has to assume that the two geodesics are labelled by the same affine parameter λ . However, since there is no unique way of relating the affine parameter on one geodesic to the affine parameter on another, we have a degeneracy in the separation vector definition. This will be clarified later.

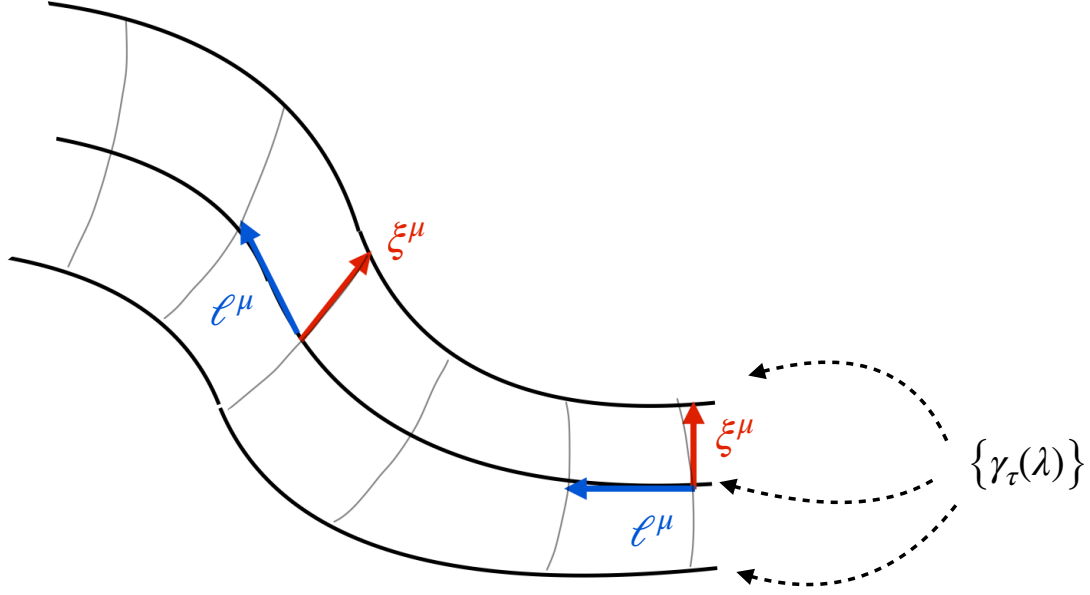


Figure 3.1: The tangent vector to the geodesics ℓ^μ and the deviation vector ξ^μ , representing the infinitesimal displacement from a nearby geodesic, characterise the geodesics of the family $\{\gamma_\tau(\lambda)\}$.

commutation of the two vector fields

$$\ell^\nu \nabla_\nu \xi^\mu = \xi^\nu \nabla_\nu \ell^\mu. \quad (3.21)$$

Let us remark that the perturbative nature of the geodesic deviation equation is already assumed when we use the Lie derivative. In fact, from the very definition of the Lie derivative we have

$$-\mathcal{L}_\ell \xi^\mu = \mathcal{L}_\xi \ell^\mu = \lim_{\Delta\tau \rightarrow 0} \frac{1}{\Delta\tau} \left[\frac{\partial x_0^\mu}{\partial x_\tau^\nu} \ell^\nu(x_\tau) - \ell^\mu(x_0) \right], \quad (3.22)$$

where ξ^μ points from $x_0^\mu \in \gamma_0$ to a nearby point $x_\tau^\mu \in \gamma_\tau$. We can now see that Eq. (3.21), which is the starting point of this derivation, expresses the vanishing of the linear order expansion of the flow of ℓ^μ along the vector field ξ^μ .

We can also go back from the right hand side of Eq. (3.22) to the Lie derivative in Eq. (3.20) by expanding the first term as an infinitesimal coordinate transform x_τ^μ to $x_0^\mu = x_\tau^\mu - \xi^\mu \Delta\tau + \mathcal{O}(\Delta\tau^2)$ acting on ℓ^μ :

$$\frac{\partial x_0^\mu}{\partial x_\tau^\nu} \ell^\nu(x_\tau) = \ell^\mu(x_\tau) - \ell^\nu(x_\tau) \partial_\nu \xi^\mu(x_0) \Delta\tau + \mathcal{O}(\Delta\tau^2). \quad (3.23)$$

Expressing $\ell^\mu(x_\tau) = \ell^\mu(x_0) + \xi^\nu(x_0) \partial_\nu \ell^\mu(x_0) \Delta\tau + \mathcal{O}(\Delta\tau^2)$ in Eq. (3.23), we indeed obtain the previous expression of the Lie derivative

$$\mathcal{L}_\xi \ell^\mu = \frac{1}{\Delta\tau} \left[\ell^\mu(x_0) + \xi^\nu \partial_\nu \ell^\mu \Delta\tau - \ell^\nu \partial_\nu \xi^\mu \Delta\tau + \mathcal{O}(\Delta\tau^2) - \ell^\mu(x_0) \right] = \xi^\nu \partial_\nu \ell^\mu - \ell^\nu \partial_\nu \xi^\mu. \quad (3.24)$$

Let us move back on the derivation. Following the interpretation that ξ^μ represents the displacement between nearby geodesics, the left hand side of Eq. (3.21) defines the relative

velocity between geodesics. Similarly, the relative acceleration between the geodesics of the family is $w^\mu = \ell^\rho \nabla_\rho (\ell^\nu \nabla_\nu \xi^\mu)$. From Eq. (3.21) then we have

$$\begin{aligned}
w^\mu &= \ell^\rho \nabla_\rho (\xi^\nu \nabla_\nu \ell^\mu) \\
&= (\ell^\rho \nabla_\rho \xi^\nu) (\nabla_\nu \ell^\mu) + \ell^\rho \xi^\nu \nabla_\rho \nabla_\nu \ell^\mu \\
&= (\xi^\rho \nabla_\rho \ell^\nu) (\nabla_\nu \ell^\mu) + \ell^\rho \xi^\nu (\nabla_\nu \nabla_\rho \ell^\mu + R^\mu_{\sigma\rho\nu} \ell^\sigma) \\
&= (\xi^\rho \nabla_\rho \ell^\nu) (\nabla_\nu \ell^\mu) + \xi^\nu \nabla_\nu (\ell^\rho \nabla_\rho \ell^\mu) - (\xi^\nu \nabla_\nu \ell^\rho) (\nabla_\rho \ell^\mu) + R^\mu_{\sigma\rho\nu} \ell^\sigma \ell^\rho \xi^\nu \\
&= R^\mu_{\sigma\rho\nu} \ell^\sigma \ell^\rho \xi^\nu.
\end{aligned} \tag{3.25}$$

The result is the geodesic deviation equation (GDE),

$$\ell^\rho \nabla_\rho (\ell^\nu \nabla_\nu \xi^\mu) = R^\mu_{\sigma\rho\nu} \ell^\sigma \ell^\rho \xi^\nu, \tag{3.26}$$

which relates the relative acceleration between infinitesimally close geodesics with the spacetime curvature, [185]. The GDE for timelike geodesics plays an important role in the foundation of General Relativity, since it can be used to characterize the spacetime curvature as the relative motion of free falling bodies. This was covered by many authors, see e.g. [143, 171, 28, 27, 13, 56, 183, 146, 80]). For analysis on the GDE for null geodesics see [23, 57, 58, 110, 179, 88].

3.1.2 Properties of the GDE

Let us discuss now two general properties of the GDE solutions which hold irrespectively of the underlying geometry, as shown in [183, 110, 88]. The first property is derived by multiplying the GDE, Eq. (3.26), by ℓ_μ to obtain

$$\nabla_\ell \nabla_\ell (\ell_\mu \xi^\mu) = 0, \tag{3.27}$$

with $\nabla_\ell = \ell^\sigma \nabla_\sigma$, and we use the fact that ℓ^μ is a solution of Eq. (3.13) and $\ell_\mu R^\mu_{\alpha\beta\nu} \ell^\alpha \ell^\beta = 0$ from the symmetry of the Riemann tensor. Then we have

$$\xi^\mu \ell_\mu = C + D \lambda,$$

with $C, D = \text{const.}$ In this way we have defined 2 constants of motion for the GDE, namely the quantities

$$D = (\nabla_\ell \xi^\mu) \ell_\mu \tag{3.28}$$

$$C = \xi^\mu \ell_\mu - D \lambda, \tag{3.29}$$

are conserved along the geodesics.

The second property states that if $\xi^\mu(\lambda)$ is a solution of the GDE, then also $\tilde{\xi}^\mu = \xi^\mu + \alpha(\lambda) \ell^\mu$ is a solution. The form of the proportionality function $\alpha(\lambda)$ is easily obtained by inserting $\tilde{\xi}^\mu$ into Eq. (3.26) to find that $\alpha(\lambda) = (E + F \lambda)$, with $E, F = \text{const.}$ In other words, we have that

$$\tilde{\xi}^\mu = \xi^\mu + (E + F \lambda) \ell^\mu \tag{3.30}$$

is a solution of Eq. (3.26). This ‘‘gauge freedom’’ of adding terms proportional to ℓ^μ to the solution of the GDE is a direct consequence of the freedom we have in choosing the affine parametrisation of a geodesic. In fact, as previously discussed, if λ is the affine parameter of the geodesic $\gamma_0 \in \{\gamma_\tau\}$, then $A(\tau) \lambda + B(\tau)$ is the only possible form for the affine parameter of any of the other geodesics of the family $\{\gamma_\tau\}$. Geometrically, $\tilde{\xi}^\mu$ corresponds to the same

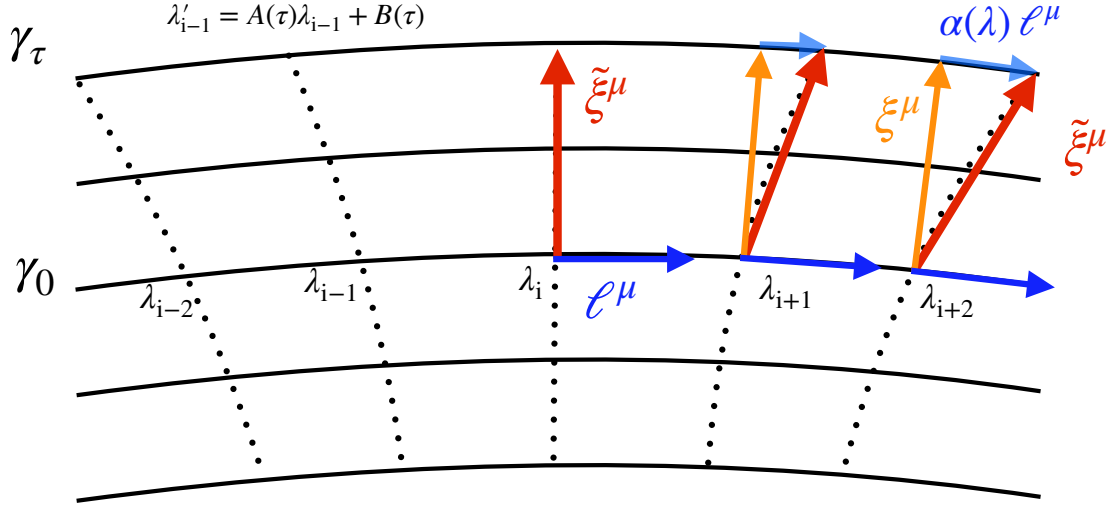


Figure 3.2: The two deviation vectors ξ^μ and $\tilde{\xi}^\mu = \xi^\mu + \alpha(\lambda)\ell^\mu$ identify the same geodesic γ_τ . This invariance of the GDE is related to the gauge freedom one has in choosing the affine parameter. Indeed, the different deviation vector $\tilde{\xi}^\mu$ can be obtained by introducing the different affine parametrisation λ' of the geodesic γ_τ .

congruence of geodesics as ξ^μ , but with a change of parametrisation of the geodesics around γ_0 , see Fig. 3.2.

Assuming that the character of the geodesics is conserved, i.e. the geodesics of the family are all of the same type, we can draw some conclusions regarding C and D . Let us start by using Eq. (3.29) to write Eq. (3.30) as

$$\tilde{C} + \lambda\tilde{D} = \tilde{\xi}^\mu \ell_\mu = C + \lambda D + (E + F\lambda)\ell^\mu \ell_\mu, \quad (3.31)$$

where $C + \lambda D = \xi^\mu \ell_\mu$, and the equality is satisfied for

$$\tilde{C} = C + E \ell^\mu \ell_\mu \quad (3.32)$$

$$\tilde{D} = D + F \ell^\mu \ell_\mu. \quad (3.33)$$

We distinguish two cases:

- for a time-like or space-like family we have $\ell^\mu \ell_\mu = \epsilon \neq 0$, implying that it is always possible to choose a different reparametrisation of the geodesics around γ_0 such that the vectors ξ^μ and ℓ^μ stay perpendicular along γ_0 , namely

$$\tilde{C} = C + \frac{-C}{\ell^\mu \ell_\mu} \ell^\mu \ell_\mu = 0 \quad (3.34)$$

$$\tilde{D} = D + \frac{-D}{\ell^\mu \ell_\mu} \ell^\mu \ell_\mu = 0. \quad (3.35)$$

- for a null family one has $\ell^\mu \ell_\mu = 0$ for all geodesics, implying that for any choice of E and F we have $\tilde{C} = C$ and $\tilde{D} = D$.

We conclude that for a congruence of null geodesics there is no⁹ affine reparametrisation of the geodesics around γ_0 which makes the deviation vector ξ^μ perpendicular to ℓ^μ , [110, 88]. In this sense the null families represent a special class of families of geodesics.

⁹Note that we are not saying that $\xi^\mu \ell_\mu \neq 0$ for null geodesics. This is possible and it represent a specific choice of the initial conditions for the null geodesics of the family. What we meant is that if $\xi^\mu \ell_\mu \neq 0$, then it is not possible to chose a proper affine reparametrisation to transform ξ^μ into a vector orthogonal to ℓ^μ .

Let us proceed in our analysis by noting that Eq. (3.28) can be expressed as $D = \frac{1}{2}\xi^\nu \nabla_\nu(\ell^\mu \ell_\mu)$, which follows multiplying by ℓ_μ the relation in Eq. (3.21), and using the equality¹⁰ $\xi^\nu(\nabla_\nu \ell^\mu)\ell_\mu = \frac{1}{2}\xi^\nu \nabla_\nu(\ell^\mu \ell_\mu)$. Again we have different conclusions depending on the character of the family:

- for a time-like or space-like family we have a preferred normalisation of the tangent vector $\ell^\mu \ell_\mu = \epsilon$, which in general may differ among the geodesics of the family. In other words, the value of $\ell^\mu \ell_\mu = \epsilon$ changes along ξ^μ , implying that $D = \xi^\nu \nabla_\nu(\ell^\mu \ell_\mu) \neq 0$. To impose $D = 0$ we need to perform a reparametrisation of the other geodesics of the family such that the normalisation of the tangent vector remains constant: this is precisely what we demanded in Eq. (3.35).
- for a null family one has $\ell^\mu \ell_\mu = 0$ for all geodesics, implying $D = 0$ and $C = \xi^\mu \ell_\mu = \text{const}$ irrespectively of the parametrisation.

The condition $D = 0$ for null geodesics leads to the *flat lightcone approximation* (FLA) for the time of arrival of the electromagnetic signals¹¹, which is a direct consequence of the linearity of the GDE in ξ^μ , [88]. Indeed, if γ_0 is a null geodesic with tangent vector ℓ^μ and γ is a nearly displaced geodesic of the same family, with tangent vector $k^\mu = \ell^\mu + \nabla_\ell \xi^\mu$, the condition for γ to remain null reads

$$g_{\mu\nu}(\ell^\mu + \nabla_\ell \xi^\mu)(\ell^\nu + \nabla_\ell \xi^\nu) = 2\ell_\mu \nabla_\ell \xi^\mu + \nabla_\ell \xi_\mu \nabla_\ell \xi^\mu = 0, \quad (3.36)$$

where we have already removed the term $\ell_\mu \ell^\mu = 0$. Since we are considering small displacements, the term $\nabla_\ell \xi_\mu \nabla_\ell \xi^\mu$ is quadratic in ξ^μ and it can be neglected. The null condition for γ reduces to $\ell_\mu \nabla_\ell \xi^\mu = 0$, that from Eq. (3.28) reads $D = 0$.

3.2 The bilocal geodesic operators

In the geometric optics regime, the geodesic equation (3.13) and the GDE (3.26) are the two master equations governing light propagation in the presence of curvature. In the following we apply these concepts to describe a typical situation in observational astronomy.

Consider the physical system consisting of an observer \mathcal{O} and a source \mathcal{S} far apart and moving freely along their timelike worldlines. We denote the regions of spacetime where the observer and the source are moving $N_{\mathcal{O}}$ and $N_{\mathcal{S}}$, and we suppose that $N_{\mathcal{O}}$ and $N_{\mathcal{S}}$ are causally connected, meaning that any signal emitted by \mathcal{S} is received by \mathcal{O} at any later time. If L is typical size of $N_{\mathcal{O}}$ and $N_{\mathcal{S}}$, it must be much smaller than the characteristic curvature scale of the spacetime \mathcal{R} , i.e. $L \ll \mathcal{R}$. In this case, we may effectively treat both $N_{\mathcal{O}}$ and $N_{\mathcal{S}}$ as flat, and use special relativity to describe the effects on light propagation in these regions. From a geometric prospective, the local flatness of the two regions allows us to identify points in $N_{\mathcal{O}}$ and $N_{\mathcal{S}}$ with points in the corresponding tangent spaces $T_{x_{\mathcal{O}}}\mathcal{M}$ and $T_{x_{\mathcal{S}}}\mathcal{M}$, up to quadratic terms in x^μ .

Since $N_{\mathcal{O}}$ and $N_{\mathcal{S}}$ are causally connected, it is possible to find a *fiducial null geodesic* γ_0 going from \mathcal{S} to \mathcal{O} , i.e. such that $\gamma(\lambda_{\mathcal{S}}) = x_{\mathcal{S}}^\mu$ and $\gamma(\lambda_{\mathcal{O}}) = x_{\mathcal{O}}^\mu$ are the source's and observer's positions, respectively¹². The vector $\ell_{\mathcal{O}}^\mu$ is the tangent vector to γ_0 at \mathcal{O} and $\ell_{\mathcal{S}}^\mu$

¹⁰It is derived as follows: $\nabla_\nu(\ell^\mu \ell_\mu) = (\nabla_\nu \ell^\mu)\ell_\mu + (\nabla_\nu \ell_\mu)\ell^\mu = (\nabla_\nu \ell^\mu)\ell_\mu + [\nabla_\nu(g_{\mu\sigma}\ell^\sigma)]g^{\mu\rho}\ell_\rho$. Using $\nabla_\nu g_{\mu\sigma} = 0$, we have $\nabla_\nu(\ell^\mu \ell_\mu) = (\nabla_\nu \ell^\mu)\ell_\mu + (\nabla_\nu \ell^\sigma)\delta_{\sigma}^\rho \ell_\rho = 2(\nabla_\nu \ell^\mu)\ell_\mu = 2(\nabla_\nu \ell_\mu)\ell^\mu$.

¹¹It will be clarified later when we introduce the semi-null frame.

¹²Note that the two values $\lambda_{\mathcal{S}}$ and $\lambda_{\mathcal{O}}$, for which $\gamma(\lambda_{\mathcal{S}}) = x_{\mathcal{S}}^\mu$ and $\gamma(\lambda_{\mathcal{O}}) = x_{\mathcal{O}}^\mu$, may change if we consider a different affine parameter for γ_0 . However, in geometric optics we are interested only in the question whether or not a null geodesic passes through a given event and what null direction it follows at that moment.

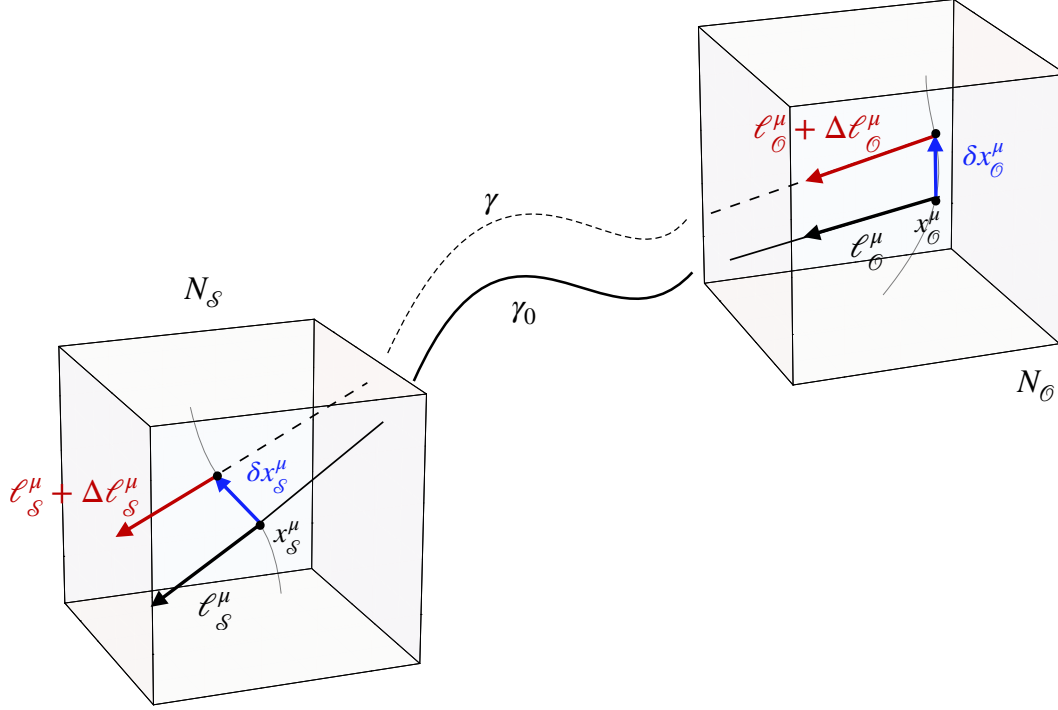


Figure 3.3: The observer \mathcal{O} and the source \mathcal{S} are free to move along their worldlines in the two small regions $N_{\mathcal{O}}$ and $N_{\mathcal{S}}$. The point $x_{\mathcal{S}}^{\mu}$ on the \mathcal{S} 's worldline is connected to $x_{\mathcal{O}}^{\mu}$ on the \mathcal{O} 's worldline by the null geodesic γ_0 . γ_0 can be identified by the initial position and initial tangent vector at the observer $(x_{\mathcal{O}}^{\mu}, \ell_{\mathcal{O}}^{\mu})$. Since the observer and source are free to move, they will be connected at a later time by another geodesic γ identified by the displacement vectors $(\delta x_{\mathcal{O}}^{\mu}, \Delta \ell_{\mathcal{O}}^{\mu})$.

is the corresponding tangent vector at \mathcal{S} . To simplify the notation we will denote $T_{x_{\mathcal{O}}}\mathcal{M}$ by $T_{\mathcal{O}}\mathcal{M}$ and $T_{x_{\mathcal{S}}}\mathcal{M}$ by $T_{\mathcal{S}}\mathcal{M}$. Now, we generalise the definition of light beam by considering all null geodesics connecting points from $N_{\mathcal{O}}$ with $N_{\mathcal{S}}$, which are contained in a four-dimensional tube around γ_0 . We consider that this tube is sufficiently narrow such that we can use the first-order geodesic deviation equation, Eq. (3.26), for describing the deviation between these geodesics. Within this assumptions, the geodesics are uniquely specified by giving their initial points and initial tangent vectors in $N_{\mathcal{O}}$ (or in $N_{\mathcal{S}}$). Alternatively, we can characterize the geodesics by their deviation from the fiducial null geodesic γ_0 : we use this second method of identification, see Figure 3.3, defining the *initial displacement vector* $\delta x(\lambda_{\mathcal{O}}) \in T_{\mathcal{O}}\mathcal{M}$ as the displacement between two nearby geodesics of the family γ and γ_0 at $N_{\mathcal{O}}$

$$\delta x^{\mu}(\lambda_{\mathcal{O}}) \equiv \delta x_{\mathcal{O}}^{\mu} = y_{\mathcal{O}}^{\mu} - x_{\mathcal{O}}^{\mu}, \quad (3.37)$$

where $y_{\mathcal{O}}^{\mu} = \gamma(\lambda_{\mathcal{O}})$ and $x_{\mathcal{O}}^{\mu} = \gamma_0(\lambda_{\mathcal{O}})$. Note that the displacement $\delta x_{\mathcal{O}}^{\mu}$ can be in all spatial and temporal directions. The variation of $\delta x_{\mathcal{O}}^{\mu}$ along the fiducial geodesic gives the *initial direction deviation vector* $\Delta \ell_{\mathcal{O}}^{\mu}$, defined as

$$\Delta \ell_{\mathcal{O}}^{\mu} \equiv \nabla_{\epsilon} \delta x^{\mu}(\lambda)|_{\mathcal{O}} = \delta \ell_{\mathcal{O}}^{\mu} + \Gamma^{\mu}_{\nu\sigma}(x_{\mathcal{O}}) \ell_{\mathcal{O}}^{\nu} \delta x_{\mathcal{O}}^{\sigma}, \quad (3.38)$$

where $\Delta \ell_{\mathcal{O}}^{\mu} \equiv \Delta \ell^{\mu}(\lambda_{\mathcal{O}})$, $\delta \ell_{\mathcal{O}}^{\mu} \equiv \delta \ell^{\mu}(\lambda_{\mathcal{O}}) = \frac{d\delta x^{\mu}}{d\lambda}|_{\mathcal{O}}$, and $\Gamma^{\mu}_{\nu\sigma}(x_{\mathcal{O}})$ are the Christoffel symbols at \mathcal{O} . The pair $(\delta x_{\mathcal{O}}^{\mu}, \Delta \ell_{\mathcal{O}}^{\mu})$ labels all the geodesics in the vicinity of γ_0 and will be referred to as *the displacement vectors*. Let us notice that the choice of setting the initial displacement and direction deviation at $N_{\mathcal{O}}$ is arbitrary. In the rest of the chapter we adopt this choice

but in principle we could choose to parametrise the geodesics of the family by starting from $N_{\mathcal{S}}$ giving $(\delta x_{\mathcal{S}}^{\mu}, \Delta \ell_{\mathcal{S}}^{\mu})$. This second method is described in [89] and it is one of the original results of this thesis.

Since the geodesics are expected to be confined within the narrow tube all along γ_0 , the initial displacement vectors must be small. In this case, their propagation from \mathcal{O} to \mathcal{S} is described by the GDE

$$\nabla_{\ell} \nabla_{\ell} \delta x^{\mu} - R^{\mu}_{\alpha\beta\nu} \ell^{\alpha} \ell^{\beta} \delta x^{\nu} = 0, \quad (3.39)$$

with the initial data

$$\delta x^{\mu}(\lambda)|_{\mathcal{O}} = \delta x_{\mathcal{O}}^{\mu} \quad (3.40)$$

$$\nabla_{\ell} \delta x^{\mu}(\lambda)|_{\mathcal{O}} = \Delta \ell_{\mathcal{O}}^{\mu}. \quad (3.41)$$

The solution gives the displacements at the other end for $\lambda = \lambda_{\mathcal{S}}$: $\delta x^{\mu}(\lambda_{\mathcal{S}}) = \delta x_{\mathcal{S}}^{\mu}$ and $\nabla_{\ell} \delta x^{\mu}(\lambda)|_{\mathcal{S}} = \Delta \ell_{\mathcal{S}}^{\mu}$. The combination $R^{\mu}_{\alpha\beta\nu} \ell^{\alpha} \ell^{\beta}$ is the *optical tidal matrix* expressing the spacetime curvature along the line of sight γ_0 . The condition for applicability of the GDE excludes the possibility of multiple imaging for light rays contained within the tube.

Due to the linearity of the GDE, the solutions at $\lambda_{\mathcal{S}}$ are given as linear combination of the initial conditions $(\delta x_{\mathcal{O}}^{\mu}, \Delta \ell_{\mathcal{O}}^{\mu})$

$$\delta x_{\mathcal{S}}^{\mu} = W_{XX}{}^{\mu}_{\nu} \delta x_{\mathcal{O}}^{\nu} + W_{XL}{}^{\mu}_{\nu} \Delta \ell_{\mathcal{O}}^{\nu} \quad (3.42)$$

$$\Delta \ell_{\mathcal{S}}^{\mu} = W_{LX}{}^{\mu}_{\nu} \delta x_{\mathcal{O}}^{\nu} + W_{LL}{}^{\mu}_{\nu} \Delta \ell_{\mathcal{O}}^{\nu}, \quad (3.43)$$

with W_{XX} , W_{XL} , W_{LX} , W_{LL} being bilocal operators (also known as 2-point tensors [170] or bitensors [144, 183]), acting from $T_{\mathcal{O}}\mathcal{M}$ to $T_{\mathcal{S}}\mathcal{M}$. We refer to the four operators W_{XX} , W_{XL} , W_{LL} and W_{LX} as the *bilocal geodesic operators* (BGO), [88]. In the context of timelike geodesics the first two are the *Jacobi propagators* K and H introduced in [63, 67, 183]. Moreover, the BGO can also be related to the Synge's worldfunction [170, 67, 183]. Recently the BGO defined along a timelike geodesic have been used as a tool to study of the gravitational waves memory effect [80]. Here, we will focus exclusively on the application of the BGO to describe null geodesics as presented in [88]. The notation we introduced in Eqs. (3.42)-(3.43) highlights their relation with the resolvent operator, or the Wroński matrix [81] for the GDE,

$$\mathcal{W} = \begin{pmatrix} W_{XX}{}^{\mu}_{\nu} & W_{XL}{}^{\mu}_{\sigma} \\ W_{LX}{}^{\rho}_{\nu} & W_{LL}{}^{\rho}_{\sigma} \end{pmatrix}. \quad (3.44)$$

$\mathcal{W} = \mathcal{W}(\mathcal{S}, \mathcal{O})$ is the linear mapping between vector sums of two copies of the tangent space, i.e.

$$\mathcal{W} : T_{\mathcal{O}}\mathcal{M} \oplus T_{\mathcal{O}}\mathcal{M} \rightarrow T_{\mathcal{S}}\mathcal{M} \oplus T_{\mathcal{S}}\mathcal{M}, \quad (3.45)$$

defined by the relation

$$\begin{pmatrix} \delta x_{\mathcal{S}}^{\mu} \\ \Delta \ell_{\mathcal{S}}^{\rho} \end{pmatrix} = \begin{pmatrix} W_{XX}{}^{\mu}_{\nu} & W_{XL}{}^{\mu}_{\sigma} \\ W_{LX}{}^{\rho}_{\nu} & W_{LL}{}^{\rho}_{\sigma} \end{pmatrix} \begin{pmatrix} \delta x_{\mathcal{O}}^{\nu} \\ \Delta \ell_{\mathcal{O}}^{\sigma} \end{pmatrix} = \mathcal{W} \begin{pmatrix} \delta x_{\mathcal{O}}^{\nu} \\ \Delta \ell_{\mathcal{O}}^{\sigma} \end{pmatrix}. \quad (3.46)$$

It is also a symplectic mapping, as noted by Uzun [179], since in GR the ordinary differential equations (ODE) for null geodesics can be expressed as a Hamiltonian system, both in general and in the first-order perturbation theory [81]. In contrast to other approaches, here we evaluate displacements in all four dimensions, including time. The Wroński matrix formalism extends to the fully four-dimensional GDE without any problems, preserving its properties (as shown in [163]).

It follows easily from the geodesic deviation equation (3.39) and from Eqs. (3.42)-(3.43) that the BGO can be expressed as solutions to the GDE along γ_0 and with initial data at $\lambda_{\mathcal{O}}$. Let us start by using the fact $\nabla_{\ell}\delta x^{\mu}(\lambda) = \Delta\ell^{\mu}(\lambda)$ to express the GDE (3.39) as a system of two first-order ODE as

$$\begin{cases} \nabla_{\ell}\delta x^{\mu} = \Delta\ell^{\mu} \\ \nabla_{\ell}\Delta\ell^{\rho} = R^{\rho}_{\alpha\beta\nu}\ell^{\alpha}\ell^{\beta}\delta x^{\nu} \end{cases}, \quad (3.47)$$

with initial conditions

$$\delta x^{\mu}(\lambda_{\mathcal{O}}) = \delta x^{\mu}_{\mathcal{O}} \quad (3.48)$$

$$\Delta\ell^{\rho}(\lambda_{\mathcal{O}}) = \Delta\ell^{\rho}_{\mathcal{O}}. \quad (3.49)$$

In a more compact form the system becomes

$$\nabla_{\ell} \begin{pmatrix} \delta x^{\mu} \\ \Delta\ell^{\rho} \end{pmatrix} = \begin{pmatrix} 0 & \delta^{\mu}_{\sigma} \\ R^{\rho}_{\ell\ell\nu} & 0 \end{pmatrix} \begin{pmatrix} \delta x^{\nu} \\ \Delta\ell^{\sigma} \end{pmatrix}, \quad (3.50)$$

where we defined $R^{\rho}_{\alpha\beta\nu}\ell^{\alpha}\ell^{\beta} = R^{\rho}_{\ell\ell\nu}$. Making use of Eq. (3.46), one obtains a matrix ODE for \mathcal{W}

$$\nabla_{\ell}\mathcal{W} = \begin{pmatrix} 0 & \mathbb{1} \\ R_{\ell\ell} & 0 \end{pmatrix} \cdot \mathcal{W}, \quad (3.51)$$

where the dot indicates usual matrix product operation. The initial conditions for the BGO are

$$\mathcal{W} = \mathbb{1}_{8 \times 8}. \quad (3.52)$$

Let us clarify that the action of the covariant derivative is intended as acting on bitensors [144], i.e.

$$\nabla_{\ell}\mathcal{W} = \begin{pmatrix} \partial_{\ell}W_{XX^{\mu}\nu} + \Gamma^{\mu}_{\alpha\beta}W_{XX^{\alpha}\nu}\ell^{\beta} & \partial_{\ell}W_{XL^{\mu}\sigma} + \Gamma^{\mu}_{\alpha\beta}W_{XL^{\alpha}\sigma}\ell^{\beta} \\ \partial_{\ell}W_{LX^{\rho}\nu} + \Gamma^{\rho}_{\alpha\beta}W_{LX^{\alpha}\nu}\ell^{\beta} & \partial_{\ell}W_{LL^{\rho}\sigma} + \Gamma^{\rho}_{\alpha\beta}W_{LL^{\alpha}\sigma}\ell^{\beta} \end{pmatrix}. \quad (3.53)$$

The relations in Eq. (3.51) are the evolution equations for the BGO along γ_0 . They show that the BGO can be expressed as non-local functionals of the Riemann tensor along the line of sight. Even though the GDE and the matrix equations (3.51) are linear, the BGO are *nonlinear* functionals of the curvature tensor along γ_0 . This can be easily checked as follows: let us take two solutions of Eq. (3.51), $\mathcal{W}^{(1)}$ and $\mathcal{W}^{(2)}$, each ones corresponding to two different optical tidal tensor functions, $R_{\ell\ell}^{(1)}$ and $R_{\ell\ell}^{(2)}$

$$\nabla_{\ell}\mathcal{W}^{(1)} = \begin{pmatrix} 0 & \mathbb{1} \\ R_{\ell\ell}^{(1)} & 0 \end{pmatrix} \mathcal{W}^{(1)} \quad (3.54)$$

$$\nabla_{\ell}\mathcal{W}^{(2)} = \begin{pmatrix} 0 & \mathbb{1} \\ R_{\ell\ell}^{(2)} & 0 \end{pmatrix} \mathcal{W}^{(2)}. \quad (3.55)$$

Then let us see if the linear combination of these solutions $a\mathcal{W}^{(1)} + b\mathcal{W}^{(2)}$, with $a, b \in \mathbb{R}$, is also a solution of Eq. (3.51) for the same linear combination of the optical tidal tensor functions, i.e.

$$\nabla_{\ell}(a\mathcal{W}^{(1)} + b\mathcal{W}^{(2)}) = \begin{pmatrix} 0 & \mathbb{1} \\ aR_{\ell\ell}^{(1)} + bR_{\ell\ell}^{(2)} & 0 \end{pmatrix} (a\mathcal{W}^{(1)} + b\mathcal{W}^{(2)}). \quad (3.56)$$

Rearranging the terms we finally get

$$a \left[\nabla_\ell \mathcal{W}^{(1)} - \begin{pmatrix} 0 & \mathbb{1} \\ aR_{\ell\ell}^{(1)} & 0 \end{pmatrix} \mathcal{W}^{(1)} \right] + b \left[\nabla_\ell \mathcal{W}^{(2)} - \begin{pmatrix} 0 & \mathbb{1} \\ bR_{\ell\ell}^{(1)} & 0 \end{pmatrix} \mathcal{W}^{(2)} \right] = b \begin{pmatrix} 0 & 0 \\ aR_{\ell\ell}^{(1)} & 0 \end{pmatrix} \mathcal{W}^{(2)} + a \begin{pmatrix} 0 & 0 \\ bR_{\ell\ell}^{(2)} & 0 \end{pmatrix} \mathcal{W}^{(1)}, \quad (3.57)$$

from which it is easy to see that a linear combination of the solutions of (3.51) *does not* satisfy the same equations proving the nonlinearity of the BGO with respect to the optical tidal tensor¹³. The nonlinearity of the BGO with respect to the curvature reflects the fact that, although they describe small deviations from the fiducial geodesics, the BGO captures all nonlinear effects of light bending combined along γ_0 .

3.2.1 Algebraic properties of the BGO.

From its very definition, the \mathcal{W} matrix satisfies the following properties

$$\mathcal{W}(\mathcal{O}, \mathcal{S}) = \mathcal{W}^{-1}(\mathcal{S}, \mathcal{O}) \quad (3.58)$$

$$\mathcal{W}(\mathcal{S}, \mathcal{O}) = \mathcal{W}(\mathcal{S}, p_\lambda) \mathcal{W}(p_\lambda, \mathcal{O}), \quad (3.59)$$

with p_λ an arbitrary point on the fiducial geodesic γ_0 , [88]. We also have that \mathcal{W} is a symplectic mapping, [179].

Moreover, the properties of the GDE (3.29)-(3.30) can be immediately translated to corresponding properties of the BGO, which hold irrespective of the spacetime geometry or whether γ_0 is null or not, [88]. From the first property, Eqs. (3.29) and (3.28), we have that for any initial data $\delta x_{\mathcal{O}}^\mu$ and $\Delta \ell_{\mathcal{O}}^\mu$ the values of C and D need to remain equal in \mathcal{O} and \mathcal{S} . This means that

$$\ell_{\mathcal{O}\mu} \Delta \ell_{\mathcal{O}}^\mu = \ell_{\mathcal{S}\mu} \Delta \ell_{\mathcal{S}}^\mu \quad (3.60)$$

$$\ell_{\mathcal{O}\mu} \delta x_{\mathcal{O}}^\mu - \lambda_{\mathcal{O}} \ell_{\mathcal{O}\mu} \Delta \ell_{\mathcal{O}}^\mu = \ell_{\mathcal{S}\mu} \delta x_{\mathcal{S}}^\mu - \lambda_{\mathcal{S}} \ell_{\mathcal{S}\mu} \Delta \ell_{\mathcal{S}}^\mu. \quad (3.61)$$

We make use of Eqs.(3.42)-(3.43) in order to express $\delta x_{\mathcal{S}}^\mu$ and $\Delta \ell_{\mathcal{S}}^\mu$ by $\delta x_{\mathcal{O}}^\mu$ and $\Delta \ell_{\mathcal{O}}^\mu$. The resulting equations are equivalent to the following 4 relations:

$$\ell_{\mathcal{S}\mu} W_{XX}{}^\mu{}_\nu = \ell_{\mathcal{O}\nu} \quad (3.62)$$

$$\ell_{\mathcal{S}\mu} W_{XL}{}^\mu{}_\nu = (\lambda_{\mathcal{S}} - \lambda_{\mathcal{O}}) \ell_{\mathcal{O}\nu} \quad (3.63)$$

$$\ell_{\mathcal{S}\mu} W_{LX}{}^\mu{}_\nu = 0 \quad (3.64)$$

$$\ell_{\mathcal{S}\mu} W_{LL}{}^\mu{}_\nu = \ell_{\mathcal{O}\mu}. \quad (3.65)$$

The ‘‘inverted’’ relations are obtained by considering the solution (3.30) at \mathcal{O} and \mathcal{S} : we have $\delta \tilde{x}_{\mathcal{O}}^\mu = \delta x_{\mathcal{O}}^\mu + (E + \lambda_{\mathcal{O}} F) \ell_{\mathcal{O}}^\mu$, $\Delta \tilde{\ell}_{\mathcal{O}}^\mu = \Delta \ell_{\mathcal{O}}^\mu + F \ell_{\mathcal{O}}^\mu$ and $\delta \tilde{x}_{\mathcal{S}}^\mu = \delta x_{\mathcal{S}}^\mu + (E + \lambda_{\mathcal{S}} F) \ell_{\mathcal{S}}^\mu$, $\Delta \tilde{\ell}_{\mathcal{S}}^\mu = \Delta \ell_{\mathcal{S}}^\mu + F \ell_{\mathcal{S}}^\mu$. We substitute these equations to (3.42)-(3.43) and assuming the resulting relations must hold for all E and F we get

$$W_{XX}{}^\mu{}_\nu \ell_{\mathcal{O}}^\nu = \ell_{\mathcal{S}}^\mu \quad (3.66)$$

$$W_{XL}{}^\mu{}_\nu \ell_{\mathcal{O}}^\nu = (\lambda_{\mathcal{S}} - \lambda_{\mathcal{O}}) \ell_{\mathcal{S}}^\mu \quad (3.67)$$

$$W_{LX}{}^\mu{}_\nu \ell_{\mathcal{O}}^\nu = 0 \quad (3.68)$$

$$W_{LL}{}^\mu{}_\nu \ell_{\mathcal{O}}^\nu = \ell_{\mathcal{S}}^\mu. \quad (3.69)$$

¹³In the case $a = b = 1$, the left hand side of Eq (3.57) vanishes while the right hand side is in general non zero.

Finally, let us note that two of the BGO undergo rescaling under the affine reparametrisations of the fiducial null geodesic γ_0 . Namely, under the transformation Eq. (3.15) we have the following rescaling for the BGO¹⁴

$$W_{XX} \rightarrow \tilde{W}_{XX} = W_{XX} \quad (3.70)$$

$$W_{XL} \rightarrow \tilde{W}_{XL} = A \cdot W_{XL} \quad (3.71)$$

$$W_{LX} \rightarrow \tilde{W}_{LX} = \frac{1}{A} \cdot W_{LX} \quad (3.72)$$

$$W_{LL} \rightarrow \tilde{W}_{LL} = W_{LL}. \quad (3.73)$$

3.2.2 BGO for light propagation and the quotient space

The considerations we have made so far are independent of the character of the geodesics we are considering, so they are valid for BGO describing the properties of all types of geodesics in the vicinity of γ_0 . Since our goal is the application of the BGO to describe light propagation, from now on we will consider only families of null geodesics. Let us start by noting that the BGO distinguish differently parametrised geodesics sharing the same path. However, from the point of view of geometric optics, an affine reparametrisation of null geodesics is just a gauge freedom, as we have already discussed in Eq.(3.30). The change in the affine parameter of the geodesics around γ_0 transforms solutions of the GDE ξ^μ as $\tilde{\xi}^\mu = \xi^\mu + \alpha(\lambda)\ell^\mu$, with ξ^μ and $\tilde{\xi}^\mu$ pointing at the same displaced geodesic. Here, we want to isolate this gauge freedom in order to consider only geodesics having different path. In other words, we want to identify the initial data for which the position and directional deviations only differ by a multiple of $\ell^\mu_{\mathcal{O}}$

$$\begin{pmatrix} \delta x_{\mathcal{O}}^\mu \\ \Delta \ell_{\mathcal{O}}^\mu \end{pmatrix} \sim \begin{pmatrix} \delta x_{\mathcal{O}}^\mu + C_1 \ell_{\mathcal{O}}^\mu \\ \Delta \ell_{\mathcal{O}}^\mu + C_2 \ell_{\mathcal{O}}^\mu \end{pmatrix}, \quad (3.74)$$

for some non-vanishing constants C_1 and C_2 . Substituting Eq. (3.74) in Eqs. (3.42)-(3.43), and making use of Eqs. (3.66)-(3.69), we obtain that adding this type of terms in $N_{\mathcal{O}}$ leads to a similar change in the final data

$$\begin{pmatrix} \delta x_{\mathcal{S}}^\mu \\ \Delta \ell_{\mathcal{S}}^\mu \end{pmatrix} \sim \begin{pmatrix} \delta x_{\mathcal{S}}^\mu + D_1 \ell_{\mathcal{S}}^\mu \\ \Delta \ell_{\mathcal{S}}^\mu + D_2 \ell_{\mathcal{S}}^\mu \end{pmatrix}, \quad (3.75)$$

with constants D_1 and D_2 related to C_1 and C_2 . The relation $Y^\mu \sim X^\mu$ in Eqs. (3.74)-(3.75) defines equivalence classes $[X]$ in both $T_{\mathcal{O}}\mathcal{M}$ and $T_{\mathcal{S}}\mathcal{M}$. To remove this gauge freedom, one can consider the BGO as maps between vectors $[X]$ in the quotient spaces $\mathcal{Q}_{\mathcal{O}} = T_{\mathcal{O}}\mathcal{M}/\ell_{\mathcal{O}}$ and $\mathcal{Q}_{\mathcal{S}} = T_{\mathcal{S}}\mathcal{M}/\ell_{\mathcal{S}}$, see Fig. 3.4. The equivalence relation $Y^\mu \sim X^\mu$ effectively suppresses one dimension (the one along the tangent vector) in the tangent spaces in $N_{\mathcal{S}}$ and $N_{\mathcal{O}}$, leaving only three non-trivial directions in \mathcal{Q} .

Let us consider the subspaces $\ell_{\mathcal{O}}^\perp \subset T_{\mathcal{O}}\mathcal{M}$ and $\ell_{\mathcal{S}}^\perp \subset T_{\mathcal{S}}\mathcal{M}$ consisting of all vectors orthogonal to $\ell_{\mathcal{O}}^\mu$ and $\ell_{\mathcal{S}}^\mu$, respectively. In analogy to \mathcal{Q} , it is possible to define the two-dimensional *perpendicular spaces* $\mathcal{P}_{\mathcal{O}} = \ell_{\mathcal{O}}^\perp/\ell_{\mathcal{O}}$ and $\mathcal{P}_{\mathcal{S}} = \ell_{\mathcal{S}}^\perp/\ell_{\mathcal{S}}$ as the subspaces orthogonal to $\ell_{\mathcal{O}}^\mu$ and $\ell_{\mathcal{S}}^\mu$, respectively [110, 88]. The physical meaning of the quotient spaces \mathcal{Q} and \mathcal{P} will be clear once we introduce a reference frame.

¹⁴The derivation of these relations uses the fact that under the affine reparametrisation the tangent to the geodesic transforms as Eq. (3.16). Then one can use the GDE, Eq. (3.51), together with Eqs. (3.66)-(3.69) to obtain the relations Eqs. (3.70)-(3.73).

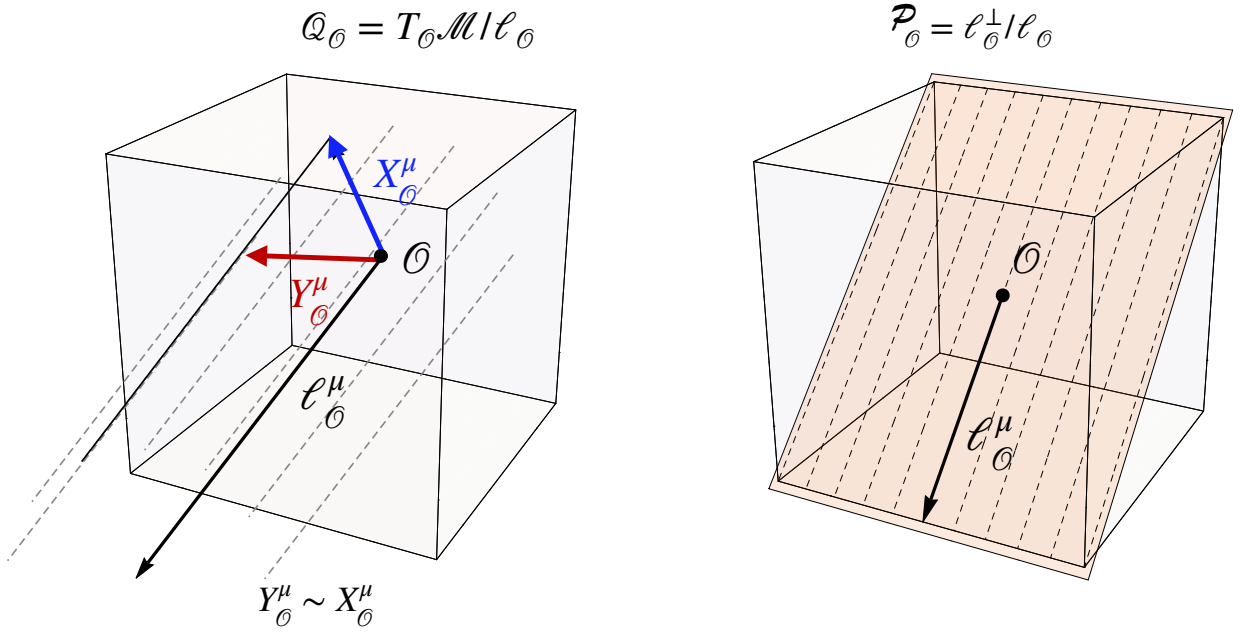


Figure 3.4: Geometry of the quotient spaces \mathcal{Q}_O and \mathcal{P}_O . Elements $[X] \in \mathcal{Q}_O$ correspond to the vectors X^μ and Y^μ in $T_O\mathcal{M}$ identified by the relation $Y^\mu \sim X^\mu$, i.e. such that $Y^\mu = X^\mu + c\ell_O^\mu$. Geometrically is the space containing all geodesics in N_O parallel to γ_0 . Elements $\mathbf{X} \in \mathcal{P}_O$ corresponds to the vectors X^μ and Y^μ in $T_O\mathcal{M}$, which are perpendicular to ℓ_O (i.e. $X^\mu \ell_{O\mu} = 0$ and $Y^\mu \ell_{O\mu} = 0$) and identified by $Y^\mu \sim X^\mu$. Geometrically, \mathcal{P}_O is the space containing the geodesics parallel to γ_0 and lying on the null hypersurface orthogonal to ℓ_O .

3.2.3 The semi-null frame and the observer's sky

Up to this point, the GDE formulation in terms of bilocal operators we just presented is completely covariant, namely it was derived without invoking explicitly a coordinate system or a frame of reference. However, in order to relate the BGO to actual observable quantities, we need to introduce a reference frame. In the context of relativistic geometric optics, it is customary to introduce a frame that relates to the results of observations at \mathcal{O} . The standard approach is to use the Sachs orthonormal frame, consisting of the observer four-velocity u_O^μ , the direction vector r^μ , being the direction from which the observer sees the light coming, and two perpendicular, spatial vectors ϕ_A^μ spanning the so called Sachs screen space [140, 158, 71]. However, here we use a different frame called the *semi-null frame* (SNF) [88], in which the two quotient spaces \mathcal{Q} and \mathcal{P} have a simple physical interpretation. The SNF consists of u_O^μ , the same two perpendicular, spatial vectors ϕ_A^μ and the null vector ℓ^μ instead of r^μ . It is not orthonormal and we can check that the products of the basis vectors read

$$\begin{aligned}
 \ell^\mu \ell_\mu &= 0 \\
 \phi_A^\mu \ell_\mu &= 0 \\
 u_O^\mu \phi_{A\mu} &= 0 \\
 \phi_A^\mu \phi_{B\mu} &= \delta_{AB} \\
 u_O^\mu u_{O\mu} &= -1 \\
 \ell^\mu u_{O\mu} &= Q,
 \end{aligned} \tag{3.76}$$

where we have introduced the constant¹⁵ Q for the product of ℓ^μ and $u_\mathcal{O}^\mu$. We denote the frame indices by boldface letters: capital Latin indices $\mathbf{A}, \mathbf{B}, \dots$, running over the spatial components $\mathbf{1}$ and $\mathbf{2}$, lower case Latin indices i, j, \dots , running over $\mathbf{1}, \mathbf{2}$ and $\mathbf{3}$, and the boldface Greek indices $\boldsymbol{\mu}, \boldsymbol{\nu}, \dots$, running over all 4 dimensions from $\mathbf{0}$ to $\mathbf{3}$. The associated coframe ψ_μ^α is composed of the tetrad of vectors $\psi_\mu^\alpha = (\frac{\ell_\mu}{Q}, \phi_\mu^{\mathbf{A}}, \frac{u_\mu}{Q} + \frac{\ell_\mu}{Q^2})$. In the SNF the displacement vector δx^μ has components $\delta x^\mu = \delta x^\nu \hat{\psi}_\nu^\mu = (\frac{\delta x^\nu \ell_\nu}{Q}, \delta x^\nu \hat{\phi}_\nu^{\mathbf{A}}, \frac{\delta x^\nu u_{\mathcal{O}\nu}}{Q} + \frac{\delta x^\nu \ell_\nu}{Q^2})$, where hatted vectors are parallel transported along the fiducial geodesic γ_0 .

In the SNF the presence of the quotient spaces have a natural explanation: the first three components of the GDE (3.39) in the SNF¹⁶

$$\frac{d^2 \delta x^{\mathbf{0}}}{d\lambda^2} = 0 \quad (3.77)$$

$$\frac{d^2 \delta x^{\mathbf{A}}}{d\lambda^2} = R^{\mathbf{A}}{}_{\ell\mathbf{0}} \delta x^{\mathbf{0}} + R^{\mathbf{A}}{}_{\ell\mathbf{B}} \delta x^{\mathbf{B}}, \quad (3.78)$$

decouple from the fourth one, $\frac{d^2 \delta x^{\mathbf{3}}}{d\lambda^2} = R^{\mathbf{3}}{}_{\ell\mathbf{0}} \delta x^{\mathbf{0}} + R^{\mathbf{3}}{}_{\ell\mathbf{B}} \delta x^{\mathbf{B}}$. Moreover, from $\frac{d^2 \delta x^{\mathbf{0}}}{d\lambda^2} = 0$ we have that $\delta x^{\mathbf{0}} = \frac{\delta x^\mu \ell_\mu}{Q} = \text{const}$, according to Eq. (3.29) for null geodesics in the flat lightcones approximation, in which we have $\frac{d\delta x^{\mathbf{0}}}{d\lambda} \propto \ell_\mu \Delta \ell^\mu = 0$.

Geometrically, the condition $\ell_{\mathcal{O}\mu} \delta x_{\mathcal{O}}^\mu = \ell_{\mathcal{S}\mu} \delta x_{\mathcal{S}}^\mu$ defines foliations of $N_{\mathcal{O}}$ and $N_{\mathcal{S}}$ by families of null hypersurfaces, see Fig. 3.5, implying that the observers located on a leaf in $N_{\mathcal{O}}$ can only perceive the events lying on the corresponding leaf in $N_{\mathcal{S}}$, as explained in [88]. The interpretation of the two null foliations is straightforward: at two ends of γ_0 the foliations $\delta x^\mu \ell_\mu = \text{const}$ are the degenerate families of light cones centred at the opposite ends of γ_0 . In other words, the past lightcone of the point p in $N_{\mathcal{O}}$ degenerate to a flat hypersurface in $N_{\mathcal{S}}$ due to the large distance between the two regions and their small size. Similarly, the future light cone of any point on that null hypersurface will degenerate to the null hypersurface containing p in $N_{\mathcal{O}}$. These clarifies the name used for the condition $\ell_\mu \Delta \ell^\mu = 0$. In the special case $\delta x^{\mathbf{0}} = 0$, Eqs. (3.78) decouple from Eq. (3.77), and their solutions $(\delta x^{\mathbf{A}}, \Delta \ell^{\mathbf{A}})$ form a subspace of solutions in \mathcal{P} .

Vectors expressed in the SNF have a very simple representation in the quotient spaces $\mathcal{Q}_{\mathcal{O}} = T_{\mathcal{O}}\mathcal{M}/\ell_{\mathcal{O}}$ and $\mathcal{Q}_{\mathcal{S}} = T_{\mathcal{S}}\mathcal{M}/\ell_{\mathcal{S}}$. In fact, for vectors $[X] \in \mathcal{Q}$ we can “forget” about the fourth component $X^{\mathbf{3}}$, namely $(X^{\mathbf{0}}, X^{\mathbf{1}}, X^{\mathbf{2}}, X^{\mathbf{3}}) \rightarrow (X^{\mathbf{0}}, X^{\mathbf{1}}, X^{\mathbf{2}})$. Similarly, vectors in any perpendicular subspace \mathcal{P} along γ_0 have additionally vanishing first component, i.e. $(0, X^{\mathbf{1}}, X^{\mathbf{2}})$.

The introduction of a frame is mandatory to perform measurements like the positions of celestial objects: the observer \mathcal{O} sees the source \mathcal{S} in the direction corresponding to the line of sight γ_0 as

$$r_0^\mu = \frac{1}{\ell_\sigma u_{\mathcal{O}}^\sigma} \ell^\mu + u_{\mathcal{O}}^\mu. \quad (3.79)$$

The direction r_0^μ serves as a reference point on the observer screen, indeed in the SNF gives $r_0^{\mathbf{A}} = (0, 0)$. Similarly, for the geodesic γ emitted by a another source \mathcal{S}' in $N_{\mathcal{S}}$, the observer sees the light from the direction

$$r^\mu = \frac{1}{k_\sigma u_{\mathcal{O}}^\sigma} k^\mu + u_{\mathcal{O}}^\mu, \quad (3.80)$$

¹⁵Note that the sign of the constant Q depends on the temporal orientation of ℓ^μ . The standard convention in cosmology is to consider the tangent vector past-oriented, from the observer \mathcal{O} to the source \mathcal{S} , which cause to have $Q > 0$. However, we will later consider the case when ℓ^μ is future-oriented and in that case $Q < 0$.

¹⁶The optical tidal matrix in the SNF components is defined as $R^\mu{}_{\ell\nu} = \hat{\psi}_\rho^\mu R^\rho{}_{\ell\sigma} \hat{\phi}_\nu^\sigma$ and from the symmetries of the Riemann tensor follows that $R^{\mathbf{0}}{}_{\ell\ell\nu} = R^\mu{}_{\ell\ell\mathbf{3}} = 0$.

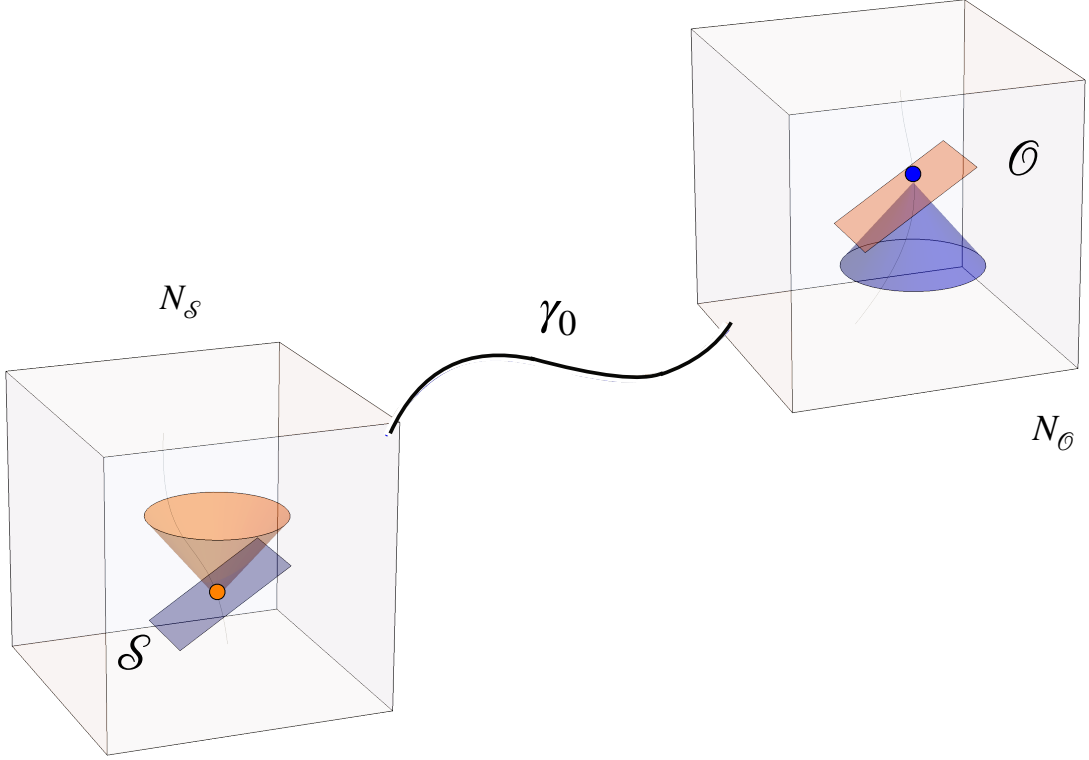


Figure 3.5: The past light cone (blue) in $N_{\mathcal{O}}$ degenerates to the flat null hypersurface (blue plane) in $N_{\mathcal{S}}$. Similarly, the future light cone (orange) in $N_{\mathcal{S}}$ degenerates to the flat null hypersurface (orange plane) in $N_{\mathcal{O}}$. \mathcal{O} can observe only those events on the corresponding hypersurface in $N_{\mathcal{S}}$.

where k^μ is the tangent vector of the geodesic. The position of \mathcal{S}' is identified by the observer \mathcal{O} measuring the angle between r_0^μ and r^μ , that for a source which lies close¹⁷ to r_0^μ is simply

$$\delta\theta^A \approx r^A. \quad (3.81)$$

Therefore, all objects in the observer's view can be conceived as being projected on an ideal sphere, representing the observer's sky, where the apparent positions of objects in the sky are determined from the transversal components of r^μ in the semi-null frame of the observer, denoted as r^A . The expression Eq. (3.79) defines an observer-dependent mapping from the set of null tangent vectors $\mathcal{N}_{\mathcal{O}} = \{\ell \in T_{\mathcal{O}}\mathcal{M} | \ell^\mu \ell_\mu = 0, \ell^0 < 0\}$ to the observer's sky of directions $\text{Dir}(u_{\mathcal{O}}) = \{r \in T_{\mathcal{O}}\mathcal{M} | r^\mu r_\mu = 1, u_{\mathcal{O}}^\mu r_\mu = 0\}$, i.e. the set of normalised, purely spatial vectors for the observer [139, 119, 110, 88].

The introduction of the observer's sky provides an observer-dependent method to identify the apparent position of sources. Now we will see how observations made by observers with different four-velocities and at different points in $N_{\mathcal{O}}$ may be compared. This is not a simple task in a generic spacetime because the position on the sky is a vector in the observer-dependent space of directions. Let us split the task in two simpler problems:

1. how do we compare position vectors at different points,
2. how do we compare directions on the sky measured by observers boosted with respect to each other.

¹⁷The approximation is valid for $\delta\theta^A \ll 1$ rad. The relation for larger angles requires the use of the standard trigonometric formulae.

The first issue is overcome by the assumed flatness of $N_{\mathcal{O}}$, which allows to use the parallel propagation of the frame for \mathcal{O} to identify $T_{\mathcal{O}}\mathcal{M}$ as the tangent space at all points. Thus, we can introduce a parallel propagated SNF $\phi_{\alpha}^{\mu} = (u_{\mathcal{O}}^{\mu}, \phi_{\mathbf{A}}^{\mu}, \ell_{\mathcal{O}}^{\mu})$ from \mathcal{O} throughout the whole region $N_{\mathcal{O}}$ to compare vector or tensor defined at different points. From now on all equations are expressed in this type of parallel transported SNF at $N_{\mathcal{O}}$ (and a similar one at $N_{\mathcal{S}}$). The tangent vector of γ_0 is $\ell_{\mathcal{O}}^{\mu}$, while for the other null geodesics the tangent vector is simply $k_{\mathcal{O}}^{\mu} = \ell_{\mathcal{O}}^{\mu} + \Delta\ell_{\mathcal{O}}^{\mu}$. Then, the direction vector r^{μ} in the SNF of the observer $u_{\mathcal{O}}^{\mu}$ become

$$\begin{aligned} r^{\mathbf{A}} &= r^{\mu} \phi_{\mu}^{\mathbf{A}} = \left(\frac{\ell_{\mathcal{O}}^{\mu} + \Delta\ell_{\mathcal{O}}^{\mu}}{u_{\mathcal{O}\sigma} (\ell_{\mathcal{O}}^{\sigma} + \Delta\ell_{\mathcal{O}}^{\sigma})} + u_{\mathcal{O}}^{\mu} \right) \phi_{\mu}^{\mathbf{A}} = \frac{\Delta\ell_{\mathcal{O}}^{\mathbf{A}}}{u_{\mathcal{O}\sigma} (\ell_{\mathcal{O}}^{\sigma} + \Delta\ell_{\mathcal{O}}^{\sigma})} \\ &= \frac{\Delta\ell_{\mathcal{O}}^{\mathbf{A}}}{u_{\mathcal{O}\sigma} \ell_{\mathcal{O}}^{\sigma} \left(1 + \frac{u_{\mathcal{O}\sigma} \Delta\ell_{\mathcal{O}}^{\sigma}}{u_{\mathcal{O}\sigma} \ell_{\mathcal{O}}^{\sigma}} \right)} = \frac{\Delta\ell_{\mathcal{O}}^{\mathbf{A}}}{u_{\mathcal{O}\sigma} \ell_{\mathcal{O}}^{\sigma}} \left(1 - \frac{\Delta\ell_{\mathcal{O}}^{\mathbf{0}}}{u_{\mathcal{O}\sigma} \ell_{\mathcal{O}}^{\sigma}} + \Delta\ell_{\mathcal{O}}^{\mathbf{3}} \right)^{-1}, \end{aligned} \quad (3.82)$$

where in the last equality we have used Eq. (3.76) to express

$$u_{\mathcal{O}\sigma} \Delta\ell_{\mathcal{O}}^{\sigma} = u_{\mathcal{O}\sigma} (\phi_{\nu}^{\sigma} \Delta\ell_{\mathcal{O}}^{\nu}) = -\Delta\ell_{\mathcal{O}}^{\mathbf{0}} + u_{\mathcal{O}\sigma} \ell_{\mathcal{O}}^{\sigma} \Delta\ell_{\mathcal{O}}^{\mathbf{3}}. \quad (3.83)$$

Let us remark that we are in the regime of the first-order GDE, so we only need to consider linear terms in the displacement (and its derivatives). This is indeed the condition of the FLA, i.e. $\ell_{\mathcal{O}\mu} \Delta\ell_{\mathcal{O}}^{\mu} = 0$, that we have considered in Eq. (3.36). If we express this condition in the SNF we have $0 = \ell_{\mathcal{O}\mu} (\phi_{\nu}^{\mu} \Delta\ell_{\mathcal{O}}^{\nu}) = \ell_{\mathcal{O}\mu} (u_{\mathcal{O}}^{\mu} \Delta\ell_{\mathcal{O}}^{\mathbf{0}})$, or in other words the FLA gives that $\Delta\ell_{\mathcal{O}}^{\mathbf{0}}$ is an higher-order correction. Now, we can expand Eq. (3.82) in terms of the components of the direction deviation vector $\Delta\ell$, to obtain

$$r^{\mathbf{A}} = \frac{\Delta\ell_{\mathcal{O}}^{\mathbf{A}}}{u_{\mathcal{O}\sigma} \ell_{\mathcal{O}}^{\sigma}} (1 - \Delta\ell_{\mathcal{O}}^{\mathbf{3}}) + h.o.t. = \frac{\Delta\ell_{\mathcal{O}}^{\mathbf{A}}}{u_{\mathcal{O}\sigma} \ell_{\mathcal{O}}^{\sigma}} + h.o.t. \quad (3.84)$$

From Eq. (3.42), the direction deviation vector $\Delta\ell_{\mathcal{O}}^{\mathbf{A}}$ is related to the BGO as

$$\Delta\ell_{\mathcal{O}}^{\mathbf{A}} = (W_{XL}^{-1})^{\mathbf{A}}_{\nu} [\delta x_{\mathcal{S}}^{\nu} - W_{XX}{}^{\nu}{}_{\sigma} \delta x_{\mathcal{O}}^{\sigma}]. \quad (3.85)$$

Should be emphasised that the vector $[\delta x_{\mathcal{S}}^{\mu} - W_{XX}{}^{\mu}{}_{\sigma} \delta x_{\mathcal{O}}^{\sigma}]$ is an element of the perpendicular space $\ell_{\mathcal{S}}^{\perp}$, in fact from Eq. (3.61) for null geodesics in the FLA and Eq. (3.62) follow that [88]

$$\ell_{\mathcal{S}\mu} \delta x_{\mathcal{S}}^{\mu} - \ell_{\mathcal{S}\mu} W_{XX}{}^{\mu}{}_{\sigma} \delta x_{\mathcal{O}}^{\sigma} = \ell_{\mathcal{S}\mu} \delta x_{\mathcal{S}}^{\mu} - \ell_{\mathcal{O}\sigma} \delta x_{\mathcal{O}}^{\sigma} = 0. \quad (3.86)$$

Therefore, although $\delta x_{\mathcal{S}}^{\mu}$ and $W_{XX}{}^{\mu}{}_{\sigma} \delta x_{\mathcal{O}}^{\sigma}$ are not necessarily orthogonal to $\ell_{\mathcal{S}}^{\mu}$, the combination $[\delta x_{\mathcal{S}} - W_{XX}(\delta x_{\mathcal{O}})]^{\mu}$ certainly is¹⁸, and it can be pulled back to the quotient space $\mathcal{P}_{\mathcal{S}}$ to finally obtain

$$r^{\mathbf{A}} = \frac{(W_{XL}^{-1})^{\mathbf{A}}_{\mathbf{B}}}{u_{\mathcal{O}\sigma} \ell_{\mathcal{O}}^{\sigma}} [\delta x_{\mathcal{S}} - W_{XX}(\delta x_{\mathcal{O}})]^{\mathbf{B}}. \quad (3.87)$$

The second question is how we compare directions registered by another observer \mathcal{O}' with a different four-velocity $U_{\mathcal{O}}^{\mu}$. As for \mathcal{O} , we introduce a SNF $f_{\alpha}^{\mu} = (U_{\mathcal{O}}^{\mu}, f_{\mathbf{A}}^{\mu}, \ell_{\mathcal{O}}^{\mu})$ adapted to the observer \mathcal{O}' that is used to define directions on $U_{\mathcal{O}}^{\mu}$'s sky. The relation between directions measured by the two observers is contained in the expression of the spatial vectors $f_{\mathbf{A}}^{\mu}$ in components of ϕ_{α}^{μ}

$$f_{\mathbf{A}}^{\mu} = \omega^{\mathbf{B}}{}_{\mathbf{A}} \phi_{\mathbf{B}}^{\mu} + C_{\mathbf{A}} \ell_{\mathcal{O}}^{\mu}, \quad (3.88)$$

where the coefficients $\omega^{\mathbf{B}}{}_{\mathbf{A}}$ and $C_{\mathbf{A}}$ are found using the relations for the SNF. In particular, from $f_{\mathbf{A}}^{\mu} (f_{\mathbf{B}})_{\mu} = \delta_{\mathbf{A}\mathbf{B}}$ follows that $\omega^{\mathbf{B}}{}_{\mathbf{A}} \omega^{\mathbf{D}}{}_{\mathbf{C}} \delta_{\mathbf{B}\mathbf{D}} = \delta_{\mathbf{A}\mathbf{C}}$. In the case that $f_{\mathbf{A}}^{\mu}$ and $\phi_{\mathbf{A}}^{\mu}$ have the

¹⁸Since $\Delta\ell_{\mathcal{O}} \in \mathcal{P}_{\mathcal{O}}$, this implies also that $W_{XL}{}^{\mathbf{A}}{}_{\mathbf{B}} : \mathcal{P}_{\mathcal{O}} \rightarrow \mathcal{P}_{\mathcal{S}}$ is the operator mapping direction deviations in $\mathcal{P}_{\mathcal{O}}$ to images in $\mathcal{P}_{\mathcal{S}}$.

same orientation, i.e. $\det(\omega^{\mathbf{B}}_{\mathbf{A}}) > 0$, then the matrix coefficient $\omega \in SO(2)$. In conclusion, Eq. (3.88) tell us that the two screen vectors are related by a rotation around the direction vector r^μ and possibly by a component along $\ell_{\mathcal{O}}^\mu$. We can always choose the spatial vectors $f_{\mathbf{A}}^\mu$ aligned along $\phi_{\mathbf{A}}^\mu$, such that $f_{\mathbf{A}}^\mu = \phi_{\mathbf{A}}^\mu + C_{\mathbf{A}} \ell_{\mathcal{O}}^\mu$, with appropriate C_1 and C_2 [110]. The two pairs of vectors $f_{\mathbf{A}}^\mu$ and $\phi_{\mathbf{A}}^\mu$ belong to the same equivalence classes in $\mathcal{P}_{\mathcal{O}}$. This way both $u_{\mathcal{O}}^\mu$ and U^μ may use the fiducial null vector $\ell_{\mathcal{O}}^\mu$ to provide the reference direction on their skies and the screen vectors $\phi_{\mathbf{A}}^\mu$ and $f_{\mathbf{A}}^\mu$ as the two perpendicular vectors on the celestial sphere. Now, the two spatial components of the direction vector $r^{\mathbf{A}}$ can be used to compare the registered directions on the sky between the two observers. In general, to any SNF $(u^\mu, \phi_{\mathbf{A}}^\mu, \ell_{\mathcal{O}}^\mu)$ we can take $\mathbf{u} = [u]$, $\phi_{\mathbf{A}} = [\phi_{\mathbf{A}}]$ to obtain a frame $(\mathbf{u}, \phi_{\mathbf{A}})$ in $\mathcal{Q}_{\mathcal{O}}$ and a frame $(\phi_{\mathbf{A}})$ in $\mathcal{P}_{\mathcal{O}}$. By parallel propagating the SNF and repeating this procedure we obtain similar parallel propagated frames $(\hat{u}^\mu, \hat{\phi}_{\mathbf{A}}^\mu, \hat{\ell}_{\mathcal{O}}^\mu)$, $(\hat{\mathbf{u}}, \hat{\phi}_{\mathbf{A}})$ and $(\hat{\phi}_{\mathbf{A}})$, in $T_p\mathcal{M}$, \mathcal{Q}_p and \mathcal{P}_p , respectively.

3.3 Observables with the BGO: momentary observables and drift effects

In this section we apply the machinery of the BGO to compute multiple observables within the same framework. We show the derivation of the angular diameter distance, the parallax distance, the position drift, and the redshift drift as functionals of the BGO, following the results in [140, 110, 88, 109]. We also recall the definition of the redshift and the luminosity distance, as these are fundamental quantities in cosmology.

3.3.1 The redshift

The redshift is a dimensionless quantity which measures the relative difference in the light wavelength between the emission and the observation points. In our system, the photons travelling along γ_0 from the source \mathcal{S} to the observer \mathcal{O} will experience the redshift z

$$1 + z = \frac{(\ell_\sigma u^\sigma)|_{\mathcal{S}}}{(\ell_\sigma u^\sigma)|_{\mathcal{O}}}, \quad (3.89)$$

where ℓ^σ is the tangent to γ_0 , and $u_{\mathcal{O}}^\sigma$ and $u_{\mathcal{S}}^\sigma$ are the observer and source four-velocities. In practical applications we distinguish the following sources of the redshift:

- when \mathcal{S} and \mathcal{O} are moving with respect to each other, we have *the relativistic Doppler effect*,
- when \mathcal{S} is immersed in a different gravitational potential than \mathcal{O} , i.e. when one end of γ_0 is in a region of the spacetime more curved than the other end, we have *the gravitational redshift*,
- when the spacetime between \mathcal{S} and \mathcal{O} is expanding, we have *the cosmological redshift*.

In FLRW spacetimes, the cosmological redshift is directly related to the scale factor $1 + z = a_0/a$ and can be used as an independent variable to express other quantities, such as distance measurements.

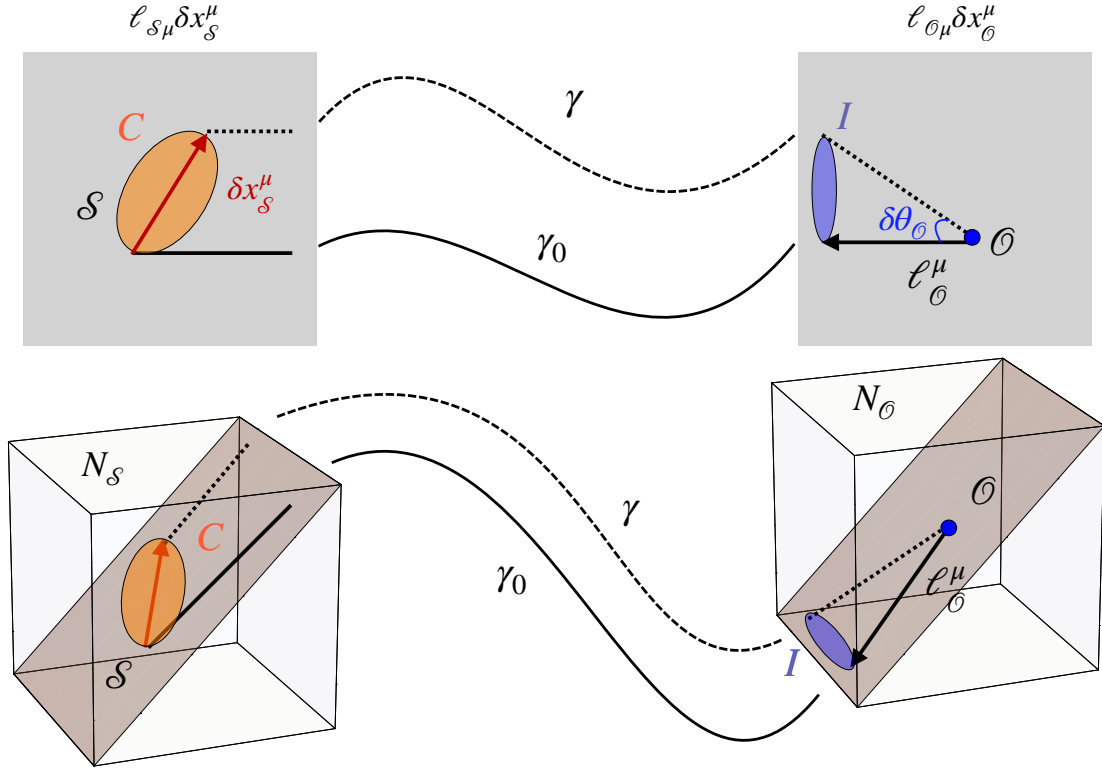


Figure 3.6: On the null hypersurface $\ell_{S\mu}\delta x_S^\mu = 0$ the cross section C of the source \mathcal{S} has area A_S . On the corresponding null hypersurface $\ell_{O\mu}\delta x_O^\mu = 0$, the observer \mathcal{O} measures the solid angle Ω_O occupied by the image I of the source.

3.3.2 The angular diameter distance

In astronomy there are several methods to measure the distance of faraway objects, each based on different techniques. The *angular diameter distance* (or *area distance*¹⁹) is a measure of distance based on the idea that the farther away an object is, the smaller it appears to be, and it is defined as

$$D_{ang} = \sqrt{\left| \frac{A_S}{\Omega_O} \right|}, \quad (3.90)$$

with A_S being the area of the cross-section C of the emitting body measured in its own frame $\phi_{S\nu}^\mu$, and Ω_O is the solid angle²⁰ occupied by the image I in the observer's celestial sphere, see Fig. 3.6. Now, the area and the solid angle can be expressed in terms of the deviation vector δx^μ as

$$A_S = \int_C \delta x_S^1 \wedge \delta x_S^2$$

$$\Omega_O = \int_I \delta \theta_O^1 \wedge \delta \theta_O^2 = \frac{1}{(u_{O\sigma} \ell_O^\sigma)^2} [\det(W_{XL}{}^A{}_B)]^{-1} \int_C \delta x_S^1 \wedge \delta x_S^2, \quad (3.91)$$

where we have used Eq. (3.87) with $\delta x_O^\mu = 0$ to express small angles $\delta \theta^A \sim r^A$. Inserting Eqs. (3.91) in the definition Eq. (3.90) we obtain the angular diameter distance in terms of

¹⁹Actually, the angular diameter distance and the area distance have different definitions, as pointed out in [140]. However, here we will consider the two as synonyms to the definition in Eq. (3.90).

²⁰Note that A_S and Ω_O are signed quantities depended on the orientation. To remove this dependence we have introduced an absolute value in Eq. (3.90).

BGO as

$$D_{ang} = (\ell_\sigma u^\sigma)|_{\mathcal{O}} |\det(W_{XL}^{\mathbf{A}})|^{\frac{1}{2}}. \quad (3.92)$$

By direct comparison with the standard definition of the angular diameter distance, see e.g. [140], we have that the two-by-two submatrix of W_{XL} is the well-known Jacobi operator $\mathcal{D}_{\mathbf{B}}^{\mathbf{A}}$, namely the map between physical separations $\delta x_{\mathcal{S}}^{\mathbf{A}}$ at the source position and direction deviations $\Delta \ell_{\mathcal{O}}^{\mathbf{A}}$ at the observer position.

3.3.3 The luminosity distance

Similar to the angular diameter distance, the *luminosity distance* is based on the idea that the farther away an object is located, the fainter appears its light. Indeed, if we consider an isotropic light emission, the energy flux of the light F decreases with distance from the source D according to the flux-luminosity relation $F = L/(4\pi D^2)$. The luminosity distance is then defined as the ratio between the luminosity L of the source and the flux measured at the observer

$$D_{lum} = \sqrt{\frac{L}{4\pi F}}. \quad (3.93)$$

As we did for D_{ang} , also in this case we can express eq. (3.93) in terms of geometrical quantities by inverting the role of observer and emitter and calculating the flux of photons. However, in this case we prefer to use the well-known result obtained by Etherington, see [76, 77], that relates the luminosity distance D_{lum} to the angular diameter distance D_{ang} via the *distance duality relation*

$$D_{lum} = (1 + z)^2 D_{ang}. \quad (3.94)$$

3.3.4 The parallax and the parallax distance

Another distance estimator in astronomy is the parallax distance, called this way because it takes into account the apparent change in position of a source on the celestial sphere when viewed from at least two different viewpoints, known as the parallax effect. Unlike angular diameter distance or luminosity distance, it does not require knowledge of the source's properties. For this reason, parallax is an attractive method of measuring distance. However, studying the parallax of distant objects is complex and requires accurate astrometric measurements [65, 120, 98]. On top of that, the parallax has a straightforward interpretation only in a flat space and in non-relativistic context: its generalization to general relativity is more cumbersome, generating confusion on its interpretation [128, 186, 104, 156, 152, 124]. A covariant treatment of cosmic parallax was proposed by Räsänen in [152], where the author distinguishes different definitions of parallax by the distance between observation points $\delta x_{\mathcal{O}}^\mu$. In the following we will focus on two definitions of parallax: the classic parallax, that we use to define the (classical) parallax distance, and the position drift.

Let us examine the classic parallax of a source \mathcal{S} as it is seen by a number of observers in $N_{\mathcal{O}}$. The observers are chosen such that they all perceive signals emitted exactly at the same moment by \mathcal{S} . In other words, all observation points lie on the same null hypersurface $\delta x_{\mathcal{O}}^\mu \ell_{\mathcal{O}\mu} = \text{const}$: for simplicity we assume that the observers are comoving²¹ and they all perform the measurement when their worldlines cross the null hypersurface $\delta x_{\mathcal{O}}^\mu \ell_{\mathcal{O}\mu} = 0$. Therefore, at the moment of observation we have $[\delta x_{\mathcal{O}}] \in \mathcal{P}_{\mathcal{O}}$ for the equivalence class of their displacement vectors, see Fig. 3.7.

²¹This way we do not need to consider the aberration effects when comparing the results of their measurements.

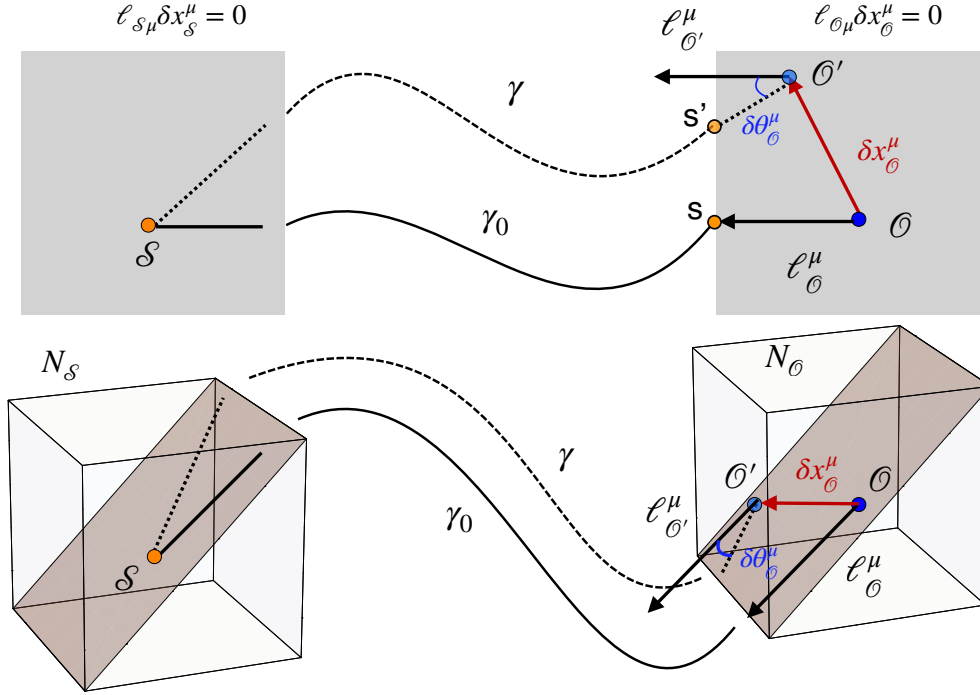


Figure 3.7: The worldlines of two observers \mathcal{O} and \mathcal{O}' cross the same null hypersurface $\delta x_{\mathcal{O}}^\mu \ell_{\mathcal{O}\mu} = 0$ and observe the source \mathcal{S} , which lies on the corresponding null hypersurface $\delta x_{\mathcal{S}}^\mu \ell_{\mathcal{S}\mu} = 0$ in $N_{\mathcal{S}}$. \mathcal{O} and \mathcal{O}' are displaced by $\delta x_{\mathcal{O}}^\mu$, and they perceive the source in the apparent positions \mathbf{s} and \mathbf{s}' , respectively. The difference between \mathbf{s} and \mathbf{s}' gives the parallax angle $\delta\theta_{\mathcal{O}}^\mu$. On the screen $\hat{\phi}_{\mathcal{A}}^\mu$, the displacement $\delta x_{\mathcal{O}}^{\mathcal{A}}$ and the angular distance $\delta\theta_{\mathcal{O}}^{\mathcal{A}}$ are related by the parallax matrix $\Pi^{\mathcal{A}}_{\mathcal{B}}$.

The difference in the apparent position of the source, as measured by the two observers \mathcal{O} and \mathcal{O}' , defines the classic parallax. Using Eq. (3.87) with $\delta x_{\mathcal{S}}^\mu = 0$ the classic parallax takes the form

$$\delta\theta_{\mathcal{O}}^{\mathcal{A}} = -\frac{1}{\ell_{\mathcal{O}\sigma} u_{\mathcal{O}}^\sigma} (W_{XL}^{-1})^{\mathcal{A}}_{\mathcal{B}} W_{XX}^{\mathcal{B}}{}_{\mathcal{C}} \delta x_{\mathcal{O}}^{\mathcal{C}}. \quad (3.95)$$

The product

$$\Pi^{\mathcal{A}}_{\mathcal{B}} = \frac{1}{\ell_{\mathcal{O}\sigma} u_{\mathcal{O}}^\sigma} (W_{XL}^{-1})^{\mathcal{A}}_{\mathcal{B}} W_{XX}^{\mathcal{B}}{}_{\mathcal{C}}, \quad (3.96)$$

defines the observer-dependent *parallax matrix*, namely the map between perpendicular displacement on the observer's side $\delta x_{\mathcal{O}}^{\mathcal{A}}$, and two-dimensional angles $\delta\theta_{\mathcal{O}}^{\mathcal{A}}$ measuring the observed position on the sky in comparison with the position observed by \mathcal{O}' at \mathcal{O} , see Fig. 3.8.

In astronomy the parallax has been used to measure the distances to objects up to few kiloparsecs [142, 153]. In the following we present the parallax distance formula in terms of BGO²² by using the definition of the classic parallax discussed earlier. Let us consider an observer \mathcal{O} and two additional observers \mathcal{O}_1 and \mathcal{O}_2 , comoving with \mathcal{O} and such that their displacement with respect to \mathcal{O} are on $\mathcal{P}_{\mathcal{O}}$. We also introduce a screen frame $[\hat{\phi}_{\mathcal{A}}] \in \mathcal{P}_{\mathcal{O}}$, which is parallel transported on $N_{\mathcal{O}}$. The three observers define a triangle T_2 on the screen space perpendicular to $\ell_{\mathcal{O}}$ with area $A_{\mathcal{O}} = \int_{T_2} \delta x_{\mathcal{O}}^1 \wedge \delta x_{\mathcal{O}}^2$. Now, the observers measure the apparent position of a source \mathcal{S} and, using the parallel transported frame, they combine their

²²As noted in [152, 88], for curved spacetimes the trigonometric parallax angle depends on the direction of the baseline $\delta x_{\mathcal{O}}^\mu$. To overcome this problem, we use the baseline-averaged definition of parallax distance as presented in [88].

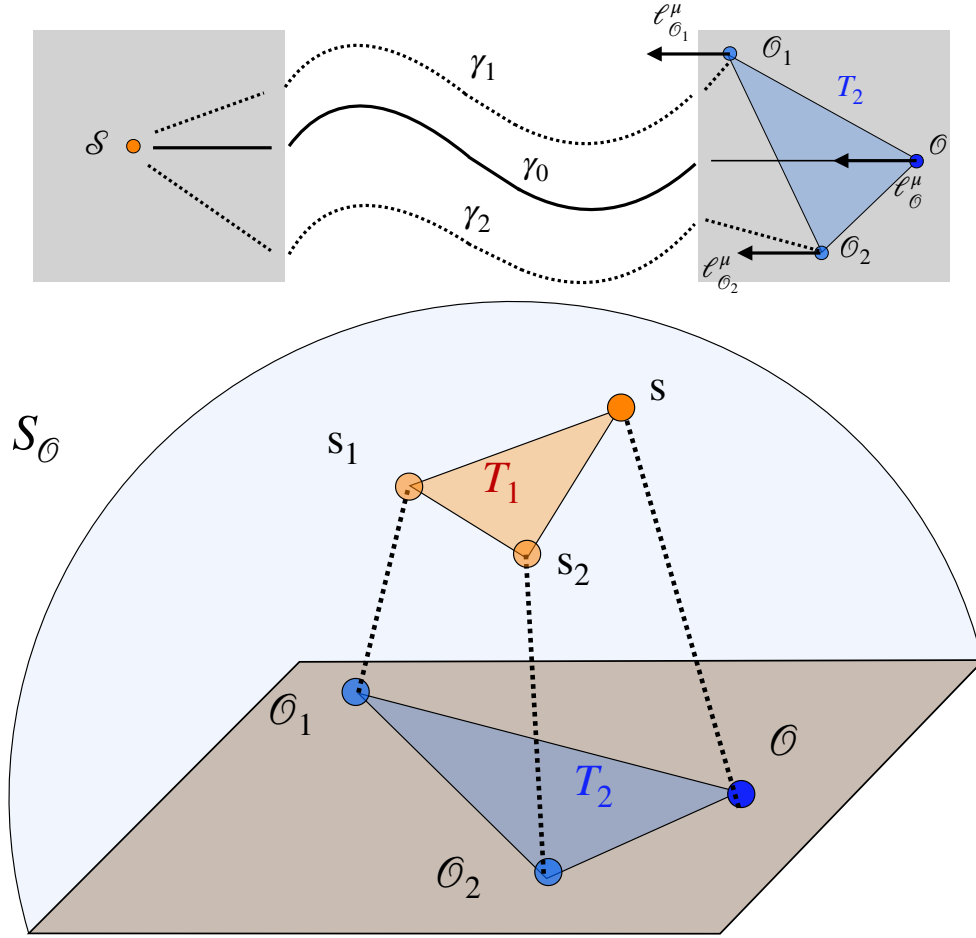


Figure 3.8: The source \mathcal{S} is observed by \mathcal{O} , \mathcal{O}_1 , and \mathcal{O}_2 in $N_{\mathcal{O}}$. The positions of the three observers form the blue triangle T_2 in the space perpendicular to $\ell_{\mathcal{O}}$. Similarly, on the shared celestial sphere $S_{\mathcal{O}}$, the apparent positions of the source \mathbf{s} , \mathbf{s}_1 , and \mathbf{s}_2 form the orange triangle T_1 . The parallax distance is defined as the ratio between the area of T_2 and the solid angle of T_1 .

observations on a shared celestial sphere $S_{\mathcal{O}}$, see Fig. 3.8. The combined observation form a solid triangle T_1 on $S_{\mathcal{O}}$. Denoting as $\Omega_{\mathcal{O}} = \int_{T_1} \delta\theta_{\mathcal{O}}^1 \wedge \delta\theta_{\mathcal{O}}^2$ the solid angle taken up by T_1 , we define the parallax distance as

$$D_{par} = \sqrt{\left| \frac{A_{\mathcal{O}}}{\Omega_{\mathcal{O}}} \right|}. \quad (3.97)$$

Using Eq. (3.95) to express the solid angle, i.e.

$$\Omega_{\mathcal{O}} = \int_{T_1} \delta\theta_{\mathcal{O}}^1 \wedge \delta\theta_{\mathcal{O}}^2 = \frac{1}{(\ell_{\mathcal{O}\sigma} u^{\sigma})^2} \det[(W_{XL}^{-1})^{\mathbf{A}}_{\mathbf{B}} W_{XX}^{\mathbf{B}}_{\mathbf{C}}] \int_{T_2} \delta x_{\mathcal{O}}^1 \wedge \delta x_{\mathcal{O}}^2, \quad (3.98)$$

the expression for the parallax distance becomes

$$D_{par} = (\ell_{\sigma} u^{\sigma})|_{\mathcal{O}} \frac{|\det(W_{XL}^{\mathbf{A}}_{\mathbf{B}})|^{\frac{1}{2}}}{|\det(W_{XX}^{\mathbf{A}}_{\mathbf{B}})|^{\frac{1}{2}}}. \quad (3.99)$$

3.3.5 Position drift

Among the various definitions of parallax, there is also the case where a single observer measures the temporal changes in the position of the source in the sky. This momentary

rate of change of the source's position in the observer's sky is the *position drift* $\delta_{\mathcal{O}}r^A$ [110, 88] and is one of the real-time measurements commonly referred to as *drift effects*. In contrast to the classic parallax, the position drift depends on the four-velocities of both the observer and the emitter, involving also the observer's four-acceleration [110, 96, 124]. A general formula for the position drift has already been presented in [110], while a special case for spherically symmetric metrics was presented in [149, 148]. Here we present the general formula for the position drift in terms of BGO as derived in [88].

As was said many times, the position drift measures the temporal change of directions on the observer's sky as the observer moves along its worldline. This means that, contrary to the other observables considered so far, we are actually measuring changes in the direction vector as the observer crosses different null hypersurfaces $\delta x^\sigma \ell_\sigma = \text{const}$. This implies that, having fixed a reference frame, we need to find a way to transport it along the observer's worldline in order to be able to measure the changes in the directions registered on the next null hypersurface. The choice we make is to use the Fermi-Walker transport, which reduces to the usual parallel transport if the \mathcal{O} 's worldline is a geodesic. The Fermi-Walker transport of vectors in the observer's sphere $\text{Dir}(u_{\mathcal{O}})$ along the worldline defines our "fixed directions on the sky" [96, 110]. The Fermi-Walker derivative of the direction vector r_0^μ in Eq. (3.79) is expressed as

$$\delta_{\mathcal{O}}r^\mu = u_{\mathcal{O}}^\sigma \nabla_\sigma r_0^\mu - u_{\mathcal{O}}^\mu w_{\mathcal{O}\sigma} r_0^\sigma + w_{\mathcal{O}}^\mu u_{\mathcal{O}\sigma} r_0^\sigma, \quad (3.100)$$

where $u_{\mathcal{O}}^\mu$ and $w_{\mathcal{O}}^\mu$ are the observer's four-velocity and four-acceleration respectively. From Eq. (3.79) follows that the last term in Eq. (3.100) vanishes, since $u_{\mathcal{O}\sigma} r_0^\sigma = 0$, while the covariant derivative $u_{\mathcal{O}}^\sigma \nabla_\sigma r_0^\mu$ is²³

$$u_{\mathcal{O}}^\sigma \nabla_\sigma r_0^\mu = \frac{u_{\mathcal{O}}^\sigma \nabla_\sigma \ell_{\mathcal{O}}^\mu}{(\ell_{\mathcal{O}}^\rho u_{\mathcal{O}\rho})} + u_{\mathcal{O}}^\sigma \nabla_\sigma u_{\mathcal{O}}^\mu = \frac{\Delta \ell_{\mathcal{O}}^\mu}{(\ell_{\mathcal{O}}^\rho u_{\mathcal{O}\rho})} + w_{\mathcal{O}}^\mu, \quad (3.101)$$

with $\delta\tau_{\mathcal{O}}$ the observer's proper time. The pull-back to $\mathcal{P}_{\mathcal{O}}$ of Eq. (3.100) defines the position drift $\delta_{\mathcal{O}}r^A$ measured with respect to inertially dragged fixed directions

$$\delta_{\mathcal{O}}r^A = \frac{\Delta \ell_{\mathcal{O}}^A}{(\ell_{\mathcal{O}}^\rho u_{\mathcal{O}\rho})} + w_{\mathcal{O}}^A. \quad (3.102)$$

The first term in Eq. (3.102) can be obtained from Eq. (3.85) as

$$\frac{\Delta \ell_{\mathcal{O}}^A}{\delta\tau_{\mathcal{O}}} = (W_{XL}^{-1})^A_B \left[\frac{1}{1+z} u_S - W_{XX}(u_{\mathcal{O}}) \right]^B, \quad (3.103)$$

where we expressed the two displacements as

$$\delta x_{\mathcal{O}}^\mu = u_{\mathcal{O}}^\mu \delta\tau_{\mathcal{O}} \quad (3.104)$$

$$\delta x_S^\mu = u_S^\mu \delta\tau_S, \quad (3.105)$$

and we used the relation²⁴

$$\delta\tau_S = \frac{\delta\tau_{\mathcal{O}}}{1+z}, \quad (3.106)$$

²³The relation $\Delta \ell^\mu = \delta\tau_{\mathcal{O}} u_{\mathcal{O}}^\sigma \nabla_\sigma \ell_{\mathcal{O}}^\mu$ follows from the definition $\Delta \ell^\mu = \ell^\sigma \nabla_\sigma \delta x_{\mathcal{O}}^\mu$ by using Eqs. (3.21) and expressing $\delta x_{\mathcal{O}}^\mu = u_{\mathcal{O}}^\mu \delta\tau_{\mathcal{O}}$.

²⁴The relation is obtained from the condition $\delta x_{\mathcal{O}}^\mu \ell_{\mathcal{O}\mu} = \delta x_S^\mu \ell_{S\mu}$, by using Eq. (3.105) and the definition of redshift Eq. (3.89).

between the proper time as measured at the observer $\delta\tau_{\mathcal{O}}$ and the proper time as measured at the source $\delta\tau_{\mathcal{S}}$, [139, 105, 110]. Combining (3.102) and (3.103) yields

$$\delta_{\mathcal{O}}r^{\mathbf{A}} = \frac{1}{\ell_{\mathcal{O}\sigma}u_{\mathcal{O}}^{\sigma}} (W_{XL}^{-1})^{\mathbf{A}\mathbf{B}} \left[\frac{1}{1+z} u_{\mathcal{S}} - W_{XX}(u_{\mathcal{O}}) \right]^{\mathbf{B}} + w_{\mathcal{O}}^{\mathbf{A}}. \quad (3.107)$$

Note that the last term is the perpendicular component of the observer's four-acceleration. It corresponds to the special relativistic effect of the position drift due to the drift of the aberration [152, 110, 124]. For a longer discussion of the position drift formula and its physical and astrophysical consequences see [110, 88].

3.3.6 The redshift drift formula

The last observable under consideration is the redshift drift, a real time observable expressing the temporal changing of the redshift, due to cosmic expansion and proper motion of the source and the observer. The formulation of the redshift drift was firstly proposed by Sandage in 1962 [159], and later applied by A. Loeb [116] as a tracer of the expansion of the Friedmann-Lemaître-Robertson-Walker Universe. Here, we will present the derivation of the general formula of the redshift drift in terms of BGO, [164].

Let us consider two consecutive measurements of the redshift z as taken by the observer \mathcal{O} at the two instants $\tau_{\mathcal{O}}$ and $\tau_{\mathcal{O}} + \delta\tau_{\mathcal{O}}$. In the time lapse $\delta\tau_{\mathcal{O}}$ the observer and the source are shifted along their worldlines by:

$$\begin{aligned} \delta x_{\mathcal{O}}^{\mu} &= u_{\mathcal{O}}^{\mu} \delta\tau_{\mathcal{O}} \\ \delta x_{\mathcal{S}}^{\mu} &= u_{\mathcal{S}}^{\mu} \delta\tau_{\mathcal{S}} = \frac{1}{1+z} u_{\mathcal{S}}^{\mu} \delta\tau_{\mathcal{O}}, \end{aligned} \quad (3.108)$$

where we have used the relation between $\delta\tau_{\mathcal{S}}$ and $\delta\tau_{\mathcal{O}}$ in Eq. (3.106). Now, the redshift drift is obtained varying with respect to the observer proper time the definition of the redshift. For our convenience, let us take the logarithm of the redshift in Eq. (3.89)

$$\log(1+z) = \log(\ell^{\mu}u_{\mu}|_{\mathcal{S}}) - \log(\ell^{\mu}u_{\mu}|_{\mathcal{O}}), \quad (3.109)$$

and do its variation

$$\delta \log(1+z) = \frac{(\Delta \ell_{\mathcal{S}}^{\mu} u_{\mathcal{S}\mu} + \ell_{\mathcal{S}}^{\mu} \Delta u_{\mathcal{S}\mu})}{\ell_{\mathcal{S}}^{\mu} u_{\mathcal{S}\mu}} - \frac{(\Delta \ell_{\mathcal{O}}^{\mu} u_{\mathcal{O}\mu} + \ell_{\mathcal{O}}^{\mu} \Delta u_{\mathcal{O}\mu})}{\ell_{\mathcal{O}}^{\mu} u_{\mathcal{O}\mu}}. \quad (3.110)$$

The two terms

$$\begin{aligned} \Delta u_{\mathcal{O}}^{\mu} &= w_{\mathcal{O}}^{\mu} \delta\tau_{\mathcal{O}}, \\ \Delta u_{\mathcal{S}}^{\mu} &= w_{\mathcal{S}}^{\mu} \delta\tau_{\mathcal{S}} = \frac{1}{1+z} w_{\mathcal{S}}^{\mu} \delta\tau_{\mathcal{O}}, \end{aligned} \quad (3.111)$$

define the four-acceleration of the observer $w_{\mathcal{O}}$ and the emitter $w_{\mathcal{S}}$.

The variation in Eq. (3.110) can be reshuffled as

$$\delta \log(1+z) = \left(\frac{1}{1+z} \frac{\ell_{\mathcal{S}}^{\mu} w_{\mathcal{S}\mu}}{\ell_{\mathcal{S}}^{\mu} u_{\mathcal{S}\mu}} - \frac{\ell_{\mathcal{O}}^{\mu} w_{\mathcal{O}\mu}}{\ell_{\mathcal{O}}^{\mu} u_{\mathcal{O}\mu}} \right) \delta\tau_{\mathcal{O}} + \left(\frac{\Delta \ell_{\mathcal{S}}^{\mu} u_{\mathcal{S}\mu}}{\ell_{\mathcal{S}}^{\mu} u_{\mathcal{S}\mu}} - \frac{\Delta \ell_{\mathcal{O}}^{\mu} u_{\mathcal{O}\mu}}{\ell_{\mathcal{O}}^{\mu} u_{\mathcal{O}\mu}} \right). \quad (3.112)$$

The first term is a special relativistic term representing the Doppler effect along the line of sight caused by the four-acceleration of the observer and the emitter

$$\Xi_{\text{Doppler}} = \left[\frac{1}{1+z} \frac{(\ell^{\mu} w_{\mu})|_{\mathcal{S}}}{(\ell^{\mu} u_{\mu})|_{\mathcal{S}}} - \frac{(\ell^{\mu} w_{\mu})|_{\mathcal{O}}}{(\ell^{\mu} u_{\mu})|_{\mathcal{O}}} \right]. \quad (3.113)$$

The second term contains the effects of the spacetime curvature on the redshift drift and it can be expressed in terms of the BGO. Let us start by writing the second term in the matrix form:

$$\frac{\Delta \ell_S^\mu u_{S\mu}}{\ell_S^\mu u_{S\mu}} - \frac{\Delta \ell_O^\mu u_{O\mu}}{\ell_O^\mu u_{O\mu}} = - \begin{pmatrix} u_{O\nu} & u_{S\mu} \\ \ell_O^\mu u_{O\mu} & \ell_S^\mu u_{S\mu} \end{pmatrix} \cdot \begin{pmatrix} \Delta \ell_O^\nu \\ -\Delta \ell_S^\mu \end{pmatrix}. \quad (3.114)$$

The vector $(\Delta \ell_O^\nu \quad -\Delta \ell_S^\mu)^\top$ is expressed in terms of the BGO using Eqs. (3.42)-(3.43)

$$\begin{cases} \Delta \ell_O^\nu = W_{XL}^{-1\nu}{}_\rho \delta x_S^\rho - W_{XL}^{-1\nu}{}_\rho W_{XX}{}^\rho{}_\sigma \delta x_O^\sigma \\ -\Delta \ell_S^\mu = -W_{LX}{}^\mu{}_\rho \delta x_O^\rho - W_{LL}{}^\mu{}_\nu W_{XL}^{-1\nu}{}_\rho \delta x_S^\rho + W_{LL}{}^\mu{}_\nu W_{XL}^{-1\nu}{}_\rho W_{XX}{}^\rho{}_\sigma \delta x_O^\sigma \end{cases}, \quad (3.115)$$

from which we finally get

$$\begin{pmatrix} \Delta \ell_O^\nu \\ -\Delta \ell_S^\mu \end{pmatrix} = \begin{pmatrix} -W_{XL}^{-1\nu}{}_\rho W_{XX}{}^\rho{}_\sigma & W_{XL}^{-1\nu}{}_\rho \\ W_{LL}{}^\mu{}_\nu W_{XL}^{-1\nu}{}_\rho W_{XX}{}^\rho{}_\sigma - W_{LX}{}^\mu{}_\sigma & -W_{LL}{}^\mu{}_\nu W_{XL}^{-1\nu}{}_\rho \end{pmatrix} \begin{pmatrix} \delta x_O^\sigma \\ \delta x_S^\rho \end{pmatrix} \quad (3.116)$$

Denoting

$$U = \begin{pmatrix} -W_{XL}^{-1\nu}{}_\rho W_{XX}{}^\rho{}_\sigma & W_{XL}^{-1\nu}{}_\rho \\ W_{LL}{}^\mu{}_\nu W_{XL}^{-1\nu}{}_\rho W_{XX}{}^\rho{}_\sigma - W_{LX}{}^\mu{}_\sigma & -W_{LL}{}^\mu{}_\nu W_{XL}^{-1\nu}{}_\rho \end{pmatrix} \quad (3.117)$$

as the large 8×8 block matrix containing the BGO, Eq. (3.116) becomes

$$\begin{pmatrix} \Delta \ell_O^\nu \\ -\Delta \ell_S^\mu \end{pmatrix} = U \begin{pmatrix} \delta x_O^\sigma \\ \delta x_S^\rho \end{pmatrix} = U \begin{pmatrix} u_O^\sigma \delta \tau_O \\ \frac{\delta \tau_O}{1+z} u_S^\rho \end{pmatrix}, \quad (3.118)$$

and it can then inserted in Eq. (3.114) that finally becomes

$$\begin{aligned} & - \begin{pmatrix} u_{O\nu} & u_{S\mu} \\ \ell_O^\mu u_{O\mu} & \ell_S^\mu u_{S\mu} \end{pmatrix} \cdot \begin{pmatrix} \Delta \ell_O^\nu \\ -\Delta \ell_S^\mu \end{pmatrix} = \\ & - \frac{\delta \tau_O}{\ell_O^\mu u_{O\mu}} \begin{pmatrix} u_{O\nu} & u_{S\mu} \\ \ell_O^\mu u_{O\mu} & \ell_S^\mu u_{S\mu} \end{pmatrix} \cdot U \cdot \begin{pmatrix} u_O^\sigma \\ \frac{u_S^\rho}{1+z} \end{pmatrix}, \end{aligned} \quad (3.119)$$

where we invite the reader to notice that this derivation was made considering U with upper-down indices distribution.

Finally, Eq. (3.112) in terms of the new defined quantities gives the expression of the redshift drift $\frac{\delta \log(1+z)}{\delta \tau_O} \equiv \zeta$ in terms of the BGO

$$\zeta = \Xi_{\text{Doppler}} - \begin{pmatrix} u_{O\nu} & u_{S\mu} \\ \ell_O^\mu u_{O\mu} & \ell_S^\mu u_{S\mu} \end{pmatrix} \cdot U \cdot \begin{pmatrix} u_O^\sigma \\ \frac{u_S^\rho}{1+z} \end{pmatrix}. \quad (3.120)$$

The expression Eq. (3.120) is completely general in the sense that it was derived from general considerations and without referring to a specific model. Of course, the specific expression of the BGO is dictated by the particular form of the spacetime in which they are calculated, but once the BGO are computed, they can be used to calculate the redshift drift with the formula above.

In conclusion, the BGO are fundamental objects describing multiple effects on light propagation in the regime of geometric optics. Let us notice that, although the BGO formalism is independent of the frame used, the observables depend on the emitter and observer kinematics, as shown by the explicit dependence of u_O^μ , u_S^μ , w_O^μ and w_S^μ in Eqs. (3.92)-(3.120). Indeed, it is possible to apply the Lorentz transformations to change reference frame, but

this modifies the observables introducing special relativistic effects such as the Doppler effect or aberration. In this sense, the BGO provide a unified framework for computing all optical observables, such us those in Eqs. (3.92),(3.99), (3.107), and (3.120). Moreover, while there are already analogous formulas for D_{ang} and D_{par} , where instead of the BGO we have the magnification and the parallax matrix (see [109] for the comparison), there was no general formula for the position drift and the redshift drift: Eqs. (3.107) and (3.120) look the same for each spacetime model considered.

PAPER I: “BiGONLight: LIGHT PROPAGATION WITH BILOCAL OPERATORS IN NUMERICAL RELATIVITY”

The chapter presents `BiGONLight`, a `Wolfram` package designed to implement the BGO framework in $3 + 1$ form to compute optical observables from numerically generated spacetimes. The package is completely general: it can simulate light propagation in geometric optics approximation in any spacetime, with no assumptions on the gauge or coordinate system used. It was specifically designed to be compatible with the full-GR codes in numerical relativity based on the ADM formalism. Nevertheless, it also takes advantage of `Mathematica`’s symbolic algebra manipulation to compute the BGO from the analytical expression of the metric tensor. The output of the package are the BGO, which are then combined with the observer \mathcal{O} and source \mathcal{S} four-velocities ($u_{\mathcal{O}}^{\mu}$, $u_{\mathcal{S}}^{\mu}$) and four-accelerations ($w_{\mathcal{O}}^{\mu}$, $w_{\mathcal{S}}^{\mu}$) to compute observables.

This work is conceptually divided into two parts. In the first part, `BiGONLight` is presented together with the theoretical formulation of the BGO framework in $3 + 1$ form. In the second part, the code is tested by calculating observables in three well-known cosmological models: the Λ CDM and the Szekeres (analytical) spacetimes, and a dust Universe obtained from numerical simulation.

Author’s contribution

`BiGONLight` is my original contribution in [89] and my main achievement in this thesis. On the 13th of July 2021, I released the stable version of the package (v1.0), which is publicly available on the GitHub repository <https://github.com/MicGrasso/bigonlight> under the GPL-3.0 license. The `BiGONLight` package is a collection of `Wolfram` functions that can be used in a `Mathematica` notebook to compute observables. The procedure to compute observables with `BiGONLight` can be summarised as follows:

- (i) the user provides the metric $g_{\mu\nu}$, and the observer \mathcal{O} and source \mathcal{S} kinematics as input. They can be given already in $3 + 1$ decomposition or as four-dimensional quantities. In the last instance, the user can use the functions `ADM[]` and `Vsplit[]` to perform the $3 + 1$ decomposition of $g_{\mu\nu}$ and of the vectors (u^{μ} , w^{μ}), respectively;
- (ii) set the initial conditions ($x_{\mathcal{O}}^{\mu}$, $\ell_{\mathcal{O}}^{\mu}$) for the photon’s geodesic, provided as $3 + 1$ components or using `Vsplit[]` and `InitialConditions[]`;
- (iii) obtain the expression of the geodesic equation in $3+1$ with the functions `GeodesicEquations[]`

and `EnergyEquations[]`. The functions implement the 3 + 1 geodesic equations obtained by Vincent et. al. in [182];

- (iv) solve the geodesic equations numerically with `SolveGeodesic[]` and `SolveEnergy[]`;
- (v) set the initial conditions for the SNF, directly in ADM components or using `SNF[]`. Then the function `PTransportedFrame[]` computes the parallel transported SNF along the geodesic by solving the 3 + 1 parallel transport equations Eq. (31) in [89];
- (vi) compute the optical tidal matrix projected into the SNF with the `OpticalTidalMatrix[]` function, as expressed in Eq. (39) in [89];
- (vii) compute the expressions of the evolution equations for the BGO with `BGOequations[]`, as in Eq. (44) in [89], and solve them with `SolveBGO[]` for obtaining $\mathcal{W}(\mathcal{S}, \mathcal{O})$.

Step (vii) is the starting point for obtaining the observables by combining the BGO with the observer and source four-velocities and four-accelerations as discussed in Sec. 3.3.

Other of my original contributions in [89] are the expressions of the parallel transport equation and the optical tidal matrix in terms of ADM quantities (Eq. (31) and Eq. (39) in [89]), and the explicit transformation relations from forward to backward integrated BGO (Eqs. (49)-(52) in [89]). I also obtained the specific form of the optical tidal matrix and the BGO in the SNF, and I used these expressions to simplify the calculations of their components.

I have also performed the tests computing the redshift, the angular diameter distance, the parallax distance, and the redshift drift for two analytical spacetimes corresponding to the Λ CDM and the (axially-symmetric) Szekeres models (presented in [130]), and for a numerically evolved dust Universe (EdS). The tests were designed jointly by E. Villa and me. I have performed the numerical calculations of the observables with `BiGONLight` and the comparisons with their analytical expressions in the Λ CDM and EdS models (Fig. 2 and Figs. 4-5 in [89]). The numerical evolution of the dust Universe was done by me with the `Einstein Toolkit` and the `FLRWSolver`, [117, 122].

In the axially-symmetric Szekeres model we were considering, there are no analytical expressions for the observables: the redshift and the angular diameter distance can be obtained numerically as shown in [131] and the results compared with those obtained with `BiGONLight` (Fig. 3 in [89]). Conversely, there was no known way to calculate the redshift drift. To this end, I derived an ODE whose solution gives the redshift drift for a geodesic along the axis of symmetry of the model (Eq. (96) in [89]). Finally, I have compared the redshift drift obtained from this result with the one obtained with the package. The results were discussed jointly by E. Villa and me, and published in [89].

BiGONLight: light propagation with bilocal operators in numerical relativity

Michele Grasso*  and Eleonora Villa 

Center for Theoretical Physics Polish Academy of Sciences, Al. Lotników 32/46,
02-668 Warsaw, Poland

E-mail: grasso@cft.edu.pl and villa@cft.edu.pl

Received 21 July 2021, revised 6 October 2021

Accepted for publication 2 November 2021

Published 7 December 2021



CrossMark

Abstract

BiGONLight, Bilocal Geodesic Operators framework for Numerical Light propagation, is a new tool for light propagation in numerical relativity. The package implements the bilocal geodesic operators formalism, a new framework for light propagation in general relativity. With BiGONLight it is possible to extract observables such as angular diameter distance, luminosity distance, magnification as well as new real-time observables like parallax and redshift drift within the same computation. As a test-bed for our code we consider two exact cosmological models, the Λ CDM and the inhomogeneous Szekeres model, and a simulated dust Universe. All our tests show an excellent agreement with known results.

Keywords: cosmology, numerical relativity, relativistic light propagation

(Some figures may appear in colour only in the online journal)

1. Introduction

Electromagnetic and gravitational radiation are the primary means by which cosmologists and astronomers try to learn about the structure and the evolution of the Universe. All the information we receive from distant objects is inferred from these signals which are affected by the presence of cosmic structures between the source and the observer. These effects are accumulated along the line of sight and they modify the perception of the observer which e.g. can receive the image of the source as if it were in a different position on the sky or with a

* Author to whom any correspondence should be addressed.



Original content from this work may be used under the terms of the [Creative Commons Attribution 4.0 licence](https://creativecommons.org/licenses/by/4.0/). Any further distribution of this work must maintain attribution to the author(s) and the title of the work, journal citation and DOI.

distorted shape or measure a redshift in the source light spectrum. Actually, most of the information comes from these distortions and they will be measured with unprecedented precision in a wider range of scales and redshift by the next generation of galaxy survey and cosmic microwave background experiments¹. On top of that, thanks to the improvements in the modern experimental apparatus, nowadays we will be able of measuring small temporal changes of those effects, the so-called optical drift effects. They may provide important and new information about the Universe structure and evolution, marking the beginning of real-time cosmology [1]. In order to make the most from this revolution in observational astronomy and cosmology, the same accuracy is required in the theoretical predictions and interpretations of what we measure. This tough task requires much effort from two sides. At one hand the most recent progress on cosmological dynamics are represented by general-relativistic simulations of cosmic structures with no assumed symmetries employing exact solutions of Einstein equations [2–8], or approximated treatments [9, 10]. The common ambitious aim is to have a description valid from large to small scales which accounts for relativistic effects. On the other hand relativistic effects in the non-linear regime have recently become to be investigated with relativistic simulations in galaxy clustering and lensing observables, and the Hubble diagram, see e.g. [11–19] and references therein.

From the point of view of the basic theory of light propagation a new approach was presented in [20]. The key ingredients of this new formulation are the bilocal geodesic operators (BGO) which constitute the map from the portion of spacetime occupied by the observer to that occupied by the source and give the full description of the distortion of light rays in between. The main advantage of the BGO formalism is that it provides a unified framework to compute all optical observables, namely those inferred from gravitational lensing effects, like e.g. magnification, shear, and angular diameter distance. The novelty is that source(s) and observer(s) are allowed to move and therefore the observables originated by the variation in time and the motion of sources and observers, like e.g. parallax, and redshift and position drifts, are automatically included, see [20]. In addition, by having the observables written in terms of the BGO, it is easy to disentangle the contributions of the spacetime curvature from those due to observer and source motion and construct specific new probes, e.g. for the curvature as the distance slip investigated in [21] in the Λ CDM cosmology.

In this paper we present `BiGONLight`², **Bilocal Geodesic Operators** framework for Numerical **Light** propagation, a `Mathematica` package developed for extracting observables from numerically generated spacetimes using the BGO formalism. The principal aim of the package is to provide a unified procedure to calculate multiple observables in numerical relativity: this is guaranteed since, once that the BGO are determined from the output metric of a numerical simulation, a all set of observables are obtained within the same computation. In order to be compatible with the majority of the codes in numerical cosmology, `BiGONLight` encodes the BGO formalism in $3 + 1$ form and it uses the `Mathematica` powerful symbolic algebra manipulation and precision control options.

The paper is organized as follows: in section 2, we give the fundamentals of light propagation and its formulation in terms of BGOs. In section 3 we present `BiGONLight` and the equations to compute the BGO in $3 + 1$ form encoded into the package. The recipe to compute observables in numerical relativity using `BiGONLight` and the expressions of the observables in terms of BGO are given in section 4. The last section of this paper, section 5, is dedicated to the code tests, which are performed in the following three cosmological models:

¹ <https://skatelescope.org>, <https://euclid-ec.org>, <https://lsst.org>, <https://litebird.jp/eng/>, <https://jpl.nasa.gov/missions/spherex>.

² The package is publicly available at <https://github.com/MicGrasso/bigonlight.git>.

Λ CDM (see section 5.1), Szekeres (see section 5.2), and a numerically evolved dust Universe (see section 5.3). We draw our conclusions in section 6. In the appendix A we show how to set physical units in `BiGONLight`.

Notation: Greek indices (α, β, \dots) run from 0 to 3, while Latin indices (i, j, \dots) run from 1 to 3 and refer to spatial coordinates only. Latin indices (A, B, \dots) run from 1 to 2. Tensors and bitensors expressed in a semi-null frame (SNF) are denoted using boldface indices: Greek boldface indices ($\boldsymbol{\alpha}, \boldsymbol{\beta}, \dots$) run from 0 to 3, Latin boldface indices ($\mathbf{a}, \mathbf{b}, \dots$) run from 1 to 3 and capital Latin boldface indices ($\mathbf{A}, \mathbf{B}, \dots$) run from 1 to 2. Latin tilded indices ($\tilde{a}, \tilde{b}, \dots$), running from 0 to 7, denote indices for the components of the 8×8 BGO matrix \mathcal{W} . A dot denotes derivative with respect to conformal time. Quantities with a subscript 0 are meant to be evaluated at present, whereas the subscript ‘in’ indicates the initial time. Quantities with a subscript \mathcal{S} (or \mathcal{O}) are meant to be evaluated at the source (observer) position.

2. Light propagation and the bilocal geodesic operators

Let us start by considering an observer \mathcal{O} and a source \mathcal{S} separated by a large distance and moving freely along their time-like worldlines. Naming $\mathcal{N}_{\mathcal{O}}$ and $\mathcal{N}_{\mathcal{S}}$ the regions of the space-time in which the observer and the source are moving, we assume that $\mathcal{N}_{\mathcal{O}}$ and $\mathcal{N}_{\mathcal{S}}$ are causally connected, so that any signal emitted by \mathcal{S} is received by \mathcal{O} at any later time. We also assume that the typical length scales of $\mathcal{N}_{\mathcal{O}}$ and $\mathcal{N}_{\mathcal{S}}$ are small compared to the distance between them. Within the geometric optics approximation, we can describe the signal as moving along null geodesics $\gamma(\lambda)$ connecting the source and the observer, such that $\gamma(\lambda_{\mathcal{S}}) = x_{\mathcal{S}}^{\mu}$ and $\gamma(\lambda_{\mathcal{O}}) = x_{\mathcal{O}}^{\mu}$, where $x_{\mathcal{O}}^{\mu}$ and $x_{\mathcal{S}}^{\mu}$ are the observer’s and source’s positions, respectively. The curve γ is given by the geodesic equation

$$\ell^{\sigma} \nabla_{\sigma} \ell^{\mu} = \frac{D}{D\lambda} \ell^{\mu} = 0, \quad (1)$$

where ℓ^{μ} is the tangent vector, λ is the affine parameter spanning the geodesic γ , $\frac{D}{D\lambda} \equiv \ell^{\sigma} \nabla_{\sigma}$ is the covariant derivative along γ . A solution of equation (1) is specified by the initial position and the initial tangent vector. In astronomy, we are the only observer performing every measurement, thus it is natural to set the initial conditions $(x_{\mathcal{O}}^{\mu}, \ell_{\mathcal{O}}^{\mu})$ at the observer location and to trace the geodesic back to the source. Now, if the observer is displaced by $\delta x_{\mathcal{O}}^{\mu}$, a new geodesic connects \mathcal{O} and \mathcal{S} , and it is characterized by the new initial conditions $(x_{\mathcal{O}}^{\mu} + \delta x_{\mathcal{O}}^{\mu}, \ell_{\mathcal{O}}^{\mu} + \Delta \ell_{\mathcal{O}}^{\mu})$, see figure 1, where we define $\Delta \ell_{\mathcal{O}}^{\mu}$ as the covariant deviation of the tangent vector $\ell_{\mathcal{O}}^{\mu}$, namely

$$\Delta \ell_{\mathcal{O}}^{\mu} = \delta \ell_{\mathcal{O}}^{\mu} + \Gamma^{\mu}_{\alpha\beta}(x_{\mathcal{O}}) \ell_{\mathcal{O}}^{\alpha} \delta x_{\mathcal{O}}^{\beta}. \quad (2)$$

The deviations $(\delta x_{\mathcal{O}}^{\mu}, \Delta \ell_{\mathcal{O}}^{\mu})$ can be used to parameterize a family of null geodesics and they propagate according to the geodesic deviation equation (GDE)

$$\begin{cases} \frac{D}{D\lambda} \delta x^{\mu} = \Delta \ell^{\mu} \\ \frac{D}{D\lambda} \Delta \ell^{\mu} = R^{\mu}_{\ell\nu} \delta x^{\nu} \end{cases} \quad (3)$$

with initial conditions

$$\delta x^{\mu}(\lambda_{\mathcal{O}}) = \delta x_{\mathcal{O}}^{\mu} \quad (4)$$

$$\Delta \ell^{\mu}(\lambda_{\mathcal{O}}) = \Delta \ell_{\mathcal{O}}^{\mu}, \quad (5)$$

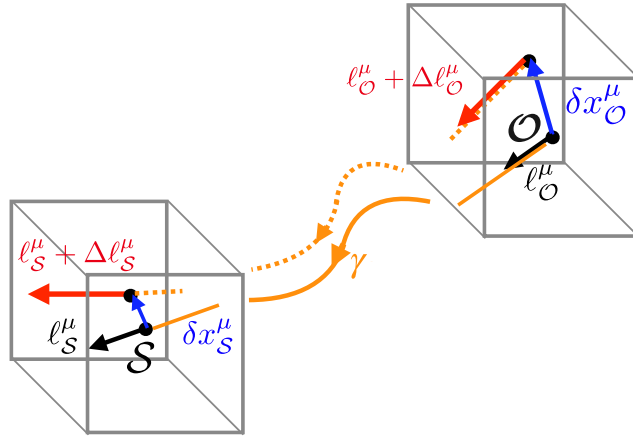


Figure 1. When the observations are repeated over time, the observer and the source may change their positions. This implies that the null geodesic connecting \mathcal{O} to \mathcal{S} has to change its path accordingly. This situation is described with the deviations of the positions δx^μ and of the tangent vectors $\Delta \ell^\mu$ at the two new extremes \mathcal{S} and \mathcal{O} .

provided that all the geodesics of the family stay close enough to γ .³ In equation (3) $R^\mu{}_{\ell\nu}$ is the short-hand for the optical tidal matrix $R^\mu{}_{\ell\nu} \equiv R^\mu{}_{\alpha\beta\nu} \ell^\alpha \ell^\beta$. The standard procedure to solve the GDE (3) was introduced by Sachs in 1961 [22]. The key quantity of this approach is the deformation of the light bundle’s cross section, i.e. the projection of the beam on a 2D screen spanned by two orthonormal vectors orthogonal to ℓ^μ and parallelly transported along γ (the Sachs basis). The GDE is projected onto this basis and then re-written in terms of the deformation matrix, a 2×2 matrix containing the expansion and the shear: the GDE recasted this way gives the well-known Sachs equations, see [23] for a complete introduction to the Sachs formalism. Despite its great success, the Sachs formalism describes only momentary observations, so that it cannot be used to take into account what happens when the observations are repeated in time and/or the observer and the source move. Obviously, this can be overcome by considering a new fiducial geodesic at some later time and solving again the Sachs equations but this procedure can be very complicated in some cases. In this paper we will use a different approach, which accounts also for these situations in a unified framework, based on the BGOs, introduced in [20] and summarised below.

Let us start by noticing that the GDE (3) defines a linear, bijective map $\mathcal{W}(\mathcal{S}, \mathcal{O})$ between its solutions $(\delta x_S^\mu, \Delta \ell_S^\mu)$ and initial conditions $(\delta x_O^\mu, \Delta \ell_O^\mu)$, namely

$$\begin{aligned} \delta x_S^\mu &= \mathcal{W}_{XX}{}^\mu{}_\nu \delta x_O^\nu + \mathcal{W}_{XL}{}^\mu{}_\nu \Delta \ell_O^\nu \\ \Delta \ell_S^\mu &= \mathcal{W}_{LX}{}^\mu{}_\nu \delta x_O^\nu + \mathcal{W}_{LL}{}^\mu{}_\nu \Delta \ell_O^\nu, \end{aligned} \tag{6}$$

assuming the optical tidal matrix $R^\mu{}_{\ell\nu}$ to be a smooth tensor field. The bi-tensors \mathcal{W}_{XX} , \mathcal{W}_{XL} , \mathcal{W}_{LX} , \mathcal{W}_{LL} acting from \mathcal{O} to \mathcal{S} are called BGOs. Equation (6) can then be written in the more

³ Here the GDE is presented as a system of two first-order ODE. The reader may find more familiar the following form of the GDE as a second order ODE $\frac{D^2}{D\lambda^2} \xi^\mu = R^\mu{}_{\alpha\beta\nu} \ell^\alpha \ell^\beta \xi^\nu$, where $\xi^\nu = \delta x^\nu$ and $\frac{D}{D\lambda} \xi^\nu = \Delta \ell^\nu$. In general, the GDE describes the deviation between any two infinity close null-like, time-like or space-like geodesics.

compact form

$$\begin{pmatrix} \delta x_{\mathcal{S}} \\ \Delta \ell_{\mathcal{S}} \end{pmatrix} = \begin{pmatrix} \mathcal{W}_{\text{XX}} & \mathcal{W}_{\text{XL}} \\ \mathcal{W}_{\text{LX}} & \mathcal{W}_{\text{LL}} \end{pmatrix} \begin{pmatrix} \delta x_{\mathcal{O}} \\ \Delta \ell_{\mathcal{O}} \end{pmatrix} = \mathcal{W}(\mathcal{S}, \mathcal{O}) \begin{pmatrix} \delta x_{\mathcal{O}} \\ \Delta \ell_{\mathcal{O}} \end{pmatrix}, \quad (7)$$

where $\mathcal{W}(\mathcal{S}, \mathcal{O})$ is the 8×8 Wronski matrix of the GDE acting from \mathcal{O} to \mathcal{S} . By inserting (7) in the GDE (3), we obtain the propagation equation for the BGO

$$\frac{D}{D\lambda} \mathcal{W} = \begin{pmatrix} 0 & 1 \\ R^{\mu}{}_{\ell\nu} & 0 \end{pmatrix} \mathcal{W} \quad (8)$$

with initial conditions

$$\mathcal{W}|_{\mathcal{O}} = \begin{pmatrix} 1_{4 \times 4} & 0 \\ 0 & 1_{4 \times 4} \end{pmatrix}. \quad (9)$$

The BGO \mathcal{W} is a symplectic mapping, as firstly noticed in [24], since equation (8) for null geodesics can be formulated as a Hamiltonian system, and it satisfies the properties

$$\mathcal{W}(\mathcal{O}, \mathcal{S}) = \mathcal{W}^{-1}(\mathcal{S}, \mathcal{O}) \quad (10)$$

$$\mathcal{W}(\mathcal{S}, \mathcal{O}) = \mathcal{W}(\mathcal{S}, p_{\lambda}) \mathcal{W}(p_{\lambda}, \mathcal{O}), \quad (11)$$

with p_{λ} an arbitrary point on the fiducial geodesic γ . The usual set up is specified by giving the initial conditions at \mathcal{O} and by integrating the GDE backward in time, up to the source \mathcal{S} . The physical motivation is of course that every measurement is done from the observer position. The BGO $\mathcal{W}(p_{\lambda}, \mathcal{O})$ obtained by integrating equation (8) backwards connect the observer with an arbitrary point p_{λ} on the geodesic, ending at the source $p_{\lambda_{\mathcal{S}}} = \mathcal{S}$. Although it is natural to study light propagation this way, there are circumstances in which it is more convenient to think forward in time, namely to integrate equation (8) from the source to p_{λ} , ending at the observer $p_{\lambda_{\mathcal{O}}} = \mathcal{O}$, and obtain $\mathcal{W}(p_{\lambda}, \mathcal{S})$. To this second case belong all the simulations of cosmological dynamics, in which the Einstein equations are solved forward in time, with initial conditions given at the end of inflation. It follows that forward integration of light propagation, on-the-fly with the simulation of the spacetime dynamics, would be a cost-efficient and time-saving methodology instead of using the natural approach for light propagation in post-processing. These two opposing procedures find a meeting point within the BGO framework, which provides a relatively easy way to transform from forward integrated $\mathcal{W}(p_{\lambda}, \mathcal{S})$ to backward integrated $\mathcal{W}(p_{\lambda}, \mathcal{O})$. The transformation follows from the BGO properties and it is found by multiplying equation (11) by $\mathcal{W}^{-1}(\mathcal{S}, p_{\lambda})$ from the left and using equation (10) to obtain⁴

$$\begin{aligned} \mathcal{W}(p_{\lambda}, \mathcal{O}) &= \mathcal{W}^{-1}(\mathcal{S}, p_{\lambda}) \mathcal{W}(\mathcal{S}, \mathcal{O}) \\ &= \mathcal{W}(p_{\lambda}, \mathcal{S}) \mathcal{W}^{-1}(\mathcal{O}, \mathcal{S}). \end{aligned} \quad (12)$$

We will give the explicit transformation rules for all the BGO components in section 3.3.

Let us finally recall that the most important feature of the BGO formalism is that it provides a unified framework to compute optical observables, including also real-time ones, like e.g. parallax, and redshift and position drifts [20]. In section 4 we will give the explicit expressions of the observables considered in this work in terms of the BGO.

⁴In the last equality of equation (12) we used equation (10). The symplectic property is useful for getting the inverse matrix, see section 3.3.

3. BiGONLight: light propagation with the BGO in numerical relativity

The BGO framework finds a natural application in studying light propagation in numerical relativity, since it allows to obtain multiple optical observables within the same calculation and this is easily adaptable to perform light propagation on-the-fly with a simulation of relativistic dynamics. For this purpose, we develop BiGONLight (**Bilocal Geodesic Operator framework for Numerical Light propagation**), a *Mathematica* package which simulates light propagation in numerical relativity within the BGO formalism, described in section 2. It is publicly available at the repository <https://github.com/MicGrasso/bigonlight.git> and it works as an external library that can be called inside a *Mathematica* notebook. *Mathematica* provides a large variety of numerical methods that can be used and customized to adapt them to the particular problem. This is exploited in the functions `SolveGeodesic[]`, `SolveEnergy[]`, `PTransportedFrame[]` and `SolveBGO[]` in which the user can choose the numerical methods used to solve the system of ODE⁵. Another useful feature is the *Mathematica*'s precision control options, which allows the user to set the precision and accuracy of numerical result through the commands `WorkingPrecision`, `SetPrecision` and `SetAccuracy`. In the following we give a detailed description of the equations for light propagation and the procedure to obtain the BGO implemented in the code. We dedicate a separate section, section 4, to the computation of the observables once the BGO are known.

The required input for BiGONLight are the spacetime metric and the source/observer kinematics, which can be provided in two different ways: (i) from the analytical expression of the metric $g_{\mu\nu}$ and the emitter/observer four-velocities (u_S^μ , u_O^μ) and four-accelerations (w_S^μ , w_O^μ) for some exact model, and (ii) from the output of a relativistic numerical simulation of the spacetime dynamics. A large variety of numerical codes used in cosmology and astrophysics employs the 3 + 1 formalism to solve the Einstein equations and simulate full-GR dynamical systems. To be compatible with the numerical output generated by these codes, in BiGONLight we recasted the BGO formalism in the 3 + 1 form. In the following we summarise some basic definitions of the 3 + 1 formalism and report the 3 + 1 version of all the equations for light propagation used to compute the BGO. For comprehensive references of the 3 + 1 formalism see e.g. [25–28].

The procedure of splitting a four-dimensional spacetime $(\mathcal{M}, g_{\mu\nu})$ into its 3 + 1 form, the so-called ADM formalism, was introduced by Arnowitt, Deser and Misner in [29]. It is constructed by foliating a four-dimensional manifold \mathcal{M} with a family of 3D space-like hypersurfaces Σ_t , labelled by a monotonic function t , such that $t = \text{const.}$ on each slice. This space-like foliation defines the time-like vector field n^μ , which is orthonormal to the slices and it can be regarded as the four-velocity of Eulerian observers. The geometry on each hypersurface is described by the following quantities:

- The induced metric $\gamma_{\mu\nu}$ is defined as the covariant form of the orthogonal projector onto the slices

$$\gamma_{\mu\nu} = g_{\mu\nu} + n_\mu n_\nu \quad (13)$$

and it is used to measure proper distances on Σ_t ;

⁵The user can choose between three different methods: 'RK' a 4th order Runge–Kutta method, 'A' which lets *Mathematica* to decide what is the best method to use, and 'SS' denoting the stiffness–switching method, which allows to switch between implicit and explicit methods to resolve stiff problems.

- The covariant derivative on the slice

$$D_\nu V^\mu = \gamma^\sigma{}_\nu \gamma^\mu{}_\rho \nabla_\sigma V^\rho, \quad (14)$$

which is written in terms of the 3D Christoffel symbol ${}^{(3)}\Gamma^k{}_{ij} = \frac{1}{2}\gamma^{kl}(\frac{\partial\gamma_{lj}}{\partial x^i} + \frac{\partial\gamma_{il}}{\partial x^j} - \frac{\partial\gamma_{ij}}{\partial x^l})$, once a coordinate system x^i on Σ_t is introduced;

- The extrinsic curvature $K_{\mu\nu}$ defined as

$$K_{\mu\nu} = -\gamma^\sigma{}_\mu \gamma^\rho{}_\nu \nabla_\sigma n_\rho, \quad (15)$$

which represents the curvature of the 3D hypersurfaces with respect to the 4D embedding spacetime.

A natural choice for a coordinate system x^μ is the one adapted to the foliation: the corresponding reference frame is such that the three vectors $\partial_i^\mu = (\frac{\partial}{\partial x^i})^\mu$ are tangent to the hypersurface while $\partial_0^\mu = (\frac{\partial}{\partial t})^\mu$ is transverse to it. In particular, the time-like vector field $(\frac{\partial}{\partial t})^\mu$ is tangent to a congruence of world-lines of coordinate observers and it is given by

$$\left(\frac{\partial}{\partial t}\right)^\mu = \alpha n^\mu + \beta^\mu, \quad (16)$$

where α is the lapse function, which measures the proper time of the Eulerian observers, and β^μ is the shift vector, which quantifies the displacement on Σ_t of the coordinate observer $(\frac{\partial}{\partial t})^\mu$ with respect to the Eulerian observer n^μ . The components of the normal vector and the metric $g_{\mu\nu}$ in the adapted coordinates are written with the lapse, the shift and the induced metric as

$$n^\mu = \left(\frac{1}{\alpha}, -\frac{\beta^i}{\alpha}\right), \quad (17)$$

and

$$g_{\mu\nu} = \begin{pmatrix} \beta_i \beta^i - \alpha^2 & \beta_i \\ \beta_j & \gamma_{ij} \end{pmatrix}, \quad (18)$$

where the Latin indices runs from 1 to 3. A generic 4D tensor is projected on the slice as

$${}^{(3)}T^{\mu_1 \dots \mu_m}_{\nu_1 \dots \nu_n} = {}^{(4)}T^{\rho_1 \dots \rho_m}_{\sigma_1 \dots \sigma_n} \gamma^{\mu_1}{}_{\rho_1} \dots \gamma^{\mu_m}{}_{\rho_m} \gamma^{\sigma_1}{}_{\nu_1} \dots \gamma^{\sigma_n}{}_{\nu_n}. \quad (19)$$

BiGONLight is designed to accept as input directly the ADM quantities $(\alpha, \beta^i, \gamma_{ij}, K_{ij})$ generated by a numerical simulation. However, the powerful symbolic algebra manipulation of the Wolfram language allows also to use the analytical form of the metric $g_{\mu\nu}$ as input. In this case, the ADM quantities are computed in BiGONLight by the function `ADM[]` accordingly to equations (15), (17) and (18). On top of that, BiGONLight contains other functions to calculate the Christoffel symbols, `Christoffel[]`, and the Riemann tensor, `Riemann[]`. Note that in both cases, the input metric is provided in form of components within a specific coordinate system and not in full tensorial form. The package is designed to work in any gauge and any coordinate system, leaving the choice to the user. Now that we have summarized the basics, we will describe in more details and step by step the procedure for obtaining the BGO in the 3 + 1 decomposition: we report the 3 + 1 version of the geodesic equation following [30] and we derive all the 3 + 1 ingredients for the evolution equation of the BGO.

3.1. Geodesic equation in 3 + 1 decomposition

The first code solving the 3 + 1 geodesic equation was presented in [31] and it was used to map the event horizon in numerical simulations with black holes (like heads-on collision of two black holes), while a more recent formulation of the 3 + 1 geodesic equation was presented in [30]. Here, we briefly resume the procedure in [30], since we will use their approach throughout all our calculations.

The null geodesics representing light rays connecting source and observer is obtained by solving

$$\ell^\sigma \nabla_\sigma \ell^\mu = 0 \quad (20)$$

where ℓ^μ is the tangent vector which obeys to the null condition

$$\ell^\sigma \ell_\sigma = 0. \quad (21)$$

It is 3 + 1 decomposed as:

$$\ell^\mu = \mathcal{E}(n^\mu + V^\mu), \quad (22)$$

where \mathcal{E} is defined by $\mathcal{E} = -n^\mu \ell_\mu$ and $V^\mu n_\mu = 0$. In other words, $\mathcal{E}V^\mu$ is the component of ℓ^μ tangent to Σ_t and $\mathcal{E}n_\nu$ is the orthogonal one. Substituting equation (22) in the geodesic equation (20) after a long but straightforward calculation, see [30], the geodesic equation decouples in two differential equations

$$\frac{d\mathcal{E}}{dt} = \mathcal{E} (\alpha K_{ik} V^j V^k - V^j \partial_j \alpha), \quad (23)$$

$$\begin{cases} \frac{dx^i}{dt} = \alpha V^i - \beta^i \\ \frac{dV^i}{dt} = \alpha V^j [V^i (\partial_j \log \alpha - K_{jk} V^k) + 2K^i_j - {}^{(3)}\Gamma^i_{jk} V^k] - \gamma^{ij} \partial_j \alpha - V^j \partial_j \beta^i \end{cases} \quad (24)$$

for the orthogonal and the tangent components, respectively.

In the `BiGONLight` package the two functions `EnergyEquations[]` and `GeodesicEquations[]` give the differential equations (23) and (24), respectively. Next, we need to specify the initial conditions. The function `InitialConditions[]` is specifically constructed to get the initial conditions for V^i and \mathcal{E} consistent with the null condition (21) and the decomposition (22). The ODE (23) and (24) are then solved by using two customized versions of the Mathematica `NDSolve[]` function: `SolveEnergy[]` and `SolveGeodesic[]`.

3.2. Parallel transport equation in the 3 + 1 decomposition

The BGO map the changes of the deviations (δx^μ , $\Delta \ell^\mu$) between the observer \mathcal{O} and the source \mathcal{S} along the photon geodesic γ , see equation (7). This is possible only if we introduce a frame parallel transported along γ , which allows us to compare quantities at the observation point and at source position. For our purposes, the definition and the parallel transport of the frame have to be split into the 3 + 1 form. Let us start with the parallel transport of a generic vector e^μ along a given geodesic with tangent ℓ^μ , which is governed by

$$\ell^\alpha \nabla_\alpha e^\mu = 0. \quad (25)$$

The 3 + 1 decomposition of e^μ reads

$$e^\mu = Cn^\mu + E^\mu, \quad (26)$$

where we have defined the orthogonal component $Cn^\mu = -n_\alpha e^\alpha n^\mu$ and the tangent component $E^\mu = \gamma^\mu_\alpha e^\alpha$. The parallel transport equation (25) becomes

$$n^\mu (n^\alpha \nabla_\alpha C + V^\alpha \nabla_\alpha C) + C(n^\alpha \nabla_\alpha n^\mu + V^\alpha \nabla_\alpha n^\mu) + n^\alpha \nabla_\alpha E^\mu + V^\alpha \nabla_\alpha E^\mu = 0. \quad (27)$$

Now, we make use of some 3 + 1 well-known relations: for the first term we have $n^\mu \nabla_\mu C = \frac{1}{\alpha} \mathcal{L}_{\alpha\bar{n}} C$, in the second bracket we substitute $n^\alpha \nabla_\alpha n^\mu = D^\mu \log \alpha$ and the definition of the extrinsic curvature $\nabla_\alpha n^\mu = -K^\mu_\alpha$, and for the expansion of the last two terms we use the two identities:

$$\begin{aligned} V^\alpha \nabla_\alpha E^\mu &= V^\alpha D_\alpha E^\mu - K_{\alpha\beta} V^\alpha E^\beta n^\mu \\ n^\nu \nabla_\nu E^\mu &= \frac{1}{\alpha} (\mathcal{L}_{\alpha\bar{n}} E^\mu + E^\nu \nabla_\nu (\alpha n^\mu)) = \frac{1}{\alpha} \mathcal{L}_{\alpha\bar{n}} E^\mu - E^\nu K^\mu_\nu + E^\nu \partial_\nu (\log \alpha) n^\mu. \end{aligned}$$

We then re-write equation (27) split into two parts, the one proportional to n^μ and the other tangent to Σ_t as

$$\begin{cases} \frac{1}{\alpha} \mathcal{L}_{\alpha\bar{n}} C + V^\nu \partial_\nu C + E^\nu \partial_\nu (\log \alpha) - K_{\nu\rho} V^\nu E^\rho = 0 \\ \frac{1}{\alpha} \mathcal{L}_{\alpha\bar{n}} E^\mu - E^\nu K^\mu_\nu + V^\nu D_\nu E^\mu + C (\gamma^{\mu\nu} D_\nu \log \alpha - K^\mu_\nu V^\nu) = 0, \end{cases} \quad (28)$$

where both must vanish individually in order to satisfy the parallel transport condition (25). The last steps consist in expanding the Lie derivative

$$\mathcal{L}_{\alpha\bar{n}} = \frac{\partial}{\partial t} - \mathcal{L}_{\bar{\beta}} \quad (29)$$

and converting partial derivatives with respect to the time t into total derivative via

$$\frac{\partial}{\partial t} = \frac{d}{dt} - \alpha V^j \partial_j + \beta^j \partial_j. \quad (30)$$

The final result for the 3 + 1 parallel transport equation is

$$\begin{cases} \frac{1}{\alpha} \frac{dC}{dt} + E^i \partial_i \log \alpha - K_{ij} V^i E^j = 0 \\ \frac{1}{\alpha} \left(\frac{dE^i}{dt} + E^j \partial_j \beta^i \right) + {}^{(3)}\Gamma^i_{jk} V^j E^k - K^i_j E^j + C (\gamma^{ij} D_j \log \alpha - K^i_j V^j) = 0, \end{cases} \quad (31)$$

where we have only spatial indices $i, j = 1, 2, 3$ since all the quantities lie on Σ_t .

The system of equation (31) has to be solved for each vector of the frame we choose. Following [20], we choose the SNF composed by the tetrad of vectors

$$\phi^\mu_\alpha = (u^\mu, \phi^\mu_1, \phi^\mu_2, \ell^\mu), \quad (32)$$

where u^μ is the matter four-velocity, ℓ^μ is the tangent of the photon geodesic. The two vectors $\phi^\mu_{\mathbf{A}}$ are orthonormal to both u^μ and ℓ^μ , namely:

$$\begin{cases} g_{\mu\nu}u^\mu\phi^\mu_{\mathbf{A}} = 0 \\ g_{\mu\nu}\ell^\mu\phi^\mu_{\mathbf{A}} = 0 \\ g_{\mu\nu}u^\mu\ell^\nu = Q \\ g_{\mu\nu}\phi^\mu_{\mathbf{A}}\phi^\mu_{\mathbf{B}} = \delta_{\mathbf{AB}} \end{cases} \quad (33)$$

with Q a real number. Each vector of the SNF is then decomposed in 3 + 1 form as

$$\phi^\mu_{\alpha} = \Phi_{\alpha}n^\mu + F^\mu_{\alpha} \quad (34)$$

and parallelly propagated by solving equation (31) for its orthogonal and tangent components, i.e. $\Phi_{\alpha}n^\mu = -n_{\sigma}\phi^{\sigma}_{\alpha}n^\mu$ and $F^\mu_{\alpha} = \gamma^{\mu}_{\sigma}\phi^{\sigma}_{\alpha}$.

In `BiGONLight` this is demanded to the function `PTransportedFrame[]`, which gives as output the components in (34) of the SNF parallel transported. The function `PTransportedFrame[]` uses `ParallelTransport[]` to obtain equation (31) for each vector of the frame and then solve them with a customised `NDSolve[]` function.

3.3. The optical tidal matrix and the GDE for the BGO

So far the 3 + 1 equations equations (23), (24) and (31) we presented are valid for any type of geodesics and to parallelly transport any type of vectors along that geodesic. From now on, we will restrict the BGO formalism to the case of a SNF parallelly propagated along a null-like geodesic. The equation for the BGO has then to be projected onto the SNF. The result is simply given by

$$\frac{d}{d\lambda}\mathcal{W} = \begin{pmatrix} 0 & 1 \\ R^\mu_{\ell\nu} & 0 \end{pmatrix} \mathcal{W}, \quad (35)$$

where the only formal difference with respect to equation (8) is that the covariant derivative along the photon geodesic $D/D\lambda$ reduces to the total derivative $d/d\lambda$ in the SNF. In equation (35), the optical tidal matrix is projected in the SNF and it is given by

$$R^\mu_{\ell\nu} = h^{\mu\omega}R_{\omega\ell\nu} = \phi^{\rho\mu}R_{\rho\alpha\beta\sigma}\ell^\alpha\ell^\beta\phi^\sigma_{\nu}, \quad (36)$$

where $h^{\mu\omega}$ is the inverse of the induced metric of the frame defined as

$$h^{\mu\omega} = \begin{pmatrix} 0 & 0 & 0 & \frac{1}{Q} \\ 0 & 1 & 0 & 0 \\ 0 & 0 & 1 & 0 \\ \frac{1}{Q} & 0 & 0 & \frac{1}{Q^2} \end{pmatrix} \quad (37)$$

with Q as in equation (33). In general $R^\mu_{\ell\nu}$ is a 4×4 matrix with non trivial components. However, in the SNF it is easy to use the symmetries of the Riemann tensor to show that the components $R^0_{\ell\nu} = R^\ell_{\ell\nu}$ and $R^\mu_{\ell 0} = R^\mu_{\ell\ell}$ vanish. Now, let us use equations (22) and (34) in (36) to write the optical tidal matrix in terms of 3 + 1 quantities

$$R^\mu_{\ell\nu} = (\Phi^\mu n^\rho + F^{\mu\rho})R_{\rho\alpha\beta\sigma}\mathcal{E}^2(n^\alpha n^\beta + n^\alpha V^\beta + V^\alpha n^\beta + V^\alpha V^\beta)(\Phi_\nu n^\sigma + F^\sigma_\nu) \quad (38)$$

After some tedious but straightforward calculations, we finally obtain

$$\begin{aligned} R^\mu{}_{\ell\nu} = & \mathcal{E}^2 h^{\mu\rho} \left[\mathcal{R}_{\beta\alpha} \left(\Phi_\rho F^\beta{}_\nu V^\alpha + \Phi_\nu F^\beta{}_\rho V^\alpha - \Phi_\rho \Phi_\nu V^\beta V^\alpha - F^\alpha{}_\rho F^\beta{}_\nu \right) \right. \\ & + \mathcal{C}_{\sigma\beta\alpha} \left(\Phi_\rho F^\sigma{}_\nu V^\alpha V^\beta + \Phi_\nu F^\sigma{}_\rho V^\alpha V^\beta - F^\alpha{}_\rho F^\sigma{}_\nu V^\beta - F^\alpha{}_\nu F^\sigma{}_\rho V^\beta \right) \\ & \left. + \mathcal{G}_{\omega\alpha\beta\sigma} F^\omega{}_\rho V^\alpha V^\beta F^\sigma{}_\nu \right] \end{aligned} \quad (39)$$

where

$$\mathcal{G}_{\mu\alpha\beta\nu} = R_{\rho\delta\theta\sigma} \gamma^\rho{}_\mu \gamma^\delta{}_\alpha \gamma^\theta{}_\beta \gamma^\sigma{}_\nu = {}^{(3)}R_{\mu\alpha\beta\nu} + K_{\mu\beta} K_{\alpha\nu} - K_{\mu\nu} K_{\beta\alpha} \quad (40)$$

$$\mathcal{C}_{\mu\alpha\beta} = R_{\rho\delta\theta\sigma} n^\rho \gamma^\delta{}_\alpha \gamma^\theta{}_\beta \gamma^\sigma{}_\mu = D_\alpha K_{\mu\beta} - D_\mu K_{\alpha\beta} \quad (41)$$

$$\mathcal{R}_{\mu\nu} = R_{\rho\delta\theta\sigma} n^\rho \gamma^\delta{}_\nu \gamma^\theta{}_\mu n^\sigma = \mathcal{L}_n K_{\nu\alpha} + \frac{1}{\alpha} D_\nu D_\alpha \alpha + K^\rho{}_\alpha K_{\nu\rho} \quad (42)$$

are the Gauss relation, the Codazzi relation and the Ricci relation, respectively (see e.g. [27]). In `BiGONLight`, the three functions `GaussRelation[]`, `CodazziRelation[]`, `RicciRelation[]` compute the relations in equations (40)–(42) and the function `OpticalTidalMatrix[]` collects all previous results together in order to obtain the optical tidal matrix $R^\mu{}_{\ell\nu}/\mathcal{E}^2$ in equation (39) as output. We now have the equation for the BGO, equation (35), projected onto the SNF and written in terms of 3 + 1 quantities. To solve it, it is easier to change the derivation variable from the affine parameter λ to the time t according to

$$\frac{d}{d\lambda} = \frac{dt}{d\lambda} \frac{d}{dt} = \frac{\mathcal{E}}{\alpha} \frac{d}{dt}, \quad (43)$$

where we used the time component of the tangent vector in equation (22), i.e. $\ell^0 = dt/d\lambda = \mathcal{E}/\alpha$. The GDE for the BGO, equation (35), decouples in two systems of first-order ODE, one for $(\mathcal{W}_{XX}, \mathcal{W}_{LX})$ and the other for $(\mathcal{W}_{XL}, \mathcal{W}_{LL})$, computed separately using the function `BGOequations[]`:

$$\left\{ \begin{aligned} \frac{d\mathcal{W}_{XX}{}^\mu{}_\nu}{dt} &= \frac{\alpha}{\mathcal{E}} \mathcal{W}_{LX}{}^\mu{}_\nu \\ \frac{d\mathcal{W}_{LX}{}^\mu{}_\nu}{dt} &= \frac{\alpha}{\mathcal{E}} R^\mu{}_{\ell\sigma} \mathcal{W}_{XX}{}^\sigma{}_\nu \end{aligned} \right\}, \quad \left\{ \begin{aligned} \frac{d\mathcal{W}_{XL}{}^\mu{}_\nu}{dt} &= \frac{\alpha}{\mathcal{E}} \mathcal{W}_{LL}{}^\mu{}_\nu \\ \frac{d\mathcal{W}_{LL}{}^\mu{}_\nu}{dt} &= \frac{\alpha}{\mathcal{E}} R^\mu{}_{\ell\sigma} \mathcal{W}_{XL}{}^\sigma{}_\nu \end{aligned} \right\} \quad (44)$$

with initial conditions:

$$\left\{ \begin{aligned} \mathcal{W}_{XX}{}^\mu{}_\nu|_{\mathcal{O}} &= \delta^\mu{}_\nu \\ \mathcal{W}_{XL}{}^\mu{}_\nu|_{\mathcal{O}} &= 0 \\ \mathcal{W}_{LX}{}^\mu{}_\nu|_{\mathcal{O}} &= 0 \\ \mathcal{W}_{LL}{}^\mu{}_\nu|_{\mathcal{O}} &= \delta^\mu{}_\nu. \end{aligned} \right. \quad (45)$$

The systems in equation (44) are solved separately in `BiGONLight` by `SolveBGO[]`. Getting the BGO with the procedure just described is one important part of `BiGONLight`. Let us recall that the only inputs required are the spacetime metric, the observer four-velocity components and the initial and ending points.

With initial conditions in equation (45), equation (44) gives the BGO $\mathcal{W}(p_\lambda, \mathcal{O})$ integrated backward in time from the observer. The relation with the BGO $\mathcal{W}(p_\lambda, \mathcal{S})$ integrated forward in time from the source can be explicitly written down for all the BGO components from

equation (12). To this end we need the inverse matrix \mathcal{W}^{-1} which is easily found from the symplectic property

$$\mathcal{W}^{T\bar{m}} \Omega_{\bar{m}\bar{s}} \mathcal{W}^{\bar{s}}_{\bar{b}} = \Omega_{\bar{a}\bar{b}}, \quad (46)$$

where Ω is the 8×8 non-singular, skew-symmetric matrix

$$\Omega_{\bar{a}\bar{b}} = \begin{pmatrix} 0 & h_{\alpha\beta} \\ -h_{\gamma\delta} & 0 \end{pmatrix}, \quad (47)$$

with Latin tilded indices running from 0 to 7 ($\bar{a}, \dots = 0, 1, \dots, 7$) and the Greek bold indices ($\alpha = 0, 1, \dots, 3$) indicate the components in the SNF. By inverting equation (46) we find

$$\begin{aligned} \mathcal{W}^{-1} &= \Omega^{-1} \mathcal{W}^T \Omega \\ &= \begin{pmatrix} 0 & -h^{\alpha\rho} \\ h^{\beta\sigma} & 0 \end{pmatrix} \begin{pmatrix} \mathcal{W}_{XX}^{\nu\sigma} & \mathcal{W}_{LX}^{\mu\sigma} \\ \mathcal{W}_{XL}^{\nu\rho} & \mathcal{W}_{LL}^{\mu\rho} \end{pmatrix} \begin{pmatrix} 0 & h_{\nu\gamma} \\ -h_{\mu\delta} & 0 \end{pmatrix}. \end{aligned} \quad (48)$$

The transformation from forward to backward BGO in equation (12) finally reads

$$\begin{aligned} \mathcal{W}_{XX}(p_\lambda, \mathcal{O})^\sigma_{\nu} &= \mathcal{W}_{XX}(p_\lambda, \mathcal{S})^\sigma_{\alpha} h^{\alpha\rho} \mathcal{W}_{LL}^T(\mathcal{O}, \mathcal{S})^\mu_{\rho} h_{\mu\nu} \\ &\quad - \mathcal{W}_{XL}(p_\lambda, \mathcal{S})^\sigma_{\alpha} h^{\alpha\rho} \mathcal{W}_{LX}^T(\mathcal{O}, \mathcal{S})^\mu_{\rho} h_{\mu\nu} \end{aligned} \quad (49)$$

$$\begin{aligned} \mathcal{W}_{XL}(p_\lambda, \mathcal{O})^\sigma_{\nu} &= -\mathcal{W}_{XX}(p_\lambda, \mathcal{S})^\sigma_{\alpha} h^{\alpha\rho} \mathcal{W}_{XL}^T(\mathcal{O}, \mathcal{S})^\mu_{\rho} h_{\mu\nu} \\ &\quad + \mathcal{W}_{XL}(p_\lambda, \mathcal{S})^\sigma_{\alpha} h^{\alpha\rho} \mathcal{W}_{XX}^T(\mathcal{O}, \mathcal{S})^\mu_{\rho} h_{\mu\nu} \end{aligned} \quad (50)$$

$$\begin{aligned} \mathcal{W}_{LX}(p_\lambda, \mathcal{O})^\sigma_{\nu} &= \mathcal{W}_{LX}(p_\lambda, \mathcal{S})^\sigma_{\alpha} h^{\alpha\rho} \mathcal{W}_{LL}^T(\mathcal{O}, \mathcal{S})^\mu_{\rho} h_{\mu\nu} \\ &\quad - \mathcal{W}_{LL}(p_\lambda, \mathcal{S})^\sigma_{\alpha} h^{\alpha\rho} \mathcal{W}_{LX}^T(\mathcal{O}, \mathcal{S})^\mu_{\rho} h_{\mu\nu} \end{aligned} \quad (51)$$

$$\begin{aligned} \mathcal{W}_{LL}(p_\lambda, \mathcal{O})^\sigma_{\nu} &= -\mathcal{W}_{LX}(p_\lambda, \mathcal{S})^\sigma_{\alpha} h^{\alpha\rho} \mathcal{W}_{XL}^T(\mathcal{O}, \mathcal{S})^\mu_{\rho} h_{\mu\nu} \\ &\quad + \mathcal{W}_{LL}(p_\lambda, \mathcal{S})^\sigma_{\alpha} h^{\alpha\rho} \mathcal{W}_{XX}^T(\mathcal{O}, \mathcal{S})^\mu_{\rho} h_{\mu\nu}. \end{aligned} \quad (52)$$

These relations are coded in the section ‘forward to backward transformation for \mathcal{W} operators’ of each sample notebook in the repository <https://github.com/MicGrasso/bigonlight.git>.

4. Optical observables with BiGONLight

The recipe to obtain optical observables using BiGONLight can be summarized as follows. One needs to:

- (a) Specify the spacetime metric $g_{\mu\nu}$ and the source \mathcal{S} and observer \mathcal{O} kinematics, namely four-velocity u^μ and four-acceleration w^μ . They can be given already in $3 + 1$ components or as 4D quantities and the functions `ADM[]` and `Vsplit[]` will do the splitting of $g_{\mu\nu}$, and u^μ and w^μ respectively;
- (b) Set up the initial photon geodesic using `Vsplit[]` for the null tangent ℓ^μ , which gives its $3 + 1$ components \mathcal{E} and V^i . Alternatively one can give \mathcal{E} and a vector V^i that has to be assigned by specifying the spatial direction V^2 and V^3 and use `InitialConditions[]` to get V^1 from the null condition;

- (c) Obtain the geodesic equations equations (23) and (24) from `GeodesicEquations []` and `EnergyEquations []`, and then solve them with `SolveGeodesic []` and `SolveEnergy []`⁶;
- (d) Set up the initial conditions for the SNF according to equation (33), directly in 3 + 1 components or using `SNF []`, which is specifically designed to compute the SNF in 3 + 1. Then `PTransportedFrame []` will give the SNF parallel transported along the light ray;
- (e) Compute separately $R^\mu{}_{\ell\nu}$ projected into the SNF with `OpticalTidalMatrix []`;
- (f) Obtain the ODE system for the BGO in equation (44) with `BGOequations []` and, together with the initial conditions in equation (45), solve it using `SolveBGO []` to finally find the full \mathcal{W} matrix;

Note that the components of the optical tidal matrix can have a very complicated expression, that may cause problems in solving the GDE (44). This can be overcome by using an interpolated form of $R^\mu{}_{\ell\nu}$: the `Mathematica interpolation []` function allows to use different methods and reach an excellent precision, see section 5.

Step (f) is the starting point to compute the optical observables, which are all given by different combinations and/or functions of the \mathcal{W} components. It is important to remark that all the observables in the BGO formalism are written in terms of $\mathcal{W}(\mathcal{S}, \mathcal{O})$, namely the map computed from the observer to the source. As we already recalled, this is obtained directly by integrating the GDE backward in time. However in some cases, e.g. if the spacetime model comes from a numerical simulation, it may be more convenient to get the inverse BGO map $\mathcal{W}^{-1}(\mathcal{S}, \mathcal{O})$ and then use the transformations equations (49)–(52) to obtain the \mathcal{W} needed for the observables.

Here we list the four observables that we study in this paper. The redshift is simply given by its definition

$$1 + z = \frac{(\ell_\sigma u^\sigma)|_{\mathcal{S}}}{(\ell_\sigma u^\sigma)|_{\mathcal{O}}}, \quad (53)$$

where ℓ^σ is the tangent to the light ray, and $u_{\mathcal{O}}^\sigma$ and $u_{\mathcal{S}}^\sigma$ are the observer and source four-velocities. The same definition in 3 + 1 splitting reads:

$$1 + z = \frac{\mathcal{E}_{\mathcal{S}}}{\mathcal{E}_{\mathcal{O}}} \frac{1 - (\gamma_{ij} V^i U^j)|_{\mathcal{S}}}{1 - (\gamma_{ij} V^i U^j)|_{\mathcal{O}}} \left[\frac{1 - (\gamma_{ij} U^i U^j)|_{\mathcal{S}}}{1 - (\gamma_{ij} U^i U^j)|_{\mathcal{O}}} \right]^{\frac{1}{2}}. \quad (54)$$

The angular diameter distance is formally given by

$$D_{\text{ang}} = (\ell_\sigma u^\sigma)|_{\mathcal{O}} |\det(\mathcal{W}_{\text{XL}}^A{}_{\mathcal{B}})|^{\frac{1}{2}}, \quad (55)$$

where $\mathcal{W}_{\text{XL}}^A{}_{\mathcal{B}}$ is the map between the physical size of the source and the angle subtended in the sky, as measured at the observer position, namely

$$\delta\theta^A = (\ell_\sigma u^\sigma)|_{\mathcal{O}}^{-1} (\mathcal{W}_{\text{XL}}^A{}_{\mathcal{B}})^{-1} \delta x_{\mathcal{S}}^{\mathcal{B}}. \quad (56)$$

Conversely, the parallax distance is related to the displacement of the observer position and the apparent angular shift of the source position, as measured from the observer

$$\delta\theta^A = -(\ell_\sigma u^\sigma)|_{\mathcal{O}}^{-1} (\mathcal{W}_{\text{XL}}^A{}_{\mathcal{C}})^{-1} \mathcal{W}_{\text{XX}}^{\mathcal{C}}{}_{\mathcal{B}} \delta x_{\mathcal{O}}^{\mathcal{B}}. \quad (57)$$

⁶For the purposes of our paper, we need to solve only photon geodesics. However, the code can be used to trace any type of geodesics, namely time-like and space-like also, by specifying the appropriate initial tangent vector in the 3 + 1 splitting with `Vsplit []`.

The expression for the parallax distance is

$$D_{\text{par}} = (\ell_\sigma u^\sigma)|_{\mathcal{O}} \frac{|\det(\mathcal{W}_{\text{XL}}^A{}^B)|^{\frac{1}{2}}}{|\det(\mathcal{W}_{\text{XX}}^A{}^B)|^{\frac{1}{2}}}. \quad (58)$$

The last observable that we consider in this paper is the redshift drift ζ , given in terms of the BGO by [32],

$$\zeta \equiv \frac{\delta \log(1+z)}{\delta \tau_{\mathcal{O}}} = \Xi_{\text{Doppler}} - \left(u_{\mathcal{O}}, \frac{u_S}{1+z}\right) \mathbf{U} \begin{pmatrix} u_{\mathcal{O}} \\ u_S \\ 1+z \end{pmatrix}. \quad (59)$$

In the above expression $\tau_{\mathcal{O}}$ is the proper time of the observer, the first term

$$\Xi_{\text{Doppler}} = \left[\frac{1}{1+z} \frac{(\ell^\mu w_\mu)|_S}{(\ell^\mu u_\mu)|_S} - \frac{(\ell^\mu w_\mu)|_{\mathcal{O}}}{(\ell^\mu u_\mu)|_{\mathcal{O}}} \right] \quad (60)$$

represents the Doppler effect caused by the four-acceleration w^σ of the observer and the source, and \mathbf{U} is an 8×8 matrix given by the following combinations of the BGO

$$\mathbf{U} = \begin{pmatrix} -\mathcal{W}_{\text{XL}}^{-1\nu}{}_\rho \mathcal{W}_{\text{XX}}^\rho{}_\sigma & \mathcal{W}_{\text{XL}}^{-1\nu}{}_\rho \\ \mathcal{W}_{\text{LL}}^\mu{}_\nu \mathcal{W}_{\text{XL}}^{-1\nu}{}_\rho \mathcal{W}_{\text{XX}}^\rho{}_\sigma - \mathcal{W}_{\text{LX}}^\mu{}_\sigma & -\mathcal{W}_{\text{LL}}^\mu{}_\nu \mathcal{W}_{\text{XL}}^{-1\nu}{}_\rho \end{pmatrix}. \quad (61)$$

Let us notice that, even if the BGO formalism is independent of the specific choice of the frame used, the observables are dependent on this choice, as evident by the explicit dependence on $u_{\mathcal{O}}^\mu$, u_S^μ , $w_{\mathcal{O}}^\mu$ and w_S^μ in equations (55)–(60). Indeed, it is possible to transform locally between two different frames using an appropriate Lorentz transformation, but this modifies the observables introducing special relativistic effects like Doppler effect or aberration.

The reader can find the derivation of the equations (55)–(59) in [20, 32, 33]. All the expressions in equations (55), (58) and (59) are new with respect to the standard approach, in the sense that these observables are expressed within a new, unified framework. However, while for D_{ang} and D_{par} there already exist analogous formulas, where instead of the BGO we have the magnification and the parallax matrix (see [21] for the comparison), it did not exist a general formula for the redshift drift: equation (59) looks the same for every spacetime model under consideration. Instead, in the standard approach the redshift drift is calculated by taking the derivative with respect to the time coordinate of the definition of the redshift, and this depends on the specific form of the metric tensor and null-geodesic, the latter depending in turns on the symmetries that one gives to the initial conditions. This means that the equations to get the redshift drift in the standard approach look different for each specific model and/or configuration of the light rays⁷.

5. Code tests

In this section we test the accuracy of `BiGONLight` within well-known cosmological models. The tests are performed by considering the following observables: redshift, angular diameter distance, parallax distance, and redshift drift. We compare the results obtained with two

⁷ To be more precise, equation (68) is valid for the Friedmann–Lemaître–Robertson–Walker (FLRW) model only as well as equation (96) is valid for the Szekeres model and geodesics along the symmetry axis only. Instead, equation (59) looks the same in both cases.

different procedures, by defining the estimator $\Delta O(\text{BGO}, X)$

$$\Delta O(\text{BGO}, X) \equiv \frac{O^{\text{BGO}} - O^X}{O^X}, \quad (62)$$

where O^{BGO} refers to equations (53), (55), (58) and (59). We consider the following three cases: (i) the Λ CDM model, where the spacetime metric is the analytical input for `BiGONLight` to compute O^{BGO} and for O^X we use the analytical well-known solutions for all the four observables, see section 5.1; (ii) the inhomogeneous Szekeres model [34], where the spacetime metric is again the analytical input for `BiGONLight` but to obtain O^X we solve numerically a specific differential equation for each observable, see section 5.2; (iii) the Einstein-de Sitter model, where the input for `BiGONLight` are the $3 + 1$ quantities coming from the `Einstein Toolkit` (ET) simulation and O^X is obtained analytically, see section 5.3.

It worth noting that if O^X is obtained analytically, then $\max |\Delta O(\text{BGO}, X)|$ represents the simulation error: in case (i) we have just the computational error from `BiGONLight` whereas in case (iii) the final error in the observables is the combined effect of both the ET and `BiGONLight` finite precision. On the other hand, if O^X is obtained numerically, as in case (ii), then $\Delta O(\text{BGO}, X)$ gives only an estimation of the accuracy of the two methods used.

5.1. The Λ CDM model

The first group of tests regards the study of light propagation in the flat Λ CDM model. This is an exact solution of the Einstein field equations representing an homogeneous and isotropic spacetime and the matter–energy content consists of irrotational dust of cold dark matter and a cosmological constant Λ . The line element is given by

$$ds^2 = a(\eta)^2 (-d\eta^2 + \delta_{ij} dx^i dx^j) \quad (63)$$

where η is the conformal time and $a(\eta)$ is the scale factor, which is the solution of Einstein equations and describes the dynamics of the model. The explicit result is found to be [35]

$$a(\eta) = \frac{\sqrt[3]{\frac{\Omega_{m_0}}{\Omega_\Lambda}} (1 - \text{cn}(y|r))}{(\sqrt{3} - 1) + (\sqrt{3} + 1)\text{cn}(y|r)}, \quad (64)$$

where $\text{cn}(y|r)$ is the Jacobi elliptic cosine function, with $y = (\sqrt[4]{3} \sqrt[3]{\Omega_\Lambda} \sqrt[3]{\Omega_{m_0}}) \mathcal{H}_0 \eta$, \mathcal{H}_0 being the Hubble parameter $\mathcal{H} = \frac{1}{a} \frac{da}{d\eta}$ evaluated today, Ω_Λ and Ω_{m_0} are the cosmological parameters representing the amount of dark energy (Ω_Λ) and dark matter (Ω_{m_0}) today, and $r = \sqrt{\frac{\sqrt{3}+2}{4}}$.

To test `BiGONLight` we consider two classical observables, namely the redshift z and the angular diameter distance D_{ang} , and two interesting observables that are not yet measured in the cosmological context as they belong to the new research field named real-time cosmology, see reference [1]. One is the parallax distance which exploits the motion of the Solar System with respect to the cosmic microwave background frame providing a baseline of 78 AU per year for the cosmic parallax⁸. Cosmic parallax was first proposed in 1986 in reference [37] and it is expected to be measured by the Gaia satellite [38], in the next few years. For discussions and forecasts about the measurements of the cosmological parallax distance we refer to references

⁸For an exhaustive definition of the parallax see e.g. reference [36], in which the author distinguishes between the three different cases: one source observed by two observers separated by spacelike interval (classic parallax), two sources observed by two observers separated by spacelike interval and two sources observed by one observer at two different moments (cosmic parallax also known as position drift).

[1, 36, 39–44] and references therein. The other is the redshift drift, i.e. the time variation of the redshift of a source. It was first derived for the FLRW models in references [45, 46]. Since then, and particularly in recent years, a lot of work has been done to investigate the measurability of the redshift drift in cosmology and the information gained, see e.g. references [47–51].

The analytical expressions in the flat FLRW cosmologies for the four observables that we consider are

$$z^{\Lambda\text{CDM}} = \frac{a_0}{a} - 1 \quad (65)$$

$$D_{\text{ang}}^{\Lambda\text{CDM}} = \frac{a_0}{1+z} \int_0^z \frac{dz'}{(1+z')\mathcal{H}(z')} \quad (66)$$

$$D_{\text{par}}^{\Lambda\text{CDM}} = \frac{a_0}{\mathcal{H}_0} \frac{\int_0^z \frac{\mathcal{H}_0 dz'}{(1+z')\mathcal{H}(z')}}{1 + \int_0^z \frac{\mathcal{H}_0 dz'}{(1+z')\mathcal{H}(z')}} \quad (67)$$

$$\zeta^{\Lambda\text{CDM}} = \frac{\mathcal{H}_0}{a_0} \left(1 - \frac{\mathcal{H}(z)}{\mathcal{H}_0} \right), \quad (68)$$

where the Hubble parameter in the ΛCDM model is given by

$$\mathcal{H}(z) = \mathcal{H}_0 \sqrt{\Omega_{\text{m}0}(1+z) + \Omega_{\Lambda}(1+z)^{-2}}. \quad (69)$$

We normalize the today scale factor $a_0 = 1$ and we take $\mathcal{H}_0 = 67.36 \text{ kms}^{-1} \text{ Mpc}^{-1}$, the matter parameter today $\Omega_{\text{m}0} = 0.315$, and the cosmological constant parameter $\Omega_{\Lambda} = 0.685$ from [52]. The integral in equations (66) and (67) can be solved analytically and the results is [35],

$$\int_0^z \frac{dz'}{(1+z')\mathcal{H}(z')} = \frac{F[\xi(z)|r] - F[\xi(0)|r]}{(\Omega_{\text{m}0})^{\frac{1}{3}}(\Omega_{\Lambda})^{\frac{1}{6}}3^{\frac{1}{4}}} \quad (70)$$

where $F[\xi(z)|r]$ the elliptic integral of the first kind, with arguments $r = \sqrt{\frac{2+\sqrt{3}}{4}}$ and

$$\xi(z) = \arccos \left(\frac{2\sqrt{3}}{1 + \sqrt{3} + (1+z)\sqrt[3]{\frac{\Omega_{\text{m}0}}{\Omega_{\Lambda}}}} - 1 \right). \quad (71)$$

The fact that we have analytical expressions for the observables makes this model a perfect test-bed for the code. We compare the results from `BiGONLight` with the one in equations (65)–(68) by considering the variation

$$\Delta O(\text{BGO}, \Lambda\text{CDM}) \equiv \frac{O^{\text{BGO}} - O^{\Lambda\text{CDM}}}{O^{\Lambda\text{CDM}}}. \quad (72)$$

As shown in figure 2, the numerical implementation of the BGO method is in excellent agreement with the analytical formulas in ΛCDM , the variation ΔO being $10^{-22} \div 10^{-31}$. The maximum value of ΔO , of the order of 10^{-22} , represents the numerical error over the observables and we reached such small values by using the precision control options `WorkingPrecision`, `PrecisionGoal` and `AccuracyGoal` implemented in `Mathematica`.

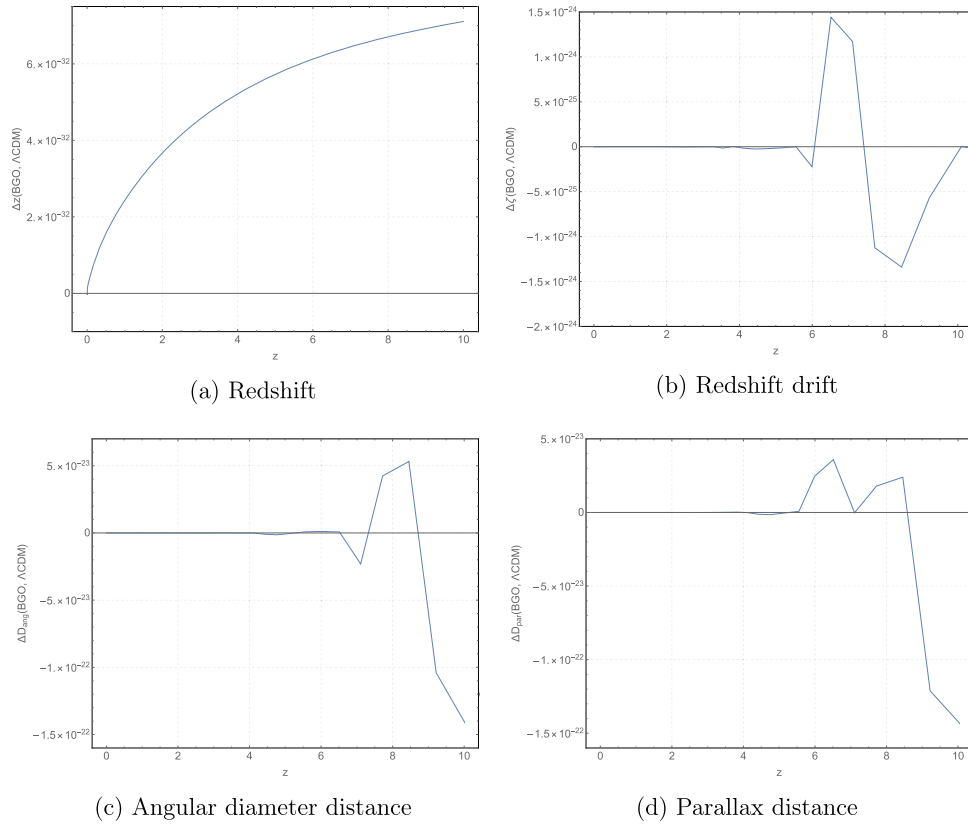


Figure 2. Variations in the Λ CDM model, equation (72), for the redshift (a), the redshift drift (b), the angular diameter distance (c), and the parallax distance (d). The variable in the horizontal axis is the redshift in Λ CDM. The values for the cosmological parameters are taken from [52].

5.2. The Szekeres model

The second group of code tests is performed considering an inhomogeneous cosmological model which is an exact solution of Einstein equations, firstly presented in [53]. The line element for the Szekeres spacetime is:

$$ds^2 = -dt^2 + e^{2\alpha} dx^{12} + e^{2\beta} (dx^{22} + dx^{32}) \quad (73)$$

with α and β functions of the spacetime coordinates (t, x^1, x^2, x^3) that are determined by solving the Einstein equations. We can distinguish two different families of Szekeres models depending whether $\partial_{x^3}\beta \neq 0$ or $\partial_{x^3}\beta = 0$: the first case defines the ‘class I’ family, which is a generalization of Lemaître–Tolman–Bondi models (with non-concentric shells), while the case $\partial_{x^3}\beta = 0$ corresponds to a simultaneous generalization of the Friedmann and Kantowski–Sachs models and it defines the ‘class II’ family. For a cosmological formulation of the Szekeres spacetimes see e.g. [54]. For our tests, we will use a class II Szekeres model filled with dust and a positive

cosmological constant as presented in [34]. For this model, the line element (73) is rewritten as:

$$ds^2 = a(\eta)^2 \left[-d\eta^2 + dx^{12} + dx^{22} + Z(\eta, x^1, x^2, x^3)^2 dx^{32} \right] \quad (74)$$

and, for the special case of axial symmetry around x^3 , we have the following form for the function Z :

$$Z(\eta, x^1, x^2, x^3) = 1 + \beta_+(x^3)\mathcal{D}(\eta) + \beta_+(x^3)B \left(x^{12} + x^{22} \right). \quad (75)$$

The function \mathcal{D} is the growing mode solution of the first-order Newtonian density contrast defined as $\delta = \frac{\rho - \rho_{\Lambda\text{CDM}}}{\rho_{\Lambda\text{CDM}}}$ and it is given by, see e.g. [55],

$$\mathcal{D}(\eta) = \frac{a}{\frac{5}{2}\Omega_{m0}} \sqrt{1 + \frac{\Omega_{\Lambda}}{\Omega_{m0}} a^3} {}_2F_1 \left(\frac{3}{2}, \frac{5}{6}, \frac{11}{6}, -\frac{\Omega_{\Lambda0}}{\Omega_{m0}} a^3 \right), \quad (76)$$

with ${}_2F_1(a, b, c, y)$ being the Gaussian (or ordinary) hypergeometric function. The term B in equation (75) is constant and given by (see appendix C in [56])

$$B = \frac{5}{4} \mathcal{H}_0^2 \Omega_{m0} \frac{\mathcal{D}_{in}}{a_{in}}, \quad (77)$$

where $\mathcal{D}_{in} = a_{in}$ for initial conditions set deeply in the matter-dominated era. The function β_+ specifies the spatial distribution of the first-order density contrast and it can be related to the peculiar gravitational potential ϕ_0 via the cosmological Poisson equation at present time

$$\beta_+ = -\frac{2}{3} \frac{\partial_{x^3}^2 \phi_0}{\mathcal{H}_0^2 \Omega_{m0}}. \quad (78)$$

For the tests, we will use a sinusoidal profile for the peculiar gravitational potential $\phi_0 = \mathcal{A} \sin(\omega x^3)$ with $\omega = \frac{2\pi}{500 \text{ Mpc}}$ and amplitude \mathcal{A} such that $\delta_0 = 0.1$ for the density contrast today.

In the following, we will present the tests over the redshift, the angular diameter distance and the redshift drift. Contrary to the ΛCDM case, here the observables are obtained using two numerical methods and the difference is expressed by

$$\Delta O(\text{BGO}, \text{Sz}) \equiv \frac{O^{\text{BGO}} - O^{\text{Sz}}}{O^{\text{Sz}}}. \quad (79)$$

All the three tests are done considering that the observer \mathcal{O} is located at the origin of the reference frame, with coordinates $(\eta_0, 0, 0, 0)$, and she/he sees the light coming from a comoving distant source \mathcal{S} , with coordinates $(\eta, 0, 0, x^3)$. The light beam is propagating along the x^3 axis, with tangent vector $\ell^\mu = (\ell^0, 0, 0, \ell^3)$.

The first observable we test is the redshift: for a photon travelling along the x^3 -axis it is

$$1 + z^{\text{Sz}} = \frac{(a\ell^0)|_{\mathcal{S}}}{(a\ell^0)|_{\mathcal{O}}}, \quad (80)$$

where ℓ^0 is obtained by solving the geodesic equation

$$\frac{d\ell^0}{d\eta} = -\ell^0 \left(2\mathcal{H} + \frac{\dot{Z}}{Z} \right). \quad (81)$$

In the above expressions Z is given in equation (75), a is the scale factor (64), and \mathcal{H} the Hubble parameter (69) of the Λ CDM background. The variation $\Delta z(\text{BGO}, \text{Sz})$ refers to the numerical solution of equation (81) as opposite to the 3 + 1 geodesic solved by `BiGONLight`.

The second observable under analysis is the angular diameter distance D_{ang} . The standard procedure to compute D_{ang} is solving the Sachs focusing equation

$$\frac{d^2 D_{\text{ang}}}{d\lambda^2} = - \left(|\sigma|^2 + \frac{1}{2} R_{\mu\nu} \ell^\mu \ell^\nu \right) D_{\text{ang}}, \quad (82)$$

where the initial conditions given at \mathcal{O} (i.e. the focusing point) are $D_{\text{ang}}|_{\mathcal{O}} = 0$ and $\left. \frac{dD_{\text{ang}}}{d\lambda} \right|_{\mathcal{O}} = (\ell_\sigma u^\sigma)|_{\mathcal{O}}$, and $|\sigma|$ is the shear that in the Szekeres model equations (74) and (75) simply vanishes, as shown in [57]. Using the Einstein equations to express $R_{\mu\nu} \ell^\mu \ell^\nu$ in terms of the density contrast and using conformal time instead of the affine parameter, the focusing equation assumes the form

$$\ddot{D}_{\text{ang}}^{\text{Sz}} + \frac{\dot{\ell}^0}{\ell^0} \dot{D}_{\text{ang}}^{\text{Sz}} = - \frac{3}{2} \frac{\mathcal{H}_0^2 \Omega_{\text{m}0}}{a} (\delta + 1) D_{\text{ang}}^{\text{Sz}}, \quad (83)$$

where the dots refers to derivatives respect to conformal time η and the initial conditions at the observation point are $D_{\text{ang}}|_{\mathcal{O}} = 0$ and $\dot{D}_{\text{ang}}|_{\mathcal{O}} = \frac{(\ell_\sigma u^\sigma)|_{\mathcal{O}}}{\ell^0}$. In synchronous-comoving gauge the density contrast along the geodesic comes directly from the continuity equation and reads

$$\delta = - \frac{\mathcal{D}\beta_+}{Z} = \frac{\frac{2}{3} \frac{\partial_{x^3}^2 \phi_0}{\mathcal{H}_0^2 \Omega_{\text{m}0}} \mathcal{D}}{1 - \frac{2}{3} \frac{\partial_{x^3}^2 \phi_0}{\mathcal{H}_0^2 \Omega_{\text{m}0}} \mathcal{D} - \frac{2}{3} \frac{\partial_{x^3}^2 \phi_0}{\mathcal{H}_0^2 \Omega_{\text{m}0}} B(x^{1^2} + x^{2^2})}. \quad (84)$$

In our estimator equation (79) the angular diameter distance $D_{\text{ang}}^{\text{Sz}}$ is obtained by integrating equation (83), whereas $D_{\text{ang}}^{\text{BGO}}$ is obtained from equation (55) with `BiGONLight`.

The last test concerns the calculation of the redshift drift, namely the secular variation of the redshift of the source. It was calculated for some inhomogeneous cosmological models, see e.g. [40, 58–61], but to our knowledge there is no expression for the Szekeres model considered here, thus we give in the following a short derivation. Let us consider that during the proper time lapse $\delta\tau_{\mathcal{O}}$ the spacetime coordinates of the observer change from $x_{\mathcal{O}}^\mu = (\eta_{\mathcal{O}}, 0, 0, 0)$ to $X_{\mathcal{O}}^\mu = (\Theta_{\mathcal{O}}, 0, 0, 0)$. Similarly, in the corresponding proper time lapse $\delta\tau_{\mathcal{S}}$, the spacetime coordinates of the source change from $x_{\mathcal{S}}^\mu = (\eta_{\mathcal{S}}, 0, 0, x^3)$ to $X_{\mathcal{S}}^\mu = (\Theta_{\mathcal{S}}, 0, 0, x^3)$. Note that in this gauge \mathcal{O} and \mathcal{S} are comoving, meaning that they both have fixed spatial positions (i.e. $\delta x_{\mathcal{O}}^i = \delta x_{\mathcal{S}}^i = 0$), but the time changes differently at \mathcal{O} and at \mathcal{S} (i.e. $\Theta_{\mathcal{O}} - \eta_{\mathcal{O}} \neq \Theta_{\mathcal{S}} - \eta_{\mathcal{S}}$). The redshift and the conformal time of the source change according to⁹

$$\mathcal{Z}(\Theta_{\mathcal{S}}, x_{\mathcal{S}}^i) = z(\eta_{\mathcal{S}}, x_{\mathcal{S}}^3) + \delta z(\eta_{\mathcal{S}}, x_{\mathcal{S}}^3) \quad (85)$$

$$\Theta(x_{\mathcal{S}}^i) = \eta(x_{\mathcal{S}}^3) + \delta\eta(x_{\mathcal{S}}^3), \quad (86)$$

while the same quantities at the observer position $X_{\mathcal{O}}^\mu$ are $\mathcal{Z}(X_{\mathcal{O}}^\mu) = z(x_{\mathcal{O}}^\mu) = 0$ and $\Theta(X_{\mathcal{O}}^i) = \eta(x_{\mathcal{O}}^i) + \delta\eta(x_{\mathcal{O}}^i)$. Our final aim is to compute the redshift drift, namely

$$\zeta = \frac{\delta \ln(1+z)}{\delta\tau_{\mathcal{O}}}. \quad (87)$$

⁹ On the rhs of equations (85) and (86) we use the fact that the source location $x_{\mathcal{S}}^i$ has components on the x^3 axis only.

Let us begin with the variation of the source redshift with respect to the observer proper time $\frac{\delta z}{\delta \tau_{\mathcal{O}}}$, where it is better to obtain first $\frac{d\delta z}{dx^3}$ (equation (91)) and $\frac{d\delta \tau}{dx^3}$ (equation (94)) separately, and then combine them to get an ODE (equation (96)), whose solution gives the redshift drift. The starting point are the differentials $\frac{d\eta}{dx^3}$ and $\frac{dz}{dx^3}$. The first is simply given by the null condition $\ell^0 = -Z\ell^3$, and reads

$$\frac{d\eta}{dx^3} = -Z, \quad (88)$$

while $\frac{dz}{dx^3}$ is obtained by differentiating equation (80)¹⁰

$$\begin{aligned} \frac{dz}{dx^3} &= \frac{1}{(a\ell^0)|_{\mathcal{O}}} \left(\frac{da}{dx^3} \ell^0 + \frac{d\ell^0}{dx^3} a \right) |_{\mathcal{S}} = \frac{(a\ell^0)|_{\mathcal{S}}}{(a\ell^0)|_{\mathcal{O}}} \left(\frac{1}{a} \frac{da}{d\eta} \frac{d\eta}{dx^3} + \frac{1}{\ell^0} \frac{d\ell^0}{d\eta} \frac{d\eta}{dx^3} \right) |_{\mathcal{S}} \\ &= (1+z) (\mathcal{H}Z + \dot{Z}), \end{aligned} \quad (89)$$

where we used equations (88) and (81), and the fact that the redshift at the observer is fixed. Now we use equation (88) to differentiate equation (86)

$$\begin{aligned} \frac{d\delta\eta}{dx^3} &= \frac{d\Theta}{dx^3} - \frac{d\eta}{dx^3} = -Z(\Theta, x^3) + Z(\eta, x^3) = -[Z(\eta, x^3) + \dot{Z}(\eta, x^3)\delta\eta] + Z(\eta, x^3) \\ &= -\dot{Z}\delta\eta, \end{aligned} \quad (90)$$

and similarly for the redshift we have

$$\frac{d\delta z}{dx^3} = \frac{dZ}{dx^3} - \frac{dz}{dx^3} = (1+z)(Z\mathcal{H} + \dot{Z})\delta\eta + (Z\mathcal{H} + \dot{Z})\delta z, \quad (91)$$

where we keep first-order terms in $\delta\eta$ and δz only. Rearranging terms and using equation (89) again, we get

$$\frac{d}{dx^3} \left(\frac{\delta z}{1+z} \right) = (Z\mathcal{H} + \dot{Z})\delta\eta. \quad (92)$$

The final step is to express the variation of the conformal time $\delta\eta$ in terms of the proper time at the observer $\delta\tau_{\mathcal{O}}$. We use their relation, which is simply

$$\delta\tau = \sqrt{|g_{\mu\nu}\delta x^\mu\delta x^\nu|} = a\sqrt{|-\delta\eta^2 + Z^2\delta x^3{}^2|} = a\delta\eta, \quad (93)$$

since $\delta x^i = 0$. We need the derivative with respect to x^3 , which reads

$$\frac{d\delta\tau}{dx^3} = \frac{d(a\delta\eta)}{dx^3} = \frac{da}{dx^3}\delta\eta + a\frac{d\delta\eta}{dx^3} = \left(\frac{1}{a} \frac{da}{d\eta} \frac{d\eta}{dx^3} - \dot{Z} \right) a\delta\eta = -(\mathcal{H}Z + \dot{Z})\delta\tau, \quad (94)$$

and, together with equations (89) and (93), the solution of the last equality is

$$\delta\eta = \frac{1}{a} \frac{\delta\tau_{\mathcal{O}}}{1+z}. \quad (95)$$

¹⁰From now on we drop the index \mathcal{S} , since all the quantities are evaluated at the source.

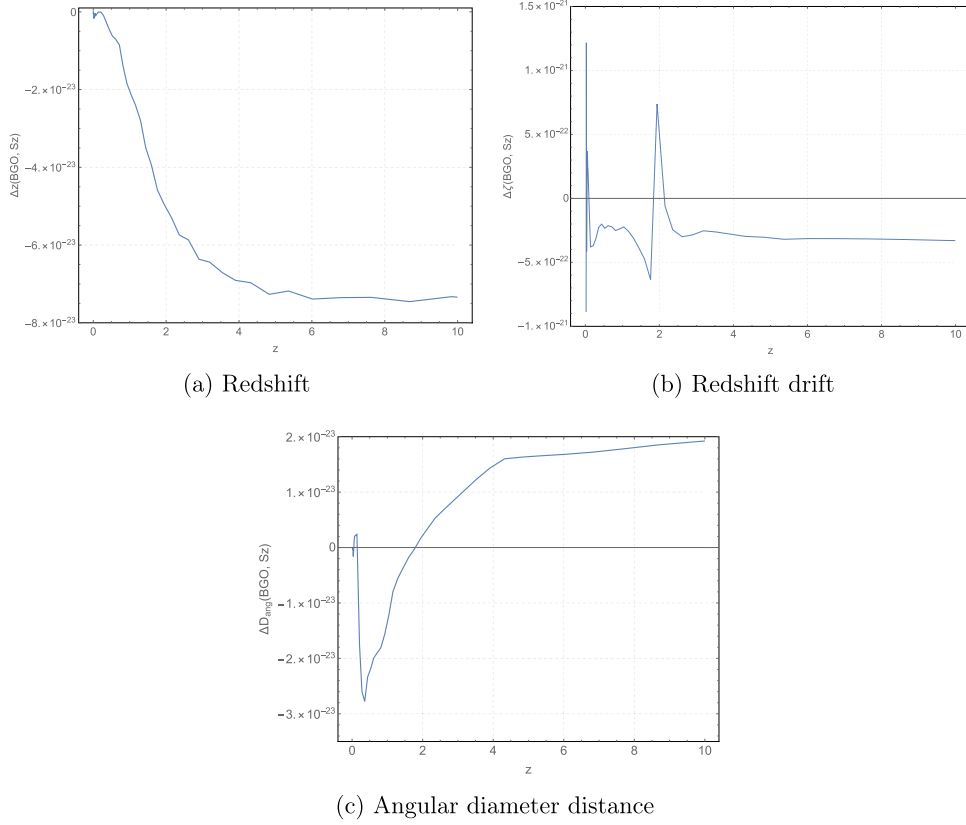


Figure 3. Variations in the Szekeres model, equation (79), for the redshift (a), the redshift drift (b), and the angular diameter distance (c). The variable in the horizontal axis is the redshift in the Szekeres model.

By changing x^3 to conformal time η with the chain rule $\frac{d}{dx^3} = \frac{d\eta}{dx^3} \frac{d}{d\eta} = -Z \frac{d}{d\eta}$, we get from equation (92) the ODE in η for the redshift drift in the Szekeres model

$$\frac{d\zeta}{d\eta} \equiv \frac{d}{d\eta} \left(\frac{\delta \log(1+z)}{\delta\tau_{\mathcal{O}}} \right) = -\frac{1}{a(1+z)} \frac{(HZ + \dot{Z})}{Z}. \quad (96)$$

For our test, in the estimator equation (79), ζ^{Sz} is the numerical solution of equation (96) and ζ^{BGO} is the expression in equation (59) obtained with `BiGONLight`. Let us mention that we did not include the parallax distance in our study of the observables in the Szekeres model because the forecasted measures of the parallax distance for inhomogeneous models are nowadays all below the instrumental precision.

As for the Λ CDM model, also for the Szekeres model we have a very good agreement between the observables calculated using the standard procedure and the observables from `BiGONLight`. The smallness of all the variations $\Delta z(\text{BGO}, Sz)$, $\Delta\zeta(\text{BGO}, Sz)$ and $\Delta D_{\text{ang}}(\text{BGO}, Sz)$ shown in figure 3 means that our code could be a reliable tool for light propagation in inhomogeneous cosmologies, represented here with the Szekeres model, which is computationally more complicated than the homogeneous Λ CDM case.

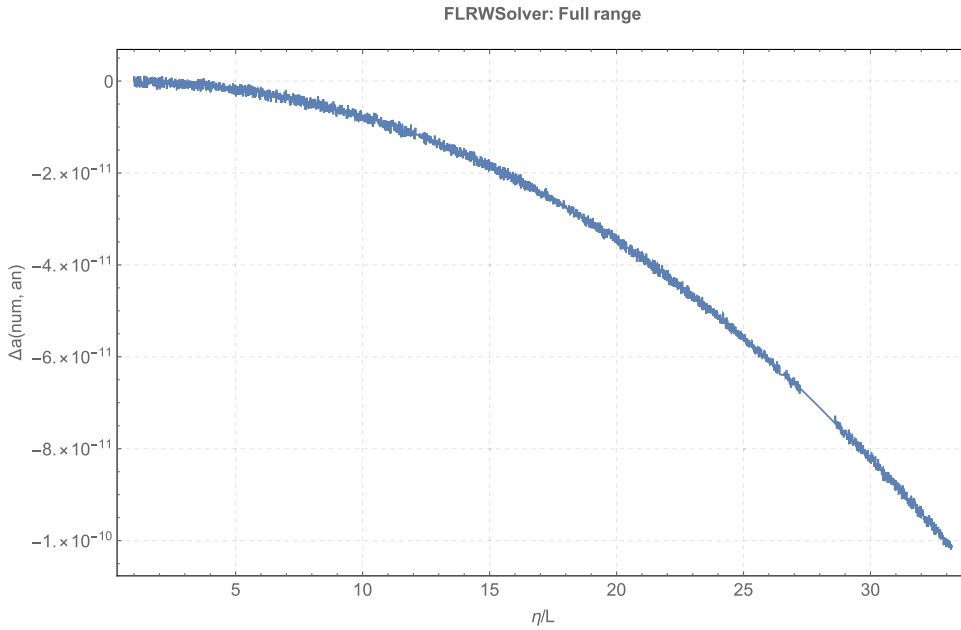


Figure 4. Scale factor in EdS: ET simulation precision. The variable on the horizontal axis is the conformal time in computational units (see appendix A).

5.3. A dust Universe in numerical relativity

The main application of the `BiGONLight` package is the computation of observables from numerically simulated spacetimes. For our test we choose to use the `FLRWSolver`¹¹, [5], which is a module (or *thorn*) of the ET [2]: the ET is a collection of open-source codes, called thorns, based on the `Cactus` framework [62], which allows to solve the Einstein equations in the BSSN formulation of the 3 + 1 splitting [63, 64]. The role of the `FLRWSolver` is to provide the initial conditions in the form of linear perturbations around a homogeneous dust Universe, i.e. the Einstein–de Sitter (EdS) background, which are then evolved with the ET. Here, we limit ourselves to the EdS background model and set perturbations to zero. In other words, we consider a FLRW model in which the Universe is flat and contains only cold dark matter. The line element of the EdS model in conformal time is

$$ds^2 = a_{\text{EdS}}^2(\eta) \left(-d\eta^2 + dx^{2^2} + dx^{2^2} + dx^{3^2} \right), \quad (97)$$

where $a_{\text{EdS}}(\eta) = \eta^2$ is the scale factor. We carry out the simulation in a cubic domain $-L \leq \{x^1, x^2, x^3\} \leq L$ with periodic boundary conditions and spatial resolution $\Delta x = \Delta y = \Delta z = \frac{L}{20}$, where L is the simulation unit length in Mpc¹². The initial data are given at $\eta_{\text{in}} = L$ and such that $\gamma_{ij}^{\text{in}} = \delta_{ij}$. The simulation runs with the ET up to $\eta_0 = 33.2L$, which corresponds to integrating from redshift $z = 1100$ to present time $z = 0$, and we choose a fixed temporal resolution $\Delta\eta = \frac{L}{100}$ due to computational time convenience. To give an estimation of the

¹¹ https://github.com/hayleyjm/FLRWSolver_public.

¹² The physical value is $L = 268.11$ Mpc, as it is explained in appendix A.

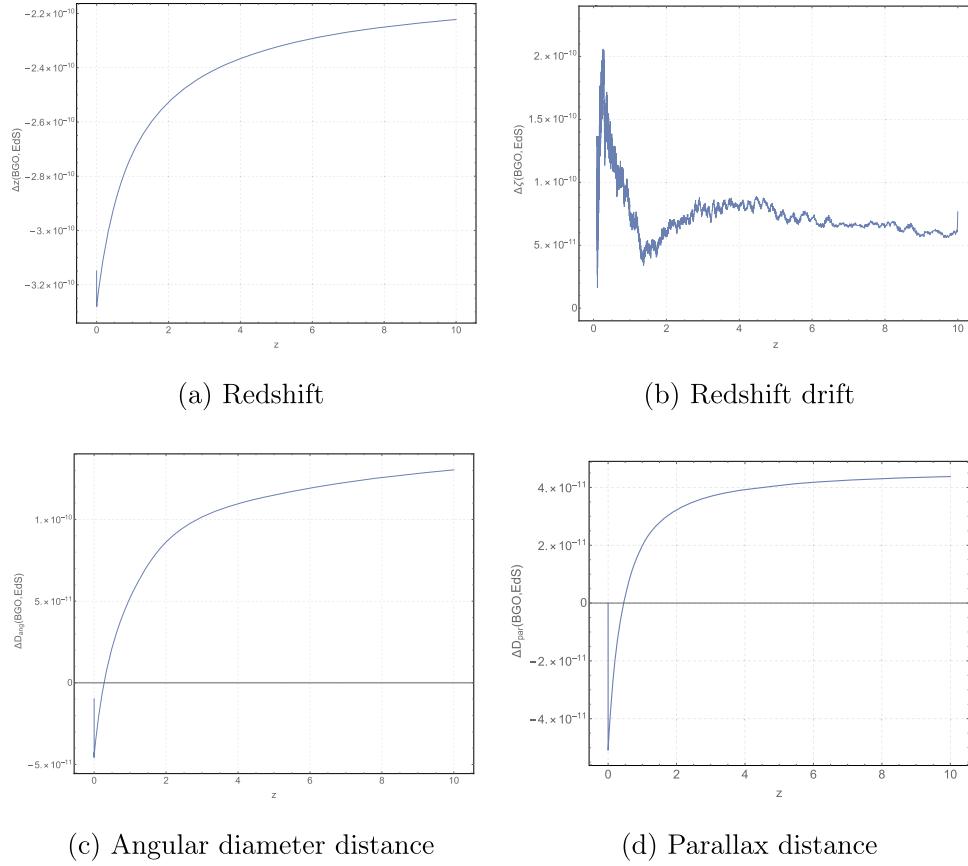


Figure 5. Variations in the EdS model with ET, equation (99), for the redshift (a), the redshift drift (b), the angular diameter distance (c), and the parallax distance (d). The variable in the horizontal axis is the redshift in EdS.

simulation error we define

$$\Delta a(\text{ET}, \text{EdS}) \equiv \frac{a^{\text{ET}} - a^{\text{EdS}}}{a^{\text{EdS}}}, \quad (98)$$

which is the variation between the analytical scale factor in EdS, i.e. $a^{\text{EdS}} = \eta^2$ and the scale factor from the numerical simulation $a^{\text{ET}} = \det(\gamma_{ij})^{\frac{1}{6}}$. The result, shown in figure 4, is of the order of 10^{-10} and this value is determined by the specific setting that we choose for the ET simulation.

The simulated EdS model constitutes the playground of our tests. We perform light propagation with `BiGONLight` using forward integration in time with the method described in section 3.3. We start from the source \mathcal{S} , placed at redshift $z = 10$ in $x_{\mathcal{S}}^{\mu} = (\eta_{\mathcal{S}}, 0, 0, 0)$, and we end at the observer \mathcal{O} . The emitted light moves along the diagonal of the cubic domain with initial tangent vector $\ell_{\mathcal{S}}^{\mu} = (-1, -\frac{1}{2}, \frac{1}{2}, \frac{\sqrt{2}}{2})$, until it reaches the observer at $x_{\mathcal{O}}^{\mu}$. The numerical

accuracy in the calculation of the observables is tested by means of the variation $\Delta O(\text{BGO}, \text{ET})$ defined as

$$\Delta O(\text{BGO}, \text{EdS}) \equiv \frac{O^{\text{BGO}} - O^{\text{EdS}}}{O^{\text{EdS}}}, \quad (99)$$

where O^{BGO} is computed numerically with `BiGONLight` using as input the EdS model simulated with the ET and O^{EdS} is the analytical expression in the EdS model that reads

$$D_{\text{ang}}^{\text{EdS}} = \frac{2a_0 \sqrt{1+z} - 1}{\mathcal{H}_0 (1+z)^{\frac{3}{2}}}, \quad (100)$$

$$D_{\text{par}}^{\text{EdS}} = \frac{a_0 \sqrt{1+z} - 1}{\mathcal{H}_0 \frac{3}{2} \sqrt{1+z} - 1}, \quad (101)$$

$$\zeta^{\text{EdS}} = \frac{\mathcal{H}_0}{a_0} (1 - \sqrt{1+z}). \quad (102)$$

These are obtained by integrating equations (66)–(68) with $\Omega_{\text{m}_0} = 1$ and $\Omega_{\Lambda} = 0$. The results are shown in figure 5. What we see is the error on $\Delta O(\text{BGO}, \text{EdS})$ which has in principle two contributions: one from the simulation of the EdS model and the other from the simulation of light propagation. We have already isolated the second contribution coming from `BiGONLight` in the ΛCDM test. Indeed, since we use the analytical solution for ΛCDM both in the numerical and analytical computation for the observables, the error $\Delta O(\text{BGO}, \Lambda\text{CDM})$ we find in figure 2 is entirely due to the simulation of light propagation and is of the order of $10^{-22} \div 10^{-31}$. On the other hand, in figure 4 we see that the accuracy of the ET simulation we use is much larger, i.e. of the order of 10^{-10} , which is of the same order of the one for $\Delta O(\text{BGO}, \text{EdS})$ in figure 5. Therefore we can conclude that the final error on the observables we find in figure 5 is settled by the accuracy of the ET in simulating the EdS model. Let us finally remark that for this test we perform light propagation using forward integration, namely from the source \mathcal{S} to the observer \mathcal{O} . We also repeated the computation of $\Delta O(\text{BGO}, \text{EdS})$ using backward integration, from \mathcal{O} to \mathcal{S} , in `BiGONLight` and we found the same results.

6. Conclusions

In this paper we present and test `BiGONLight`, a `Mathematica` package for relativistic light propagation in numerical relativity. Our new code implements the BGO formalism, a new approach to geometric optics in general relativity, firstly introduced in reference [20], which we recasted here in the $3+1$ form to be compatible with the structure of relativistic numerical simulations. The generality of the BGO framework allows `BiGONLight` to be suitable to study light propagation in different contexts: from small scales, e.g. inside our Galaxy, to the ultra-large scales of Cosmology, as long as light propagation can be treated within the assumptions of geometric optics. `BiGONLight` is extremely flexible also from the technical point of view, requiring as input only the spacetime metric and the observer and source kinematics: the user can choose any gauge and also the type of input to use, namely numerical from a relativistic simulation or analytical from an exact solution of the Einstein field equations. An analytical solution for the spacetime metric in any perturbative scheme can be also given as input but the code does not apply the perturbative scheme to light propagation. This is indeed the approach we adopted in reference [56]. We plan to implement perturbation theory in a future version of `BiGONLight`. A key feature of the BGO framework is that all optical effects are encoded in the bi-ejective \mathcal{W} map, which can be written from the observer

\mathcal{O} to the source \mathcal{S} or viceversa. In this paper we give the ready-to-use transformation relations in equations (49)–(52). This property in `BiGONLight` means that the user is free to adopt different approaches to trace light propagation. On one hand, one can trace the photons from the observer to the source using the conventional backward integration, on the other hand one can choose to do the other way around and use forward integration. This second method is particularly convenient in numerical relativity because it allows us to perform light propagation on-the-fly with a simulation of spacetime dynamics, which employs integration forward in time by construction.

We decide to test `BiGONLight` in the computation of four cosmological observables: the redshift, the angular diameter distance, the parallax distance, and the redshift drift, the last two being real-time observables that are new in the cosmological context. We perform three different kinds of tests. In the first we test the accuracy of the code against the analytical results in the Λ CDM model and we find an excellent agreement of the order of $10^{-22} \div 10^{-31}$, see figure 2. We are able to reach this extremely good accuracy by using the precision control options and the many well-tested numerical methods to solve ODE implemented in `Mathematica`. For the second test we consider the Szekeres inhomogeneous cosmological model as presented in references [56, 57] and we compare the BGO formalism with the standard procedures used for the angular diameter distance and the redshift drift. Let us point out here that the BGO formalism provides a unified way to compute multiple observables within the same framework, contrary to the standard approach. In particular, for the angular diameter distance we compare the result obtained from the BGO, equation (55), with the one from the Sachs equation, equation (83). For the redshift drift we compare the BGO general formula, equation (59), with the result of the standard calculation, equation (96), that we derive here for the specific set up for light propagation in the Szekeres model considered. Also in this case we find a very good agreement of the order of 10^{-22} , see figure 3. For our final test we consider the EdS background simulated with the ET together with the `FLRWSolver`. The numerical output of this simulation is used to compute the observables with the BGO in `BiGONLight` which are then compared with the usual analytical formulas. Our findings are shown in figure 5 where we see that the accuracy on the observables calculated with `BiGONLight` is ruled by the accuracy of the ET simulation, which is limited to the order of 10^{-10} for the specifications that we use in our paper. Contrary to the first two tests, here the BGO are calculated by integrating the GDE forward in time and then we use the BGO property in equation (12) to obtain the observables, see section 4. The current version of `BiGONLight` is designed to perform light propagation in post-processing and not on-the-fly, with the advantage of being able to accept input from different numerical codes for cosmological dynamics. The `Wolfram` language is at the base of the `BiGONLight`'s versatility, providing an entire ecosystem with build-in libraries for symbolic and numerical computations, but also plotting functions and various types of data. The computational time required to complete the analysis depends on the calculation's precision we want to achieve and it can be estimated using the function `AbsoluteTiming[]`. For instance, to obtain the results presented in section 5.2 for the Szekeres model, with our average laptop¹³, we needed $\sim 10^5$ sec to complete the analysis, and it was the most computationally expensive. For the Λ CDM model we spent $\sim 3 \times 10^4$ sec, due to the fact we use a simpler analytical model. As for the simulated dust Universe with the ET the computational time was only $\sim 2.5 \times 10^4$ sec, since the precision of the input simulation acted as an upper limit for our computations of the observables.

¹³ We used a laptop with a quad-core processor (cores clock speed 2.6 \div 3.5 GHz) and 16 GB of RAM.

Acknowledgments

This work was supported by the National Science Centre, Poland (NCN) via the SONATA BIS programme, Grant No. 2016/22/E/ST9/00578 for the project ‘*Local relativistic perturbative framework in hydrodynamics and general relativity and its application to cosmology*’. We thank Mikołaj Korzyński for carefully reading the draft, Hayley Macpherson for useful comments and tips about the FLRWSOLVER, and Hayley Macpherson and Julian Adamek for insightful discussions during the workshop ‘*GR simulations in cosmology*’, Queen Mary University of London, 7–8 September 2020.

Data availability statement

All data that support the findings of this study are included within the article (and any supplementary files).

Appendix A. Units

Throughout this article all quantities are expressed in geometric units, i.e. units defined by the relation $G = c = 1$, thus such that masses, time and lengths have the same unit of measurement. For instance, we can fix a unit of length¹⁴ $[\text{length}] = L$ and define $[\text{mass}] = \frac{c^2 L}{G}$ as unit of mass and $[\text{time}] = \frac{L}{c}$ as unit of time: in geometric units they all reduce to $[\text{mass}] = [\text{time}] = [\text{length}] = L$. Within this choice, every physical quantity Q_{phys} can be expressed as $Q_{\text{phys}} = Q_{\text{comp}} L^\alpha$, where Q_{comp} is dimensionless, L is a arbitrary length to be chosen, and α is a certain exponent. This way of writing is particularly useful in numerical simulations, where all physical quantities are represented as dimensionless numbers and units are assigned when analysing the results. Usually L is fixed to be a length meaningful for the specific physical situation under consideration. For example, a common choice in numerical cosmological dynamics is to set L equal to a characteristic length of the simulation (e.g. N -body and GR hydrodynamics), such as the side of the simulated box. In cosmology it is usually chosen to set L equal to the conformal time in Mpc, i.e. $L = \eta^{\text{phys}}$, thus $\eta^{\text{comp}} = 1$, at some special instant like e.g. at initial time or today. This choice is particularly convenient, since conformal time is found by integrating the Friedmann equation and reads

$$\eta = \frac{1}{H_0} \int_0^a \frac{d\tilde{a}}{\tilde{a}^2 E(\tilde{a})}, \quad (\text{A.1})$$

where $E(a) = \sqrt{\Omega_{\text{m}_0} \left(\frac{a_0}{a}\right)^3 + \Omega_\Lambda}$ for a Universe containing cold dark matter and a cosmological constant.

For the Λ CDM model, section 5.1, and for the Szekeres model, section 5.2, we choose $L = \eta_0$ and we normalize the scale factor to 1 today. This is the natural choice for this two cases since we studied light propagation backward in time. By integrating equation (A.1) together with the normalization $a_0 = 1$ for the value of the today scale factor we have

$$\eta^{\Lambda\text{CDM}} = \frac{1}{H_0 3^{\frac{1}{4}} \Omega_\Lambda^{\frac{1}{4}} \Omega_{\text{m}_0}^{\frac{1}{3}}} F \left(\arccos \left(\frac{1 + (1 - \sqrt{3}) \sqrt[3]{\frac{\Omega_\Lambda}{\Omega_{\text{m}_0}}} a}{1 + (1 + \sqrt{3}) \sqrt[3]{\frac{\Omega_\Lambda}{\Omega_{\text{m}_0}}} a} \right); \frac{\sqrt{2 + \sqrt{3}}}{2} \right), \quad (\text{A.2})$$

¹⁴ The same can be done by fixing a unit of time T to define $[\text{mass}] = T \frac{c^3}{G}$ as unit of mass and $[\text{length}] = Tc$ as unit of length, or fixing a unit of mass M to define $[\text{time}] = M \frac{G}{c^3}$ as unit of time and $[\text{length}] = M \frac{G}{c^2}$ as unit of length.

with $F(x; y)$ being the elliptic integral of the first kind. Substituting the values of the cosmological parameters from [52], $\Omega_{m_0} = 0.315$ and $\Omega_{\Lambda} = 0.685$ and expressing the Hubble constant in Mpc, i.e. $\mathcal{H}_0 = 2.2469 \times 10^{-4} \text{ Mpc}^{-1}$, equation (A.2) gives $L = \eta_0^{\Lambda\text{CDM}} = \eta_0^{\text{Sz}} = 14.4152 \text{ Gpc}$.

For the EdS model, section 5.3, we study light propagation forward in time and we decided to use the same conventions as the one implemented in the ET. Here, the simulation is carried out in a cubic domain volume of comoving side $2L$, which is initialised at initial time η_{in} (and not today) and the scale factor is normalised to 1 at η_{in} . Let us start by integrating (A.1) for the EdS model, i.e. $\Omega_{m_0} = 1$ and $\Omega_{\Lambda} = 0$, which gives

$$\eta^{\text{EdS}} = \frac{2}{\mathcal{H}_0} \sqrt{\frac{a}{a_0}}. \quad (\text{A.3})$$

The value of L is set by evaluating equation (A.3) at initial time and choosing $\eta_{\text{in}}^{\text{EdS}} = L$. Substituting $a_{\text{in}} = 1$ and $\sqrt{a_0} = 33.2$ from the numerical simulation, and $\mathcal{H}_0 = 2.2469 \times 10^{-4} \text{ Mpc}^{-1}$ from [52] in equation (A.3), it follows that the value of L is

$$L = 268.11 \text{ Mpc}. \quad (\text{A.4})$$

We report for completeness the dimensions of all the main quantities in units of the characteristic length L

Physical quantities in units of L	
Hubble constant	$\mathcal{H}_0^{\text{phys}} = \mathcal{H}_0^{\text{comp}} L^{-1}$
Conformal time	$\eta_{\text{phys}} = \eta_{\text{comp}} L$
Spatial coordinates	$x_{\text{phys}}^i = x_{\text{comp}}^i L$
Gravitational potential	$\phi_0^{\text{phys}} = \phi_0^{\text{comp}} L^0$
Velocity field	$\nabla \phi_0^{\text{phys}} = \nabla \phi_0^{\text{comp}} L^{-1}$
Density field	$\nabla^2 \phi_0^{\text{phys}} = \nabla^2 \phi_0^{\text{comp}} L^{-2}$
Frequency	$\omega^{\text{phys}} = \omega^{\text{comp}} L^{-1}$
Angular diameter distance	$D_{\text{ang}}^{\text{phys}} = D_{\text{ang}}^{\text{comp}} L$
Parallax distance	$D_{\text{par}}^{\text{phys}} = D_{\text{par}}^{\text{comp}} L$
Redshift drift	$\zeta^{\text{phys}} = \zeta^{\text{comp}} L^{-1}$
Redshift z	Dimensionless
Scale factor $a(\eta)$	Dimensionless
Growing mode $\mathcal{D}(\eta)$	Dimensionless
Cosmological parameters Ω_i	Dimensionless

ORCID iDs

Michele Grasso  <https://orcid.org/0000-0001-6193-3363>

Eleonora Villa  <https://orcid.org/0000-0003-2203-0254>

References

- [1] Quercellini C, Amendola L, Balbi A, Cabella P and Quartin M 2012 *Phys. Rep.* **521** 95–134

- [2] Löffler F *et al* 2012 *Class. Quantum Grav.* **29** 115001
- [3] Giblin J T, Mertens J B and Starkman G D 2016 *Phys. Rev. Lett.* **116** 251301
- [4] Bentivegna E 2017 *Phys. Rev. D* **95** 044046
- [5] Macpherson H J, Lasky P D and Price D J 2017 *Phys. Rev. D* **95** 064028
- [6] Clesse S, Roisin A and Füzfa A 2017 arXiv:1702.06643
- [7] East W E, Wojtak R and Abel T 2018 *Phys. Rev. D* **97** 043509
- [8] Daverio D, Dirian Y and Mitsou E 2019 *J. Cosmol. Astropart. Phys.* JCAP10(2019)065
- [9] Adamek J, Daverio D, Durrer R and Kunz M 2016 *Nat. Phys.* **12** 346–9
- [10] Barrera-Hinojosa C and Li B 2020 *J. Cosmol. Astropart. Phys.* JCAP01(2020)007
- [11] Borzyszkowski M, Bertacca D and Porciani C 2017 *Mon. Not. R. Astron. Soc.* **471** 3899–914
- [12] Zhu H, Alam S, Croft R A C, Ho S and Giusarma E 2017 *Mon. Not. R. Astron. Soc.* **471** 2345–56
- [13] Giblin J T, Mertens J B, Starkman G D and Zentner A R 2017 *Phys. Rev. D* **96** 103530
- [14] Breton M-A, Rasera Y, Taruya A, Lacombe O and Saga S 2019 *Mon. Not. R. Astron. Soc.* **483** 2671–96
- [15] Adamek J, Clarkson C, Coates L, Durrer R and Kunz M 2019 *Phys. Rev. D* **100** 021301
- [16] Beutler F and Dio E D 2020 *J. Cosmol. Astropart. Phys.* JCAP07(2020)048
- [17] Lepori F, Adamek J, Durrer R, Clarkson C and Coates L 2020 *Mon. Not. R. Astron. Soc.* **497** 2078–95
- [18] Guandalin C, Adamek J, Bull P, Clarkson C, Abramo L R and Coates L 2021 *Mon. Not. R. Astron. Soc.* **501** 2547–61
- [19] Lepori F, Adamek J and Durrer R 2021 arXiv:2106.01347
- [20] Grasso M, Korzyński M and Serbenta J 2019 *Phys. Rev. D* **99** 064038
- [21] Korzyński M and Villa E 2020 *Phys. Rev. D* **101** 063506
- [22] Sachs R 1961 *Proc. R. Soc. A* **264** 309–38
- [23] Perlick V 2004 *Living Rev. Relativ.* **7** 9
- [24] Uzun N 2020 *Class. Quantum Grav.* **37** 045002
- [25] Smarr L and York J W Jr 1978 *Phys. Rev. D* **17** 2529–51
- [26] Alcubierre M 2008 *Introduction to 3+1 Numerical Relativity* vol 140 (Oxford: Oxford University Press)
- [27] Baumgarte T W and Shapiro S L 2010 *Numerical Relativity* (Cambridge: Cambridge University Press)
- [28]ourgoulhon E 2012 *3+1 Formalism in General Relativity* vol 846 (Berlin: Springer)
- [29] Arnowitt R, Deser S and Misner C W 1959 *Phys. Rev.* **116** 1322–30
- [30] Vincent F H,ourgoulhon E and Novak J 2012 *Class. Quantum Grav.* **29** 245005
- [31] Hughes S A *et al* 1994 *Phys. Rev. D* **49** 4004
- [32] Serbenta J and Korzyński M 2021 in preparation
- [33] Korzyński M and Kopiński J 2018 *J. Cosmol. Astropart. Phys.* JCAP03(2018)012
- [34] Meures N and Bruni M 2011 *Phys. Rev. D* **83** 123519
- [35] Gradshteyn I S and Ryzhik I M 2014 *Table of Integrals, Series, and Products* (New York: Academic)
- [36] Räsänen S 2014 *J. Cosmol. Astropart. Phys.* JCAP03(2014)035
- [37] Kardashev N S 1986 *Sov. Astron.* **30** 82
- [38] Lindegren L *et al* 2016 *Astron. Astrophys.* **595** A4
- [39] Ding F and Croft R A C 2009 *Mon. Not. R. Astron. Soc.* **397** 1739
- [40] Quartin M and Amendola L 2010 *Phys. Rev. D* **81** 043522
- [41] Quercellini C, Quartin M and Amendola L 2009 *Phys. Rev. Lett.* **102** 151302
- [42] Singal A K 2015 *Astrophys. Space Sci.* **359** 1–6
- [43] Marcori O H, Pitrou C, Uzan J P and Pereira T S 2018 *Phys. Rev. D* **98** 023517
- [44] Bel J and Marinoni C 2018 *Phys. Rev. Lett.* **121** 021101
- [45] Sandage A 1962 *Astrophys. J.* **136** 319
- [46] McVittie G C 1962 *Astrophys. J.* **136** 334
- [47] Corasaniti P S, Huterer D and Melchiorri A 2007 *Phys. Rev. D* **75** 062001
- [48] Uzan J P, Bernardeau F and Mellier Y 2008 *Phys. Rev. D* **77** 021301
- [49] Uzan J-P, Clarkson C and Ellis G F R 2008 *Phys. Rev. Lett.* **100** 191303
- [50] Martinelli M, Pandolfi S, Martins C J A P and Vielzeuf P E 2012 *Phys. Rev. D* **86** 123001
- [51] Lazkoz R, Leanizbarrutia I and Salzano V 2018 *Eur. Phys. J. C* **78** 11
- [52] Aghanim N *et al* (Planck) 2020 *Astron. Astrophys.* **641** A6
- [53] Szekeres P 1975 *Commun. Math. Phys.* **41** 55–64
- [54] Goode S W and Wainwright J 1982 *Phys. Rev. D* **26** 3315–26

- [55] Villa E and Rampf C 2016 *J. Cosmol. Astropart. Phys.* [JCAP01\(2016\)030](#)
- [56] Grasso M, Villa E, Korzyński M and Matarrese S 2021 [arXiv:2105.04552](#)
- [57] Meures N and Bruni M 2012 *Mon. Not. R. Astron. Soc.* **419** 1937
- [58] Yoo C M, Kai T and Nakao K 2011 *Phys. Rev. D* **83** 043527
- [59] Mishra P, Célérier M N and Singh T P 2012 *Phys. Rev. D* **86** 083520
- [60] Balcerzak A and Dabrowski M P 2013 *Phys. Rev. D* **87** 063506
- [61] Mishra P and Célérier M N 2014 [arXiv:1403.5229](#)
- [62] Goodale T, Allen G, Lanfermann G, Massó J, Radke T, Seidel E and Shalf J 2002 The cactus framework and toolkit: design and applications *Int. Conf. High Performance Computing for Computational Science* (Berlin: Springer) pp 197–227
- [63] Shibata M and Nakamura T 1995 *Phys. Rev. D* **52** 5428
- [64] Baumgarte T W and Shapiro S L 1998 *Phys. Rev. D* **59** 024007

PAPER II: “ISOLATING NONLINEARITIES OF LIGHT PROPAGATION IN INHOMOGENEOUS COSMOLOGIES”

This chapter presents the application of `BiGONLight` to study the nonlinear contributions to light propagation in an inhomogeneous cosmological model. The ultimate goal of this work is to isolate and quantify how different sources of inhomogeneities contribute to nonlinearities in cosmological observables. To this end, instead of using a realistic model of the Universe, it is preferable to have a toy model, whose properties can be tuned easily by changing its parameters. The *wall Universe*, in which the matter is condensed in a sequence of plane-symmetric perturbations around a homogeneous distribution (FLRW background), is the toy model employed in this investigation. The analytical expression of its metric in PN approximation is given in [180] and is used in this analysis at three different approximations: linear PT, Newtonian, and PN. The forms of the metric at Newtonian and PN approximations are provided as input metric in `BiGONLight` to compute numerically the observables at Newtonian and PN order, respectively. The observables at linear PT are obtained analytically from the expressions of the BGO at linear order. The nonlinear contributions are determined as relative differences between observables computed within these three different approximations.

The study answers the following four questions:


1. what are the Newtonian and PN corrections to the linear PT observables?
2. what is the impact of the size of inhomogeneities?
3. how much do the free parameters of the model affect the comparison?
4. how important are the nonlinear PN corrections?

Although many other authors have already examined the first question (see e.g. [69, 18, 44, 131, 178, 121]), the other three questions penetrate deeply into the origin of nonlinearities, whose contributions are precisely evaluated by `BiGONLight`.

Author’s contribution

The work described in this Chapter was performed in collaboration with E. Villa, M. Kozłowski, and S. Matarrese. The idea of this analysis was proposed by E. Villa and later discussed with the other authors. The Λ CDM extension of the metric in [180] (originally formulated for an EdS background) have been obtained jointly by me and E. Villa (Eq. 2 in

[90]). I have performed the simulations for light propagation and the computations of the observables in the three approximations. E. Villa and I did the preliminary analysis on the comparisons of the observables, and the results were discussed with all the other authors in order to draw conclusions. The comparison of the metric in Eq. (7) in [90] with the Szekeres metric in [130] was done jointly by E. Villa and me. We also derived the analytical expressions of the linear observables with the BGO, and we did the match with the known formulas in the literature (i.e. without BGO). The draft was written by E. Villa and me and jointly published by all authors.

Isolating nonlinearities of light propagation in inhomogeneous cosmologiesMichele Grasso^{1,*}, Eleonora Villa^{1,†}, Mikołaj Korzyński^{1,‡} and Sabino Matarrese^{2,3,4,5,§}¹*Center for Theoretical Physics, Polish Academy of Science,
Al. Lotników 32/46, 02-668 Warszawa, Poland*²*Dipartimento di Fisica e Astronomia G. Galilei, Università degli Studi di Padova, I-35131 Padova, Italy*³*INFN, Sezione di Padova, via F. Marzolo 8, I-35131 Padova, Italy*⁴*INAF—Osservatorio Astronomico di Padova, vicolo dell'Osservatorio 5, I-35122 Padova, Italy*⁵*Gran Sasso Science Institute, viale F. Crispi 7, I-67100 L'Aquila, Italy* (Received 12 May 2021; accepted 6 July 2021; published 5 August 2021)

A new formulation for light propagation in geometric optics by means of the bilocal geodesic operators is considered. We develop the *BIGONLIGHT Mathematica* package, uniquely designed to apply this framework to compute optical observables in numerical relativity. Our package can be used for light propagation on a wide range of scales and redshifts and accepts numerical as well as analytical input for the spacetime metric. In this paper we focus on two cosmological observables, the redshift and the angular diameter distance, specializing our analysis to a wall universe modeled within the post-Newtonian approximation. With this choice and the input metric in analytical form, we are able to estimate nonlinearities of light propagation by comparing and isolating the contributions coming from Newtonian and post-Newtonian approximations as opposed to linear perturbation theory. We also clarify the role of the dominant post-Newtonian contribution represented by the linear initial seed which, strictly speaking, is absent in the Newtonian treatment. We found that post-Newtonian nonlinear corrections are below 1%, in agreement with previous results in the literature.

DOI: 10.1103/PhysRevD.104.043508

I. INTRODUCTION

Upcoming galaxy surveys like Euclid, LSST, SKA and others¹ mark the beginning of a new exciting era, dubbed *precision cosmology*. The reason behind this name is twofold: on one side these future observations will map almost all the visible universe with the unprecedented precision of 1% and on the other side cosmological modelling aim at the same precision target.

In this view treating non-linearities, i.e., going beyond (linear) cosmological perturbation theory is of crucial importance and new approximation schemes were developed specifically or approximations used in other contexts were applied to cosmology. They include: the post-Newtonian (PN) approximation (see [1,2] for formulations of PN cosmology in two different gauges), the post-Friedmann approximation (see [3,4] for a different approach, which adapts to cosmology the weak-field post-Minkowskian approximation and reproduces linear-order cosmological perturbation theory at their zeroth-

order), the weak-field approximation² (see [6] for the development of the framework and [7] for estimations with the use of Newtonian simulations for a plane-symmetric universe), and, more recently, a two-parameters gauge-invariant approximation (see [8]). In addition, over the past few decades, numerical simulations have increasingly become a powerful tool in cosmology to model the growth of non-linear structures. Since Newtonian dynamics seems to be a good approximation to describe late-time structure formation, the first generation of cosmological simulations adopted Newtonian gravity to simulate cosmological dynamics. Then, Newtonian simulations were used to feed approximate field equations coming from general relativity (GR) as e.g., in [9–11]. Only recently we assist to a revolution in cosmological simulations with the birth of codes aiming at simulating fully general relativistic dynamics, [12–17]: for the state of the art and the comparison among different codes, see [18].

However, a sophisticated general relativistic (exact or approximated) description of cosmological dynamics is not the end of the story. The key point is how (much) it affects

*grasso@cft.edu.pl

†villa@cft.edu.pl

‡korzynski@cft.edu.pl

§sabino.matarrese@pd.infn.it

¹<http://sci.esa.int/euclid/>, <https://www.lsst.org>, <http://skatelescope.org/>²The leading order of the last two approximation schemes were shown to be equivalent for a dust universe in the Poisson gauge in [5], whereas [1,2] were constructed on purpose to include second-order perturbation theory at their PN order.

light propagation, the final aim being to characterize and (hopefully) measure nonlinear GR effects in the observables on cosmological scales or, at least, quantify their bias in observations. These studies are still in their infancy but they are addressed with several approaches most of which we briefly sketched above. A noncomprehensive list includes [19–27]. Despite being too early to draw definitive conclusions, it seems that the codes that approximate GR dynamics are in agreement with Newtonian simulations for what concerns weak-lensing observables [19,26] but a modification in the statistics of the luminosity distance [24] was found. In addition, the PN approximation for some models gives predictions different from Λ CDM [22]. A bit of work is still needed to adapt to (observational) cosmology the truly GR numerical codes.

In this paper we examine the differences between linear and nonlinear light propagation. An accurate treatment of the problem would require to analyse light propagation in a realistic model of the universe. However, our aim is not to make general predictions, but rather to deeply investigate the various factors and effects on observables coming from nonlinearities. For this purpose, we decided to employ a toy-model of the universe in which light rays pass through a series of plane-symmetric perturbations around a Friedmann-Lemaître-Robertson-Walker (FLRW) background. This model is known as plane-parallel or wall universe, and it was used in the past to study the back-reaction from the small-scale inhomogeneities [28–31]. We start by extending the results of [28] by providing the so-called Zel’dovich solution with a Λ CDM background. In this model, we compute the redshift and the angular diameter distance within three different approximation schemes: linear, Newtonian and post-Newtonian. In order to quantify and isolate nonlinear contributions, we present our results in terms of the relative differences between observables computed with these three different approximations (see Sec. IV for details). We also analyze different aspects of nonlinearities, e.g., scale-dependence, non-Gaussianity, etc. Even if our modeling is very simple, we believe that this kind of analysis is representative of more general configurations.

Besides, an important novelty of this work is that we make use of the new *BIGONLIGHT Mathematica* package to study light propagation in GR and compute observables numerically, [32]. Contrary to other software, *BIGONLIGHT* implements light propagation within the new bilocal geodesic operator (BGO) framework, which is applicable to more general situations than the standard formalism and it is also suitable to construct new observables, [33,34]. This unique design makes the package adaptable to study various light propagation problems in numerical simulations.

We begin by presenting in Sec. II the plane-parallel toy-model as introduced in [28]. Then, in Sec. III we briefly describe the BGO framework, pointing out to [33,34] for further details. In Sec. IV, we introduce the goals of our

analysis and the method which led to the results presented in Sec. V. Finally, we address our conclusions in Sec. VI.

Notation: Greek indices (α, β, \dots) run from 0 to 3, while Latin indices (i, j, \dots) run from 1 to 3 and refer to spatial coordinates only. Latin indices (A, B, \dots) run from 1 to 2. Tensors and bitensors expressed in a semi-null frame are denoted using boldface indices: Greek boldface indices $(\boldsymbol{\alpha}, \boldsymbol{\beta}, \dots)$ run from 0 to 3, Latin boldface indices $(\boldsymbol{a}, \boldsymbol{b}, \dots)$ run from 1 to 3 and capital Latin boldface indices $(\boldsymbol{A}, \boldsymbol{B}, \dots)$ run from 1 to 2. Latin tilded indices $(\tilde{a}, \tilde{b}, \dots)$ run from 0 to 7 and refer to the indices of 8×8 matrices \mathcal{W} and Ω . A dot denotes derivative with respect to conformal time. Quantities with a subscript 0 are meant to be evaluated at present, whereas the subscript “in” indicates the initial time. Similarly, we indicate with a subscript \mathcal{O} (\mathcal{S}) quantities defined at the observer (source). An overbar indicates quantities evaluated in the Λ CDM model. In this paper we use three different approximations and consequently three different notations: “N” for Newtonian, “PN” for post-Newtonian, “Lin” for first-order perturbation theory. We place these abbreviations up or down depending on convenience.

II. THE PLANE-PARALLEL DYNAMICS IN THREE APPROXIMATIONS

We consider a toy-model characterized by the choice of globally plane-parallel configurations, i.e., the case where the initial perturbation field depends on a single coordinate. The dynamics of this very simple universe consists of a collection of parallel planes that collapse along the direction of their normal to form a pancake. For the purposes of our work, we are not interested in a more realistic modelling of the Universe; rather our main aim is to estimate, isolate and compare purely nonlinear and non-Newtonian contributions in light propagation, e.g., in fundamental observables such as redshift and angular diameter distance.

We work in the synchronous-comoving gauge and leave to future work the gauge issue of every perturbation scheme that affects the observables as well as the estimate of the related contributions in other gauges. Despite gauge effects in the observables are known in standard cosmological perturbation theory (see Ref. [35] for a recent discussion of gauge invariance of cosmological observables up to second order), the issue is more delicate for nonstandard approximations, such as those considered in this paper.

The starting point of our analysis is the results of Ref. [28]: the authors started from the Newtonian background given by the well-known Zel’dovich approximation, [36], which, for plane-parallel perturbations in the Newtonian limit, represents an exact solution. They then obtained the exact analytical form for the PN metric, thereby providing the exact PN extension of the Zel’dovich solution. Let us remark how the Zel’dovich

approximation is constructed: in its conformal version, it is an expansion around the three-dimensional spatial displacement vector of the CDM particles between the position comoving with the Hubble flow and the true position governed by perturbations. The peculiarity is the following: the solution for the displacement vector is strictly linear, as it is found from the linear Newtonian equations of motion. But all other dynamical quantities, such as the mass density, are written in terms of such a displacement vector, as if it was exact, i.e., from their nonperturbative definition. The same construction was first extended to the PN approximation of general relativity,

where the metric tensor also is a dynamical variable, in Ref. [1] and specialized in the plane-parallel case in Ref. [28]. The Zel'dovich specific feature is evident in the form of the metric tensor (7), which is quadratic in the perturbations, and the density contrast in Eq. (9) for the Newtonian background and in Eqs. (2) and (10) for the PN solution found in Ref. [28].

We provide here the Λ CDM extension of the PN metric found in Ref. [28], which was obtained for the Einstein-de Sitter background model, i.e., the dust-only universe. Starting from the line element

$$ds^2 = a^2(\eta) \{-c^2 d\eta^2 + \gamma_{11}^{\text{PN}}(\eta, q_1) dq_1^2 + \gamma_{22}^{\text{PN}}(\eta, q_1) dq_2^2 + \gamma_{33}^{\text{PN}}(\eta, q_1) dq_3^2\} \quad (1)$$

we then obtain the conformal metric given by³

$$\begin{aligned} \gamma_{11}^{\text{PN}} &= \left(1 - \frac{2}{3} \frac{\partial_{q_1}^2 \phi_0}{\mathcal{H}_0^2 \Omega_{m0}} \mathcal{D}\right)^2 \\ &+ \frac{1}{c^2} \left[-\frac{10}{3} \phi_0 + (4a_{\text{nl}} - 5) \frac{10 (\partial_{q_1} \phi_0)^2}{9 \mathcal{H}_0^2 \Omega_{m0}} \mathcal{D} + (a_{\text{nl}} - 1) \frac{40 \phi_0 \partial_{q_1}^2 \phi_0}{9 \mathcal{H}_0^2 \Omega_{m0}} \mathcal{D} \right. \\ &\left. + \left(\frac{41}{7} - 4a_{\text{nl}}\right) \frac{20 (\partial_{q_1} \phi_0)^2 \partial_{q_1}^2 \phi_0}{27 (\mathcal{H}_0^2 \Omega_{m0})^2} \mathcal{D}^2 + (3 - 2a_{\text{nl}}) \frac{40 \phi_0 (\partial_{q_1}^2 \phi_0)^2}{27 (\mathcal{H}_0^2 \Omega_{m0})^2} \mathcal{D}^2 - \frac{80 (\partial_{q_1} \phi_0)^2 (\partial_{q_1}^2 \phi_0)^2}{189 (\mathcal{H}_0^2 \Omega_{m0})^3} \mathcal{D}^3 \right] \\ \gamma_{22}^{\text{PN}} &= 1 + \frac{1}{c^2} \left[\frac{10}{9} \left(\frac{\mathcal{D} (\partial_{q_1} \phi_0)^2}{\mathcal{H}_0^2 \Omega_{m0}} - 3\phi_0 \right) \right] \\ \gamma_{33}^{\text{PN}} &= 1 + \frac{1}{c^2} \left[\frac{10}{9} \left(\frac{\mathcal{D} (\partial_{q_1} \phi_0)^2}{\mathcal{H}_0^2 \Omega_{m0}} - 3\phi_0 \right) \right]. \end{aligned} \quad (2)$$

In the above expression η is the conformal time, a is the scale-factor encoding the evolution of the Λ CDM background, \mathcal{H}_0 , Ω_{m0} , and ϕ_0 are the (conformal) Hubble parameter $\mathcal{H} \equiv \dot{a}/a$, the matter (ordinary plus dark) density parameter, and the peculiar gravitational potential, respectively, all evaluated at present. The dot denotes differentiation with respect to conformal time. \mathcal{D} is the growing mode solution of the first-order equation for the density contrast which is defined as

$$\delta(\eta, q_1) \equiv \frac{\rho(\eta, q_1)}{\bar{\rho}(\eta)} - 1, \quad (3)$$

where $\bar{\rho}$ the Λ CDM background matter density. At first order in standard perturbation theory and without loss of generality, the space and time dependence of the expression of the

growing density contrast can be factored out. In our one-dimensional case we have $\delta^{\text{Lin}}(\eta, q_1) = \mathcal{D}(\eta) \delta_0^{\text{Lin}}(q_1)$, where we fix the constant δ_0 at the present time, and the growing mode \mathcal{D} obeys the well-known equation

$$\ddot{\mathcal{D}} + \mathcal{H} \dot{\mathcal{D}} - \frac{3}{2} \mathcal{H}_0^2 \Omega_{m0} \frac{\mathcal{D}}{a} = 0. \quad (4)$$

It is worth noticing that these quantities are all connected via the cosmological Poisson equation

$$\mathcal{D} \nabla^2 \phi_0 - \frac{3}{2} \mathcal{H}_0^2 \Omega_{m0} \delta_{\text{Lin}} = 0. \quad (5)$$

Finally, we follow here the parametrization for primordial non-Gaussianity defined in Ref. [37]: the number a_{nl} parametrizes local primordial non-Gaussianity of the gauge-invariant curvature perturbation of uniform density hypersurfaces. This is linked to the parametrization of the primordial gravitational potential by a simple relation between the respective parameters: $f_{\text{nl}} = (5/3)(a_{\text{nl}} - 1)$.

³We take this chance to point out a typo in Eq. (4.37) of Ref. [28]: in the first term of the second line of the expression for γ_{11} the correct coefficient is 5/756 instead of 5/576.

The metric in (2) corresponds to the most sophisticated approximation that we will use in this paper: although being referred to the 1D toy-model, it is fully nonlinear in the standard perturbative sense, i.e., it is not assumed that density perturbations are small. On the contrary, taking advantage of the Zel'dovich prescription, we calculate the density contrast nonperturbatively, see Eq. (10) below. The PN approximation extends standard perturbation theory including the leading-order corrections to the Newtonian treatment, which are the terms proportional to $1/c^2$. For the convergence of the PN expansion in the metric (2), see Ref. [28]. We will compare light propagation in the spacetime described by (2) with other two cases, that are both extended in (2): the linear order of standard cosmological perturbation theory and the Newtonian approximation. The linear spacetime metric in the synchronous-comoving gauge is very well known and in 1D it reads

$$\begin{aligned}\gamma_{11}^{\text{Lin}} &= 1 - \frac{4}{3} \frac{\mathcal{D}\partial_{q_1}^2 \phi_0}{\mathcal{H}_0^2 \Omega_{m0}} - \frac{10}{3c^2} \phi_0 \\ \gamma_{22}^{\text{Lin}} &= 1 - \frac{10}{3c^2} \phi_0 \\ \gamma_{33}^{\text{Lin}} &= 1 - \frac{10}{3c^2} \phi_0.\end{aligned}\quad (6)$$

This metric is the solution of the Einstein's equations expanded at first order around the FLRW background.

$$\begin{aligned}\delta_{\text{PN}} &= \frac{\frac{2}{3} \frac{\mathcal{D}\partial_{q_1}^2 \phi_0}{\mathcal{H}_0^2 \Omega_{m0}}}{\left(1 - \frac{2}{3} \frac{\mathcal{D}\partial_{q_1}^2 \phi_0}{\mathcal{H}_0^2 \Omega_{m0}}\right)} \\ &+ \frac{1}{c^2} \frac{1}{\left(1 - \frac{2}{3} \frac{\mathcal{D}\partial_{q_1}^2 \phi_0}{\mathcal{H}_0^2 \Omega_{m0}}\right)^2} \left[\frac{5}{9} (3 - 4a_{\text{nl}}) \frac{\mathcal{D}}{\mathcal{H}_0^2 \Omega_{m0}} (\partial_{q_1} \phi_0)^2 + \frac{20}{9} (2 - a_{\text{nl}}) \frac{\mathcal{D}}{\mathcal{H}_0^2 \Omega_{m0}} (\phi_0 \partial_{q_1}^2 \phi_0) + \frac{20}{21} \left(\frac{2}{3} \frac{\mathcal{D}}{\mathcal{H}_0^2 \Omega_{m0}}\right)^2 \partial_{q_1}^2 \phi_0 (\partial_{q_1} \phi_0)^2 \right]\end{aligned}\quad (10)$$

Note that the Newtonian density contrast, according to the Zel'dovich approximation, is calculated exactly from the continuity equation in the synchronous-comoving gauge (see Eq. (25)) as the PN one, which is just expanded in powers of $1/c^2$. We take our initial conditions at η_{in} , after the end of inflation and in the matter-dominated era, when linear theory around the Einstein-de Sitter model is still a good approximation. The explicit expression for the initial density contrast is thus

$$\delta_{\text{in}} = \frac{2}{3} \frac{\mathcal{D}_{\text{in}} \partial_{q_1}^2 \phi_0}{\mathcal{H}_0^2 \Omega_{m0}} \quad (11)$$

where $\mathcal{D}_{\text{in}} \propto \eta_{\text{in}}^2$ is the linear growing mode of the Einstein-de Sitter model. We model the profile of the gravitational

Note however that the planar symmetry reduces the degrees of freedom to be only scalar (there are no vector or tensor mode in 1D, by construction) and confines the dynamical part in γ_{11}^{Lin} only, i.e., only in the direction of the perturbations, while in the other two directions we have just the (PN) initial conditions. On the other hand, in the Newtonian approximation we have

$$\begin{aligned}\gamma_{11}^{\text{N}} &= \left(1 - \frac{2}{3} \frac{\mathcal{D}\partial_{q_1}^2 \phi_0}{\mathcal{H}_0^2 \Omega_{m0}}\right)^2 \\ \gamma_{22}^{\text{N}} &= 1 \\ \gamma_{33}^{\text{N}} &= 1.\end{aligned}\quad (7)$$

This metric can be read off (2) by discarding the PN corrections proportional to $1/c^2$.

For completeness we report here the expressions of the density contrast in the three cases:

$$\delta_{\text{Lin}} = \frac{2}{3} \frac{\mathcal{D}\partial_{q_1}^2 \phi_0}{\mathcal{H}_0^2 \Omega_{m0}} \quad (8)$$

$$\delta_{\text{N}} = \frac{\frac{2}{3} \frac{\mathcal{D}\partial_{q_1}^2 \phi_0}{\mathcal{H}_0^2 \Omega_{m0}}}{1 - \frac{2}{3} \frac{\mathcal{D}\partial_{q_1}^2 \phi_0}{\mathcal{H}_0^2 \Omega_{m0}}} \quad (9)$$

potential at present as $\phi_0 = \mathcal{I} \sin(\omega q_1)$, with frequency $\omega = \frac{2\pi}{500 \text{ Mpc}}$ and amplitude \mathcal{I} such that $\max(\delta_{\text{PN}}(\eta_0, q_1)) = 0.1$. We set the fiducial values of the cosmological parameters from [38,39] with $\Omega_{m0} = 0.3153$, $\Omega_{\Lambda} = 0.6847$, $\mathcal{H}_0 = 67.36$ and $a_{\text{nl}} = \frac{3}{5} f_{\text{nl}} + 1 = 0.46$. The three profiles (8), (9) and (10) of the density contrast at the present time are shown in Fig. 1. The plot shows the amplitudes of the curves of the N and PN density contrast are shifted to higher values compared to the linear one, namely the N and PN corrections have the effect of increasing both the under- and the over-density peaks by the same amount $\approx 4.15 \times 10^{-3}$. The differences in the evolution of the density contrast in the three approximations are more evident from Fig. 2, in which we analyse the growth of an initial under-density, $\delta_{\text{in}} < 0$, over-density, $\delta_{\text{in}} > 0$, and the case of vanishing δ_{in} .

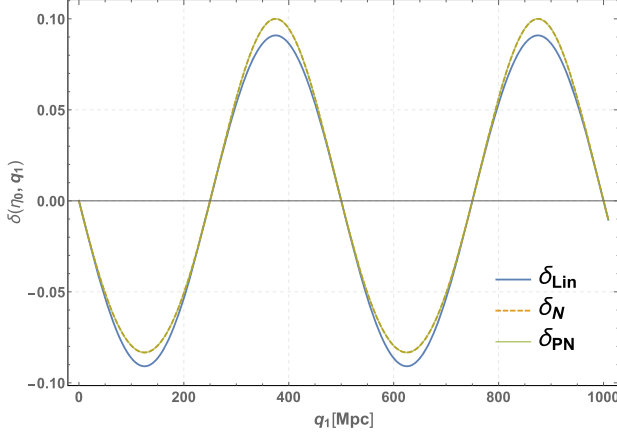


FIG. 1. Density contrast at present (conformal) time η_0 in the three approximations δ_{Lin} , δ_{N} and δ_{PN} , as in Eqs. (8), (9) and (10) respectively. The plots are obtained setting up the potential as $\phi_0 = \mathcal{I} \sin(\omega q_1)$ with $\omega = \frac{2\pi}{500 \text{ Mpc}}$ and amplitude \mathcal{I} such that $\max(\delta_{\text{PN}}(\eta_0, q_1)) = 0.1$. The values for Ω_{m0} , Ω_{Λ} , f_{nl} and \mathcal{H}_0 are taken from [38,39].

In Figs. 2(a) and 2(b) we show the deviations $|\frac{\delta_{\text{Lin}} - \delta_{\text{N}}}{\delta_{\text{N}}}|$ and $|\frac{\delta_{\text{PN}} - \delta_{\text{N}}}{\delta_{\text{N}}}|$ respectively, at fixed position as a function of time for the two cases of initial over- and underdensities. In Fig. 2(a) we clearly see that the variation Lin vs N grows with time, reaching $\approx 9\%$ at present, which is exactly the shift of 4.15×10^{-3} that we see in Fig. 1. The variation PN vs N grows with time as well, Fig. 2(b), but the value at present is 4 orders of magnitude less. Furthermore, in this figure we can also appreciate how the overdensities accrete faster than the underdensities, as one should expect. This is not visible in Fig. 2(a), due to the fact that the difference between the linear and the Newtonian approximation is dominant. The case of $\delta_{\text{in}} = 0$ is presented in Fig. 2(c), where we plot the differences $|\delta_{\text{Lin}} - \delta_{\text{N}}|$ and $|\delta_{\text{PN}} - \delta_{\text{N}}|$. The reason why we took the difference instead of the variation (as was done in the over- and underdensity cases) is to avoid the operation of dividing by zero, since we are considering regions with $\delta = 0$. We begin by noticing that for $\delta_{\text{in}} = 0$ both δ_{Lin} and δ_{N} vanish at any time, as evident from (8) and (9): both δ_{Lin} and δ_{N} are proportional to ϕ_0 and they are exactly zero at the same value

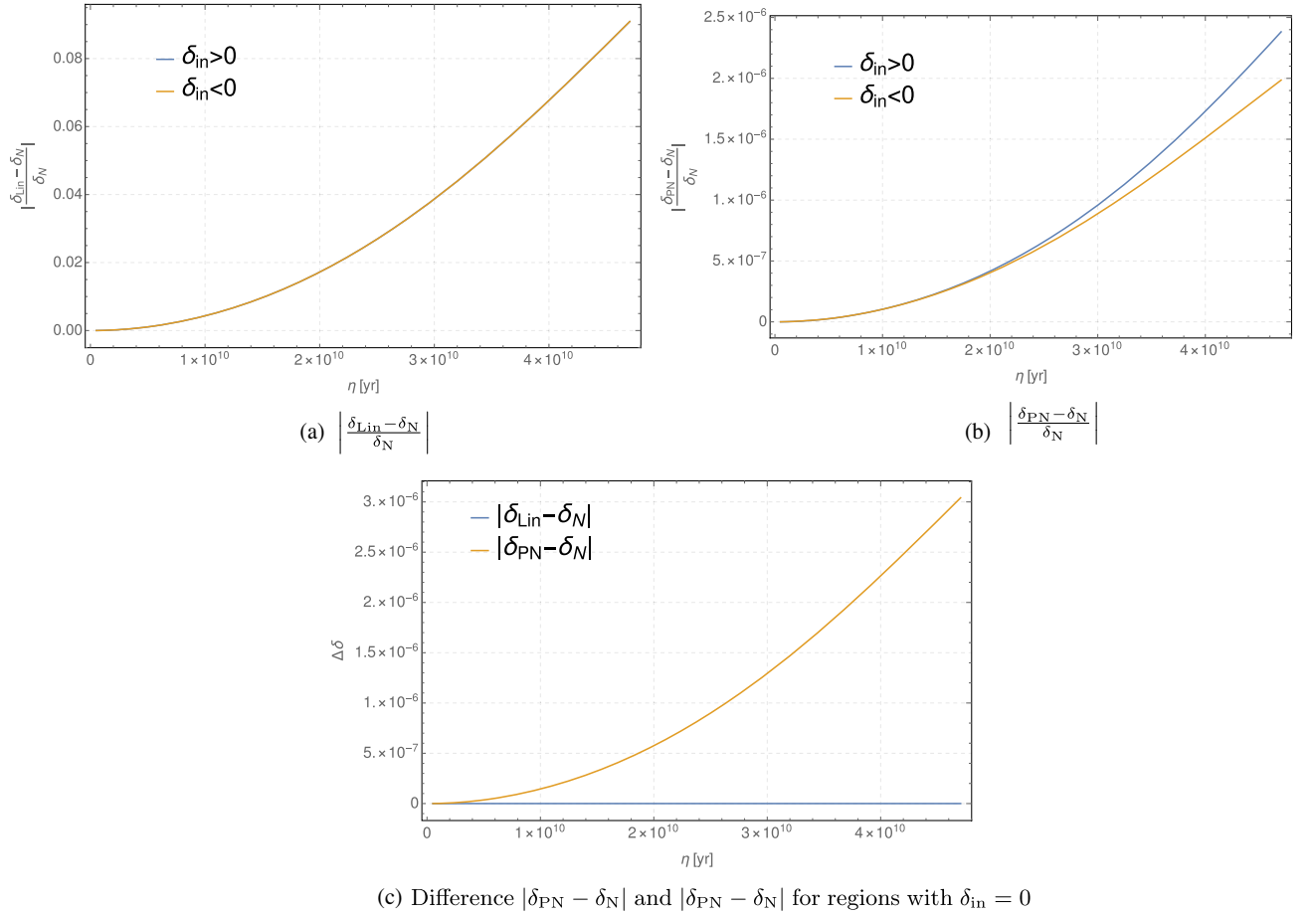


FIG. 2. Comparison between δ_{Lin} , δ_{N} and δ_{PN} as functions of conformal time η . The comparisons 2(a) and 2(b) are evaluated for an initial overdensity $\delta_{\text{in}} > 0$ and underdensity $\delta_{\text{in}} < 0$, while 2(c) is plotted for $\delta_{\text{in}} = 0$. All the three approximations are obtained for $\phi_0 = \mathcal{I} \sin(\omega q_1)$ with $\omega = \frac{2\pi}{500 \text{ Mpc}}$, amplitude \mathcal{I} such that $\max(\delta_{\text{PN}}(\eta_0, q_1)) = 0.1$, and cosmological parameters taken from [38,39].

of q_1 , in our toy model $\phi_0 \propto \sin(\omega q_1)$. Conversely, the term $\propto \partial_{q_1} \phi_0$ in $\delta_{\text{PN}}(10)$ implies that $\delta_{\text{PN}}(\eta_{\text{in}}) \neq 0$ at the position where $\delta_{\text{in}} = 0$. Therefore, what is actually shown in Fig. 2(c) is the evolution of the density contrast in the post-Newtonian approximation, whose absolute value increases up to $\approx 3 \times 10^{-6}$.

III. LIGHT PROPAGATION IN THE BGO FRAMEWORK

In this section we present the key elements of the formulation of light propagation which we are going to use in this paper: the bilocal geodesic operator (BGO) framework (for a more extended discussion of this formalism, see [33]). The physical situation we want to study is depicted in Fig. 3: an observer \mathcal{O} placed at $x_{\mathcal{O}}^{\mu}$ is connected to the source \mathcal{S} placed at $x_{\mathcal{S}}^{\mu}$ through a null geodesic γ . Both \mathcal{S} and \mathcal{O} are free to move along their timelike worldlines, but we assume that the typical length scale of the regions in which their motion takes place is small compared to the distance between them, so that their local geometry can be treated as flat. Therefore, we can safely assume that all gravitational effects on light propagation are due to the curvature of the spacetime between \mathcal{S} and \mathcal{O} .

In general, geodesics are uniquely specified by giving the initial position and the initial tangent vector, that can be assigned at the observation point. In other words, a fiducial null geodesic γ can be identified through its initial conditions $(x_{\mathcal{O}}^{\mu}, \ell_{\mathcal{O}}^{\mu})$. Now, if the observer is displaced by $\delta x_{\mathcal{O}}^{\mu}$, a new geodesic connects \mathcal{S} and \mathcal{O} and it is characterized by the new initial conditions $(x_{\mathcal{O}}^{\mu} + \delta x_{\mathcal{O}}^{\mu}, \ell_{\mathcal{O}}^{\mu} + \Delta \ell_{\mathcal{O}}^{\mu})$, where we define $\Delta \ell_{\mathcal{O}}^{\mu}$ as the covariant deviation of the tangent vector $\ell_{\mathcal{O}}^{\mu}$ at the observer position, namely

$$\Delta \ell_{\mathcal{O}}^{\mu} = \delta \ell_{\mathcal{O}}^{\mu} + \Gamma^{\mu}_{\alpha\beta}(x_{\mathcal{O}}) \ell_{\mathcal{O}}^{\alpha} \delta x_{\mathcal{O}}^{\beta}. \quad (12)$$

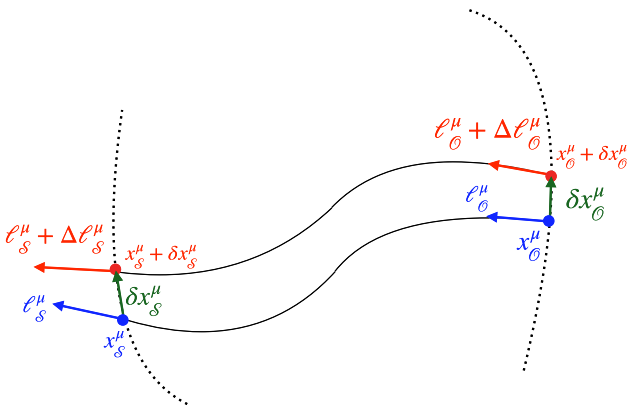


FIG. 3. Sketchy representation of the geometric set-up. Both the source \mathcal{S} and the observer \mathcal{O} are free to move along their worldlines, with the condition that at every proper time $\tau_{\mathcal{O}}$ there exists a null geodesic connecting $x_{\mathcal{O}}^{\mu}$ and $x_{\mathcal{S}}^{\mu}$.

The deviations $(\delta x_{\mathcal{O}}^{\mu}, \Delta \ell_{\mathcal{O}}^{\mu})$ can be used to parametrize a family of null geodesics around the fiducial geodesic γ , provided that the geodesics of the family stay close enough to γ , such that it can be studied by keeping all the equations linear in the displacements.

The deviation vector δx^{μ} , which is the displacement between γ and infinitesimally separated geodesics, propagates accordingly to the geodesic deviation equation (GDE)

$$\nabla_{\ell} \nabla_{\ell} \delta x^{\mu} - R^{\mu}_{\alpha\beta\nu} \ell^{\alpha} \ell^{\beta} \delta x^{\nu} = 0 \quad (13)$$

with initial conditions

$$\begin{aligned} \delta x^{\mu}(x_{\mathcal{O}}) &= \delta x_{\mathcal{O}}^{\mu} \\ \nabla_{\ell} \delta x^{\mu}(x_{\mathcal{O}}) &= \Delta \ell_{\mathcal{O}}^{\mu}. \end{aligned} \quad (14)$$

Using the linearity of the GDE and considering its projection into the parallel-propagated frame⁴ $\phi^{\mu}_{\alpha} = (u^{\mu}, \phi^{\mu}_{\mathbf{A}}, \ell^{\mu})$ (with $\alpha = 0, 1, 2, 3$ and $\mathbf{A} = 1, 2$ frame indices), the deviations at the source $(\delta x_{\mathcal{S}}^{\mu}, \Delta \ell_{\mathcal{S}}^{\mu})$ can be given as a linear combination of the initial deviations $(\delta x_{\mathcal{O}}^{\mu}, \Delta \ell_{\mathcal{O}}^{\mu})$

$$\begin{aligned} \delta x_{\mathcal{S}}^{\mu} &= W_{XX}{}^{\mu}_{\nu} \delta x_{\mathcal{O}}^{\nu} + W_{XL}{}^{\mu}_{\nu} \Delta \ell_{\mathcal{O}}^{\nu} \\ \Delta \ell_{\mathcal{S}}^{\mu} &= W_{LX}{}^{\mu}_{\nu} \delta x_{\mathcal{O}}^{\nu} + W_{LL}{}^{\mu}_{\nu} \Delta \ell_{\mathcal{O}}^{\nu}, \end{aligned} \quad (15)$$

where the BGO $W_{XX}, W_{XL}, W_{LX}, W_{LL}$ are bi-tensors acting from \mathcal{O} to \mathcal{S} . Equation (15) can then be written in the more compact form

$$\begin{aligned} \begin{pmatrix} \delta x_{\mathcal{S}} \\ \Delta \ell_{\mathcal{S}} \end{pmatrix} &= \begin{pmatrix} W_{XX} & W_{XL} \\ W_{LX} & W_{LL} \end{pmatrix} \begin{pmatrix} \delta x_{\mathcal{O}} \\ \Delta \ell_{\mathcal{O}} \end{pmatrix} \\ &= \mathcal{W}(\mathcal{S}, \mathcal{O}) \begin{pmatrix} \delta x_{\mathcal{O}} \\ \Delta \ell_{\mathcal{O}} \end{pmatrix}, \end{aligned} \quad (16)$$

where $\mathcal{W}(\mathcal{S}, \mathcal{O})$ is the resolvent of the GDE acting from \mathcal{O} to \mathcal{S} and satisfying the properties:

$$\begin{aligned} \mathcal{W}(\mathcal{O}, \mathcal{S}) &= (\mathcal{W}(\mathcal{S}, \mathcal{O}))^{-1} \\ \mathcal{W}(\mathcal{S}, \mathcal{O}) &= \mathcal{W}(\mathcal{S}, p_{\lambda}) \mathcal{W}(p_{\lambda}, \mathcal{O}), \end{aligned} \quad (17)$$

with p_{λ} being an arbitrary point on γ . A third key property of the BGO is that \mathcal{W} is symplectic, as first shown in [40]. To be precise, this property is written as

$$\mathcal{W}^{T\bar{m}}{}_{\bar{a}} \Omega_{\bar{m}\bar{s}} \mathcal{W}^{\bar{s}}{}_{\bar{b}} = \Omega_{\bar{a}\bar{b}} \quad (18)$$

where Ω is the 8×8 nonsingular, skew-symmetric matrix

⁴The frame $(u^{\mu}, \phi^{\mu}_{\mathbf{A}}, \ell^{\mu})$ is called seminull frame and it is composed by two parallel-propagated Sachs screen vectors $\phi^{\mu}_{\mathbf{A}}$, both orthogonal to u^{μ} and ℓ^{μ} . See [33] for a detailed discussion on semi-null frames properties.

$$\Omega_{\tilde{a}\tilde{b}} = \begin{pmatrix} 0 & h_{\alpha\beta} \\ -h_{\gamma\delta} & 0 \end{pmatrix}, \quad (19)$$

with $h_{\alpha\beta}$ the metric associated to the parallel-transported frame ϕ^μ_{α} , tilded indices run from 0 to 7 and bold indices $\alpha = 0, 1, 2, 3$ are those associated with the frame. Inserting (16) in the GDE equation projected in the parallel transported frame ϕ^μ_{α} , we obtain the propagation equation for the BGO

$$\frac{d}{d\lambda}\mathcal{W} = \begin{pmatrix} 0 & \mathbb{1}_{4\times 4} \\ R_{\ell\ell} & 0 \end{pmatrix}\mathcal{W} \quad (20)$$

with initial conditions

$$\mathcal{W}|_{\mathcal{O}} = \begin{pmatrix} \mathbb{1}_{4\times 4} & 0 \\ 0 & \mathbb{1}_{4\times 4} \end{pmatrix}, \quad (21)$$

where λ is the affine parameter spanning the geodesic γ and $R_{\ell\ell}$ is a short-hand notation to express the optical tidal matrix in the frame $R^\mu_{\alpha\beta\nu} \ell^\alpha \ell^\beta$.

The usual procedure for studying light propagation in numerical simulations is that the spacetime dynamics is integrated forward in time, while the study of light propagation is done in postprocessing, tracing the light beam backwards from the observer \mathcal{O} to the source \mathcal{S} . By solving (20) with initial conditions (21) at \mathcal{O} , one obtains the BGO $\mathcal{W}(p_\lambda, \mathcal{O})$ connecting the observer with the point p_λ up to the source $\mathcal{S} = p_{\lambda_S}$ and this is the procedure to compute observables, since real observations are made from the observer position. Nevertheless, in the framework we present here, one can choose to give initial conditions at \mathcal{S} (or anywhere else) and integrate forward in time to \mathcal{O} . The key advantage is that in this way one is able to integrate (20) for light propagation on-the-fly with Einstein's equations for spacetime dynamics. In this case one obtains the BGO $\mathcal{W}(p_\lambda, \mathcal{S})$ relating the point p_λ with the source. The two procedures for light propagation are fully equivalent and the relation between them, namely between $\mathcal{W}(p_\lambda, \mathcal{O})$ and $\mathcal{W}(p_\lambda, \mathcal{S})$, simply follows from the BGO properties (17) and reads⁵

$$\mathcal{W}(p_\lambda, \mathcal{O}) = \mathcal{W}(p_\lambda, \mathcal{S})(\mathcal{W}(\mathcal{O}, \mathcal{S}))^{-1} \quad (22)$$

where $\mathcal{W}(\mathcal{O}, \mathcal{S}) = \mathcal{W}(p_{\lambda_{\mathcal{O}}}, \mathcal{S})$.

In this work the input is an analytic form of the spacetime metric and we integrate the equation for the BGO (20) backwards in time and obtain directly the left-hand side (lhs) of Eq. (22). The procedure to compute observables can be summarized in the following steps:

- (1) compute the null geodesic connecting \mathcal{O} and \mathcal{S} ;
- (2) perform the parallel transport of a reference frame;

⁵The symplectic property of \mathcal{W} , Eq. (18) simplifies a lot the computation of \mathcal{W}^{-1} .

- (3) solve the evolution equation for the BGO, Eq. (20), with initial conditions, Eq. (21) from the observer to the source;
- (4) combine the BGO with the four-velocity of source and observer to obtain the observables we are interested in, which are redshift and angular diameter distance D_{ang} , written in terms of the BGO as, see [34]

$$1 + z = \frac{\ell_\sigma u^\sigma|_{\mathcal{S}}}{\ell_\sigma u^\sigma|_{\mathcal{O}}} \quad (23)$$

$$D_{\text{ang}} = \ell_\sigma u^\sigma|_{\mathcal{O}} |\det(W_{XL}{}^A{}_B)|^{\frac{1}{2}}. \quad (24)$$

The advantage of the BGO formalism is that it provides a unified approach to geometric optics. Furthermore, it extends the standard Sachs formalism, allowing also to describe what happens when the observation occurs for a prolonged period of time and the slow temporal variations of the optical observables, called the drift effects, could become measurable.

All the steps 1–4 require the ability of solving systems of coupled ODEs, that can be done either using analytical methods (exact or perturbative approach) or numerical methods. In our work we will use both methods, as we are going to explain in the next section.

IV. METHOD

The core of our analysis is to estimate the magnitude of the nonlinear effects on light propagation, through the comparison of some cosmological observables calculated within different approximation schemes. In particular, we will compare the redshift z and the angular diameter distance D_{ang} computed in the following three cases:

- (1) using the first-order expansion in standard cosmological perturbation theory of the plane-parallel metric (6) and performing light propagation perturbatively, up to first order. We will denote as O^{Lin} , the generic observable O obtained in this way, which only includes effects linear in the perturbations; (z^{Lin} and $D_{\text{ang}}^{\text{Lin}}$ are derived in App. B);
- (2) using the Newtonian part of the plane-parallel metric, namely the metric in Eq. (7), and performing exact light propagation⁶ using numerical integration.

⁶The term “exact” refers to the fact that no perturbative approach is used when we derive and solve the equations describing the propagation of light and observables. In other words, even if the spacetime metric was obtained using some perturbation scheme, we use it as if it were exact for the entire procedure to calculate the observables, starting from the very beginning, i.e., the geodesic equation. We will discuss this approach further on in this section.

The observables calculated in this way will be indicated as O^N ;

- (3) using the full PN plane-parallel metric (2) and performing exact light propagation via numerical integration. We denote the observables calculated with this method as O^{PN} .

The observables calculated with the last two methods, O^N and O^{PN} , are obtained using `BiGONLight.m` (bilocal geodesic operators framework for numerical light propagation), a publicly available *Mathematica* package (<https://github.com/MicGrasso/bigonlight>) developed to study light propagation in numerical simulations using the BGO framework. The package contains a collection of function definitions, including those to compute geodesics, parallel transported frames and solve the BGO's equation (20). `BiGONLight.m` works as an independent package that, once is called by a *Mathematica* notebook, can be used to compute numerically the BGO along the line of sight, given the spacetime metric, the four-velocities and accelerations of source and observer as inputs: a sample of the notebook we used for our analysis can be found in the repository

folder *Plane-parallel*. An exhaustive description of `BiGONLight` and several tests of the package are presented in [32]. Here we just report in Appendix A two case studies of code testing, the Λ CDM and the Szekeres model.

Let us now comment about the fact that we use exact light propagation for the Newtonian and post-Newtonian observables, despite the fact that the respective spacetime metric is obtained with perturbative techniques. First, we notice that this method used to compute O^{PN} does not produce observables strictly of PN order: the observables O^{PN} will contain also some of higher than PN contributions, coming from the fact that we start from the PN metric (2) but we do not expand further the equations for light propagation or the expressions for the observables in powers of $1/c^2$ (we set $c = 1$ everywhere). One would naively expect that the higher than PN terms are always subleading with respect to the PN ones, as in any well-defined perturbation scheme. The key point here is if this hierarchy, which starts at the level of metric perturbations, is preserved throughout the full calculation to the final results, especially in our case where the equations to

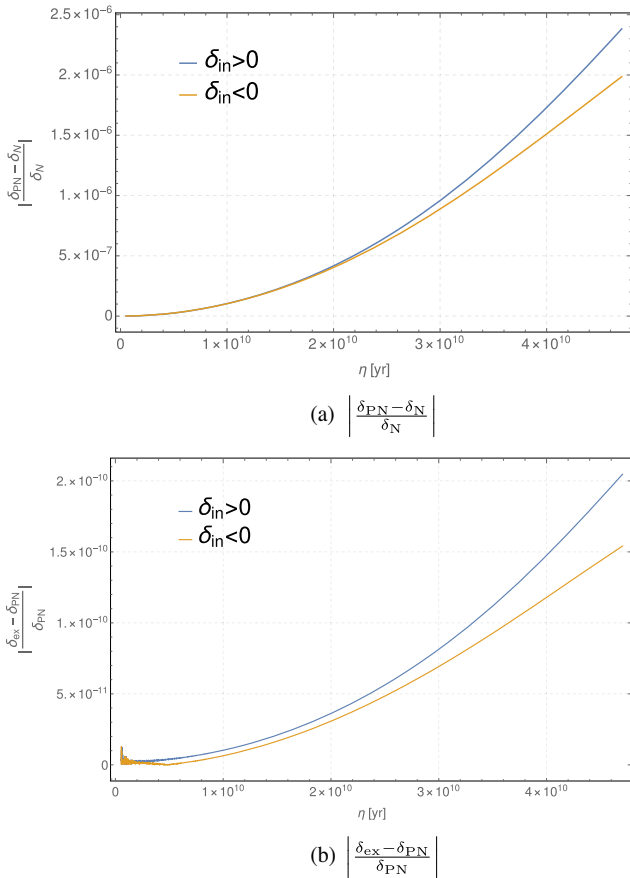


FIG. 4. Evolution of the variation δ_{PN} vs δ_N (a) and δ_{ex} vs δ_{PN} (b) for initial overdensity $\delta_{in} > 0$ and underdensity $\delta_{in} < 0$ regions for $k = 500$ Mpc. The variation δ_{ex} vs δ_{PN} (b) is 4 orders of magnitude smaller than the variation δ_{PN} vs δ_N (a).

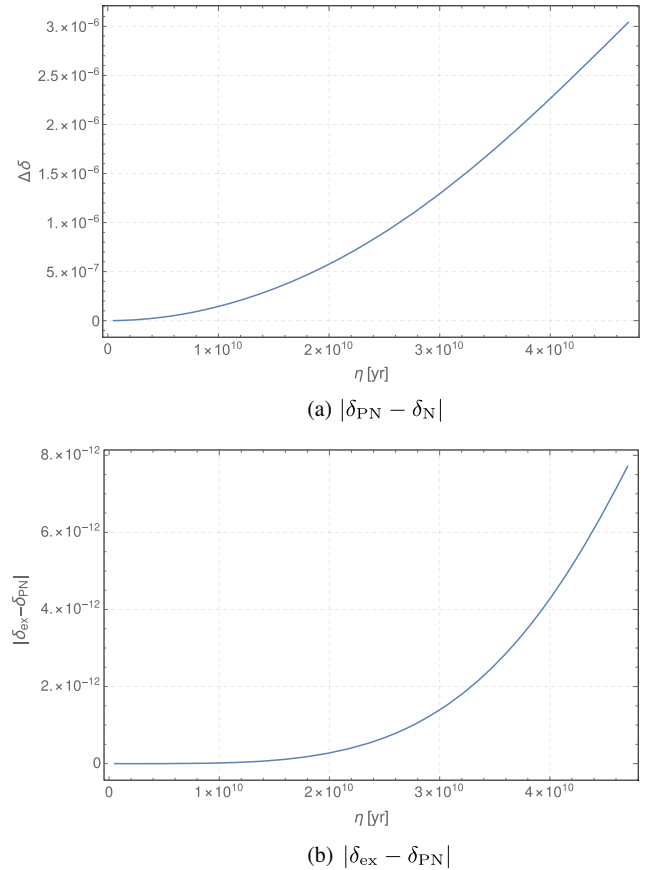


FIG. 5. Evolution of the variation δ_{PN} vs δ_N (a) and δ_{ex} vs δ_{PN} (b) for regions with $\delta_{in} = 0$ and $k = 500$ Mpc. The variation δ_{ex} vs δ_{PN} (b) is 6 orders of magnitude smaller than the variation δ_{PN} vs δ_N (a).

TABLE I. Values (k, δ_0^{\max}) used in our analysis.

k (Mpc)	500	300	100	50	30
δ_0^{\max}	0.1	0.35	1	1.5	1.8

compute the observables are fully nonlinear. We find that this is indeed the case, as indicated in similar investigations in the literature. In order to show this explicitly and to give an estimate of the higher than PN corrections, we have compared the density contrast calculated strictly up to PN order δ_{PN} (10) and the density contrast δ_{ex} obtained from its exact expression from the continuity equation in synchronous-comoving gauge, i.e.,

$$\delta_{\text{ex}}(\eta, q_1) = (\delta(\eta_{\text{in}}, q_1) + 1) \sqrt{\frac{|\gamma(\eta_{\text{in}}, q_1)|}{|\gamma(\eta, q_1)|}} - 1, \quad (25)$$

where $|\gamma|$ is the short-hand notation for the determinant of the metric (2), calculated here without expanding in powers of $1/c^2$.

The plots in Fig. 4 show that the variation between δ_{PN} and δ_{ex} is 4 orders smaller than the variation between δ_{N} and δ_{PN} for initial over- and underdense regions and it is 6 orders smaller when we consider regions with vanishing initial density contrast, Fig. 5. This is something we expected, since the impact of the corrections gets smaller and smaller with the increase of the order in the expansion and, more importantly, we were able to isolate and quantify the corrections coming from the higher than PN terms. This specific result holds for the density contrast but it is perfectly reasonable that this estimation is roughly valid for the observables too, even if the calculation to get them is different. We believe that the argument just presented validates our method of performing exact light propagation.

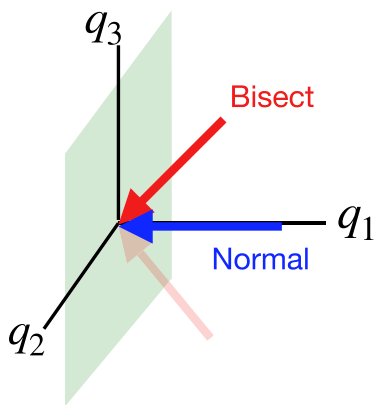


FIG. 6. Graphic representation of the direction normal to the planes (blue) and the direction along the bisect (red). Two geodesics with these directions will intersect the uniform density planes with different angles. Therefore the matter distribution profiles along the geodesics are also different.

In order to compare the observables calculated within different approximations, we introduce the dimensionless variation ΔO for the generic observable O calculated in the two approximations a and b defined as:

$$\Delta O(b, a) = \frac{O^b - O^a}{O^a} \quad (26)$$

where a and b stand for Λ CDM, Lin, N or PN, namely the Λ CDM background, the linear order in standard PT, Newtonian or post-Newtonian approximations, respectively.

Having introduced the general method we use for our analysis and we defined the key quantity for our comparisons, we have to specify the free functions and the parameters of the plane-parallel universe we are considering, of the Λ CDM background model and its perturbations. We recall that the evolution of the inhomogeneities in our

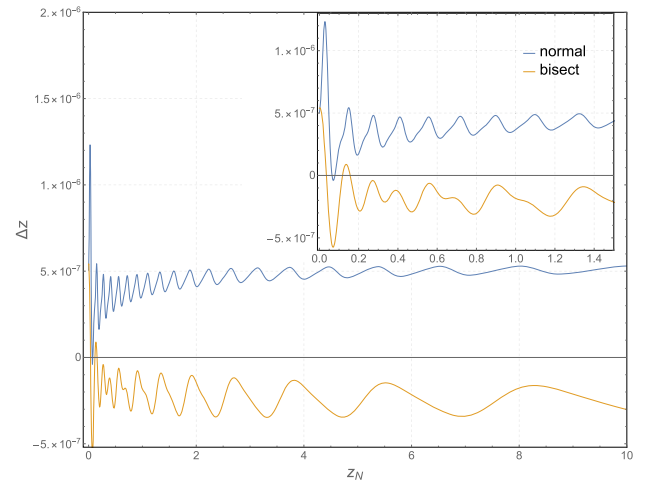
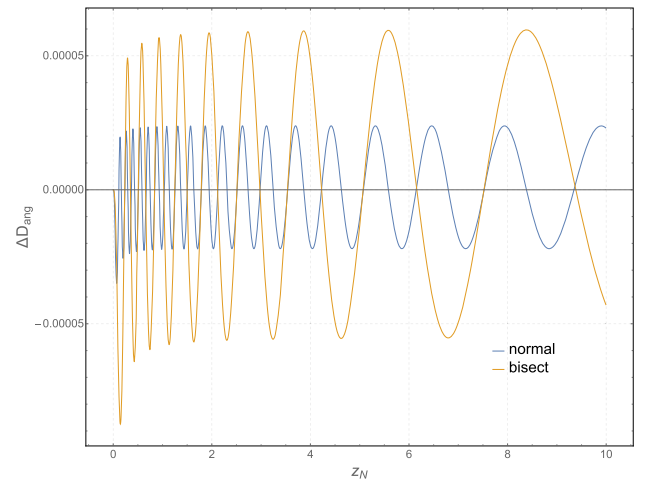
(a) Δz (b) ΔD_{ang}

FIG. 7. $\Delta z(\text{PN}, N)$ [7(a)] and $\Delta D_{\text{ang}}(\text{PN}, N)$ [7(b)] according to our definition (26) for the two geodesics with directions normal to the planes (blue lines) and parallel to the bisect (orange lines).

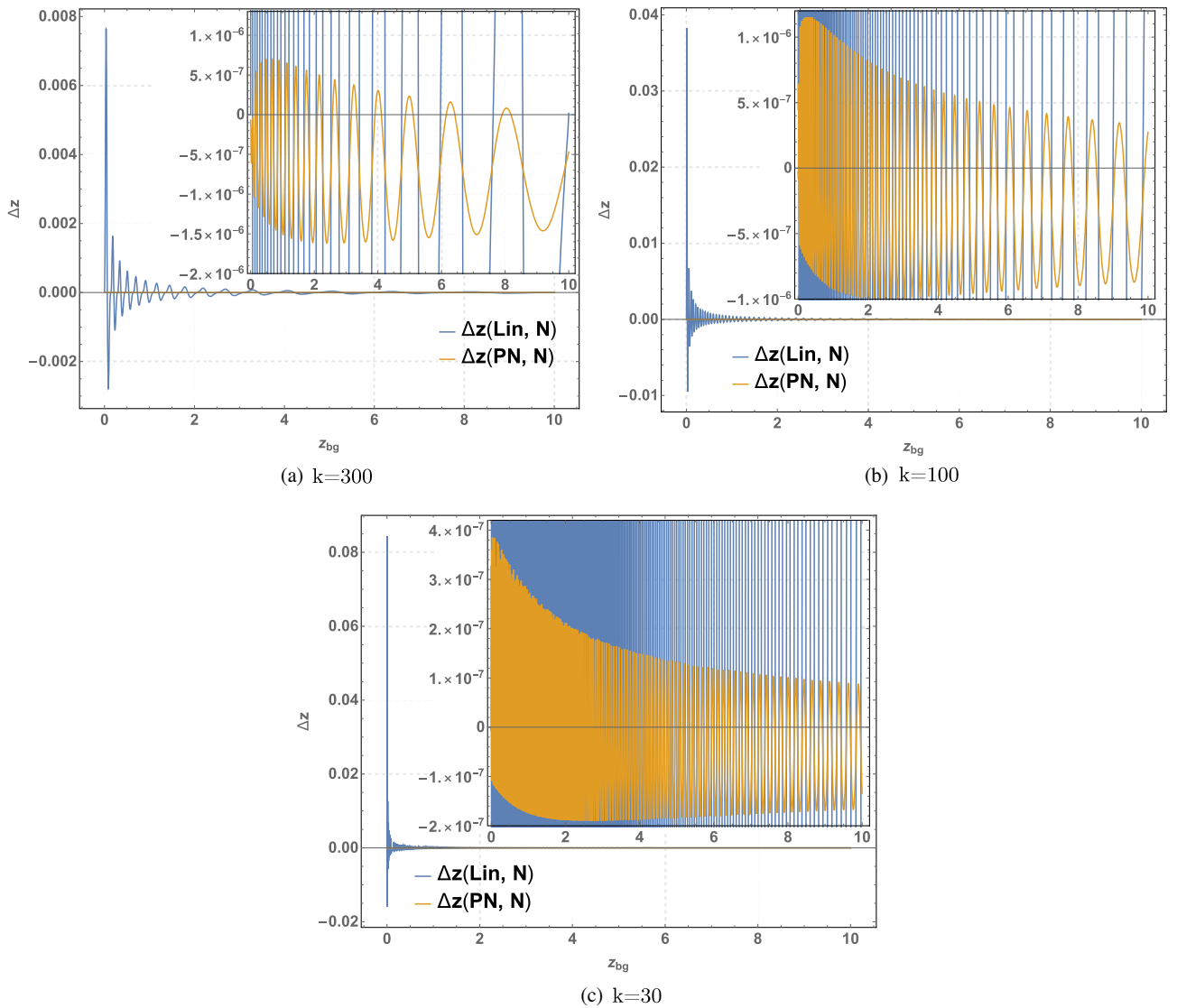


FIG. 8. Redshift variations, as defined in Eq. (29), Linear vs Newtonian (blue) and post-Newtonian vs Newtonian (orange) on three different scales $k = 30, 100, 300$ Mpc. We see that $\Delta z(\text{Lin}, \text{N}) \sim 10^2 \Delta z(\text{PN}, \text{N})$ on every scale k . The variable on the horizontal axis is the Λ CDM redshift.

model is governed by the growing mode solution \mathcal{D} (4), while the spatial part of the matter distribution is determined by the gravitational potential ϕ_0 , which is the only free function. We use a sinusoidal profile for the gravitational potential ϕ_0 defined as:

$$\phi_0 = \mathcal{I} \sin(\omega q_1) \quad (27)$$

where the frequency $\omega = 2\pi/k$ is determined from the scale of the inhomogeneities k , while the amplitude \mathcal{I} is obtained from (10) for a certain value of the maximum of post-Newtonian density contrast today δ_0^{max} . The scale k and the maximum of the density contrast δ_0^{max} are linked by the matter power spectrum and we will repeat our analysis for different values of $(k, \delta_0^{\text{max}})$ (this will be discussed in the

Sec. V). In Table I we report the chosen values for the scales and the corresponding maximum of the density contrast today. The cosmological parameters are set using the fiducial values from [38], i.e., $\Omega_{m0} = 0.3153$, $\Omega_\Lambda = 0.6847$ and $\mathcal{H}_0 = 67.36$. For primordial non-Gaussianity we use the parameter a_{nl} introduced in [37]. It is linked to the parameter f_{nl} by:

$$a_{\text{nl}} = \frac{3}{5} f_{\text{nl}} + 1 \quad (28)$$

where $a_{\text{nl}} = 1$, i.e., $f_{\text{nl}} = 0$, correspond to the case of exact Gaussian fluctuations. The latest measurement of f_{nl} from the Planck collaboration [39] gives $a_{\text{nl}} = 0.46 \pm 3.06$ that will fix $a_{\text{nl}} = 0.46$ as the fiducial value for our analysis.

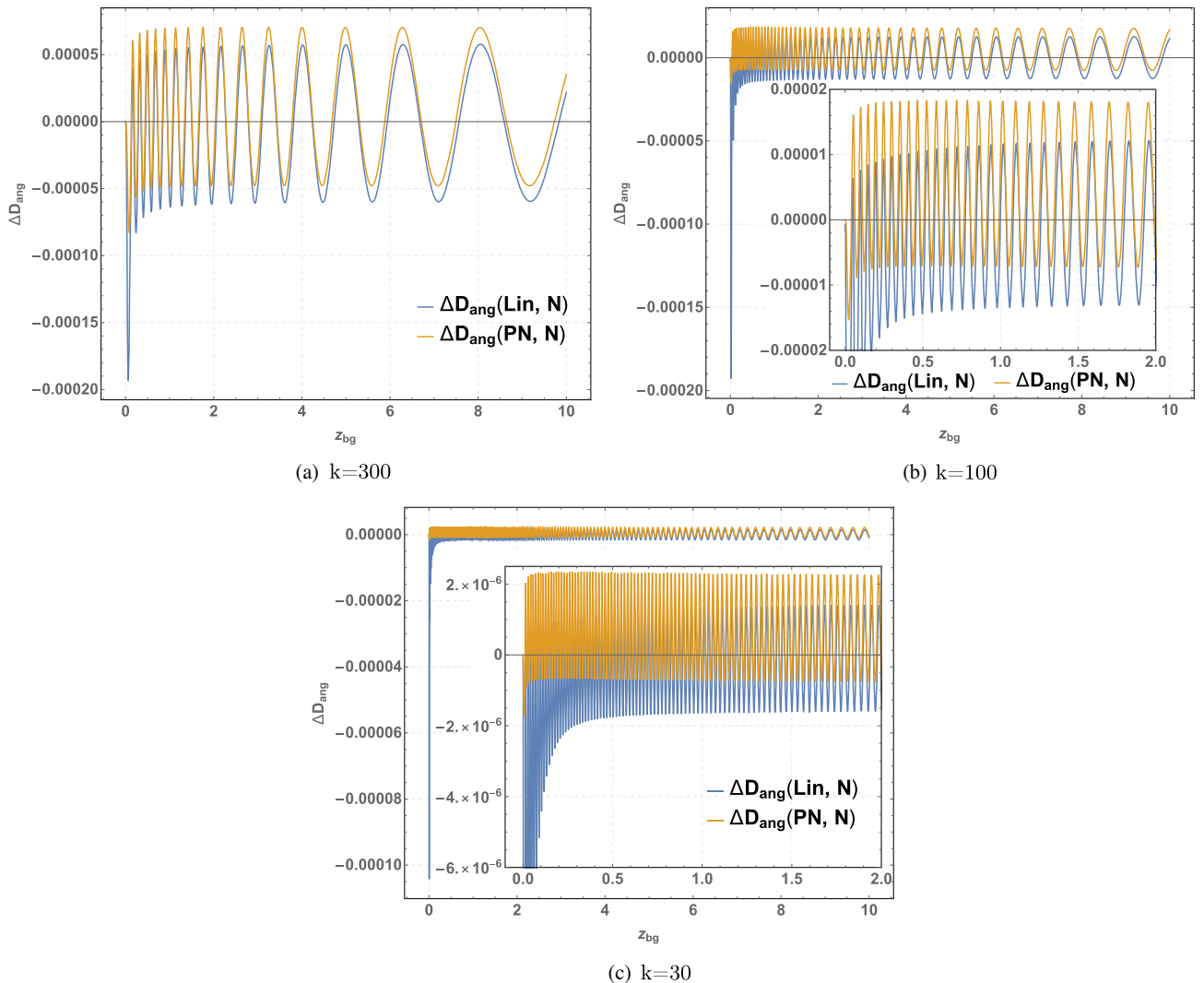


FIG. 9. Angular diameter distance variations, as defined in Eq. (29), linear vs Newtonian (blue) and post-Newtonian vs Newtonian (orange) on three different scales $k = 30, 100, 300$ Mpc. We see that $\Delta D_{\text{ang}}(\text{Lin, N}) \sim \Delta D_{\text{ang}}(\text{PN, N})$ on every scale k . The variable on the horizontal axis is the Λ CDM redshift.

However, since in our case we take deterministic initial conditions, a_{nl} merely represents an extra free parameter of our approach which tunes the post-Newtonian corrections.⁷ Given that a_{nl} has a lot of room to vary inside its confidence interval of ± 3.06 , we have also investigated how the comparison Newtonian vs post-Newtonian gets modified if we take different values of a_{nl} to calculate post-Newtonian observables O^{PN} (see section V).

The last things we need to specify are the observer and emitter positions and their kinematics. In our study we place the observer in a position with vanishing initial density contrast $\delta_{\text{in}} = 0$ and we will leave the analysis on

⁷This is evident, since a_{nl} appears only in the post-Newtonian terms and some of them can be cancelled or dimmed with an appropriate choice of the a_{nl} 's value.

how the comparison change when the observer is located in an initial overdensity or underdensity for future investigations. The geodesic equations and the BGO equations (20) are solved giving the initial conditions at the observer position and they are integrated backwards in time up to redshift $z = 10$. The choice of analyzing only sources at $z = 10$ still leaves us the freedom in selecting the direction from which the light is coming. The difference between geodesics with different directions is mainly due to the way in which the geodesics cross the parallel planes with uniform density. To investigate this effect, we have considered two geodesics, one with direction normal to the planes and one with direction parallel to the bisect as represented in Fig. 6, considering in both cases the observer in a position with $\delta_{\text{in}} = 0$ and the gravitational potential (27) set such that $k = 500$ Mpc and $\delta_0^{\text{max}} = 0.1$. For both

geodesics we have analysed what are the effects of the direction on the variations Newtonian vs post-Newtonian for Δz [Fig. 7(a)] and ΔD_{ang} [Fig. 7(b)].

From the plots we can conclude that there are small differences in the comparison post-Newtonian vs Newtonian for geodesics with different directions. However, the change in the matter distribution on the geodesic induced by the different directions does not modify the magnitude of the variations too much, but only their shapes. In conclusion, when we consider geodesics along the normal, the effects of the nonlinearities are somewhat smaller than for the geodesics along the bisect direction. Nevertheless, from now on, we will consider only geodesics directed along the bisect: this will not affect our conclusions because we will make all the comparisons using geodesics along the bisect in all the cases under study.

For clarity, the following list summarizes the conditions we set for our analysis:

- (i) If not specified, the observer \mathcal{O} is placed in a position with initial vanishing density contrast $\delta_{\text{in}} = 0$.
- (ii) The sources are at redshift $z = 10$ and such that the observer receives the light with direction parallel to the bisect.
- (iii) Our analysis is performed in synchronous comoving gauge implying that both emitter and observer are comoving with the cosmic flow.
- (iv) The primordial non-Gaussianity parameter a_{nl} is set using the fiducial value from Planck [39], i.e., $a_{\text{nl}} = 0.46$. However, in Sec. V we will also consider the case when a_{nl} is set equal to the extreme of its confidence interval.

V. RESULTS

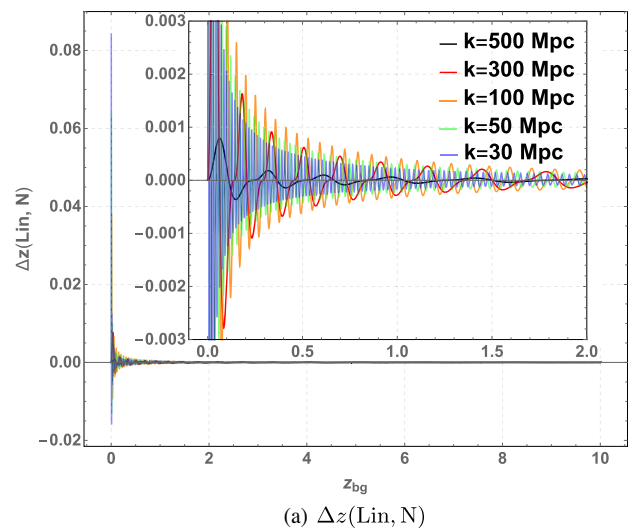
In this section we present the results of our study that we plot in terms of the quantity

$$\Delta O(b, a) = \frac{O^b - O^a}{O^a}, \quad (29)$$

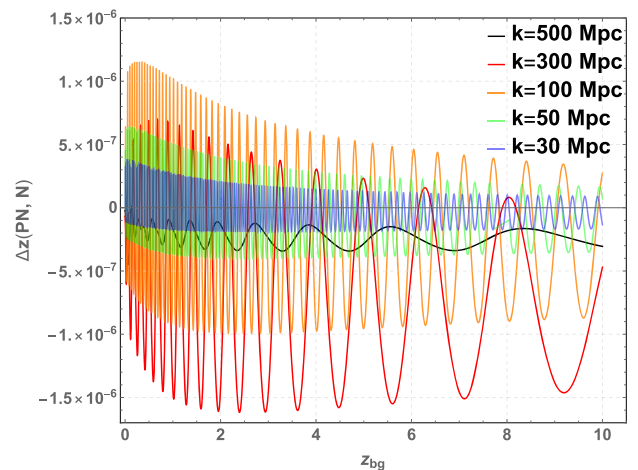
where our observables O are the redshift z and the angular diameter distance D_{ang} and a, b stand for the approximations used in turn. Let us start with Figs. 8 and 9 in which we plot the variation between linear and Newtonian approximations, $\Delta z(\text{Lin}, N)$ and $\Delta D_{\text{ang}}(\text{Lin}, N)$, and the PN corrections to the Newtonian approximation, $\Delta z(\text{PN}, N)$ and $\Delta D_{\text{ang}}(\text{PN}, N)$ for three different scales, $k = 30, 100, 300$ Mpc. The main result here is that the variations behave differently for the redshift and for the angular diameter distance. Indeed, while for z the post-Newtonian corrections are two orders of magnitude smaller than the nonlinear Newtonian contributions with respect to linear theory, for D_{ang} the two corrections are of the same order. This can be clearly seen on $k = 300$ Mpc, Figs. 8(a) and 9(a), and the same behavior also holds on smaller scales, Figs. 8(b), 8(c), 9(b), and 9(c).

For $z \lesssim 2$ we have that $\Delta z(\text{PN}, N) \sim 10^{-6}$ on $k = 300$ Mpc with oscillation damped as the redshift increases. On the other hand, for the angular diameter distance $\Delta D_{\text{ang}}(\text{Lin}, N) \sim \Delta D_{\text{ang}}(\text{PN}, N) \sim 10^{-4}$ on $k = 300$ Mpc in the full redshift range $[0, 10]$.

We dedicate a separate study, reported in Figs. 10 and 11, to the change of the amplitude of all the variations with the scale. We consider inhomogeneities scales of $k = 500, 300, 100, 50, 30$ Mpc. Figure 10 shows that both the variations $\Delta z(\text{Lin}, N)$ and $\Delta z(\text{PN}, N)$ increase from $k = 500$ Mpc to reach the maximum amplitude on $k = 100$ Mpc and then decreases down to $k = 30$ Mpc. In terms of amplitudes we have: $\Delta z(\text{Lin}, N) \sim 10^{-4}$, with a maximum $\sim 10^{-3}$ around $k = 100$ Mpc and $\Delta z(\text{PN}, N) \sim 10^{-7}$, with a maximum $\sim 10^{-6}$ around $k = 100$ Mpc. We again note that



(a) $\Delta z(\text{Lin}, N)$



(b) $\Delta z(\text{PN}, N)$

FIG. 10. Variations $\Delta z(\text{Lin}, N)$ and $\Delta z(\text{PN}, N)$, as defined in Eq. (29), on different scales in the range $[30, 500]$ Mpc. Both the variations show a maximum around $k = 100$ Mpc. The variable on the horizontal axis is the Λ CDM redshift.

the variations for the redshift are damped as z increases. This is most evident for $\Delta z(\text{Lin}, N)$. The angular diameter distance shows in Fig. 11 a different behavior: the amplitude of both variations $\Delta D_{\text{ang}}(\text{Lin}, N)$ and $\Delta D_{\text{ang}}(\text{PN}, N)$ decreases monotonically as the scale k become smaller. Both the amplitudes start from $\Delta D_{\text{ang}} \sim 10^{-4}$ on $k = 500$ Mpc and decrease to 10^{-6} on $k = 30$ Mpc.

As we mentioned in Sec. IV, different values of the primordial non-Gaussianity parameter a_{nl} tune some of the post-Newtonian terms in (2), e.g., a perfect Gaussian initial perturbation ($a_{\text{nl}} = 1$) cancels out the third term in the PN part of the metric (2). We then decided to quantify how the PN observables change when we vary the values of a_{nl} inside the confidence interval measured by Planck, [39].

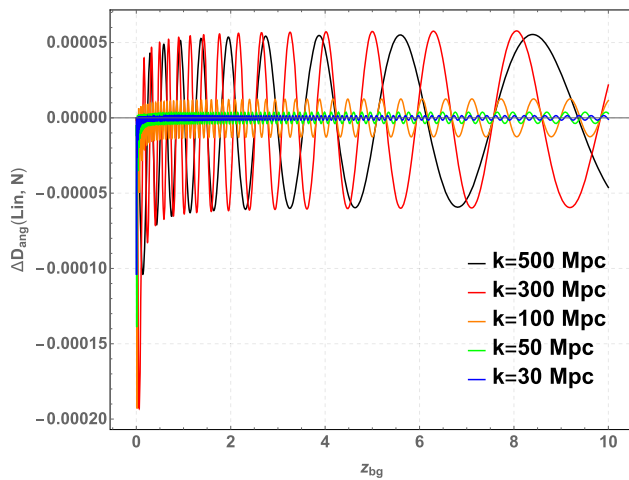
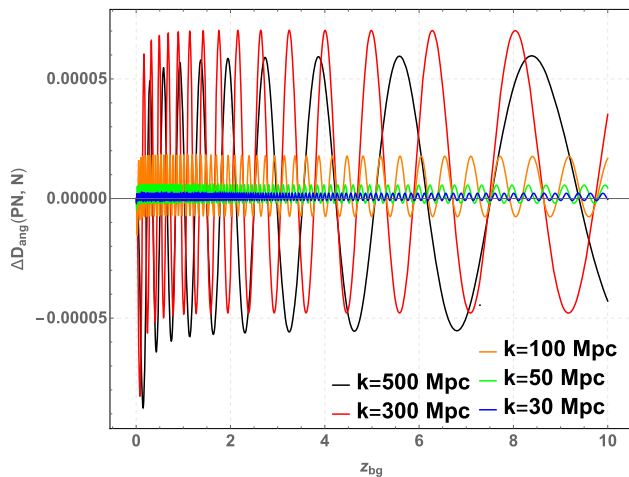
(a) $\Delta D_{\text{ang}}(\text{Lin}, N)$ (b) $\Delta D_{\text{ang}}(\text{PN}, N)$

FIG. 11. Variations $\Delta D_{\text{ang}}(\text{Lin}, N)$ and $\Delta D_{\text{ang}}(\text{PN}, N)$, as defined in Eq. (29), on different scales in the range [30, 500] Mpc. The amplitudes monotonically decrease as the scale k becomes smaller. The variable on the horizontal axis is the Λ CDM redshift.

For this analysis, we choose $a_{\text{nl}} = 1, 0.46, -2.6, 3.52$, corresponding to Gaussian perturbations ($a_{\text{nl}} = 1$), Planck 2018 fiducial value ($a_{\text{nl}} = 0.46$), and extremes of confidence interval ($a_{\text{nl}} = -2.6, 3.52$). We start the discussion of our results by looking at Figs. 12(a) and 13(a), in which we plot for the PN observables the quantity

$$\Delta O^{\text{PN}}(a_{\text{nl}_1}, a_{\text{nl}_2}) = \frac{O_{a_{\text{nl}_1}}^{\text{PN}} - O_{a_{\text{nl}_2}}^{\text{PN}}}{O_{a_{\text{nl}_2}}^{\text{PN}}}, \quad (30)$$

where we fix a_{nl_2} to the Planck best-fit value and we vary a_{nl_1} . The effect is different for the redshift and for the angular diameter distance: the variation in $D_{\text{ang}}^{\text{PN}}$ is $\sim 10^{-9}$, two orders of magnitude smaller than the one in z^{PN} . This

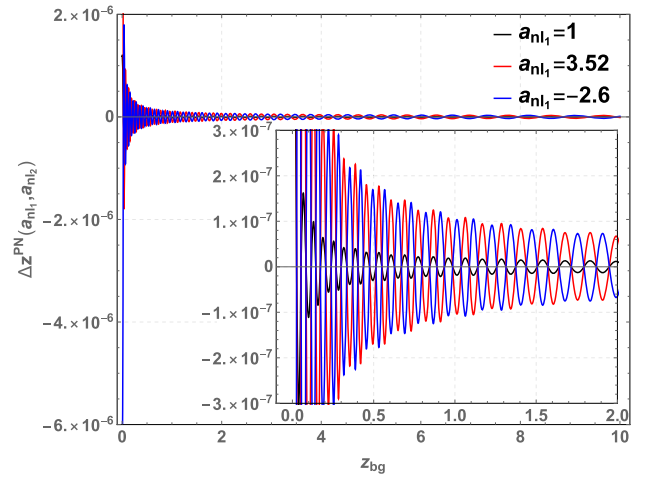
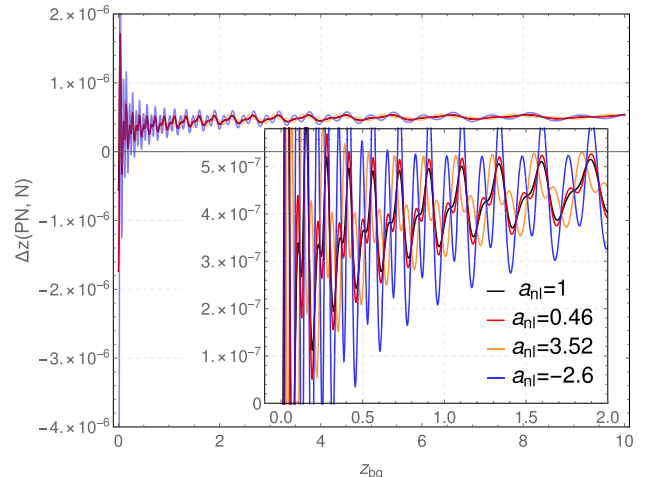
(a) $\Delta z^{\text{PN}}(a_{\text{nl}_1}, a_{\text{nl}_2})$ (b) $\Delta z(\text{PN}, N)$

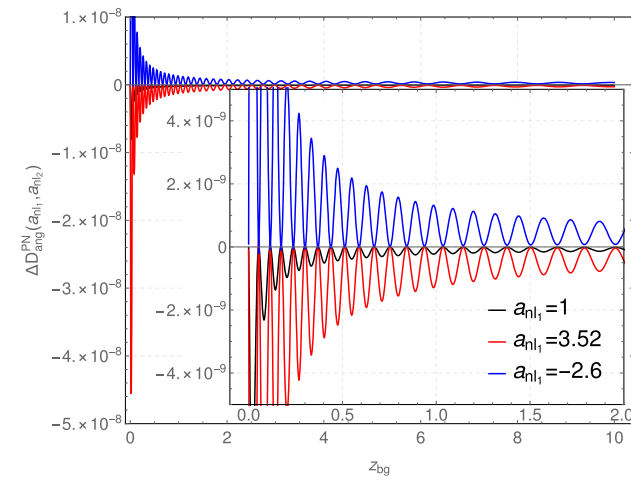
FIG. 12. The effect of varying primordial non-Gaussianity for the redshift: the variation in Eq. (30), [12(a)], and PN correction for different values of a_{nl} , [12(b)]. We find that $\Delta z^{\text{PN}}(a_{\text{nl}_1}, a_{\text{nl}_2}) \lesssim \Delta z(\text{PN}, N)$. The variable on the horizontal axis is the Λ CDM redshift.

very difference is evident when we plot the PN corrections for different values of a_{nl} , see Figs. 12(b) and 13(b). The effect of tuning primordial non-Gaussianity is roughly of the same order as the PN correction for the redshift and also changes its shape. On the contrary, D_{ang} is completely insensitive to the variation of the non-Gaussianity parameter, since $\Delta D_{\text{ang}}^{\text{PN}}(a_{nl_1}, a_{nl_2}) \sim 10^{-4} \Delta D_{\text{ang}}(\text{PN}, N)$.

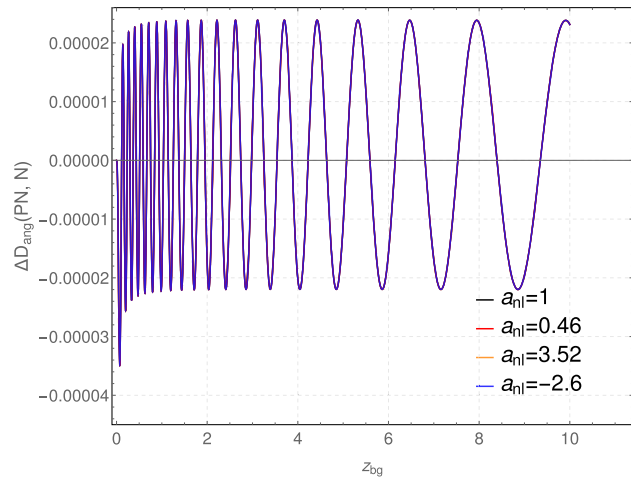
To conclude our analysis, we isolate and quantify the contribution of the linear PN initial seed proportional to the gravitational potential, i.e., $\gamma_{ij} = -\frac{10}{3c^2} \phi_0 \delta_{ij}$ in the spacetime metric (2). To do so, we define an hybrid spacetime metric, labelled with \tilde{N} , by adding the initial PN seed to the Newtonian metric (7), i.e.,

$$\begin{aligned} \gamma_{11}^{\tilde{N}} &= \left(1 - \frac{2 \mathcal{D} \partial_{q_1}^2 \phi_0}{3 \mathcal{H}_0^2 \Omega_{m0}}\right)^2 - \frac{10}{3c^2} \phi_0 \\ \gamma_{22}^{\tilde{N}} &= 1 - \frac{10}{3c^2} \phi_0 \\ \gamma_{33}^{\tilde{N}} &= 1 - \frac{10}{3c^2} \phi_0, \end{aligned} \quad (31)$$

and we have compared the angular diameter distance computed from the two have compared the angular diameter distance computed from the two approximations in Eq. (7) and in Eq. (31). The inclusion of the initial seed in

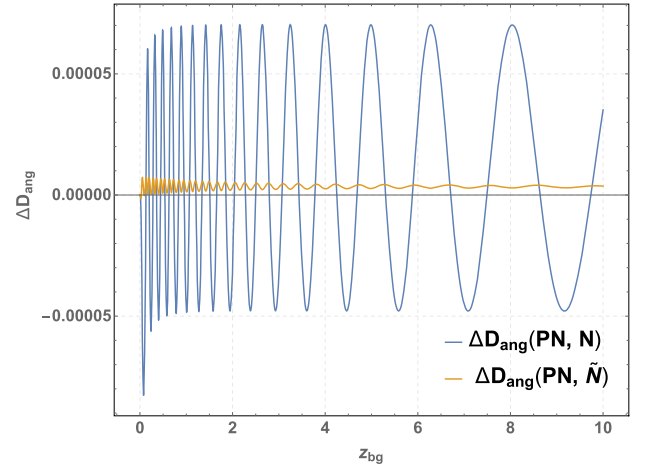


(a) $\Delta D_{\text{ang}}^{\text{PN}}(a_{nl_1}, a_{nl_2})$

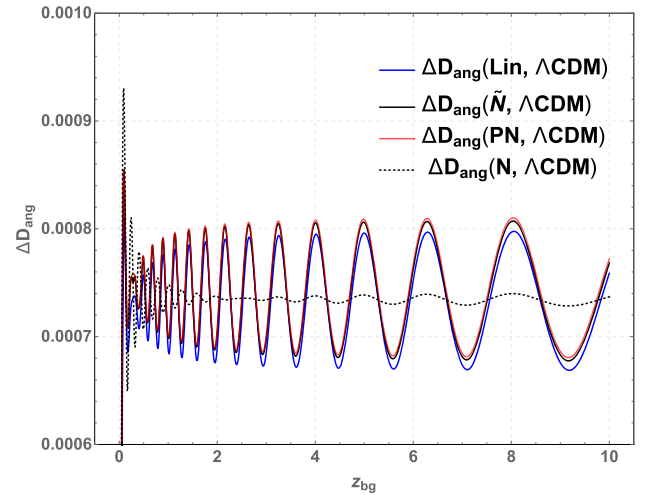


(b) $\Delta D_{\text{ang}}(\text{PN}, N)$

FIG. 13. The effect of varying primordial non-Gaussianity for the angular diameter distance: the variation in Eq. (30), [13(a)], and PN correction for different values of a_{nl} , [13(b)]. We find that $\Delta D_{\text{ang}}^{\text{PN}}(a_{nl_1}, a_{nl_2}) \sim 10^{-4} \Delta D_{\text{ang}}(\text{PN}, N)$. The variable on the horizontal axis is the ΛCDM redshift.



(a) Comparison PN vs N (blue) and PN vs \tilde{N} (orange) for the angular diameter distance, as defined in Eq. (29), on $k = 300 \text{ Mpc}$. The variation $\Delta D_{\text{ang}}(\text{PN}, \tilde{N}) \sim 10^{-6}$ is two orders of magnitude smaller than $\Delta D_{\text{ang}}(\text{PN}, N)$. The variable on the horizontal axis is the ΛCDM redshift.



(b) Comparison between the different approximations Lin, N, \tilde{N} , PN and the ΛCDM background for the angular diameter distance.

FIG. 14. Results for the contribution of the initial seeds to the angular diameter distance. For the definition of \tilde{N} see Eq. (31).

the modified Newtonian model is such that the PN variation is reduced by two orders of magnitude, see Fig. 14(a). In other words the initial seed is the leading order of the post-Newtonian correction. The effect is even more evident when we consider the variations of each of the approximation Lin, N, \tilde{N} , PN respect to the Λ CDM background: we can clearly distinguish between the two approximations, observing that \tilde{N} behaves as expected very close to the PN approximation.

VI. CONCLUSIONS

In this paper we use the new BGO framework for light propagation in general relativity, presented in [33] and applied to Λ CDM cosmology in [34]. We encoded the new framework in the *Mathematica* package called BIGONLIGHT (<https://github.com/MicGrasso/bigonlight>) that is designed to compute optical observables numerically, once the spacetime metric components and the observer and source kinematics are provided as input. The code is adaptable to work in any gauge and with analytical as well as numerical inputs. A short description of the package is given in Appendix A here and we will give a more extensive discussion on BIGONLIGHT in [32]. In the present work we focus on two observables in the cosmological context: redshift and angular diameter distance. We concentrate our analysis on a one-dimensional toy model in which the density perturbations around the Λ CDM background are distributed along parallel planes. In other words our perturbations depend on time and one spatial coordinate only. The purpose of our investigation is to isolate the contribution of nonlinearities by considering the relative differences in the observables ΔO , as defined in Eq. (29), computed within three approximations: linear cosmological perturbation theory, Newtonian and post-Newtonian approximation. Although the plane-parallel universe is a simple model, let us remark that the spacetime metric in Eq. (2) is particularly well-suited for this kind of analysis, since the terms coming from all the three approximations are clearly identified and they can be directly used as input in our code for light propagation. All our investigations are performed within a fixed setting for light propagation: (i) in the observers region $\delta_{\text{in}} = 0$, (ii) the source is at redshift $z = 10$, (iii) photon geodesics are parallel to the bisect, i.e., they have an inclination of 45° with respect to all the three spatial axes.

We now present our findings relative to the different features that we examined: the dependence on the scale of perturbations, on primordial non-Gaussianity and the role of initial conditions. We start by pointing out that the redshift and the angular diameter distance have different behavior: for the redshift the Newtonian corrections are the leading order for the nonlinearities with $\Delta z(\text{Lin}, N) \sim 10^2 \Delta z(\text{PN}, N)$, see Fig. 8, whereas for the angular diameter distance Newtonian and post-Newtonian contributions are of the same order $\Delta D_{\text{ang}}(\text{Lin}, N) \sim \Delta D_{\text{ang}}(\text{PN}, N)$, as clear from Fig. 9. Our

results confirm previous studies in the literature [30], in particular we have found that the nonlinearities from the approximations we considered are well below 1% for both the observables. To be more precise, we have that the variation linear vs Newtonian approximations is of order 10^{-3} for z and 10^{-5} for D_{ang} , while the variation post-Newtonian vs Newtonian is of order 10^{-6} for z and 10^{-5} for D_{ang} , both on $k = 100$ Mpc and $\delta_0^{\text{max}} = 1$.

In addition, we analysed the dependence of the various contributions on the inhomogeneities scale, finding again a slightly different trend for z and D_{ang} , see Figs. 10 and 11. For both observables, the change in the scale modifies the amplitude of the oscillations by more than one order of magnitude, but the amplitude of ΔD_{ang} decreases monotonically with the scale k , while that of Δz has a maximum around $k = 100$ Mpc. For the angular diameter distance the contributions from nonlinearities span from 10^{-4} on $k = 500$ Mpc to 10^{-6} on $k = 30$ Mpc.

To complete our investigation, we took advantage of having an analytical expression of our input, i.e., the spacetime metric. As one can easily verify, some of the PN terms are triggered or cancelled out for specific values of the primordial non-Gaussianity parameter a_{nl} inside Planck confidence interval. Therefore, we decided to examine the response of the post-Newtonian observables to the variation of a_{nl} . It turned out that the tuning of primordial non-Gaussianity has negligible effects on the PN observables. The only effect is the change in the shape of the PN part of the redshift but the net contribution is of the order of 10^{-6} see Figs. 12 and 13.

Finally, we have estimated the relative variations of the three approximations with respect to the Λ CDM background in Fig. 14b. We find that the post-Newtonian contribution to D_{ang} comes almost exclusively from the linear post-Newtonian initial seed. The other, i.e., non-linear, post-Newtonian corrections are below 1%, in agreement with previous results in the literature.

ACKNOWLEDGMENTS

This work was supported by the National Science Centre, Poland (NCN) via the SONATA BIS programme, grant No 2016/22/E/ST9/00578 for the project ‘‘Local relativistic perturbative framework in hydrodynamics and General Relativity and its application to cosmology’’.

APPENDIX A: BIGONLIGHT: PRESENTING AND TESTING THE CODE

In Sec. III we have introduced the BGO formalism, emphasizing that it provides a unified framework to compute all possible optical observables and how it extends the Sachs formalism: it includes the case of observations occurring for a prolonged period of time, when repeated observations are made, e.g., parallax and drifts. In this Appendix, we present the `BiGONLiGht.m` package used

in this paper to calculate the Newtonian and post-Newtonian observables numerically within the BGO framework. The main achievement of our package is to simulate light propagation in numerical relativity to extract observables. BIGONLIGHT works in any gauge and with any coordinate system and it requires the spacetime metric components and the source and observer kinematics (four-velocities and four-accelerations) as input.⁸ The flexibility of the code allows us to use two types of inputs: analytic expressions or the output of a (relativistic) numerical simulation. In fact, in order to make our code compatible with the majority of the codes in numerical relativity, we recasted the BGO framework in 3 + 1 formalism. We decided to develop BIGONLIGHT within *Mathematica* for several reasons. One of the advantages is that one can choose between a large variety of numerical methods to solve ODE without the need of modifying the code. Another useful feature in *Mathematica* are the quite detailed build-in precision control options, which allow the user to set precision and accuracy of the numerical calculations efficiently.

We devote a companion paper, [32], to the comprehensive description of the modules of package, including also benchmark testing performed in the context of several exact and simulated cosmological models and addressing more observables than in the present work. In the rest of this Appendix, we report the tests for the angular diameter distance only in the well-known Λ CDM and Szekeres models.

1. Λ CDM model

Let us start by considering the test in the flat Λ CDM model. It consists of a universe filled with a cosmological constant Λ and an homogeneous and isotropic distribution of noninteracting matter (dust) and it represents the background model of all the approximations used in this work.

We test our code by computing the variation between the angular diameter distance calculated numerically using the `BiGONLiGht.m` package and its analytic expression. We plot our results in terms of

$$\Delta D_{\text{ang}}(\text{BGO}, \text{an}) = \frac{D_{\text{ang}}^{\text{BGO}} - D_{\text{ang}}^{\text{an}}}{D_{\text{ang}}^{\text{an}}}. \quad (\text{A1})$$

The angular diameter distance is defined as

$$D_{\text{ang}} = \frac{D_{\text{com}}}{1+z} \quad (\text{A2})$$

⁸Note that the input is not in full tensorial form, but in the form of components. Let us remark that, of course, once we give the metric and the four-velocities components in practice we are making a gauge and a coordinate system choice. Nevertheless, the code can work with any choice.

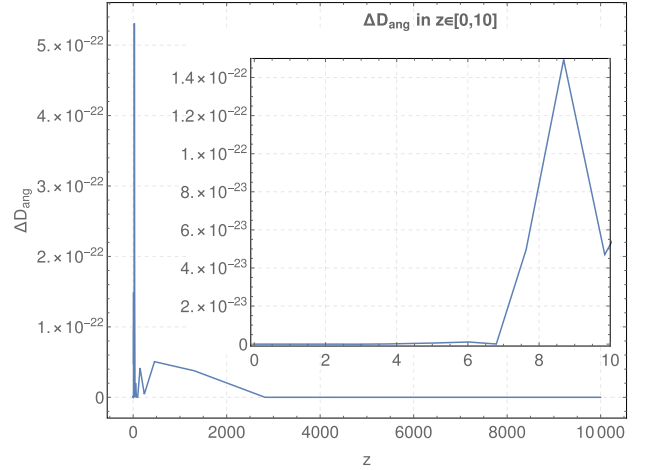


FIG. 15. $\Delta D_{\text{ang}}(\text{BGO}, \text{an})$ in the Λ CDM model. The light geodesic is traced backwards in time up to $\eta_{\text{in}} \approx \frac{1}{100} \eta_0 = 5.1738 \times 10^8$ yr. The values for the cosmological parameters $\Omega_{m0} = 0.3153$, $\Omega_{\Lambda} = 0.6847$ and $\mathcal{H}_0 = 67.36$ are taken from Planck [38].

where the comoving distance D_{com} in the flat Λ CDM model is

$$D_{\text{com}}(z) = \int_0^z \frac{dz'}{\mathcal{H}_0 \sqrt{\Omega_{m0}(1+z')^3 + \Omega_{\Lambda}}}, \quad (\text{A3})$$

where $\mathcal{H}_0 = \frac{\dot{a}}{a}|_{\eta_0}$ and $\Omega_{m0} + \Omega_{\Lambda} = 1$. By solving the integral, [41], the analytic expression of the angular diameter distance is

$$D_{\text{ang}}^{\text{an}}(z) = \frac{F[\chi(z)|r] - F[\chi(0)|r]}{(1+z)\mathcal{H}_0(\Omega_{m0})^{\frac{1}{3}}(\Omega_{\Lambda})^{\frac{1}{6}}3^{\frac{1}{4}}}, \quad (\text{A4})$$

where $F[\chi(z)|r]$ is the elliptic integral of the first kind, with arguments $r = \sqrt{\frac{2+\sqrt{3}}{4}}$ and $\chi(z) = \arccos \times \left(\frac{2\sqrt{3}}{1+\sqrt{3}+(1+z)^3 \sqrt{\frac{\Omega_{m0}}{\Omega_{\Lambda}}}} - 1 \right)$. The plot in Fig. 15 shows a

deviation of the order of 10^{-22} between the numerical and the analytical calculation, highlighting the high precision reached by our code. Such a precision was possible thanks to the precision control options implemented in *Mathematica*. We plot up to $z = 10000$ to show that the deviation stays small over the whole simulation.

2. Szekeres model

As second test-bed for the code, we decided to use a more complicated spacetime. We chose the inhomogeneous dust Szekeres model plus a cosmological constant as presented in [42], discussed in Appendix C and briefly summarized here. The line element of the model is

$$ds^2 = a(\eta)^2[-d\eta^2 + X(\eta, q_1, q_2, q_3)^2 dq_1^2 + dq_2^2 + dq_3^2]. \quad (\text{A5})$$

In particular, here we consider the case with axial symmetry around the q_1 axis in which the function X has the form

$$X(\eta, q_1, q_2, q_3) = 1 + \beta_+(q_1)\mathcal{D}(\eta) + \beta_+(q_1)B(q_2^2 + q_3^2) \quad (\text{A6})$$

with the constant B given by (C12). The function β_+ is the free function of the model and it is linked with the gravitational potential ϕ_0 via

$$\beta_+ = -\frac{2}{3} \frac{\nabla^2 \phi_0}{\mathcal{H}_0^2 \Omega_{m0}} \quad (\text{A7})$$

as we show explicitly in Appendix C. For our test, we set up β_+ using Eq. (A7) with $\phi_0 = \mathcal{I} \sin(\omega q_1)$, where $\omega = \frac{2\pi}{500 \text{ Mpc}}$, the amplitude \mathcal{I} is determined such that $\text{Max}(\delta_0^{S_z}) = 0.1$ and $\Omega_{m0} = 0.3153$ and $\mathcal{H}_0 = 67.36$ are taken from Planck [38]. Contrary to the Λ CDM case, where the spatial orientation of the geodesic is irrelevant due to the intrinsic homogeneity and isotropy of the model, in the inhomogeneous Szekeres model the light propagates differently in different directions. In order to facilitate the comparison with the literature, we decided to follow Ref. [43] and consider geodesics traveling along the symmetry axis q_1 . The observer is placed at $q_{\mathcal{O}}^\mu = (\eta_{\mathcal{O}}, 0, 0, 0)$ such that $\delta|_{\mathcal{O}} = 0$.

The testing procedure for the `BiGONLight.m` package in this case is to compare the angular diameter distance calculated numerically using the BGO formalism implemented in `BiGONLight.m` and numerically, as well, but solving the Sachs focusing equation⁹:

$$\begin{aligned} \ddot{D}_{\text{ang}} + \frac{\dot{\ell}^0}{\ell^0} \dot{D}_{\text{ang}} &= -\frac{1}{\ell^{0^2}} \left(|\sigma|^2 + \frac{3\mathcal{H}_0^2 \Omega_{m0}}{2a} (\delta + 1) \right) D_{\text{ang}} \\ \sigma &= \frac{\sigma_{\mathcal{O}} D_{\text{ang}}^2|_{\mathcal{O}}}{D_{\text{ang}}^2}, \end{aligned} \quad (\text{A8})$$

and the initial conditions are given considering that the light bundle has a vertex at the observation point and such that:

$$\sigma_{\mathcal{O}} = 0 \quad (\text{A9})$$

$$D_{\text{ang}}|_{\mathcal{O}} = 0 \quad (\text{A10})$$

$$\dot{D}_{\text{ang}}|_{\mathcal{O}} = \frac{g_{\mu\nu} \ell^\mu u^\nu|_{\mathcal{O}}}{\ell^0}. \quad (\text{A11})$$

⁹Here, the Ricci part of the optical tidal matrix is substitute using the Einstein equation $R_{\mu\nu} \ell^\mu \ell^\nu = \frac{3\mathcal{H}_0^2 \Omega_{m0}}{a} (\delta + 1) (\ell^0)^2$.

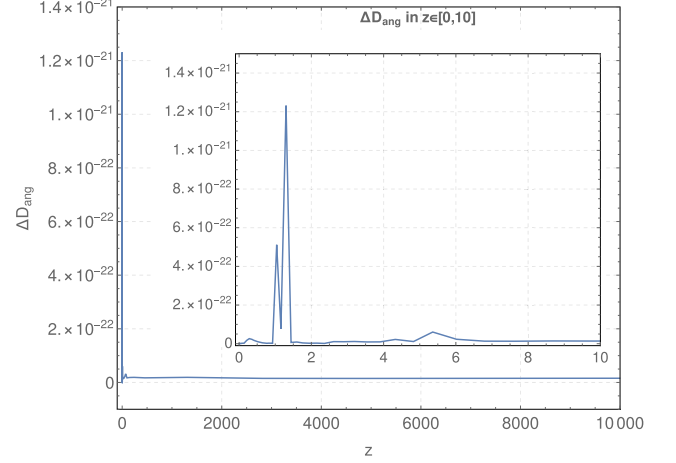


FIG. 16. Deviation ΔD_{ang} (BGO, Sachs) for the angular diameter distance in the Szekeres spacetime. The observables are evaluated for a light bundle moving along the q_3 -axis and received by the observer placed at $q_{\mathcal{O}}^\mu = (\eta_{\mathcal{O}}, 0, 0, 0)$ in a region where $\delta|_{\mathcal{O}} = 0$.

In the above the dot indicates derivative with respect to conformal time and $\tilde{\sigma}$ is the complex shear.¹⁰ All we need to solve Eq. (A8) is the expression for δ ,

$$\delta = -\frac{\beta_+ \dot{D}}{X}, \quad (\text{A12})$$

and the equation for ℓ^0

$$\frac{\dot{\ell}^0}{\ell^0} = -\frac{\beta_+ \dot{D}}{X} - 2\mathcal{H}. \quad (\text{A13})$$

We present the results of the comparison by plotting the variation

$$\Delta D_{\text{ang}}(\text{BGO, Sachs}) = \frac{\Delta D_{\text{ang}}^{\text{BGO}} - \Delta D_{\text{ang}}^{\text{Sachs}}}{\Delta D_{\text{ang}}^{\text{Sachs}}}. \quad (\text{A14})$$

From Fig. 16 we can conclude that also in the Szekeres model we have a good agreement. However, contrary to the Λ CDM case, the variation ΔD_{ang} plotted represents the comparison between two numerical computations and it cannot be considered as numerical error over the observable. Nevertheless, the very good agreement between the `BIGONLIGHT` code and the traditional method using the Sachs focusing equation is another piece of evidence that our code is a reliable tool for studying light propagation also in more complicated spacetimes.

¹⁰In general, the equation for the shear contains an additive term Ψ_0 , which is the Weyl focusing term. However, in the Szekeres model we have that $\Psi_0 = 0$, as shown in [43].

**APPENDIX B: LINEARIZING THE BGO
FORMALISM: SOLUTIONS FOR THE
PLANE-PARALLEL UNIVERSE**

In this Appendix we consider the flat FLRW background with linear perturbations in the synchronous-comoving gauge. We obtain the linearized evolution equations for the BGO, Eq. (B14), the general expressions for their solutions, Eq. (B15), and the linear angular diameter distance $D_{\text{ang}}^{\text{Lin}}$ written in terms of the BGO, Eq. (B18). We then specialise the general solutions to the Λ CDM background with perturbations at first order in standard cosmological perturbation theory and within our plane-parallel toy model and finally obtain the analytic expressions for z^{Lin} and $D_{\text{ang}}^{\text{Lin}}$ that we used in Sec. IV.

The spacetime metric has the form

$$\tilde{g}_{\mu\nu} = a^2 g_{\mu\nu} \quad (\text{B1})$$

and is expanded at first order as

$$\tilde{g}_{\mu\nu} = a^2 (\bar{g}_{\mu\nu} + \delta g_{\mu\nu}) \quad (\text{B2})$$

where $\bar{g}_{\mu\nu}$ is the conformal flat FLRW background, i.e., the Minkowski metric and $\delta g_{\mu\nu}$ represents the first-order scalar perturbations in the synchronous-comoving gauge, in general given by $\delta g_{\mu\nu} = \text{Diag}(0, \delta g_{11}, \delta g_{22}, \delta g_{33})$.

The first observable that we study in this work is the redshift, defined as

$$1 + z = \frac{\tilde{g}_{\mu\nu} \tilde{\ell}^\mu \tilde{u}^\nu|_{\mathcal{S}}}{\tilde{g}_{\mu\nu} \tilde{\ell}^\mu \tilde{u}^\nu|_{\mathcal{O}}} \quad (\text{B3})$$

In the above expression u^μ is the four-velocity of the observer (source) and ℓ^μ is the tangent vector to the photon geodesics. For our coordinates choice, all observers and sources are comoving with the cosmic flow with four-velocity given by

$$\tilde{u}^\mu \equiv \frac{1}{a} \bar{u}^\mu = \frac{1}{a} (1, 0, 0, 0) \quad (\text{B4})$$

at all orders and the null tangent vector is expanded as

$$\tilde{\ell}^\mu = \frac{a_{\mathcal{O}}^2}{a^2} (\bar{\ell}^\mu + \delta \ell^\mu) \quad (\text{B5})$$

with $\bar{\ell}^\mu = \frac{a_{\mathcal{O}}^2}{a^2} (\bar{\ell}^0, \bar{\ell}^i)$.¹¹ The linear redshift is then given by

¹¹The conformal tangent vector in the FLRW background $\bar{\ell}^\mu$ is constant. Note that usually the normalization $\bar{\ell}^0 \pm 1$ is used for the temporal component. Here, however, we leave it unnormalized.

$$1 + z = \frac{a_{\mathcal{O}}}{a_{\mathcal{S}}} \left[1 + \frac{1}{\bar{\ell}^0} (\delta \ell^0|_{\mathcal{S}} - \delta \ell^0|_{\mathcal{O}}) \right], \quad (\text{B6})$$

where $\delta \ell^0$ is founded from the first-order geodesic equation

$$\frac{d\delta \ell^\mu}{d\lambda} = \frac{1}{2} \bar{g}^{\mu\sigma} \partial_\sigma \delta g_{\alpha\beta} \bar{\ell}^\alpha \bar{\ell}^\beta - \bar{g}^{\mu\sigma} \bar{\ell}^\alpha \partial_\alpha \delta g_{\sigma\beta} \bar{\ell}^\beta. \quad (\text{B7})$$

The second observable is the angular diameter distance \tilde{D}_{ang} . However, it is more convenient to expand the conformal angular distance D_{ang} which we write here in terms of the BGO as (for a derivation see [33,34])

$$D_{\text{ang}} = \ell^\mu u_\mu|_{\mathcal{O}} |\det(W_{XL}{}^A{}_B)|^{\frac{1}{2}} \quad (\text{B8})$$

and then obtain \tilde{D}_{ang} from the very well-known conformal transformation $\tilde{D}_{\text{ang}} = \frac{a}{a_{\mathcal{O}}} D_{\text{ang}}$, that we verified for Eq. (B8). The BGO $W_{XL}{}^A{}_B$ are expanded as

$$W_{XL}{}^A{}_B = \overline{W_{XL}{}^A{}_B} + \delta W_{XL}{}^A{}_B, \quad (\text{B9})$$

where $\overline{W_{XL}}$ and δW_{XL} are found by solving the linearized GDE (20) in conformal space

$$\frac{d}{d\lambda} \mathcal{W} = \begin{pmatrix} 0 & \mathbb{1}_{4 \times 4} \\ R_{\ell\ell} & 0 \end{pmatrix} \mathcal{W} \quad (\text{B10})$$

Notice that the optical tidal matrix in the frame is purely a first-order quantity—the conformal Riemann tensor vanishes in the background—and it is given by:

$$R^\mu{}_{\ell\ell\nu} = \bar{\phi}^{\rho\mu} \delta R_{\rho\alpha\beta\sigma} \bar{\ell}^\alpha \bar{\ell}^\beta \bar{\phi}^\sigma{}_\nu \quad (\text{B11})$$

where $\delta R_{\rho\alpha\beta\sigma}$ is the first-order Riemann tensor and $\bar{\phi}^\mu{}_\alpha = (u^\mu, \bar{\phi}^\mu{}_A, \bar{\ell}^\mu)$ is the background parallel transported frame along the background geodesic.

Let us start by solving the background GDE, which reads:

$$\begin{cases} \frac{d\overline{W_{XX}{}^\mu{}_\nu}}{d\lambda} = \overline{W_{LX}{}^\mu{}_\nu} \\ \frac{d\overline{W_{LX}{}^\mu{}_\nu}}{d\lambda} = 0 \\ \frac{d\overline{W_{XL}{}^\mu{}_\nu}}{d\lambda} = \overline{W_{LL}{}^\mu{}_\nu} \\ \frac{d\overline{W_{LL}{}^\mu{}_\nu}}{d\lambda} = 0 \end{cases} \quad (\text{B12})$$

with initial conditions $\bar{\mathcal{W}} = \mathbb{1}_{8 \times 8}$. The solution is

$$\bar{\mathcal{W}} = \begin{pmatrix} \delta^\mu{}_\nu & (\lambda - \lambda_{\mathcal{O}}) \delta^\mu{}_\nu \\ 0 & \delta^\mu{}_\nu \end{pmatrix}. \quad (\text{B13})$$

Next we find the first-order BGO from:

$$\begin{cases} \frac{d\delta W_{XX^\nu}}{d\lambda} = \delta W_{LX^\nu} \\ \frac{d\delta W_{LX^\nu}}{d\lambda} = R^\mu{}_{\ell\ell\nu} \\ \frac{d\delta W_{XL^\nu}}{d\lambda} = \delta W_{LL^\nu} \\ \frac{d\delta W_{LL^\nu}}{d\lambda} = (\lambda - \lambda_{\mathcal{O}})R^\mu{}_{\ell\ell\nu} \end{cases} \quad (\text{B14})$$

with initial conditions $\delta\mathcal{W} = \mathbf{0}_{8 \times 8}$, where we have replaced the background solutions (B13). We obtain

$$\begin{cases} \delta W_{XX^\nu} = \int_{\lambda'}^{\lambda_{\mathcal{O}}} \int_{\lambda''}^{\lambda_{\mathcal{O}}} R^\mu{}_{\ell\ell\nu} d\lambda' d\lambda'' \\ \delta W_{LX^\nu} = \int_{\lambda'}^{\lambda_{\mathcal{O}}} (\lambda_{\mathcal{O}} - \lambda')(\lambda - \lambda') R^\mu{}_{\ell\ell\nu} d\lambda' \\ \delta W_{XL^\nu} = - \int_{\lambda}^{\lambda_{\mathcal{O}}} R^\mu{}_{\ell\ell\nu} d\lambda' \\ \delta W_{LL^\nu} = \int_{\lambda}^{\lambda_{\mathcal{O}}} (\lambda_{\mathcal{O}} - \lambda') R^\mu{}_{\ell\ell\nu} d\lambda' \end{cases} \quad (\text{B15})$$

In order to find $D_{\text{ang}}^{\text{Lin}}$ from the expansion of Eq. (B8) we need the second of the above solutions and we recall that the expansion of the square root of the determinant is given by

$$\sqrt{\det W_{XL}} = \sqrt{\det(\overline{W}_{XL})} \left[1 + \frac{1}{2} \text{tr}(\overline{W}_{XL}^{-1} \delta W_{XL}) \right]. \quad (\text{B16})$$

Now, looking at Eqs. (B13) and (B15) we have that

$$\begin{cases} \sqrt{\det(\overline{W}_{XL})} = (\lambda - \lambda_{\mathcal{O}}) \\ \text{tr}(\overline{W}_{XL}^{-1} \delta W_{XL}) = \frac{\int_{\lambda}^{\lambda_{\mathcal{O}}} (\lambda_{\mathcal{O}} - \lambda')(\lambda - \lambda') R^A{}_{\ell\ell A} d\lambda'}{(\lambda - \lambda_{\mathcal{O}})} \end{cases} \quad (\text{B17})$$

The final result for $D_{\text{ang}}^{\text{Lin}}$ is

$$D_{\text{ang}}^{\text{Lin}} = (\ell_{\mathcal{O}}^0 + \delta\ell_{\mathcal{O}}^0)(\lambda_{\mathcal{O}} - \lambda) - \frac{\ell_{\mathcal{O}}^0}{2} \int_{\lambda}^{\lambda_{\mathcal{O}}} (\lambda_{\mathcal{O}} - \lambda')(\lambda - \lambda') \text{tr}(R^A{}_{\ell\ell B}) d\lambda'. \quad (\text{B18})$$

It is important to stress that all the quantities are evaluated along the background geodesic, i.e., $\eta \equiv \bar{\eta}$ and $\bar{q}_1(\eta) \equiv \frac{\bar{\ell}^1}{\bar{\ell}^0}(\bar{\eta}_{\mathcal{O}} - \bar{\eta}) + \bar{q}_1(\bar{\eta}_{\mathcal{O}})$

We checked that our result coincides with the standard result in the literature, e.g., [44], by simply noting that the quantity $-\frac{1}{2} \text{tr}(R^A{}_{\ell\ell B})$ is nothing more than the Ricci part of the optical tidal matrix \mathcal{R} , usually defined as

$$\mathcal{R} = \frac{1}{2} R_{\alpha\beta} \ell^\alpha \ell^\beta = -\frac{1}{2} R^\mu{}_{\alpha\beta\mu} \ell^\alpha \ell^\beta, \quad (\text{B19})$$

and evaluated at first order.

We finally specialise the above results for our plane-parallel model. The linear perturbation of the spacetime metric around the flat Λ CDM background is

$$\delta g_{\mu\nu} = \begin{pmatrix} 0 & 0 & 0 & 0 \\ 0 & -\mathcal{F} - \frac{10}{3c^2} \phi_0 & 0 & 0 \\ 0 & 0 & -\frac{10}{3c^2} \phi_0 & 0 \\ 0 & 0 & 0 & -\frac{10}{3c^2} \phi_0 \end{pmatrix}, \quad (\text{B20})$$

where we define

$$\mathcal{F}(\eta, q_1) = \frac{4}{3} \frac{\partial_{q_1}^2 \phi_0(q_1)}{\mathcal{H}_0^2 \Omega_{m0}} \mathcal{D}(\eta). \quad (\text{B21})$$

A straightforward substitution gives for the redshift

$$1 + z^{\text{Lin}} = \frac{a_{\mathcal{O}}}{a_S} \left[1 - \left(\frac{\bar{\ell}^1}{\bar{\ell}^0} \right)^2 \int_{\bar{\eta}_S}^{\bar{\eta}_{\mathcal{O}}} \frac{2}{3} \frac{\partial_{q_1} \phi_0(q_1(\bar{\eta}'))}{\mathcal{H}_0^2 \Omega_{m0}} \partial_0 \mathcal{D}(\bar{\eta}') d\bar{\eta}' \right] \quad (\text{B22})$$

and for the angular diameter distance

$$\tilde{D}_{\text{ang}}^{\text{Lin}}(\eta) = \frac{a}{a_{\mathcal{O}}} \left[(\bar{\eta}_{\mathcal{O}} - \bar{\eta}) + \frac{\bar{\ell}^1{}^2}{2\bar{\ell}^0{}^2} \int_{\eta}^{\eta_{\mathcal{O}}} \int_{\eta'}^{\eta_{\mathcal{O}}} \mathcal{F} d\eta' d\eta'' + \int_{\eta}^{\eta_{\mathcal{O}}} (\eta_{\mathcal{O}} - \eta')(\eta - \eta') \frac{\mathcal{R}(\eta')}{\bar{\ell}^0{}^2} d\eta' \right]. \quad (\text{B23})$$

The two last relations are those we use in Sec. IV for our comparison.

APPENDIX C: COMPARISON WITH THE SZEKERES METRIC

In this section we compare the Szekeres spacetime with the plane-parallel case considered in this work. In his original paper [45], Szekeres studied all the solutions to the

Einstein field equation with irrational dust for line elements having the form

$$ds_{S_z}^2 = -dt^2 + e^{2\alpha(t, q_1, q_2, q_3)} dq_1^2 + e^{2\beta(t, q_1, q_2, q_3)} (dq_2^2 + dq_3^2) \quad (\text{C1})$$

Two different classes of solutions can be distinguished: class-I solutions are a generalization of the Lemaitre-Bondi-Tolman model while class-II solutions are a

generalization of Kantowski-Sachs and FLRW model. Subsequently, Barrow and Stein-Schabes [46] generalized the Szekeres solutions by adding a cosmological constant Λ to the dust. More recently, Bruni and Meures [42] presented a new formulation of the class-II Szekeres solutions in which the separation between inhomogeneities and the FLRW background is explicitly provided and thus the spacetime metric is presented in a more convenient form for cosmological applications. We compare our plane-parallel metric with their formulation. We begin by summarizing the results presented in [42].

The authors focused their analysis on the Szekeres solutions which admit a flat FLRW background and such that the line element¹² can be written as

$$ds_{\text{Sz}}^2 = a^2(-d\eta^2 + \gamma_{11}^{\text{Sz}}dq_1^2 + \gamma_{22}^{\text{Sz}}dq_2^2 + \gamma_{33}^{\text{Sz}}dq_3^2) \quad (\text{C2})$$

where

$$\begin{aligned} \gamma_{11}^{\text{Sz}} &= X^2(\eta, q_1, q_2, q_3) \\ \gamma_{22}^{\text{Sz}} &= 1 \\ \gamma_{33}^{\text{Sz}} &= 1. \end{aligned} \quad (\text{C3})$$

As it is shown in [42], thanks to the symmetry of the problem, the function $X(\eta, q_1, q_2, q_3)$ can be decomposed as

$$X(\eta, q_1, q_2, q_3) = F(\eta, q_1) + A(q_1, q_2, q_3), \quad (\text{C4})$$

where the function $F(\eta, q_1)$ satisfies the Newtonian evolution equation for the first-order density contrast¹³

$$\ddot{F} + \mathcal{H}\dot{F} - \frac{3}{2}\mathcal{H}_0^2\Omega_{m0}\frac{F}{a} = 0, \quad (\text{C5})$$

which admits two linearly independent solutions, the growing and decaying modes, as is well known. Then $F(\eta, q_1)$ coincides with the linear density contrast and more precisely we have $F(\eta, q_1) = -\delta_{\text{Lin}}(\eta, q_1)$.¹⁴ Neglecting

¹²We choose here to use our notation instead that of that of [42]. The line element (C3) is different from the one presented in [42] since we use conformal time and we have chosen a different axis of symmetry. Of course this does not affect any results, since it is easy to show that the two metrics are equivalent under a coordinate transformation.

¹³This was shown implicitly in Sec. V of the Szekeres' original paper [45] and subsequently by many other authors as those of [47]. However, it was Goode and Wainwright who recognized explicitly that the relativistic equations for the density fluctuations in Szekeres model are the same as in Newtonian gravity, [48]. They also provide a new formulation of the Szekeres solutions, much more useful in cosmology, in which the relationship with the FLRW solution is clarified.

¹⁴The minus sign between F and δ follows from the fact that in Eq. (A8) of [42] the authors set, in full generality, $\delta_{\text{in}} = -\frac{F_{\text{in}}}{F_{\text{in}}+A}$.

the decaying modes it is possible, without loss of generality, to factorize $F(\eta, q_1)$ as¹⁵

$$F(\eta, q_1) = \mathcal{D}(\eta)\beta_+(q_1), \quad (\text{C6})$$

where \mathcal{D} is the growing mode solution for the density contrast given by (see e.g., Eq. (5.13) in [49]), where we have already normalized in order to have $\mathcal{D}_0 = 1$)

$$\mathcal{D}(\eta) = \frac{a}{\frac{5}{2}\Omega_{m0}} \sqrt{1 + \frac{\Omega_{\Lambda0}}{\Omega_{m0}} a^3} {}_2F_1\left(\frac{3}{2}, \frac{5}{6}, \frac{11}{6}, -\frac{\Omega_{\Lambda0}}{\Omega_{m0}} a^3\right), \quad (\text{C7})$$

with ${}_2F_1(a, b, c, x)$ being the Gaussian (or ordinary) hypergeometric function.

On the other hand, our Newtonian plane-parallel metric is given by:

$$\begin{aligned} \gamma_{11}^{\text{N}} &= \left(1 - \frac{2\mathcal{D}\partial_{q_1}^2\phi_0}{3\mathcal{H}_0^2\Omega_{m0}}\right)^2 \\ \gamma_{22}^{\text{N}} &= 1 \\ \gamma_{33}^{\text{N}} &= 1. \end{aligned} \quad (\text{C8})$$

We now investigate the link between (C8) and (C3) by comparing the two forms of γ_{11} and referring to Eqs. (C4) and (C6). Let us start from (C6): to fix the time-independent function $\beta_+(q_1)$, one can take advantage from the fact that $\delta_{\text{Lin}}(\eta, q_1) = -\mathcal{D}(\eta)\beta_+(q_1)$ and use the cosmological Poisson equation (5) to find

$$\beta_+(q_1) = -\frac{2\partial_{q_1}^2\phi_0(q_1)}{3\mathcal{H}_0^2\Omega_{m0}}. \quad (\text{C9})$$

At this point we have completely fixed $F(\eta, q_1)$. Now, by looking at Eq. (C4) it is straightforward to conclude that the two metrics (C8) and (C3) are fully equivalent if $A(q_1, q_2, q_3) = 1$.¹⁶ However, this cannot be the case, as we will now show. Let us start by noticing that planar symmetry implies that the metric components can depend only on the coordinates (η, q_1) , while in the Szekeres symmetry the metric can depend in general on all spatial

¹⁵The time-dependent-only growing mode is denoted by f_+ in [42] and it is given in a dimensionless time variable τ in Eq. (11b). To match \mathcal{D} in (C7) and f_+ one needs to: first transform $f_+(\tau)$ to conformal time $f_+(\eta)$ and then normalize such that $f_+(\eta_0) = 1$. The final result is $F(\eta, q_1)$ as in (C6).

¹⁶To be more precise it would be enough to neglect the dependence on (q_2, q_3) in (C4) by imposing that $A(q_1, q_2, q_3) \equiv A(q_1)$, i.e.,

$$X(\eta, q_1) = A(q_1) + F(\eta, q_1).$$

However, if this were the case, it is easy to show that performing the coordinate transformation $\tilde{q}_1 = \int A(q_1) dq_1$ and rescaling $\tilde{F}(\eta, \tilde{q}_1) = \frac{F(\eta, q_1)}{A(q_1)}$, we obtain again $X(\eta, \tilde{q}_1) = 1 + \tilde{F}(\eta, \tilde{q}_1)$.

coordinates (and time). In [42] this dependence is encoded in $A(q_1, q_2, q_3)$ in Eq. (C4) and has the form

$$A = 1 + B\beta_+(q_1)[(q_2 + \gamma(q_1))^2 + (q_3 + \omega(q_1))^2], \quad (\text{C10})$$

thus the only possibility to have $A = 1$ is that $B = 0$. After simple manipulations of the Einstein equations together with Eq. (C10) we find that

$$2B = \frac{3\mathcal{H}_0^2\Omega_{m0}}{2a}\mathcal{D} + \mathcal{H}\dot{\mathcal{D}}. \quad (\text{C11})$$

In [49] it is shown that the R.H.S. is constant and it is always different from zero. Indeed, from Eq.(5.52) in [49] we find

$$B = \frac{5}{4}\mathcal{H}_0^2\Omega_{m0}\frac{\mathcal{D}_{\text{in}}}{a_{\text{in}}}, \quad (\text{C12})$$

where $\mathcal{D}_{\text{in}} = a_{\text{in}}$ for Einstein-de Sitter initial conditions. We finally conclude that the two metrics (C3) and (C8) cannot coincide.

-
- [1] S. Matarrese and D. Terranova, Post-newtonian cosmological dynamics in lagrangian coordinates, *Mon. Not. R. Astron. Soc.* **283**, 400 (1996).
- [2] C. Carbone and S. Matarrese, Unified treatment of cosmological perturbations from superhorizon to small scales, *Phys. Rev. D* **71**, 043508 (2005).
- [3] I. Milillo, D. Bertacca, M. Bruni, and A. Maselli, Missing link: A nonlinear post-Friedmann framework for small and large scales, *Phys. Rev. D* **92**, 023519 (2015).
- [4] C. Rampf, E. Villa, D. Bertacca, and M. Bruni, Lagrangian theory for cosmic structure formation with vorticity: Newtonian and post-Friedmann approximations, *Phys. Rev. D* **94**, 083515 (2016).
- [5] M. Kopp, C. Uhlemann, and T. Haugg, Newton to Einstein—dust to dust, *J. Cosmol. Astropart. Phys.* **03** (2014) 018.
- [6] S. R. Green and R. M. Wald, New framework for analyzing the effects of small scale inhomogeneities in cosmology, *Phys. Rev. D* **83**, 084020 (2011).
- [7] J. Adamek, D. Daverio, R. Durrer, and M. Kunz, General relativistic N -body simulations in the weak field limit, *Phys. Rev. D* **88**, 103527 (2013).
- [8] S. R. Goldberg, T. Clifton, and K. A. Malik, Cosmology on all scales: A two-parameter perturbation expansion, *Phys. Rev. D* **95**, 043503 (2017).
- [9] M. Bruni, D. B. Thomas, and D. Wands, Computing general relativistic effects from Newtonian N -body simulations: Frame dragging in the post-Friedmann approach, *Phys. Rev. D* **89**, 044010 (2014).
- [10] J. Adamek, R. Durrer, and M. Kunz, N -body methods for relativistic cosmology, *Classical Quantum Gravity* **31**, 234006 (2014).
- [11] C. Fidler, T. Tram, C. Rampf, R. Crittenden, K. Koyama, and D. Wands, General relativistic weak-field limit and Newtonian N -body simulations, *J. Cosmol. Astropart. Phys.* **12** (2017) 022.
- [12] F. Löffler, J. Faber, E. Bentivegna, T. Bode, P. Diener, R. Haas, I. Hinder, B. C. Mundim, C. D. Ott, E. Schnetter *et al.*, The Einstein toolkit: A community computational infrastructure for relativistic astrophysics, *Classical Quantum Gravity* **29**, 115001 (2012).
- [13] E. Bentivegna, An automatically generated code for relativistic inhomogeneous cosmologies, *Phys. Rev. D* **95**, 044046 (2017).
- [14] J. T. Giblin, J. B. Mertens, and G. D. Starkman, Departures from the Friedmann-Lemaître-Robertson-Walker Cosmological Model in an Inhomogeneous Universe: A Numerical Examination, *Phys. Rev. Lett.* **116**, 251301 (2016).
- [15] J. Adamek, D. Daverio, R. Durrer, and M. Kunz, General relativity and cosmic structure formation, *Nat. Phys.* **12**, 346 (2016).
- [16] H. J. Macpherson, P. D. Lasky, and D. J. Price, Inhomogeneous cosmology with numerical relativity, *Phys. Rev. D* **95**, 064028 (2017).
- [17] C. Barrera-Hinojosa and B. Li, Gramses: A new route to general relativistic n -body simulations in cosmology. Part I. Methodology and code description, *J. Cosmol. Astropart. Phys.* **01** (2020) 007.
- [18] J. Adamek, C. Barrera-Hinojosa, M. Bruni, B. Li, H. J. Macpherson, and J. B. Mertens, Numerical solutions to Einstein's equations in a shearing-dust universe: A code comparison, *Classical Quantum Gravity* **37**, 154001 (2020).
- [19] D. B. Thomas, M. Bruni, and D. Wands, Relativistic weak lensing from a fully nonlinear cosmological density field, *J. Cosmol. Astropart. Phys.* **09** (2015) 021.
- [20] A. Barreira, C. Llinares, S. Bose, and B. Li, RAY-RAMSES: A code for ray tracing on the fly in N -body simulations, *J. Cosmol. Astropart. Phys.* **05** (2016) 001.
- [21] M. Borzyszkowski, D. Bertacca, and C. Porciani, LIGER: Mock relativistic light-cones from Newtonian simulations, *Mon. Not. R. Astron. Soc.* **471**, 3899 (2017).
- [22] V. A. A. Sanghai, P. Fleury, and T. Clifton, Ray tracing and Hubble diagrams in post-Newtonian cosmology, *J. Cosmol. Astropart. Phys.* **07** (2017) 028.
- [23] J. T. Giblin, J. B. Mertens, G. D. Starkman, and A. R. Zentner, General relativistic corrections to the weak lensing convergence power spectrum, *Phys. Rev. D* **96**, 103530 (2017).
- [24] J. Adamek, C. Clarkson, L. Coates, R. Durrer, and M. Kunz, Bias and scatter in the Hubble diagram from cosmological large-scale structure, *Phys. Rev. D* **100**, 021301 (2019).

- [25] H. A. Gressel, C. Bonvin, M. Bruni, and D. Bacon, Full-sky weak lensing: A nonlinear post-Friedmann treatment, *J. Cosmol. Astropart. Phys.* **05** (2019) 045.
- [26] F. Lepori, J. Adamek, R. Durrer, C. Clarkson, and L. Coates, Weak-lensing observables in relativistic N-body simulations, *Mon. Not. R. Astron. Soc.* **497**, 2078 (2020).
- [27] H. J. Macpherson and A. Heinesen, Luminosity distance and anisotropic sky-sampling at low redshifts: A numerical relativity study, [arXiv:2103.11918](https://arxiv.org/abs/2103.11918).
- [28] E. Villa, S. Matarrese, and D. Maino, Post-newtonian cosmological dynamics of plane-parallel perturbations and back-reaction, *J. Cosmol. Astropart. Phys.* **08** (2011) 024.
- [29] E. Di Dio, M. Vonlanthen, and R. Durrer, Back reaction from walls, *J. Cosmol. Astropart. Phys.* **02** (2012) 036.
- [30] J. Adamek, E. Di Dio, R. Durrer, and M. Kunz, Distance-redshift relation in plane symmetric universes, *Phys. Rev. D* **89**, 063543 (2014).
- [31] T. Clifton and R. A. Sussman, Cosmological backreaction in spherical and plane symmetric dust-filled space-times, *Classical Quantum Gravity* **36**, 205004 (2019).
- [32] M. Grasso and E. Villa, BiGONLight: Light propagation with bi-local operators in numerical relativity, [arXiv:2107.06306](https://arxiv.org/abs/2107.06306).
- [33] M. Grasso, M. Korzyński, and J. Serbenta, Geometric optics in general relativity using bilocal operators, *Phys. Rev. D* **99**, 064038 (2019).
- [34] M. Korzyński and E. Villa, Geometric optics in relativistic cosmology: New formulation and a new observable, *Phys. Rev. D* **101**, 063506 (2020).
- [35] J. Yoo and R. Durrer, Gauge-transformation properties of cosmological observables and its application to the light-cone average, *J. Cosmol. Astropart. Phys.* **09** (2017) 016.
- [36] Y. B. Zel'dovich, Gravitational instability: An approximate theory for large density perturbations, *Astron. Astrophys.* **500**, 13 (1970), <https://ui.adsabs.harvard.edu/abs/1970A&A.....5...13Z>.
- [37] N. Bartolo, S. Matarrese, and A. Riotto, The full second-order radiation transfer function for large-scale CMB anisotropies, *J. Cosmol. Astropart. Phys.* **05** (2006) 010.
- [38] N. Aghanim *et al.* (Planck Collaboration), Planck 2018 results. VI. Cosmological parameters, *Astron. Astrophys.* **641**, A6 (2020).
- [39] Y. Akrami *et al.* (Planck Collaboration), Planck 2018 results. IX. Constraints on primordial non-Gaussianity, *Astron. Astrophys.* **641**, A9 (2020).
- [40] N. Uzun, Reduced phase space optics for general relativity: Symplectic ray bundle transfer, *Classical Quantum Gravity* **37**, 045002 (2020).
- [41] I. S. Gradshteyn and I. M. Ryzhik, *Table of Integrals, Series, and Products* (Academic Press, New York, 2014).
- [42] N. Meures and M. Bruni, Exact nonlinear inhomogeneities in λ CDM cosmology, *Phys. Rev. D* **83**, 123519 (2011).
- [43] N. Meures and M. Bruni, Redshift and distances in a λ CDM cosmology with non-linear inhomogeneities, *Mon. Not. R. Astron. Soc.* **419**, 1937 (2012).
- [44] E. Di Dio, F. Montanari, A. Raccanelli, R. Durrer, M. Kamionkowski, and J. Lesgourgues, Curvature constraints from large scale structure, *J. Cosmol. Astropart. Phys.* **06** (2016) 013.
- [45] P. Szekeres, A class of inhomogeneous cosmological models, *Commun. Math. Phys.* **41**, 55 (1975).
- [46] J. D. Barrow and J. Stein-Schabes, Inhomogeneous cosmologies with cosmological constant, *Phys. Lett.* **103A**, 315 (1984).
- [47] W. Bonnor, A. Sulaiman, and N. Tomimura, Szekeres's space-times have no killing vectors, *Gen. Relativ. Gravit.* **8**, 549 (1977).
- [48] S. W. Goode and J. Wainwright, Singularities and evolution of the Szekeres cosmological models, *Phys. Rev. D* **26**, 3315 (1982).
- [49] E. Villa and C. Rampf, Relativistic perturbations in λ CDM: Eulerian and Lagrangian approaches, *J. Cosmol. Astropart. Phys.* **01** (2016) 030.

SUMMARY

This dissertation deals with the computation of optical observables in cosmological simulations using the new `Wolfram` package `BiGONLight`. Numerical simulations have become an increasingly important instrument in modern cosmology for reconstructing the Universe's large-scale structure. To test the validity of cosmological theories, it is essential to correctly simulate the interaction of light with these structures to determine the origin of nonlinear relativistic effects measured in observations. In the past, this has been done with various methods for gravitational lensing observations. With the possibility of more precise measurements on the one hand and the observation of new quantities on the other, a unique approach to light propagation is needed to keep pace with this revolution in observational cosmology. The main feature of the package I have created is that it allows the direct implementation of the BGO formalism for computing multiple observables in a single calculation. This is possible because the BGO provide a unified framework for describing all possible optical effects caused by gravity on light propagation. Once computed along a geodesic, the BGO can be used to compute observables such as magnification, shear, and angular diameter distance, as well as new real-time observables such as parallax, redshift drift, and position drift resulting from temporal variations in the positions of sources and observers.

In the first paper, we introduce `BiGONLight` and show how it is applied to compute multiple observables in numerical relativity. In order to be compatible with most of the full-GR codes employed in numerical relativity, the package is designed to implement the BGO framework in the 3+1 form. To this end, I express the parallel transport equation, the optical tidal matrix $R^\mu{}_{\ell\nu}$, and the evolution equation for the BGO in terms of the ADM quantities (Eqs. (31), (39), and (44) in [89]). These results, together with the transformations from forward to backward integrated BGO (see Eqs. (49)-(52) in [89]), are my main theoretical contribution to this paper. Together with the 3 + 1 geodesic equation (presented in [182]), these formulas are encoded in `BiGONLight` as `Mathematica` functions. These functions take as input the ADM quantities (namely the spatial metric γ_{ij} , the extrinsic curvature K_{ij} , the lapse α and the shift β^i) and the 3 + 1 components of the velocities and accelerations of the observer \mathcal{O} and source \mathcal{S} to obtain the ODEs for computing the geodesics, to perform the parallel transport of a tetrad of vectors, and to compute the BGO. The user can provide the input as interpolated data from a numerical simulation or as analytical expressions of the components of the metric and the four-vectors (velocities and accelerations of \mathcal{O} and \mathcal{S}). For this second case, I have included functions in the package that perform the 3 + 1 splitting of the four-dimensional metric tensor and the four-vectors to obtain the ADM quantities. This hybrid design makes `BiGONLight` highly adaptable to study different types of problems in both numerical simulations and analytical (perturbation and/or exact) approaches.

The solutions of the ODEs for the geodesics, parallel transport, and GDE for BGO are found numerically using `BiGONLight` functions that solve these ODEs within a certain nu-

merical precision. The user sets the precision via the precision control options implemented in `Mathematica`. The final output of `BiGONLight` are the BGO $\mathcal{W}(\mathcal{S}, \mathcal{O})$ computed along the geodesics from the observer \mathcal{O} to the source \mathcal{S} . These can be used to obtain observables as described in Sec. 3.3. Furthermore, the ready-to-use transformations from forward-integrated BGO $\mathcal{W}(\mathcal{O}, \mathcal{S})$ to backward-integrated BGO $\mathcal{W}(\mathcal{S}, \mathcal{O})$ make `BiGONLight` potentially adaptable to perform light propagation on-the-fly with a simulation of spacetime, that is forward in time by construction. The package is currently designed to perform light propagation in post-processing rather than on-the-fly, with the advantage of processing inputs from a variety of numerical codes for cosmological dynamics. The procedure for computing observables with `BiGONLight` is described in [89] and implemented in a set of example notebooks publicly available on the GitHub repository <https://github.com/MicGrasso/bigonlight> under the GPL-3.0 license. The release of `BiGONLight` is the main result of my research and the most important achievement of this thesis.

We test `BiGONLight` by computing observables in three different cosmological models: the two homogeneous Λ CDM and EdS models and the inhomogeneous Szekeres model. The spacetime metrics corresponding to the Λ CDM and the Szekeres model are provided analytically, while the metric for the EdS model is obtained from the numerical evolution of a homogeneous dust Universe performed with the `Einstein Toolkit` and the `FLRWSolver`. In the homogeneous Λ CDM model, I have calculated the redshift, the angular diameter distance, the parallax distance, and the redshift drift using `BiGONLight` and I have compared these results with those obtained using analytical expressions from the literature. This test shows that `BiGONLight` can accurately reproduce the analytical results with a relative difference of the order of $10^{-22} \div 10^{-31}$. In the inhomogeneous Szekeres model, the metric presented in [130, 131] is provided as an analytical input to `BiGONLight` to compute the redshift and the angular diameter distance. I compare these results with those obtained by numerically solving the equations derived in [131]. I also test the calculation of the redshift drift using `BiGONLight`. In this case, the comparison is made with the formula I derived for the specific structure of light propagation in the Szekeres model under consideration (Eq. (96) in [89]). These other code tests in the Szekeres metric also show a good agreement between the observables obtained with `BiGONLight` and those obtained with other methods, with a relative difference of the order of $\sim 10^{-22}$. The last group of code tests is performed considering the homogeneous EdS model evolved numerically with the `Einstein Toolkit` and `FLRWSolver`. The data resulting from this simulation are passed as numerical input to `BiGONLight` and used to calculate the observables. These tests also differ from the other two groups, because in this case I have performed light propagation forward in time, namely from the source \mathcal{S} to the observer \mathcal{O} , and obtained the forward integrated BGO $\mathcal{W}(\mathcal{O}, \mathcal{S})$. Then I use the transformations in Eqs. (49)-(52) in the paper [89] to obtain $\mathcal{W}(\mathcal{S}, \mathcal{O})$ and compute observables. The tests on the observables (redshift, angular diameter distance, parallax distance, and redshift drift) show that the precision of the numerical simulation of the spacetime, which in our case is $\sim 10^{-10}$, determines the accuracy of the observables computed with `BiGONLight`. The very same results are obtained if $\mathcal{W}(\mathcal{S}, \mathcal{O})$ are directly computed, as was done for the tests in Λ CDM and Szekeres models.

In the second paper, we show how `BiGONLight` can be used to isolate and quantify various nonlinear contributions to light propagation. The analysis is performed in a toy model of the Universe, where the inhomogeneities in the density fluctuations form a sequence of plane-symmetric perturbations around a homogeneous Λ CDM background. The nonlinearities of light propagation are quantified by considering the relative difference of observables, defined as $\Delta O(b, a) = (O^b - O^a)/O^a$, where $a, b = \text{Lin}, \text{N}, \text{PN}$ denotes the following three different approximations: linear observables O^{Lin} , obtained using standard first-order perturbation theory, Newtonian observables O^{N} , obtained using the Newtonian approximation of the

plane-parallel metric as the analytical input to `BiGONLight`, and post-Newtonian observables O^{PN} , obtained using the post-Newtonian approximation of the plane-parallel metric as the analytical input to `BiGONLight`. The expressions of the plane-parallel metric in Newtonian and PN approximations are given in [180], and we extended them providing the corresponding metrics with a Λ CDM background. These metrics fit our analysis well, as the terms from all three approximations are easily identifiable and can be used directly as input in the package to compute observables. For our analysis, we only consider the redshift z and the angular diameter distance D_{ang} computed in the three different methods. After a preliminary analysis, we decided to fix the setting for light propagation as discussed in Sec. IV in [90].

The variations $\Delta O(\text{Lin}, \text{N})$ and $\Delta O(\text{PN}, \text{N})$ are calculated by varying the free parameters of the model. The gravitational potential $\phi_0(q^1)$ is a free function that provides the spatial profile of the matter distribution. We consider a sinusoidal distribution $\phi_0(q^1) = \mathcal{I} \sin(\frac{2\pi}{k} q^1)$, where \mathcal{I} and k denote the amplitude and scale of the inhomogeneities, respectively. We vary (k, \mathcal{I}) as described in Sec. V and according to the list of values in Table 1 in [90]. Another free parameter of the model is a_{nl} , which is related to the primordial non-Gaussianity parameter f_{nl} . It expresses the deviations from a Gaussian distribution of the primordial fluctuations and an estimate of its value is $a_{\text{nl}} = 0.46 \pm 3.06$, see [11]. In the PN metric [180], a specific value of a_{nl} can modulate the effects of some of the PN terms. We compute O^{PN} for the four values of $a_{\text{nl}} = 0.46, 3.52, -2.6, 1$, corresponding to the reference value, the two extremes of the confidence interval, and for perfect Gaussian distribution. The other (cosmological) parameters are set using the values measured by Planck satellite [10]. We isolate the various sources of nonlinear corrections in the observables by analysing the dependence of ΔO on these freely specifiable quantities.

My original contributions to this paper are all simulations in the three approximations with `BiGONLight` and calculations of ΔO , for the various choices of the free parameters $(\mathcal{I}, k, a_{\text{nl}})$. These results have led to the following findings:

- (i) We quantify the nonlinear corrections in the observables from Newtonian and PN approximations by computing $\Delta O(\text{Lin}, \text{N})$ and $\Delta O(\text{PN}, \text{N})$. In general, our results are consistent with similar results in the literature, as $\Delta z(\text{Lin}, \text{N})$ and $\Delta D_{\text{ang}}(\text{Lin}, \text{N})$ are well below 1%. However, we note a different behaviour in the two observables. For the redshift, the Newtonian corrections contribute most to the nonlinearities, with $\Delta z(\text{Lin}, \text{N}) \sim 10^2 \Delta z(\text{PN}, \text{N})$. On the other hand, for the angular diameter distance we find that $\Delta D_{\text{ang}}(\text{Lin}, \text{N}) \sim \Delta D_{\text{ang}}(\text{PN}, \text{N})$, i.e. $D_{\text{ang}}^{\text{Lin}}$ and $D_{\text{ang}}^{\text{PN}}$ have similar corrections with respect to $D_{\text{ang}}^{\text{N}}$.
- (ii) We estimate the effects of the scale of perturbations k by computing ΔO for different values of k . The observables at linear, Newtonian, and PN order are computed for $k = 500 \text{ Mpc}, 300 \text{ Mpc}, 100 \text{ Mpc}, 50 \text{ Mpc}, 300 \text{ Mpc}$. We find that the amplitude of ΔD_{ang} decreases monotonically with the scale for both linear-Newtonian and PN-Newtonian comparisons. On the other hand, the amplitude for Δz increases for $500 \text{ Mpc} \leq k \leq 100 \text{ Mpc}$ and decreases for $100 \text{ Mpc} < k \leq 30 \text{ Mpc}$, with a maximum amplitude of Δz for $k = 100 \text{ Mpc}$.
- (iii) We constrain the dependence on primordial non-Gaussianity in $\Delta O(\text{PN}, \text{N})$ and $\Delta O^{\text{PN}}(a_{\text{nl}_1}, a_{\text{nl}_2})$ with O^{PN} computed with the four different values of a_{nl} . In both cases, we found that the primordial non-Gaussianity parameter has negligible effects in our comparison, i.e. $\Delta O^{\text{PN}}(a_{\text{nl}_1}, a_{\text{nl}_2}) \ll \Delta O(\text{PN}, \text{N})$.
- (iv) Finally, we examine the relative difference $\Delta O(a, \Lambda\text{CDM})$ of the observables in the three approximations $a = \text{Lin}, \text{N}, \text{PN}$ with respect to the observable for the ΛCDM

background. This comparison for the angular diameter distance shows that the leading contribution to the PN corrections is the linear PN term $-\frac{5}{3c^2}\phi_0$, known as “initial seeds”.

The results in (iv) motivate the findings in (i) and (iii). In (i), the result $\Delta D_{\text{ang}}(\text{Lin}, \text{N}) \sim \Delta D_{\text{ang}}(\text{PN}, \text{N})$ is related to the fact that the initial seed is only present in the linear metric and the PN metric (as the leading correction), but is absent in the Newtonian metric. On the other hand, in (iii), the dependence on a_{nl} is negligible since the primordial non-Gaussian parameter can only trigger the nonlinear PN terms, and these are subleading with respect to the linear PN initial seeds.

In conclusion, I present **BiGONLight** in my thesis as a reliable numerical tool that can be easily adapted to perform numerical and analytical analyses of light propagation by computing multiple observables within a single calculation. It can be used to perform complex analyses, such as the one presented, with accuracy sufficient to constrain small nonlinear effects, such as those caused by nonlinear PN terms.

LIST OF FIGURES

2.1	Precise measurements of the CMB (Fig. 2.1a), the LSS (Fig. 2.1b), and the SnIa (Fig. 2.1c) have been used to constraint the standard model for cosmology. . . .	6
2.2	Illustration of the evolution of a group of particles in an expanding Universe in the Eulerian (left) and Lagrangian (right) frames. At the initial time t , the particles have a certain position with respect to the uniform grid. Due to the expansion and the gravitational interaction, at a later time $t + \Delta t$ the particles are in a different position with respect to the grid in the Eulerian frame (left), with the new position being marked by the vector x^μ . In the Lagrangian frame (right), on the other hand, the positions of the particles q^μ do not change with time. . . .	14
2.3	The constant-time hypersurfaces Σ_t foliating the four-dimensional spacetime $\mathcal{M}, g_{\mu\nu}$, introduce a unit normal vector n^μ orthogonal to Σ_t . The coordinate flow, i.e. the lines of constant spatial coordinates, is given in terms of the lapse α and the shift β^i gauge functions. . . .	20
3.1	The tangent vector to the geodesics ℓ^μ and the deviation vector ξ^μ , representing the infinitesimal displacement from a nearby geodesic, characterise the geodesics of the family $\{\gamma_\tau(\lambda)\}$	28
3.2	The two deviation vectors ξ^μ and $\tilde{\xi}^\mu = \xi^\mu + \alpha(\lambda)\ell^\mu$ identify the same geodesic γ_τ . This invariance of the GDE is related to the gauge freedom one has in choosing the affine parameter. Indeed, the different deviation vector $\tilde{\xi}^\mu$ can be obtained by introducing the different affine parametrisation λ' of the geodesic γ_τ	30
3.3	The observer \mathcal{O} and the source \mathcal{S} are free to move along their worldlines in the two small regions $N_{\mathcal{O}}$ and $N_{\mathcal{S}}$. The point $x_{\mathcal{S}}^\mu$ on the \mathcal{S} 's worldline is connected to $x_{\mathcal{O}}^\mu$ on the \mathcal{O} 's worldline by the null geodesic γ_0 . γ_0 can be identified by the initial position and initial tangent vector at the observer $(x_{\mathcal{O}}^\mu, \ell_{\mathcal{O}}^\mu)$. Since the observer and source are free to move, they will be connected at a later time by another geodesic γ identified by the displacement vectors $(\delta x_{\mathcal{O}}^\mu, \Delta \ell_{\mathcal{O}}^\mu)$	32
3.4	Geometry of the quotient spaces $\mathcal{Q}_{\mathcal{O}}$ and $\mathcal{P}_{\mathcal{O}}$. Elements $[X] \in \mathcal{Q}_{\mathcal{O}}$ correspond to the vectors X^μ and Y^μ in $T_{\mathcal{O}}\mathcal{M}$ identified by the relation $Y^\mu \sim X^\mu$, i.e. such that $Y^\mu = X^\mu + c\ell_{\mathcal{O}}^\mu$. Geometrically is the space containing all geodesics in $N_{\mathcal{O}}$ parallel to γ_0 . Elements $\mathbf{X} \in \mathcal{P}_{\mathcal{O}}$ corresponds to the vectors X^μ and Y^μ in $T_{\mathcal{O}}\mathcal{M}$, which are perpendicular to $\ell_{\mathcal{O}}$ (i.e. $X^\mu \ell_{\mathcal{O}\mu} = 0$ and $Y^\mu \ell_{\mathcal{O}\mu} = 0$) and identified by $Y^\mu \sim X^\mu$. Geometrically, $\mathcal{P}_{\mathcal{O}}$ is the space containing the geodesics parallel to γ_0 and lying on the null hypersurface orthogonal to $\ell_{\mathcal{O}}$	37
3.5	The past light cone (blue) in $N_{\mathcal{O}}$ degenerates to the flat null hypersurface (blue plane) in $N_{\mathcal{S}}$. Similarly, the future light cone (orange) in $N_{\mathcal{S}}$ degenerates to the flat null hypersurface (orange plane) in $N_{\mathcal{O}}$. \mathcal{O} can observe only those events on the corresponding hypersurface in $N_{\mathcal{S}}$	39
3.6	On the null hypersurface $\ell_{\mathcal{S}\mu}\delta x_{\mathcal{S}}^\mu = 0$ the cross section C of the source \mathcal{S} has area $A_{\mathcal{S}}$. On the corresponding null hypersurface $\ell_{\mathcal{O}\mu}\delta x_{\mathcal{O}}^\mu = 0$, the observer \mathcal{O} measures the solid angle $\Omega_{\mathcal{O}}$ occupied by the image I of the source. . . .	42

- 3.7 The worldlines of two observers \mathcal{O} and \mathcal{O}' cross the same null hypersurface $\delta x_{\mathcal{O}}^{\mu} \ell_{\mathcal{O}\mu} = 0$ and observe the source \mathcal{S} , which lies on the corresponding null hypersurface $\delta x_{\mathcal{S}}^{\mu} \ell_{\mathcal{S}\mu} = 0$ in $N_{\mathcal{S}}$. \mathcal{O} and \mathcal{O}' are displaced by $\delta x_{\mathcal{O}}^{\mu}$, and they perceive the source in the apparent positions \mathbf{s} and \mathbf{s}' , respectively. The difference between \mathbf{s} and \mathbf{s}' gives the parallax angle $\delta\theta_{\mathcal{O}}^{\mu}$. On the screen $\hat{\phi}_{\mathbf{A}}^{\mu}$, the displacement $\delta x_{\mathcal{O}}^{\mathbf{A}}$ and the angular distance $\delta\theta_{\mathcal{O}}^{\mathbf{A}}$ are related by the parallax matrix $\Pi^{\mathbf{A}}_{\mathbf{B}}$ 44
- 3.8 The source \mathcal{S} is observed by \mathcal{O} , \mathcal{O}_1 , and \mathcal{O}_2 in $N_{\mathcal{O}}$. The positions of the three observers form the blue triangle T_2 in the space perpendicular to $\ell_{\mathcal{O}}$. Similarly, on the shared celestial sphere $S_{\mathcal{O}}$, the apparent positions of the source \mathbf{s} , \mathbf{s}_1 , and \mathbf{s}_2 form the orange triangle T_1 . The parallax distance is defined as the ratio between the area of T_2 and the solid angle of T_1 45

BIBLIOGRAPHY

- [1] ABBOTT, B. P., ABBOTT, R., ABBOTT, T., ABERNATHY, M., ACERNESE, F., ACKLEY, K., ADAMS, C., ADAMS, T., ADDESSO, P., ADHIKARI, R., ET AL. Observation of gravitational waves from a binary black hole merger. *Physical review letters* 116, 6 (2016), 061102.
- [2] ADAMEK, J., BARRERA-HINOJOSA, C., BRUNI, M., LI, B., MACPHERSON, H. J., AND MERTENS, J. B. Numerical solutions to Einstein’s equations in a shearing-dust Universe: a code comparison. *Class. Quant. Grav.* 37, 15 (2020), 154001.
- [3] ADAMEK, J., CLARKSON, C., COATES, L., DURRER, R., AND KUNZ, M. Bias and scatter in the Hubble diagram from cosmological large-scale structure. *Phys. Rev. D* 100, 2 (2019), 021301.
- [4] ADAMEK, J., DAVERIO, D., DURRER, R., AND KUNZ, M. General Relativistic N -body simulations in the weak field limit. *Phys. Rev. D* 88, 10 (2013), 103527.
- [5] ADAMEK, J., DAVERIO, D., DURRER, R., AND KUNZ, M. General relativity and cosmic structure formation. *Nature physics* 12, 4 (2016), 346–349.
- [6] ADAMEK, J., DAVERIO, D., DURRER, R., AND KUNZ, M. gevolution: a cosmological N -body code based on General Relativity. *JCAP* 1607, 07 (2016), 053.
- [7] ADAMEK, J., DI DIO, E., DURRER, R., AND KUNZ, M. Distance-redshift relation in plane symmetric universes. *Physical Review D* 89, 6 (2014), 063543.
- [8] ADAMEK, J., DURRER, R., AND KUNZ, M. N -body methods for relativistic cosmology. *Class. Quant. Grav.* 31, 23 (2014), 234006.
- [9] AGHANIM, N., AKRAMI, Y., ASHDOWN, M., AUMONT, J., BACCIGALUPI, C., BALLARDINI, M., BANDAY, A. J., BARREIRO, R., BARTOLO, N., BASAK, S., ET AL. Planck 2018 results-v. cmb power spectra and likelihoods. *Astronomy & Astrophysics* 641 (2020), A5.
- [10] AGHANIM, N., ET AL. Planck 2018 results. VI. Cosmological parameters. *Astron. Astrophys.* 641 (2020), A6.
- [11] AKRAMI, Y., ET AL. Planck 2018 results. IX. Constraints on primordial non-Gaussianity. *Astron. Astrophys.* 641 (2020), A9.
- [12] ALCUBIERRE, M. *Introduction to 3+ 1 numerical relativity*, vol. 140. Oxford University Press, 2008.
- [13] ALEKSANDROV, A. N., AND PIRAGAS, K. A. Geodesic structure. *Theoretical and Mathematical Physics* 38, 1 (Jan 1979), 48–56.
- [14] ALEXANDER, S., BISWAS, T., NOTARI, A., AND VAID, D. Local void vs dark energy: confrontation with wmap and type ia supernovae. *Journal of Cosmology and Astroparticle Physics* 2009, 09 (2009), 025.
- [15] ARNOWITT, R., DESER, S., AND MISNER, C. W. Dynamical structure and definition of energy in general relativity. *Phys. Rev.* 116 (Dec 1959), 1322–1330.

- [16] BAIOTTI, L., GIACOMAZZO, B., AND REZZOLLA, L. Accurate evolutions of inspiralling neutron-star binaries: Prompt and delayed collapse to a black hole. *Physical Review D* 78, 8 (2008), 084033.
- [17] BAKER, J. G., CENTRELLA, J., CHOI, D.-I., KOPPITZ, M., AND VAN METER, J. Gravitational-wave extraction from an inspiraling configuration of merging black holes. *Physical review letters* 96, 11 (2006), 111102.
- [18] BARAUSSE, E., MATARRESE, S., AND RIOTTO, A. The Effect of inhomogeneities on the luminosity distance-redshift relation: Is dark energy necessary in a perturbed Universe? *Phys. Rev. D* 71 (2005), 063537.
- [19] BARDEEN, J. M. Gauge-invariant cosmological perturbations. *Physical Review D* 22, 8 (1980), 1882.
- [20] BARRERA-HINOJOSA, C., AND LI, B. Gramses: a new route to general relativistic n-body simulations in cosmology. part i. methodology and code description. *Journal of Cosmology and Astroparticle Physics* 2020, 01 (2020), 007.
- [21] BARRERA-HINOJOSA, C., LI, B., BRUNI, M., AND HE, J.-H. Vector modes in Λ CDM: the gravitomagnetic potential in dark matter haloes from relativistic N -body simulations. *Mon. Not. Roy. Astron. Soc.* 501, 4 (2021), 5697–5713.
- [22] BARROW, J. D., AND STEIN-SCHABES, J. Inhomogeneous cosmologies with cosmological constant. *Phys. Lett. A* 103 (1984), 315–317.
- [23] BARTELMANN, M. Gravitational lensing. *Classical and Quantum Gravity* 27, 23 (nov 2010), 233001.
- [24] BARTOLO, N., MATARRESE, S., AND RIOTTO, A. The full second-order radiation transfer function for large-scale cmb anisotropies. *JCAP* 05 (2006), 010.
- [25] BAUMGARTE, T. W., AND SHAPIRO, S. L. Numerical integration of einstein’s field equations. *Physical Review D* 59, 2 (1998), 024007.
- [26] BAUMGARTE, T. W., AND SHAPIRO, S. L. *Numerical relativity*. Cambridge University Press, 2010.
- [27] BAŻAŃSKI, S. L. Dynamics of relative motion of test particles in general relativity. *Annales de L’Institut Henri Poincare Section (A) Physique Theorique* 27 (Sept. 1977), 145–166.
- [28] BAŻAŃSKI, S. L. Kinematics of relative motion of test particles in general relativity. *Annales de L’Institut Henri Poincare Section (A) Physique Theorique* 27 (Sept. 1977), 115–144.
- [29] BEASLEY, A., GORDON, D., PECK, A., PETROV, L., MACMILLAN, D., FOMALONT, E., AND MA, C. The vlba calibrator survey—vcs1. *The Astrophysical Journal Supplement Series* 141, 1 (2002), 13.
- [30] BEL, J., AND MARINONI, C. Proposal for a real-time detection of our acceleration through space. *Phys. Rev. Lett.* 121 (Jul 2018), 021101.
- [31] BENTIVEGNA, E. An automatically generated code for relativistic inhomogeneous cosmologies. *Phys. Rev. D* 95, 4 (2017), 044046.

- [32] BENTIVEGNA, E., AND BRUNI, M. Effects of nonlinear inhomogeneity on the cosmic expansion with numerical relativity. *Phys. Rev. Lett.* *116*, 25 (2016), 251302.
- [33] BENTIVEGNA, E., CLIFTON, T., DURK, J., KORZYŃSKI, M., AND ROSQUIST, K. Black-hole lattices as cosmological models. *Classical and Quantum Gravity* *35*, 17 (2018), 175004.
- [34] BENTIVEGNA, E., AND KORZYŃSKI, M. Evolution of a periodic eight-black-hole lattice in numerical relativity. *Classical and quantum gravity* *29*, 16 (2012), 165007.
- [35] BENTIVEGNA, E., AND KORZYŃSKI, M. Evolution of a family of expanding cubic black-hole lattices in numerical relativity. *Classical and Quantum Gravity* *30*, 23 (2013), 235008.
- [36] BERTACCA, D., BARTOLO, N., BRUNI, M., KOYAMA, K., MAARTENS, R., MATARESE, S., SASAKI, M., AND WANDS, D. Galaxy bias and gauges at second order in general relativity. *Classical and Quantum Gravity* *32*, 17 (2015), 175019.
- [37] BERTACCA, D., MAARTENS, R., AND CLARKSON, C. Observed galaxy number counts on the lightcone up to second order: I. main result. *Journal of Cosmology and Astroparticle Physics* *2014*, 09 (2014), 037.
- [38] BERTSCHINGER, E. Cosmological Dynamics. In *Cosmology and Large Scale Structure* (Jan. 1996), R. Schaeffer, J. Silk, M. Spiro, and J. Zinn-Justin, Eds., p. 273.
- [39] BEUTLER, F., AND DI DIO, E. Modeling relativistic contributions to the halo power spectrum dipole. *JCAP* *07*, 07 (2020), 048.
- [40] BOLEJKO, K., CÉLÉRIER, M.-N., AND KRASIŃSKI, A. Inhomogeneous cosmological models: exact solutions and their applications. *Classical and Quantum Gravity* *28*, 16 (2011), 164002.
- [41] BONDI, H. Spherically symmetrical models in general relativity. *Monthly Notices of the Royal Astronomical Society* *107*, 5-6 (1947), 410–425.
- [42] BONNOR, W., SULAIMAN, A., AND TOMIMURA, N. Szekeres’s space-times have no killing vectors. *General Relativity and Gravitation* *8*, 8 (1977), 549–559.
- [43] BONVIN, C., AND DURRER, R. What galaxy surveys really measure. *Physical Review D* *84*, 6 (2011), 063505.
- [44] BONVIN, C., DURRER, R., AND GASPARINI, M. A. Fluctuations of the luminosity distance. *Physical Review D* *73*, 2 (Jan 2006).
- [45] BRUNI, M., THOMAS, D. B., AND WANDS, D. Computing general-relativistic effects from newtonian n-body simulations: Frame dragging in the post-friedmann approach. *Physical Review D* *89*, 4 (2014), 044010.
- [46] BRUNI, M., THOMAS, D. B., AND WANDS, D. Computing General Relativistic effects from Newtonian N-body simulations: Frame dragging in the post-Friedmann approach. *Phys. Rev. D* *89*, 4 (2014), 044010.
- [47] BUONANNO, A., COOK, G. B., AND PRETORIUS, F. Inspiral, merger, and ring-down of equal-mass black-hole binaries. *Physical Review D* *75*, 12 (2007), 124018.

- [48] CAMPANELLI, M., LOUSTO, C. O., MARRONETTI, P., AND ZLOCHOWER, Y. Accurate evolutions of orbiting black-hole binaries without excision. *Physical Review Letters* *96*, 11 (2006), 111101.
- [49] CARBONE, C., AND MATARRESE, S. Unified treatment of cosmological perturbations from superhorizon to small scales. *Physical Review D* *71*, 4 (2005), 043508.
- [50] CARROLL, B. W., AND OSTLIE, D. A. *An introduction to modern astrophysics*. Cambridge University Press, 2017.
- [51] CATELAN, P. Lagrangian dynamics in nonflat universes and nonlinear gravitational evolution. *Mon. Not. Roy. Astron. Soc.* *276* (1995), 115.
- [52] CATELAN, P., LUCCHIN, F., MATARRESE, S., AND MOSCARDINI, L. Eulerian perturbation theory in nonflat universes: Second order approximation. *Mon. Not. Roy. Astron. Soc.* *276* (1995), 39.
- [53] CELERIER, M.-N. Do we really see a cosmological constant in the supernovae data? *arXiv preprint astro-ph/9907206* (1999).
- [54] CHAURASIA, S. V., DIETRICH, T., JOHNSON-MCDANIEL, N. K., UJEVIC, M., TICHY, W., AND BRÜGMANN, B. Gravitational waves and mass ejecta from binary neutron star mergers: Effect of large eccentricities. *Physical Review D* *98*, 10 (2018), 104005.
- [55] CHRISTIAN, S. Re-examining the evidence of the hercules–corona borealis great wall. *Monthly Notices of the Royal Astronomical Society* *495*, 4 (May 2020), 4291–4296.
- [56] CIUFOLINI, I., AND DEMIAŃSKI, M. How to measure the curvature of space-time. *Phys. Rev. D* *34* (Aug 1986), 1018–1020.
- [57] CLARKSON, C. Roulettes: A weak lensing formalism for strong lensing - I. Overview. *Class. Quant. Grav.* *33*, 16 (2016), 16LT01.
- [58] CLARKSON, C. Roulettes: A weak lensing formalism for strong lensing - II. Derivation and analysis. *Class. Quant. Grav.* *33*, 24 (2016), 245003.
- [59] CLIFTON, T., AND FERREIRA, P. G. Archipelagian cosmology: dynamics and observables in a universe with discretized matter content. *Physical Review D* *80*, 10 (2009), 103503.
- [60] CLIFTON, T., GREGORIS, D., AND ROSQUIST, K. Applications of black hole lattices in relativistic cosmology. In *AIP Conference Proceedings* (2015), vol. 1693, AIP Publishing LLC, p. 070006.
- [61] COLLESS, M., DALTON, G., MADDOX, S., SUTHERLAND, W., NORBERG, P., COLE, S., BLAND-HAWTHORN, J., BRIDGES, T., CANNON, R., COLLINS, C., ET AL. The 2df galaxy redshift survey: spectra and redshifts. *Monthly Notices of the Royal Astronomical Society* *328*, 4 (2001), 1039–1063.
- [62] DAVERIO, D., DIRIAN, Y., AND MITSOU, E. General relativistic cosmological N-body simulations. Part I. Time integration. *JCAP* *10* (2019), 065.
- [63] DEWITT, B. S., AND BREHME, R. W. Radiation damping in a gravitational field. *Annals of Physics* *9*, 2 (1960), 220 – 259.

- [64] DI DIO, E., VONLANTHEN, M., AND DURRER, R. Back reaction from walls. *Journal of Cosmology and Astroparticle Physics* 2012, 02 (2012), 036.
- [65] DING, F., AND CROFT, R. A. C. Future dark energy constraints from measurements of quasar parallax: Gaia, SIM and beyond. *Mon. Not. Roy. Astron. Soc.* 397 (2009), 1739.
- [66] DIO, E. D., MONTANARI, F., RACCANELLI, A., DURRER, R., KAMIONKOWSKI, M., AND LESGOURGUES, J. Curvature constraints from large scale structure. *Journal of Cosmology and Astroparticle Physics* 2016, 06 (Jun 2016), 013–013.
- [67] DIXON, W. G. Dynamics of extended bodies in general relativity. i. momentum and angular momentum. *Proceedings of the Royal Society of London. A. Mathematical and Physical Sciences* 314, 1519 (1970), 499–527.
- [68] DODELSON, S. *Modern cosmology*. Elsevier, 2003.
- [69] DYER, C. C., AND ROEDER, R. C. Observations in Locally Inhomogeneous Cosmological Models. *apj* 189 (Apr. 1974), 167–176.
- [70] EAST, W. E., WOJTAK, R., AND ABEL, T. Comparing fully general relativistic and newtonian calculations of structure formation. *Physical Review D* 97, 4 (2018), 043509.
- [71] EHLERS, J., JORDAN, P., AND SACHS, R. K. *Beiträge zur Theorie der reinen Gravitationsstrahlung*, vol. 1 of *Abhandlungen der Mathematisch-Naturwissenschaftlichen Klasse*. Verlag der Akademie der Wissenschaften und der Literatur in Mainz, Wiesbaden, Germany, 1961.
- [72] EINSTEIN, A. Die Feldgleichungen der Gravitation. *Sitzungsberichte der Königlich Preussischen Akademie der Wissenschaften (Berlin)* (Jan. 1915), 844–847.
- [73] EINSTEIN, A., AND STRAUS, E. G. The influence of the expansion of space on the gravitation fields surrounding the individual stars. *Reviews of Modern Physics* 17, 2-3 (1945), 120.
- [74] ELLIS, G. F., MAARTENS, R., AND MACCALLUM, M. A. *Relativistic cosmology*. Cambridge University Press, 2012.
- [75] EPPLEY, K. Evolution of time-symmetric gravitational waves: Initial data and apparent horizons. *Physical Review D* 16, 6 (1977), 1609.
- [76] ETHERINGTON, I. Lx. on the definition of distance in general relativity. *The London, Edinburgh, and Dublin Philosophical Magazine and Journal of Science* 15, 100 (1933), 761–773.
- [77] ETHERINGTON, I. M. H. Republication of: Lx. on the definition of distance in general relativity. *General Relativity and Gravitation* 39, 7 (Jul 2007), 1055–1067.
- [78] FANIZZA, G., GASPERINI, M., MAROZZI, G., AND VENEZIANO, G. An exact jacobi map in the geodesic light-cone gauge. *Journal of Cosmology and Astroparticle Physics* 2013, 11 (Nov 2013), 019–019.
- [79] FIDLER, C., TRAM, T., RAMPF, C., CRITTENDEN, R., KOYAMA, K., AND WANDS, D. General relativistic weak-field limit and Newtonian N-body simulations. *JCAP* 12 (2017), 022.

- [80] FLANAGAN, E. E., GRANT, A. M., HARTE, A. I., AND NICHOLS, D. A. Persistent gravitational wave observables: General framework. *Physical Review D* 99, 8 (Apr 2019).
- [81] FLEURY, P. Swiss-cheese models and the Dyer-Roeder approximation. *JCAP* 1406 (2014), 054.
- [82] GIBLIN, J. T., MERTENS, J. B., AND STARKMAN, G. D. Departures from the Friedmann-Lemaitre-Robertston-Walker Cosmological Model in an Inhomogeneous Universe: A Numerical Examination. *Phys. Rev. Lett.* 116, 25 (2016), 251301.
- [83] GIBLIN, J. T., MERTENS, J. B., STARKMAN, G. D., AND ZENTNER, A. R. General Relativistic Corrections to the Weak Lensing Convergence Power Spectrum. *Phys. Rev. D* 96, 10 (2017), 103530.
- [84] GOLDBERG, S. R., CLIFTON, T., AND MALIK, K. A. Cosmology on all scales: a two-parameter perturbation expansion. *Phys. Rev. D* 95, 4 (2017), 043503.
- [85] GOODE, S. W., AND WAINWRIGHT, J. Singularities and evolution of the Szekeres cosmological models. *Phys. Rev. D* 26 (1982), 3315–3326.
- [86] GOURGOULHON, E. *3+ 1 formalism in general relativity*, vol. 846. Springer Science & Business Media, 2012.
- [87] GRADSHTEYN, I. S., AND RYZHIK, I. M. *Table of integrals, series, and products*. Academic press, 2014.
- [88] GRASSO, M., KORZYŃSKI, M., AND SERBENTA, J. Geometric optics in general relativity using bilocal operators. *Phys. Rev. D* 99, 6 (2019), 064038.
- [89] GRASSO, M., AND VILLA, E. BiGONLight: light propagation with bilocal operators in numerical relativity. *Class. Quant. Grav.* 39, 1 (2022), 015011.
- [90] GRASSO, M., VILLA, E., KORZYŃSKI, M., AND MATARRESE, S. Isolating nonlinearities of light propagation in inhomogeneous cosmologies. *Phys. Rev. D* 104, 4 (2021), 043508.
- [91] GREEN, S. R., AND WALD, R. M. New framework for analyzing the effects of small scale inhomogeneities in cosmology. *Physical Review D* 83, 8 (2011), 084020.
- [92] GREEN, S. R., AND WALD, R. M. Newtonian and relativistic cosmologies. *Physical Review D* 85, 6 (2012), 063512.
- [93] GRESSEL, H. A., BONVIN, C., BRUNI, M., AND BACON, D. Full-sky weak lensing: a nonlinear post-Friedmann treatment. *JCAP* 05 (2019), 045.
- [94] HAHN, S. G., AND LINDQUIST, R. W. The two-body problem in geometrodynamics. *Annals of Physics* 29, 2 (1964), 304–331.
- [95] HARTE, A. I. Gravitational lensing beyond geometric optics: I. Formalism and observables. *Gen. Rel. Grav.* 51, 1 (2019), 14.
- [96] HELLABY, C., AND WALTERS, A. Calculating observables in inhomogeneous cosmologies. Part I: general framework. *JCAP* 1802, 02 (2018), 015.

- [97] HINDER, I., KIDDER, L. E., AND PFEIFFER, H. P. Eccentric binary black hole inspiral-merger-ringdown gravitational waveform model from numerical relativity and post-newtonian theory. *Physical Review D* 98, 4 (2018), 044015.
- [98] HOBBS, D., ET AL. All-sky visible and near infrared space astrometry. *Exper. Astron.* 51, 3 (2021), 783–843.
- [99] HOWLETT, C., LEWIS, A., HALL, A., AND CHALLINOR, A. Cmb power spectrum parameter degeneracies in the era of precision cosmology. *Journal of Cosmology and Astroparticle Physics* 2012, 04 (2012), 027.
- [100] HUBBLE, E. A relation between distance and radial velocity among extra-galactic nebulae. *The Early Universe: Reprints* (1988), 9.
- [101] ISAACSON, R. A. Gravitational radiation in the limit of high frequency. i. the linear approximation and geometrical optics. *Phys. Rev.* 166 (Feb 1968), 1263–1271.
- [102] ISAACSON, R. A. Gravitational radiation in the limit of high frequency. ii. nonlinear terms and the effective stress tensor. *Phys. Rev.* 166 (Feb 1968), 1272–1280.
- [103] JONES, B. J. *Precision cosmology: the first half million years*. Cambridge University Press, 2017.
- [104] KASAI, M. The triangulation in a perturbed friedmann universe. *Prog. Theor. Phys.* 79 (1988), 777.
- [105] KERMAK, W. O., MCCREA, W. H., AND WHITTAKER, E. T. Iv.—on properties of null geodesics, and their application to the theory of radiation. *Proceedings of the Royal Society of Edinburgh* 53 (1934), 31–47.
- [106] KODAMA, H., AND SASAKI, M. Cosmological perturbation theory. *Progress of Theoretical Physics Supplement* 78 (1984), 1–166.
- [107] KOMATSU, E., ET AL. Five-Year Wilkinson Microwave Anisotropy Probe (WMAP) Observations: Cosmological Interpretation. *Astrophys. J. Suppl.* 180 (2009), 330–376.
- [108] KOPP, M., UHLEMANN, C., AND HAUGG, T. Newton to einstein—dust to dust. *Journal of Cosmology and Astroparticle Physics* 2014, 03 (2014), 018.
- [109] KORZYŃSKI, M., AND VILLA, E. Geometric optics in relativistic cosmology: new formulation and a new observable. *Phys. Rev. D* 101, 6 (2020), 063506.
- [110] KORZYŃSKI, M., AND KOPIŃSKI, J. Optical drift effects in general relativity. *Journal of Cosmology and Astroparticle Physics* 2018, 03 (2018), 012.
- [111] KRASINSKI, A., AND BOLEJKO, K. Drift of light rays induced by nonsymmetric cosmic flow: an observational test of homogeneity of the universe+ a few general comments on inhomogeneous models. *arXiv preprint arXiv:1212.4697* (2012).
- [112] LEMAÎTRE, G. Un univers homogène de masse constante et de rayon croissant rendant compte de la vitesse radiale des nébuleuses extra-galactiques. In *Annales de la Société scientifique de Bruxelles* (1927), vol. 47, pp. 49–59.
- [113] LEMAÎTRE, G. L’univers en expansion. In *Annales de la Société scientifique de Bruxelles* (1933), vol. 53, p. 51.

- [114] LEPORI, F., ADAMEK, J., DURRER, R., CLARKSON, C., AND COATES, L. Weak-lensing observables in relativistic N-body simulations. *Mon. Not. Roy. Astron. Soc.* *497*, 2 (2020), 2078–2095.
- [115] LINQUIST, R., AND WHEELER, J. Dynamics of a lattice universe by the schwarzschild-cell methods. *Rev. Mod. Phys* *29* (1957), 432.
- [116] LOEB, A. Direct Measurement of Cosmological Parameters from the Cosmic Deceleration of Extragalactic Objects. *Astrophys. J.* *499* (1998), L111–L114.
- [117] LÖFFLER, F., FABER, J., BENTIVEGNA, E., BODE, T., DIENER, P., HAAS, R., HINDER, I., MUNDIM, B. C., OTT, C. D., SCHNETTER, E., ET AL. The einstein toolkit: a community computational infrastructure for relativistic astrophysics. *Classical and Quantum Gravity* *29*, 11 (2012), 115001.
- [118] LOUREIRO, A., ET AL. KiDS & Euclid: Cosmological implications of a pseudo angular power spectrum analysis of KiDS-1000 cosmic shear tomography. *arXiv* (10 2021).
- [119] LOW, R. J. Celestial spheres, light cones, and cuts. *Journal of Mathematical Physics* *34* (Jan. 1993), 315–319.
- [120] LURI, X., BROWN, A. G. A., SARRO, L. M., ARENOU, F., BAILER-JONES, C. A. L., CASTRO-GINARD, A., BRUIJNE, J. DE, PRUSTI, T., BABUSIAUX, C., AND DELGADO, H. E. Gaia data release 2 - using gaia parallaxes. *A&A* *616* (2018), A9.
- [121] MACPHERSON, H. J., AND HEINESEN, A. Luminosity distance and anisotropic sky-sampling at low redshifts: A numerical relativity study. *Physical Review D* *104*, 2 (Jul 2021).
- [122] MACPHERSON, H. J., LASKY, P. D., AND PRICE, D. J. Inhomogeneous cosmology with numerical relativity. *Physical Review D* *95*, 6 (2017), 064028.
- [123] MACPHERSON, H. J., LASKY, P. D., AND PRICE, D. J. The trouble with Hubble: Local versus global expansion rates in inhomogeneous cosmological simulations with numerical relativity. *Astrophys. J.* *865*, 1 (2018), L4.
- [124] MARCORI, O. H., PITROU, C., UZAN, J.-P., AND PEREIRA, T. S. Direction and redshift drifts for general observers and their applications in cosmology. *Phys. Rev. D* *98*, 2 (2018), 023517.
- [125] MATARRESE, S., MOLLERACH, S., AND BRUNI, M. Relativistic second-order perturbations of the einstein–de sitter universe. *Physical Review D* *58*, 4 (1998), 043504.
- [126] MATARRESE, S., AND TERRANOVA, D. Post-newtonian cosmological dynamics in lagrangian coordinates. *Mon. Not. R. Astron. Soc.* *283* (1996), 400–418. astro-ph/9511093.
- [127] MCCracken, H., RADOVICH, M., BERTIN, E., MELLIER, Y., DANTEL-FORT, M., LE FEVRE, O., CUILLANDRE, J., GWYN, S., FOUCAUD, S., AND ZAMORANI, G. The virgos deep imaging survey-ii: Cfh12k bvri optical data for the 0226-04 deep field. *Astronomy & Astrophysics* *410*, 1 (2003), 17–32.
- [128] MCCREA, W. H. Observable relations in relativistic cosmology. *Zeitschrift für Astrophysik* *9* (1935), 290.

- [129] MERTENS, J. B., GIBLIN, J. T., AND STARKMAN, G. D. Integration of inhomogeneous cosmological spacetimes in the BSSN formalism. *Phys. Rev. D* *93*, 12 (2016), 124059.
- [130] MEURES, N., AND BRUNI, M. Exact nonlinear inhomogeneities in λ cdm cosmology. *Physical Review D* *83*, 12 (2011), 123519.
- [131] MEURES, N., AND BRUNI, M. Redshift and distances in a Λ CDM cosmology with non-linear inhomogeneities. *Mon. Not. Roy. Astron. Soc.* *419* (2012), 1937.
- [132] MILILLO, I., BERTACCA, D., BRUNI, M., AND MASELLI, A. Missing link: A nonlinear post-Friedmann framework for small and large scales. *Phys. Rev. D* *92*, 2 (2015), 023519.
- [133] MISNER, C. W., THORNE, K. S., AND WHEELER, J. A. *Gravitation*. W. H. Freeman and Company, New York, 1973.
- [134] NELSON, D., PILLEPICH, A., GENEL, S., VOGELSBERGER, M., SPRINGEL, V., TORREY, P., RODRIGUEZ-GOMEZ, V., SIJACKI, D., SNYDER, G., GRIFFEN, B., AND ET AL. The illustris simulation: Public data release. *Astronomy and Computing* *13* (Nov 2015), 12–37.
- [135] NELSON, D., SPRINGEL, V., PILLEPICH, A., RODRIGUEZ-GOMEZ, V., TORREY, P., GENEL, S., VOGELSBERGER, M., PAKMOR, R., MARINACCI, F., WEINBERGER, R., KELLEY, L., LOVELL, M., DIEMER, B., AND HERNQUIST, L. The illustri^{ng} simulations: Public data release, 2021.
- [136] PEEBLES, P. Structure of the coma cluster of galaxies. *The Astronomical Journal* *75* (1970), 13.
- [137] PEEBLES, P. J. E., AND PEEBLES, P. J. *Principles of physical cosmology*. Princeton university press, 1993.
- [138] PENZIAS, A. A., AND WILSON, R. W. A Measurement of Excess Antenna Temperature at 4080 Mc/s. *apj* *142* (July 1965), 419–421.
- [139] PERLICK, V. On redshift and parallaxes in general relativistic kinematical world models. *Journal of Mathematical Physics* *31*, 8 (1990), 1962–1971.
- [140] PERLICK, V. Gravitational lensing from a spacetime perspective. *Living Reviews in Relativity* *7*, 1 (Sep 2004), 9.
- [141] PERLMUTTER, S., ALDERING, G., GOLDHABER, G., KNOP, R. A., NUGENT, P., CASTRO, P. G., DEUSTUA, S., FABBRO, S., GOOBAR, A., GROOM, D. E., AND ET AL. Measurements of omega and lambda from 42 high-redshift supernovae. *The Astrophysical Journal* *517*, 2 (Jun 1999), 565–586.
- [142] PERRYMAN, M. A. C., DE BOER, K. S., GILMORE, G., HØG, E., LATTANZI, M. G., LINDEGREN, L., LURI, X., MIGNARD, F., PACE, O., AND DE ZEEUW, P. T. GAIA: Composition, formation and evolution of the Galaxy. *Astronomy and Astrophysics* *369* (Apr. 2001), 339–363.
- [143] PIRANI, F. A. E. On the Physical significance of the Riemann tensor. *Acta Phys. Polon.* *15* (1956), 389–405.

- [144] POISSON, E., POUND, A., AND VEGA, I. The motion of point particles in curved spacetime. *Living Reviews in Relativity* 14, 1 (Sep 2011), 7.
- [145] PRETORIUS, F. Evolution of binary black hole spacetimes. *Phys. Rev. Lett.* 95 (2005), 121101.
- [146] PUETZFELD, D., AND OBUKHOV, Y. N. Generalized deviation equation and determination of the curvature in General Relativity. *Phys. Rev. D* 93, 4 (2016), 044073.
- [147] QUARTIN, M., AND AMENDOLA, L. Distinguishing Between Void Models and Dark Energy with Cosmic Parallax and Redshift Drift. *Phys. Rev. D* 81 (2010), 043522.
- [148] QUERCELLINI, C., AMENDOLA, L., BALBI, A., CABELLA, P., AND QUARTIN, M. Real-time Cosmology. *Phys. Rept.* 521 (2012), 95–134.
- [149] QUERCELLINI, C., CABELLA, P., AMENDOLA, L., QUARTIN, M., AND BALBI, A. Cosmic Parallax as a probe of late time anisotropic expansion. *Phys. Rev. D* 80 (2009), 063527.
- [150] QUERCELLINI, C., QUARTIN, M., AND AMENDOLA, L. Possibility of Detecting Anisotropic Expansion of the Universe by Very Accurate Astrometry Measurements. *Phys. Rev. Lett.* 102 (2009), 151302.
- [151] RAMPF, C., VILLA, E., BERTACCA, D., AND BRUNI, M. Lagrangian theory for cosmic structure formation with vorticity: Newtonian and post-Friedmann approximations. *Phys. Rev. D* 94, 8 (2016), 083515.
- [152] RÄSÄNEN, S. A covariant treatment of cosmic parallax. *Journal of Cosmology and Astroparticle Physics* 2014, 03 (2014), 035.
- [153] RIESS, A. G., CASERTANO, S., ANDERSON, J., MACKENTY, J., AND FILIPPENKO, A. V. Parallax Beyond a Kiloparsec from Spatially Scanning the Wide Field Camera 3 on the Hubble Space Telescope. *Astrophys. J.* 785 (2014), 161.
- [154] RIESS, A. G., ET AL. New Parallaxes of Galactic Cepheids from Spatially Scanning the Hubble Space Telescope: Implications for the Hubble Constant. *Astrophys. J.* 855, 2 (2018), 136.
- [155] RIESS, A. G., FILIPPENKO, A. V., CHALLIS, P., CLOCCHIATTI, A., DIERCKS, A., GARNAVICH, P. M., GILLILAND, R. L., HOGAN, C. J., JHA, S., KIRSHNER, R. P., AND ET AL. Observational evidence from supernovae for an accelerating universe and a cosmological constant. *The Astronomical Journal* 116, 3 (Sep 1998), 1009–1038.
- [156] ROSQUIST, K. Trigonometric parallaxes of distant objects — what they could tell about the universe. *Astrophys. J.* 331 (1988), 648.
- [157] RUAN, C.-Z., CUESTA-LAZARO, C., EGGEMEIER, A., HERNÁNDEZ-AGUAYO, C., BAUGH, C. M., LI, B., AND PRADA, F. Towards an accurate model of small-scale redshift-space distortions in modified gravity. *arXiv* (10 2021).
- [158] SACHS, R. Gravitational Waves in General Relativity. VI. The Outgoing Radiation Condition. *Proceedings of the Royal Society of London Series A* 264 (Nov. 1961), 309–338.

- [159] SANDAGE, A. The Change of Redshift and Apparent Luminosity of Galaxies due to the Deceleration of Selected Expanding Universes. *Astrophys. J.* 136 (Sept. 1962), 319.
- [160] SANGHAI, V. A. A., FLEURY, P., AND CLIFTON, T. Ray tracing and Hubble diagrams in post-Newtonian cosmology. *JCAP* 07 (2017), 028.
- [161] SCARAMELLA, R., ET AL. Euclid preparation: I. The Euclid Wide Survey. *arXiv* (8 2021).
- [162] SCRIMGEOUR, M., ET AL. The WiggleZ Dark Energy Survey: the transition to large-scale cosmic homogeneity. *Mon. Not. Roy. Astron. Soc.* 425 (2012), 116–134.
- [163] SERBENTA, J., AND KORZYŃSKI, M. Bilocal geodesic operators in spherically-symmetric spacetimes. *in preparation* (2021).
- [164] SERBENTA, J., AND KORZYŃSKI, M. Redshift drift in general relativity in the bi-local formulation of geometrical optics. *in preparation* ().
- [165] SHIBATA, M., AND ASADA, H. Post-newtonian equations of motion in the flat universe. *Progress of Theoretical Physics* 94, 1 (1995), 11–31.
- [166] SHIBATA, M., AND NAKAMURA, T. Evolution of three-dimensional gravitational waves: Harmonic slicing case. *Physical Review D* 52, 10 (1995), 5428.
- [167] SMARR, L., AND YORK, JR., J. W. Kinematical conditions in the construction of space-time. *Phys. Rev. D* 17 (1978), 2529–2551.
- [168] SMOOT, G. F., ET AL. Structure in the COBE differential microwave radiometer first year maps. *Astrophys. J. Lett.* 396 (1992), L1–L5.
- [169] STAFFORD, S. G., MCCARTHY, I. G., KWAN, J., BROWN, S. T., FONT, A. S., AND ROBERTSON, A. Testing extensions to LCDM on small scales with forthcoming cosmic shear surveys. *arXiv* (9 2021).
- [170] SYNGE, J. L. *Relativity: The general theory*. North-Holland Publishing Company, Amsterdam, 1960.
- [171] SZEKERES, P. The gravitational compass. *Journal of Mathematical Physics* 6, 9 (1965), 1387–1391.
- [172] SZEKERES, P. A Class of Inhomogeneous Cosmological Models. *Commun. Math. Phys.* 41 (1975), 55.
- [173] THOMAS, D. B., BRUNI, M., AND WANDS, D. The fully non-linear post-friedmann frame-dragging vector potential: Magnitude and time evolution from n-body simulations. *Monthly Notices of the Royal Astronomical Society* 452, 2 (2015), 1727–1742.
- [174] THOMAS, D. B., BRUNI, M., AND WANDS, D. Relativistic weak lensing from a fully non-linear cosmological density field. *JCAP* 09 (2015), 021.
- [175] TOLMAN, R. C. Effect of inhomogeneity on cosmological models. *Proceedings of the national academy of sciences of the United States of America* 20, 3 (1934), 169.
- [176] TOMITA, K. Post-newtonian equations of motion in an expanding universe. *Progress of theoretical physics* 79, 2 (1988), 258–262.

- [177] TSUJIKAWA, S. Introductory review of cosmic inflation. *arXiv preprint hep-ph/0304257* (2003).
- [178] UMEH, O., CLARKSON, C., AND MAARTENS, R. Nonlinear relativistic corrections to cosmological distances, redshift and gravitational lensing magnification: I. Key results. *Class. Quant. Grav.* 31 (2014), 202001.
- [179] UZUN, N. Reduced phase space optics for general relativity: Symplectic ray bundle transfer. *Class. Quant. Grav.* 37, 4 (2020), 045002.
- [180] VILLA, E., MATARRESE, S., AND MAINO, D. Post-newtonian cosmological dynamics of plane-parallel perturbations and back-reaction. *Journal of Cosmology and Astroparticle Physics 2011*, 08 (2011), 024.
- [181] VILLA, E., AND RAMPF, C. Relativistic perturbations in λ cdm: Eulerian & lagrangian approaches. *Journal of Cosmology and Astroparticle Physics 2016*, 01 (2016), 030.
- [182] VINCENT, F. H., GOURGOULHON, E., AND NOVAK, J. 3+1 geodesic equation and images in numerical spacetimes. *Class. Quant. Grav.* 29 (2012), 245005.
- [183] VINES, J. Geodesic deviation at higher orders via covariant bitensors. *Gen. Rel. Grav.* 47, 5 (2015), 59.
- [184] VOGT, N. P., KOO, D. C., PHILLIPS, A. C., WU, K., FABER, S., WILLMER, C. N., SIMARD, L., WEINER, B. J., ILLINGWORTH, G. D., GEBHARDT, K., ET AL. The deep groth strip survey. i. the sample. *The Astrophysical Journal Supplement Series* 159, 1 (2005), 41.
- [185] WALD, R. M. *General relativity*. University of Chicago press, 2010.
- [186] WEINBERG, S. Direct determination of the metric from observed redshifts and distances. *The Astrophysical Journal* 161 (1970), L233–L234.
- [187] YADAV, J. K., BAGLA, J. S., AND KHANDAI, N. Fractal Dimension as a measure of the scale of Homogeneity. *Mon. Not. Roy. Astron. Soc.* 405 (2010), 2009.
- [188] YORK, D. G., ADELMAN, J., ANDERSON JR, J. E., ANDERSON, S. F., ANNIS, J., BAHCALL, N. A., BAKKEN, J., BARKHOUSER, R., BASTIAN, S., BERMAN, E., ET AL. The sloan digital sky survey: Technical summary. *The Astronomical Journal* 120, 3 (2000), 1579.

